A CONSTITUTIVE MODEL FOR FATIGUE AND RESIDUAL STRENGTH PREDICTIONS OF COMPOSITE LAMINATES

Jordi Llobet Vallejo

Universitat de Girona

Doctoral Thesis

A CONSTITUTIVE MODEL FOR FATIGUE AND RESIDUAL STRENGTH PREDICTIONS OF COMPOSITE LAMINATES

Jordi Llobet Vallejo

2019

Universitat de Girona

Doctoral Thesis

A CONSTITUTIVE MODEL FOR FATIGUE AND RESIDUAL STRENGTH PREDICTIONS OF COMPOSITE LAMINATES

Jordi Llobet Vallejo

2019

Doctoral Programme in Technology

Advisor:

Dr. Pere Maimí Vert

Thesis submitted to the University of Girona for the degree of Doctor of Philosophy

Acknowledgements

My deepest gratitude goes to my thesis advisor, Pere Maimí, for his continuous support and advice throughout every stage of this work. It would have been impossible to complete this work successfully without his guidance and his keen eye for proposing ideas. I would also like to thank the other professors of the group for their contributions and support in tough moments.

I would like to acknowledge the staff members of the research group AMADE for creating such a friendly and supportive work environment, and especially to the lab members for their valuable help and patience during the long fatigue test campaigns.

I would also like to thank Professors E. Lindgaard and B.L.V. Bak, from Aalborg University, for hosting me and for the insightful discussions during the three-month stay in Denmark. Furthermore, I would like to thank all the friends from Aalborg for the wonderful time and for showing me the awesome Danish Carnival.

No vull deixar d'agrair l'amistat i el suport rebut per part dels meus companys del grup de recerca AMADE, amb els quals he compartit tants bons moments durant la realització d'aquesta tesi. Per últim, vull agrair especialment a la meva família, a l'Eli i a tots els amics de Rubí, el seu suport incondicional durant tots aquest anys.

Finally, I would like to thank my late friend Søren for his kindness and for the lovely friendship created during my stay in Denmark. Your memory will always be with me. May your soul rest in peace.

Preface

The work contained in this Ph.D. thesis was conducted at AMADE research group (Department of Mechanical Engineering and Industrial Construction, University of Girona, Spain). The thesis was carried out under the predoctoral grant CBRGR-IF funded by the contract ABORDA. Part of the research presented in this thesis was developed during the Ph.D. candidate's stay at Aalborg University (Denmark) which was funded by AMADE research group.

Publications

The present Ph.D. thesis has been prepared as a compendium of peer-reviewed journal papers in accordance with the regulations of the University of Girona. The thesis is comprised of the following papers:

Peer-reviewed journal articles

- **J. Llobet**, P. Maimí, J.A. Mayugo, Y. Essa and F.M. de la Escalera. A fatigue damage and residual strength model for unidirectional carbon/epoxy composites under on-axis tension-tension loadings. *International Journal of Fatigue*, vol. 103, pp. 508–515, 2017.
`https://doi.org/10.1016/j.ijfatigue.2017.06.026`

  ISSN: 0142-1123, Impact Factor: 3.132, ranked 19/128 in the category of *Engineering, Mechanical* (Q1)[a].

- **J. Llobet**, P. Maimí, Y. Essa and F.M. de la Escalera. Progressive matrix cracking in carbon/epoxy cross-ply laminates under static and fatigue loading. *International Journal of Fatigue*, vol. 119, pp. 330-337, 2019.
`https://doi.org/10.1016/j.ijfatigue.2018.10.008`

  ISSN: 0142-1123, Impact Factor: 3.132, ranked 19/128 in the category of *Engineering, Mechanical* (Q1)[a].

- **J. Llobet**, P. Maimí, Y. Essa and F.M. de la Escalera. A continuum damage model for composite laminates. Part III: Fatigue, *submitted to Journal Mechanics of Materials*, 2019.

  ISSN: 0167-6636, Impact Factor: 2.958, ranked 21/134 in the category of *Mechanics* (Q1)[b].

[a] According to the 2017 InCites Journal Citation Reports
[b] According to the 2018 InCites Journal Citation Report

- **J. Llobet**, P. Maimí, A. Turon, B.L.V. Bak, E. Lindgaard, L. Carreras, Y. Essa and F.M. de la Escalera. A continuum damage model for composite laminates. Part IV: Experimental and numerical tests, *submitted to Journal Mechanics of Materials*, 2019.

  ISSN: 0167-6636, Impact Factor: 2.958, ranked 21/134 in the category of *Mechanics* (Q1)[b].

Other publications that have been derived from this thesis but are not included in the document are listed below:

- **P. Maimí**, N. Gascons, L. Ripoll and J.Llobet. Mixed mode delamination of asymmetric beam-like geometries with cohesive stresses. *International Journal of Solid and Structures*, vol. 155, pp. 36-46, 2018. `https://doi.org/10.1016/j.ijsolstr.2018.06.032`

Conference proceedings

- **J. Llobet**, P. Maimí, J.A. Mayugo, Y. Essa and F.M. de la Escalera. A stiffness-based phenomenological model to predict the fatigue life of unidirectional CFRP laminates under tensile fatigue loadings. XII Congreso Nacional de Materiales Compuestos (Matcomp). San Sebastián (Spain), June 2017.

- **J. Llobet**, P. Maimí, A. Turon, B.L.V. Bak, E. Lindgaard, Y. Essa and F.M. de la Escalera. Progressive damage modelling of notched carbon/epoxy laminates under tensile fatigue loadings. 18th European Conference on Composite Materials (ECCM18). Athens (Greece), June 2018.

- **J. Llobet**, P. Maimí, A. Turon, B.L.V. Bak, E. Lindgaard, Y. Essa and F.M. de la Escalera. Progressive Damage Modelling of open-hole carbon/epoxy laminates under tension-tension fatigue loading. 7th International Conference on Fatigue of Composites (ICFC 7). Vicenza (Italy), June 2018.

- **J. Llobet**, P. Maimí, A. Turon, B.L.V. Bak, E. Lindgaard, Y. Essa and F.M. de la Escalera. Progressive damage simulation in composite laminates

under in-service fatigue loadings. Society for the Advancement of Materials and Process Engineering (SAMPE). Southampton (UK), September 2018.

- **J. Llobet**, P. Maimí, A. Turon, B.L.V. Bak, E. Lindgaard, Y. Essa and F.M. de la Escalera. Fatigue damage modelling and residual strength of notched carbon/epoxy laminates. 7^{th} Thematic Conference on the Mechanical Response of Composites (ECCOMAS). Girona (Spain), September 2019.

Universitat de Girona

Dr. Pere Maimí Vert, Associate Professor at University of Girona

hereby CERTIFY that:

The thesis entitled *A constitutive model for fatigue and residual strength predictions of composite laminates*, submitted for the degree of Doctor of Philosophy by Jordi Llobet Vallejo, has been conducted under his supervision and that it fulfils the requirements for the *International Mention*.

Pere Maimí Vert
Associate Professor at University of Girona

Girona, November 2019

List of Figures

List of Tables

Contents

Abstract

Aerospace structures are often subjected to cyclic-loading conditions that, even though are far below the ultimate limit, may initiate material fatigue. In some cases, the initiation and propagation of fatigue cracks can compromise the service life and damage tolerance of the structure. Fatigue in composites is a complex material phenomena that involves the interaction of different damage mechanisms that appear at different length scales. In general, composites present an exceptional fatigue performance when compared to their metal counterparts. The substitution of metallic alloys by composites has been a great success in the aerospace industry. Despite the apparent advantages of composites against fatigue, questions about the reliability and lifetime performance of advanced composites remain unsolved and should be answered comprehensively in order to enable their use as primary structural materials.

Common practice design is still based on S-N fatigue life data, which given the inhomogeneous and anisotropic nature of composites, it results in a large number of experimental tests to ensure that the safety requirements imposed by the aviation authorities are met. At the same time, the lack of standard experimental methods specifically developed for composites gives rise to a lot of discrepancies when comparing fatigue experimental data from different laboratories. The development of advanced constitutive models to anticipate the complex mechanical behaviour of composites under different loading scenarios plays a major role in the reduction of the number of experimental tests and associated costs. Optimized structural designs by lowering safety factors as well as a reduction in the time-to-market can be only achieved by integrating these models into the latest commercial finite element codes. In this context, the main challenge is to have reliable and robust numerical models so that most experimental tests can be directly replaced by virtual simulations.

In light of the previous considerations, the present thesis aims to go one step forward into the experimental characterization and simulation methods for the design of advanced composites against fatigue loads. In the experimental field, the first consideration is to deepen the understanding on the damage mechanisms that control the fatigue degradation process in aerospace grade composite materials and to develop new experimental meth-

ods to assess the fatigue behaviour of composites. This objective is achieved by performing an extensive experimental campaign specifically designed to obtain empirical data that can be used into a new constitutive model for fatigue and residual strength predictions. The experimental campaign covers the study of different laminate configurations such as unidirectional, cross-ply and quasi-isotropic laminates. In the computational field, an extension of the former continuum damage mechanics model developed during the past ten years in AMADE research group is presented. This constitutive model has been benchmarked extensively under static and impact loading cases, and in this thesis, is upgraded to account for fatigue loads. The importance of fatigue-driven delamination on the degradation process of laminated composites made necessary the representation of this damage form within the current numerical framework. Thus, the continuum damage model for intra-laminar damage is coupled with a cohesive zone model for inter-laminar damage by means of an appropriate finite element modelling strategy. To improve the computational performance, a cycle jump strategy is implemented inside an explicit finite element code that can be executed in parallel computing. The capability of the computational model is verified by simulating the progressive damage in carbon/epoxy notched laminates under static, fatigue and residual strength tests.

Resum

Les estructures aeroespacials sovint estan sotmeses a càrregues cícliques que, tot i estar molt per sota de la resistència última, poden iniciar la fatiga del material. En aquest casos, la iniciació i propagació d'una esquerda a fatiga pot comprometre la vida útil i la tolerància al dany de l'estructura. La fatiga dels materials compòsits es considera un fenomen relativament complex a nivell material i estructural, ja que comporta la interacció de diferents mecanismes de dany que apareixen a diferents escales. En general, els compòsits presenten un comportament a fatiga excepcional en comparació amb els seus homòlegs metàl·lics. La substitució d'aliatges metàl·lics per materials compòsits avançats ha estat un gran èxit a la indústria aeronàutica. Malgrat els aparents avantatges dels compòsits en el comportament a fatiga, qüestions com la durabilitat i la predicció de la vida del material romanen sense resoldre's, i han de respondre's de manera clara per a confirmar el seu ús en l'estructura primària d'aeronaus.

A la pràctica, l'estudi de la fatiga en materials compòsits consisteix en l'aplicació de mètodes experimentals coneguts com les corbes S-N. La naturalesa no homogènia i anisòtropa del material generalment comporta la realització d'un gran nombre de proves experimentals per tal de garantir que es compleixin les condicions de seguretat imposades per les autoritats. Al mateix temps, la manca de mètodes experimentals estàndard específicament desenvolupats pels compòsits dóna lloc a moltes discrepàncies quan es comparen dades experimentals provinents de diferents laboratoris. El desenvolupament de models constitutius avançats per anticipar la resposta estructural del material sota diferents escenaris de càrrega, té un paper transcendental en la reducció dels costos de desenvolupament associats a la fase de disseny estructural. La implementació de models constitutius avançats dins d'un codi numèric d'elements finits es postula com una excel·lent eina computacional per l'optimització de components estructurals així com per la reducció del temps de disseny i per tant el cost associat. El repte esdevé la necessitat d'obtenir simulacions numèriques robustes i fiables, de manera que la majoria de proves experimentals es puguin substituir directament per simulacions numèriques.

Per tant, la present tesi té com a objectiu fer un pas endavant tan en la millora dels mètodes experimentals com en la modelització numèrica dels

materials compòsits sotmesos a càrregues cícliques. En el camp experimental, la primera consideració és aprofundir en la comprensió dels mecanismes de dany que controlen el procés de degradació a fatiga i desenvolupar nous mètodes experimentals que permetin avaluar el comportament a fatiga dels compòsits. Aquest objectiu s'aconsegueix realitzant una extensa campanya experimental dissenyada específicament per obtenir dades empíriques que es puguin utilitzar en el marc d'un model constitutiu per la predicció de la pèrdua de propietats mecàniques i de la vida a fatiga. La campanya experimental consisteix en assajar diferents tipus de laminats (unidireccionals, cross-ply i quasi-isòtrops) sota diferents escenaris de càrrega a fatiga. En el camp computacional, es proposa una extensió del model computacional de dany continu desenvolupat durant els darrers deu anys al grup de recerca AMADE. Aquest model constitutiu ha estat validat àmpliament en casos de càrrega estàtics i d'impacte, i en la present tesi s'actualitza per tal de considerar càrregues cícliques. La importància de la delaminació a fatiga en el procés de degradació a fatiga dels compòsits, fa necessària la representació d'aquest mecanisme de dany dins del marc computacional actual. Per tant, el model de dany continu per descriure el dany intra-laminar s'acobla amb un model de zona cohesiva pel dany inter-laminar. Per tal de millorar el cost computacional, el model contempla l'ús d'una estratègia de salt de cicles de càrrega ("cycle jump technique"). La resposta del model numèric es verifica simulant la degradació progressiva en provetes amb entalla o forat descobert fabricades mitjançat un laminat quasi-isòtrop amb capes de fibra de carboni i resina epoxi.

Resumen

Las estructuras aeroespaciales a menudo están sujetas a condiciones de carga cíclicas que, aunque pueden estar muy por debajo de la resistencia última, pueden iniciar la fatiga del material. En estos casos, el inicio y propagación de una grieta a fatiga pueden comprometer la vida útil y la tolerancia al daño de la estructura. La fatiga en los compuestos se considera un fenómeno de cierta complejidad que ocurre a nivel material y estructural, y que implica la interacción de diferentes mecanismos de daño que aparecen en diferentes escalas. En general, los compuestos presentan un comportamiento excepcional a fatiga en comparación con sus homólogos metálicos. La sustitución de aleaciones metálicas por materiales compuestos avanzados ha sido un gran éxito en la industria aeroespacial. A pesar de las ventajas aparentes de los materiales compuestos en términos de fatiga, cuestiones como la durabilidad y la predicción de vida del material siguen sin resolverse, y deben responderse de manera clara para confirmar su uso en la estructura primaria de aeronaves.

En la práctica, el estudio de la fatiga en materiales compuestos se basa en el uso de métodos experimentales tradicionales conocidos como las curvas S-N. La naturaleza no homogénea y anisótropa del material conlleva un gran número de pruebas experimentales para garantizar que se cumplan los requisitos de seguridad impuestos por las autoridades. Al mismo tiempo, la falta de métodos experimentales estándar específicamente desarrollados para los compuestos da lugar a ciertas discrepancias cuando se comparan datos experimentales provenientes de diferentes laboratorios. El desarrollo de modelos constitutivos avanzados para anticipar la respuesta estructural del material cuando se solicita en diferentes condiciones de carga, tiene un papel trascendental en la reducción de los costes de desarrollo asociados a la fase de diseño estructural. La implementación de modelos constitutivos avanzados dentro de un código numérico de elementos finitos se postula como una excelente herramienta computacional para la optimización de componentes estructurales, así como para la reducción del tiempo de comercialización del componente. El reto se convierte en la necesidad de obtener simulaciones numéricas robustas y fiables, para que la mayoría de pruebas experimentales se puedan sustituir directamente por simulaciones numéricas.

A la vista de las consideraciones anteriores, la presente tesis tiene como objetivo dar un paso adelante tanto en la mejora de los métodos experimen-

tales como en la modelización numérica de los materiales compuestos sometidos a cargas cíclicas. En el campo experimental, la primera consideración es profundizar en la comprensión de los mecanismos de daño que controlan el proceso de degradación a fatiga y así generar el conocimiento necesario para desarrollar nuevos métodos experimentales que permitan evaluar el comportamiento a fatiga. Este objetivo se consigue realizando una extensa campaña experimental diseñada específicamente para obtener datos empíricos que se puedan utilizar en un nuevo modelo constitutivo para la predicción de la pérdida de propiedades mecánicas y de la vida a fatiga. La campaña experimental consiste en ensayar diferentes tipos de laminados (unidireccionales, cross-ply y casi-isótropos) bajo diferentes condiciones de carga a fatiga. En el campo computacional, se propone una extensión del modelo computacional de daño continuo desarrollado durante los últimos diez años en el grupo de investigación AMADE. Este modelo constitutivo se ha estado validado ampliamente en casos de carga estáticos y de impacto, i la presente tesis se actualiza para considerar cargas cíclicas. La importancia de la delaminación a fatiga (o daño inter-laminar) en el proceso de degradación a fatiga, hace necesaria la representación de este mecanismo de daño dentro del marco computacional actual. Por esta razón, el modelo computacional de daño continuo para describir el daño intra-laminar se acopla con un modelo de zona cohesiva para el daño inter-laminar. Con el fin de reducir el coste computacional, el modelo contempla el uso de una estrategia de salto de ciclos de carga ("cycle jump technique"). La respuesta del modelo numérico se verifica simulando la degradación progresiva de probetas con entalla o agujero descubierto fabricadas mediante un laminado con capas de fibra carbono y resina epoxi.

Chapter 1

Introduction

This thesis is the result of a collaboration with the aerospace company AERNNOVA Engineering and AMADE research group under the project entitled ABORDA. The project started with the general premise of improving the available numerical design tools for composite structures subjected to fatigue loads. Thus, this Ph.D. thesis has been undertaken with the following general purpose:

To develop a computational tool capable of predicting fatigue damage and residual strength of laminated composites for primary aircraft structures

In the following sections of this chapter, the background and the motivation of this thesis are presented. Next, a state-of-the-art review on the fatigue life prediction methodologies is given with especial emphasis to the modelling of fatigue damage within the framework of continuum damage mechanics. Following that, a brief description of the main fatigue damage mechanisms that occur in laminated composites with different stacking sequences is given. To close the review section, a set of partial objectives is identified that defines the point of departure towards the general purpose of the project. In the final section, the thesis layout is presented closing this introductory chapter.

1.1 Background

In essence, a composite material is made from two or more constituents with different physical and chemical properties. When combined, the composite material exhibits beneficial physical characteristics quite different from what the individual components alone can provide. One particular standout composite material is Carbon-Fibre Reinforced Plastic, or CFRP. This type of

composite belongs to the category of Fibre-Reinforced Polymer (FRP) matrix composites. The strength of CFRP results from the interplay between its constituents. By themselves, neither the carbon fibres nor the resin is sufficient to create a product with the desired characteristics to be integrated on an aircraft. But once combined in multiple, integrated layers and bonded, the CFRP airframe takes the strength and load-bearing capacity that make it ideal for aviation use.

The presence of FRP in airframe structures has expanded progressively over the last four decades as shown in Fig. 1.1. With their winning combination of high specific stiffness and strength it is easy to see why. The principal aerospace manufacturers, like Airbus or Boeing, have pioneered the use of such materials either in their jetliners or in their military aircraft. For example, the content of CFRP in the airframe structure is more than 50% for the latest Airbus A350 XWB and the Boeing B787 Dreamliner [1]. Fig. 1.2 shows the material breakdown and its location in the Airbus A350 XWB.

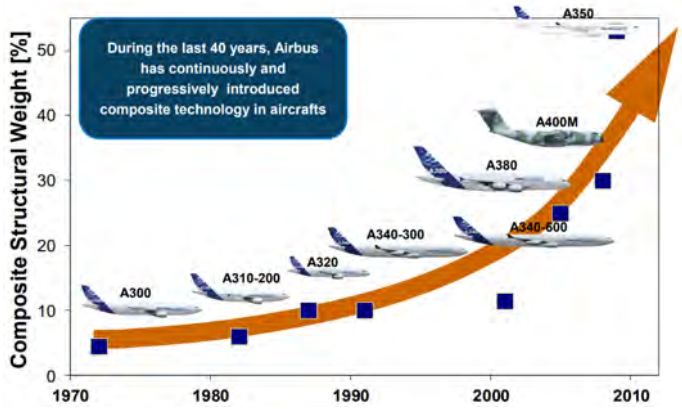

Fig. 1.1: The evolution of composite structural weight in [%]. Source from Airbus group.

A further step towards more advanced lightweight airframe parts stem from the combination of new high performance materials and the development of new experimental and computational methods to optimize the structural performance from an early stage of design. Recall that the larger operational cost of the airlines is still given by the fuel consumption and maintenance tasks of the aircraft [1]. It is evident that the choice of the airframe materials and its design can affect a large portion of the operational cost.

Fig. 1.2: Material breakdown of the Airbus A350-900 XWB family (source from Airbus group).

1.2 Motivation

The structural integrity and safety of a composite airframe are demonstrated by analytical/numerical models and by experimental tests. The usual test approach is based on the test pyramid or what it is known as the "*building block approach*" [2]. The building block approach provides different levels of testing, that start from the base of the pyramid with coupon level tests (or level 1), and move towards a higher level of complexity with elements, sub-structural details, components and full-scale tests. Thus, the certification of an aircraft relies on extensive and expensive testing programs especially those tests at the top of the pyramid (i.e., full-scale tests) under service fatigue loads.

Fatigue damage in composites is known to be conceptually different than in metals so that the traditional fatigue design philosophies applied to metals like the "*safe-life*" and "*fail-safe*" approaches are not necessarily appropriate in the current composite parts. Nowadays, the design of composites against fatigue is usually based on a "damage tolerance" approach or on the "no-growth" design philosophies. Damage tolerance means the remaining capability of a damaged structure to sustain in-service loads until the damage is detected and repaired during an scheduled inspection. The no-growth concept aims to ensure that no crack propagation will ever occur during the lifetime of a component. Though the no-growth concept reduces the maintenance tasks and associated costs, it leads to more conservative designs. Note that the need for weight minimization to reduce fuel consumption for the latest aircraft designs make them susceptible to suffer from fatigue since the

in-service loading levels are increasingly closer to the ultimate design limits. The damage tolerance requirements have been continuously revised and currently the aviation authorities insist on including new certification concepts supporting fatigue and damage tolerance. For instance, the following steps are followed to fulfil the certification of a composite part [1]:

(1.) The CFRP part is manufactured with a specified qualified material within a specially qualified process. The maximum allowable manufacturing defects and the maximum allowable impact damages (non-visible) are artificially introduced into the CFRP part.

(2.) Fatigue loads are applied to the part, simulating a complete design service goal. A load elevation factor can be used in order to compensate for any material strength reduction due to temperature and humidity. In some cases, a load elevation factor is applied to reduce the duration of the fatigue test [3].

(3.) The static ultimate load is applied, and the part must not fail meaning that the residual strength is above the ultimate load.

So far the process of certification is being updated with new safety regulations for fatigue and damage tolerance but the computational models available are still limited by the difficulty of predicting fatigue damage, service life and residual strength of composite structures. Numerical simulations with the most advanced constitutive models play a major role in the reduction of the number of mechanical tests and, consequently, in the reduction of the development costs. This approach is commonly known as *virtual mechanical testing* and its philosophy is based on replacing real mechanical tests by high-fidelity numerical simulations. Obviously, the reliability and robustness of these numerical models have to be especially high in order to convince the industrial partners to use them as reliable design computational tools.

1.3 Literature review

Establish a general classification of fatigue models and lifetime prediction methodologies for composites is difficult, but most works refer to the classification proposed by Sendeckyj [4], among other similar classifications that appear in the excellent review papers published in [5–8]. The fatigue life prediction methodologies for composites can be divided into three major categories: (I) fatigue life models, (II) phenomenological models and (III) progressive damage models. Fatigue life models (I) are based on the so-called S-N curves or Goodman-type diagrams, where the number of cycles at which failure occurs is estimated by means of log-linear functions that are fitted

from constant-amplitude load-controlled fatigue tests. Similarly to the approach taken for metals, an accumulation rule is used for variable-amplitude load cases. Under multi-axial stress states, a fatigue failure criterion is introduced. Phenomenological models (II), that are sub-classified in strength, stiffness and fracture mechanics-based models, define a empirical function to describe the gradual degradation by monitoring the residual strength, residual stiffness or the crack growth with respect to the number of cycles. Finally, progressive damage models (III) which use one or more damage variables related to measurable effects of damage (interfacial debonding, matrix cracking or delamination). Indeed, Degrieck and Van Paepegem [6] distinguished between two classes of progressive damage models. Models that correlate the damage growth with the residual mechanical properties (stiffness/strength) and mechanistic damage models that predict the damage growth using a mechanistic variable (e.g., crack density calculated as the number of matrix cracks per unit of length).

1.3.1 Fatigue life models

Fatigue life models are based on the stress-life curves (or S-N curves) which are usually fitted to a set of experimental results. They are usually defined by expressions of the form:

$$\mathrm{N} = f(\sigma_{max}, R, ...) \tag{1.1}$$

σ_{max} is the maximum applied cyclic stress (uniaxial or a norm of a multiaxial stress state) and R is the stress ratio defined as the ratio between the minimum and the maximum cyclic stress: $R = \sigma_{min}/\sigma_{max}$. The S-N curves only provide information of the number of cycles (N) required to material failure but they do not provide any indication of the underlying failure mechanism that induce fatigue failure.

By testing specimens under different maximum cyclic stresses and stress ratios is possible to construct the classical S-N curves and Goodman-type diagrams for fatigue loading cases with constant amplitude. A lot of examples of fatigue life models can be found in literature [6, 9–13]. To account for the effect of fatigue blocks of different amplitudes, Equation (1.1) can be computed with some general rule similar to the one presented by Palmgren and Miner. A review on different accumulation rules can be found in [14]. In contrast, Kawai et al. [15–17] defined a differential equation as:

$$\frac{dw}{d\mathrm{N}} = K(\Sigma^*)^{n^*} \left(\frac{1}{1-w}\right)^k \tag{1.2}$$

where w is a scalar variable that defines the degradation of the material, K, n^* and k are material constants. Σ^* is defined as a non-dimensional stress

measure based on Tsai-Hill static failure criterion to account for multiaxial stress states, but it also considers the effect of the orientation of the fibres, the maximum cyclic stress and the stress ratio. The S-N curve can be obtained by integrating Equation (1.2) when w reaches unity.

1.3.2 Phenomenological models

Phenomenological models provide a description of damage under fatigue loads by modelling the degradation of a macroscopic property such as the stiffness, the strength or the crack growth.

Strength-based models. Residual strength phenomenological models [18–20] measure the loss of strength (or residual strength) during cyclic loading. Obviously, the experimental cost of measuring the residual strength becomes extremely high, not only because of the large number of destructive tests required but for the number of factors than can affect this property such as different load levels, load ratios, lay-up configurations and so many others properties of interest from an industrial point of view. The residual strength is usually assumed to be a monotonically decreasing function of the number of cycles and its rate is defined as $\frac{d\sigma_R}{d\mathrm{N}} = f(\sigma_{\max}, \sigma_{\min}, \sigma_R, ...)$. The form of this function and its dependencies have been reviewed by numerous authors. Strength-based models are likeable in the research community since they provide a simple and clear explanation of fatigue failure, that is, failure occurs when the residual strength equals the maximum cyclic stress. Indeed, the integration of $\frac{d\sigma_R}{d\mathrm{N}}$ for the case of a constant-amplitude stress, and forcing that the residual strength is equal to the maximum cyclic stress, results in the S-N curve expression.

Stiffness-based models. Residual stiffness phenomenological models [6, 21] describe the loss of stiffness (or residual stiffness) during cyclic loading. The measure of the residual stiffness in fatigue is less problematic and costly that the residual strength (i.e., non-destructive testing). This property also presents less scatter so that it is commonly considered to be an excellent property to quantify the level of fatigue damage in composite structures. On the contrary, there is still an open discussion in the literature in order to provide a clear failure definition when using this type of models. The loss of stiffness is usually characterized by the damage rate, $\frac{dD}{d\mathrm{N}}$, where the damage variable D is defined as in continuum damage mechanics, $D = 1 - m$, being m the normalized loss of stiffness. As it happens with the residual strength, this property is influenced by many different parameters of interest such as $\frac{dD}{d\mathrm{N}} = f(\sigma_{\max}, \sigma_{\min}, D, ...)$. For instance, Van Paepegem and co-workers [22, 23] presented a one-dimensional phenomenological stiffness-based damage model to predict the life of laminated composites under bend-

ing fatigue. Fatigue failure is defined according to a modified Tsai-Wu failure criterion, in which the nominal stress is replaced by the effective stress and the ultimate strain is assumed to be constant. This last hypothesis (constant ultimate strain-to-failure) offers a link between stiffness and strength-based models, meaning that, the decrease in stiffness is proportional to the decrease in strength. This hypothesis was validated for plain woven glass/epoxy laminates and in this thesis (paper A) the same hypothesis is validated for unidirectional plies loaded in the fibre direction. Figure 1.3 illustrates the two evolution functions described in this section but plotted all together in the same figure.

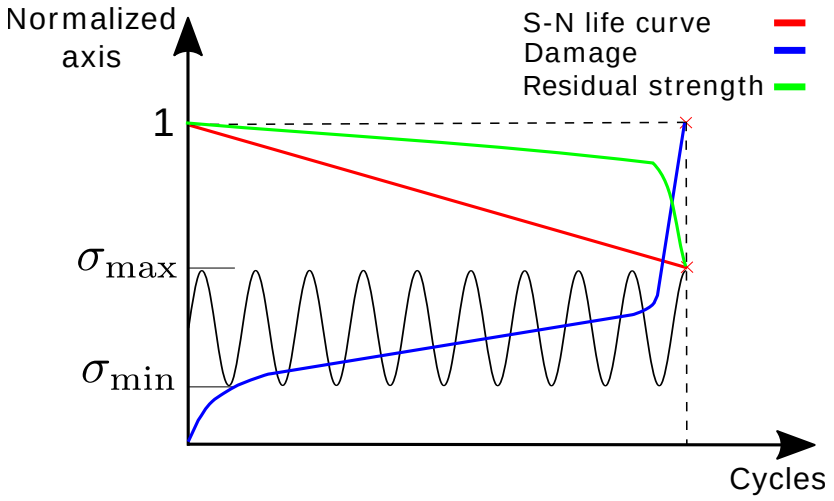

Fig. 1.3: S-N life, damage (or stiffness loss) and residual strength curves.

Fracture mechanics-based models. Fracture mechanics-based models analyse the initiation and propagation of cracks under fatigue loads. This type of models is especially used to describe the initiation and growth of delamination cracks, but also to study off-axis matrix cracking or even fibre/matrix debonding in micromechanical models. From a fracture mechanics point of view, delamination cracks experiencing cyclic loading may propagate even though the available energy release rate ($\mathcal{G}_{max}$) is below the static fracture toughness of the material ($\mathcal{G}_c$). The initiation phase deals with the emergence of delamination in pristine laminates. It can be compared with the nucleation stage in metals. Delamination onset is usually analysed by means of crack onset curves, which is similar to an S-N curve but instead of the maximum cyclic stress or strain, the maximum applied energy release rate is used. Refer to the standard test method ASTM D6115 for mode I fatigue delamination growth onset of unidirectional fibre-reinforced polymer matrix compos-

ites [24]. Onset delamination data can be fitted, as proposed by Krueger [25], by an expression of the kind:

$$\mathcal{G}_{\max} = B(\mathrm{N})^{-m} \tag{1.3}$$

where B and m are material fitting parameters (see left plot in Figure 1.4).

On the other hand, the propagation phase is typically characterized by the crack growth rate (or also the so-called Paris law inherited from metals), $\frac{da}{d\mathrm{N}}$. The expression of the crack growth rate can be related to the maximum energy release rate, $\mathcal{G}_{\max}$, by means of a power-law function:

$$\frac{da}{d\mathrm{N}} = A(\mathcal{G}_{\max})^{m} \tag{1.4}$$

where A and p are material fitting parameters. Figure 1.4 shows a qualitative representation of a typical crack onset curve (left) and crack growth rate curve (right). In Figure 1.4 (right), three regions can be distinguished: region I. limiting the energy release rate threshold, $\mathcal{G}_{\mathrm{th}}$, from which no propagation occurs, region II. governed by the log-linear crack growth of Equation 1.4, and region III. that marks the transition to quasi-static crack growth.

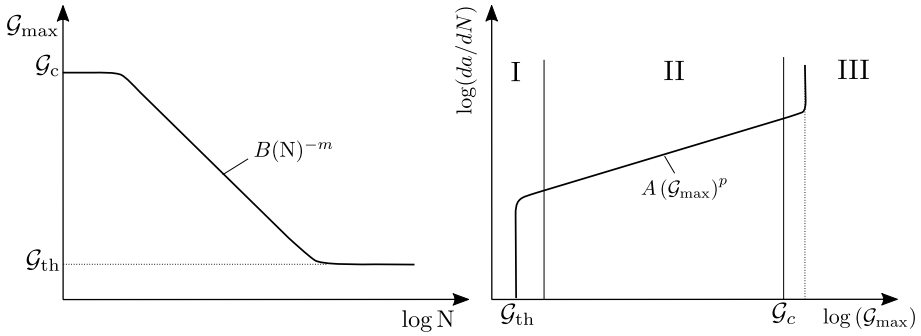

Fig. 1.4: Qualitative representations of typical crack onset (left) and crack growth rate (right) curves [26].

The fracture mechanics interpretation provided by Nairn and co-workers [27] to analyse matrix cracking in cross-ply laminates can be used as a reference source. A variational approach was used to solve the stress state in cross-ply laminates, and the stress analysis was used to calculate the energy release due to the formation of matrix cracks [28]. Not much later, Liu and Nairn [29] claimed that a modified Paris-law with the crack density can be used to predict the increase in the number of matrix cracks under fatigue loads:

$$\frac{d\rho}{d\mathrm{N}} = A(\Delta\mathcal{G})^{m} \tag{1.5}$$

where ρ is the crack density computed as the number of cracks over a certain length. Figure 1.5 shows the results presented for cross-ply laminates.The reader is referred to paper B (section 2.2) that investigates the approach proposed by Liu and Nairn [29].

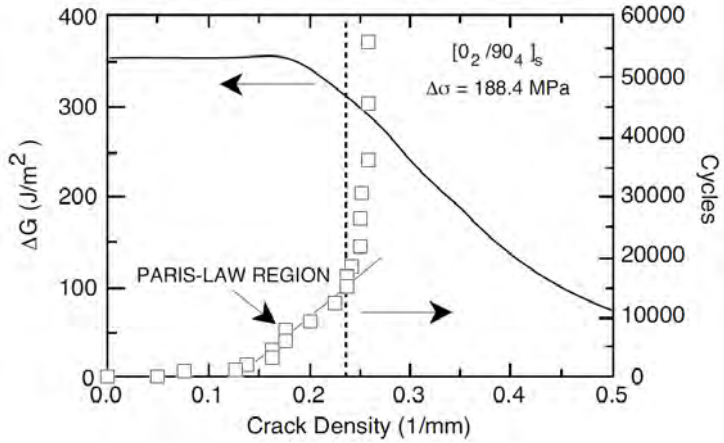

Fig. 1.5: Matrix cracking under fatigue loading for a $[0_2/90_4]$ Fiberite 934/T300 composite. The solid line shows ΔG as a function of the crack density. The squared markers show the crack density as a function of the number of cycles. The straight line through the crack density data shows the Paris-law region of a constant crack density growth rate [29].

1.3.3 Progressive damage models

The progressive damage models differ from the phenomenological models in that they estimate the fatigue behaviour of composite laminates based on a set of internal variables which describes the current state of degradation of the material. Actually, these models are usually a combination of stiffness and strength-based models along with the definition of a fatigue failure criterion (e.g., Hashin, Tsai-Wu, Puck, LaRC,...) that considers the residual strength instead of the pristine strength. These models calculate the equilibrium equations at each cycle or number of cycles, and then recompute the stress and internal variables according to some degradation rules. These damage-based models need to be implemented and solved numerically, usually by means of a finite element software.

The first consideration in defining a progressive damage model is to define a set of internal variables precise enough that describe the internal changes and the state of degradation of the material under any load case of interest. These internal variables are usually related to the damage modes, which in composites the obvious choice is to define damage in terms of the matrix and fibre failure. The common way to define these internal variables

is to relate them with the loss of stiffness and strength. Sometimes, internal variables with a mechanistic basis are used, a typical example of this would be the use of damage variables related to the density of cracks in the matrix [30–33].

Once the internal variables are defined, it is necessary to postulate a set of activation criteria and evolution laws for each of the internal variables. Under fatigue loads, the evolution laws are usually established based on the models presented in section 1.3.2. It is also important to consider the evolution of the internal variables under static loads, because the static evolution is essential to correctly predict the final structural collapse. Several fatigue models presented in literature make use of the simple ply discount method to deal with static failure once some failure criterion is satisfied.

Shokrieh and Lessard [34–36] established a model called "generalized residual material property degradation model" for unidirectional laminates. They used a Hashin-type failure criterion to identify the damage mode and consequently reduce the corresponding elastic and strength properties to zero under static loading (i.e., ply discount method). Under fatigue loading, the material properties are progressively degraded through the strength and stiffness degradation functions. Hence, the fatigue model is capable of simulating the residual strength, residual stiffness and fatigue life of composite laminates with arbitrary geometry, stress level, stress ratio and stacking sequence under multiaxial stress states. Obviously the computational model demands extensive material characterization but only with uniaxial fatigue tests at coupon level.

Similarly, Philippidis and Eliopoulos [37–39] presented a progressive damage model for life prediction of multidirectional glass/epoxy laminates under constant and variable-amplitude fatigue loading. In static, the constitutive relation accounts for non-linear hardening response under shear and transverse compression to the fibres, and the ply discount method is used on the corresponding elastic properties once the Puck failure criterion is activated. Under fatigue loads, two normalized damage functions for in-plane shear and transverse to the fibre stresses are postulated. Progressive stiffness degradation for loads parallel to the fibre direction is neglected. The residual strength model is based on the model proposed by Broutman and Sahu [19]. These functions depend implicitly on the stress ratio and the stress level through the fatigue life fraction, which is obtained directly using the constant life diagram (or Goodman-type diagram).

Several works that have been published afterwards can be considered as extensions of the previous fatigue damage models. For instance, Naderi and Maligno [40] used the original model from Shokrieh and Lessard [34] but they assigned a random distribution of material properties in order to account for the intrinsic variability of the local microstructure and the presence of defects due to the manufacturing process. They obtained reasonably good

predictions of the S-N curves for the range of laminates analysed. Lian and Yao [41] proposed a similar modelling approach that couples the residual stiffness with the strength model thus reducing the amount of experimental data to calibrate the numerical model. The model also accounts for the scatter of material properties. Hashin's failure surface envelope was used along with the ply discount method. The obtained numerical predictions are in fair agreement with experimental data except for the case in which fatigue failure was controlled by delamination. Kennedy et al. [42] proposed a method again conceptually similar to that presented in [34], based on the 3D analysis of a laminate, where the element properties were gradually degraded according to empirical laws. The element failure, followed by the sudden degradation of the ply properties, was predicted by means of a Puck-like criterion, suitably extended to fatigue loadings. They obtained a good correspondence between the simulated and the experimental stiffness trends on multidirectional laminates.

An especial consideration must be made to introduce the progressive damage models that are formulated within the framework of thermodynamics of irreversible dissipative processes. This is a general framework that can be used to formulate constitutive equations. It is a logical framework for incorporating experimental observations and a set of rules for avoiding incompatibilities. The effect of the internal variables on the elastic material response comes from the definition of a thermodynamic potential energy function, usually the Helmholtz free energy density expressed with respect to the strains and internal variables, $\Psi(\varepsilon, \text{I.V})$, or the complementary energy density function expressed by the stresses: $G(\sigma, \text{I.V})$. Both energy functions are related by means of the Legendre transformation as: $G = \Psi - \sigma : \varepsilon$. The constitutive model must ensure the irreversibility of the damage process by imposing the rate of energy dissipated, Ξ, to be positive. The evolution of damage without energy dissipation is physically not admissible in constitutive modelling. The Clausius-Duhem inequality can be postulated such that the externally supplied mechanical power, $\sigma : \dot{\varepsilon}$, minus the rate of change of the Helmholtz free energy, $\dot{\Psi}$, must be positive (for isothermal processes):

$$\Xi = \sigma : \dot{\varepsilon} - \dot{\Psi} \geq 0 \tag{1.6}$$

Finally, by means of Coleman's argument [43] the constitutive relationship: $\sigma = \frac{\partial \Psi}{\partial \varepsilon}$ and the rate of dissipation Ξ are appropriately defined. This framework defines the effect of the internal variables on the constitutive relation and defines admissible bounds for the evolution laws of these variables. There exists a long list of continuum damage mechanics (CDM) based models to predict the constitutive behaviour of laminated composites for static loads [44–50].

Within CDM-based models that consider the effect of fatigue loads, there are several studies uniquely devoted to study intralaminar off-axis matrix

cracking. In this regard, Ladevèze and co-workers [30] were one of the first to extend their static mesoscale CDM-based model mainly to study off-axis matrix cracking under fatigue loads. Only two damage variables are used represent the matrix damage caused by transverse and shear stresses. They assumed that fibre-matrix debonding (or diffuse damage) can be considered the major damage mechanism in fatigue loading. The total damage accounts for the contribution of the static and cyclic loads involved. The growing rate of diffuse damage, was defined as an intrinsic function of the thermodynamic forces and of the current level of diffuse damage. Then, they used the modified Paris-based function proposed by Liu and Nairn [29] to describe the increase in the crack density with respect to the loading cycles as a function of the available energy release rate for cracking. Equivalently, Payan and Hochard [51–53] developed a mesoscale damage model based on the work of Ladevéze [30]. Again, it was considered a brittle behaviour in fibre direction (except in [53]), but elasto-plastic and damage behaviour under transverse tension and compression, and in-plane shear stresses for the matrix. Under fatigue only diffuse damage was considered and the range of validity of the model was limited to the first intra-laminar crack.

Thionnet and Renard [31, 54] developed a similar CDM-based model to the one proposed in [30], but considering mainly the degradation of the ply due to transverse cracking. Transverse cracking was homogenized at the mesoscale by means of a single scalar damage variable that indirectly quantifies the density of cracks. They suggested an exponential decay of the transverse Young's modulus of the ply with respect to the normalized crack density. The model was benchmarked by simulating the crack density of cross-ply laminates under two block-amplitude loading levels of fatigue tests. Closely-related, Li et al. [33] developed a mesoscale damage mechanics model for cross-ply laminates following the critical element concept from Reifsnider [55]. The damage model was based on Talreja's CDM-based model [44]. The experimental fatigue lives of different cross-ply laminates with different ply thickness were compared to the theoretical predictions showing good agreement.

Sedakrian et al. [56] proposed a three-dimensional CDM-based model to describe the fatigue behaviour of $[\pm 45]_s$ laminates under torsion tests. The constitutive model follows closely the model proposed by Ladevéze [47]. The model considers five fatigue damage functions that depend on the thermodynamic forces associated with the damage variables (three of them are for the in-plane longitudinal, transverse and shear components, and the other two for the out-of-plane shear).

Later on, Kruger and Rolfes [57] presented a meso-scale CDM-based model for multi-directional laminates exposed to general states of plane-stress. The essential of the model was the use of an energy-based approach that imposes the same energy dissipated by plasticity and damage during fatigue loading

and during quasi-static loading. In this way, the stiffness and strength degradation are coupled and destructive testing to determine the residual strength is no longer required. The model is elegant but it is questionable the physical meaning and implication of their energy-based hypothesis. The model was validated by simulating open-hole specimens, and in a larger-scale, by simulating the progressive damage of a full wind turbine blade.

Recently, Mohammadi et al. [58] presented a CDM-based model based on effective average local stresses to predict the stiffness degradation and fatigue life of composite laminates. Three damage variables are defined in the framework of micromechanics of a lamina to estimate stiffness degradation in the fibre and matrix directions. The fatigue damage functions for the fibre, matrix and shear depend on the thermodynamic forces. Fatigue failure occurs when the updated stresses are greater than the corresponding static strength, or when the damage variables are greater than the critical value, then the corresponding stiffness terms are set to zero (i.e., ply discount method). The model is verified by simulating cross-ply and quasi-isotropic plain laminates, but also by simulating pin-loaded laminates reaching a reasonable correlation with the experimental results.

As a general comment, most damage-based models suffer from severe mesh-dependency and often reach to too conservative predictions when the simplified ply-discount method is used. This is especially relevant when these models are applied to structures with non-uniform stress field such as structures containing holes, notches or any other source of stress raiser. For composite structures that can accumulate damage before structural collapse, the use of the simplified ply-discount method is not sufficient to predict ultimate failure. The ply-discount can be used to predict the onset of damage, which in certain conditions might be enough to assess the structural performance, but they cannot represent with satisfactory accuracy the quasi-brittle failure of laminates that results in the accumulation of several damage mechanisms with softening until its final loss of integrity. In this respect, the CDM framework presented in references [49, 50, 59–62] establishes a bridge between the classical continuum mechanics and fracture mechanics by embedding a softening cohesive law inside a continuum element with the crack band approach [63]. Thus, the mesh sensitivity of CDM-based models is alleviated and the model ensures an objective dissipation of the fracture energy regardless of the mesh refinement. Note that Hochard et al. [64] introduced a non-local stress-based criterion to alleviate the mesh dependency in the simulation of open-hole specimens and Krueger et al. [57] followed the crack band model as in [50].

Among the different challenges associated with constitutive modelling of composite materials, fatigue clearly reveals a problem in term of experimental characterization. Any experimental campaign involving fatigue characterization raises cost and time significantly with respect to static characterization.

As a result, the use of constitutive models to analyse fatigue loading scenarios becomes economically impractical or limited by the amount of reliable experimental data. In the author's opinion, the approach that must be followed towards a reduction of the associated costs and number of tests, goes through a better understanding on the fundamental degradation mechanisms that are developed under fatigue loads, and this can only be achieved by means of mechanistic models that links different scales [65–75].

To close this review section, it is worth to mention that the vast majority of progressive damage models presented does not include the damage taking place at the interfaces between plies (i.e., delamination). Delamination is considered to be one of the most feared damage modes in laminated composites under fatigue loads. The reader is referred to following references [26,76,77] for further details on this subject.

1.4 Fatigue damage mechanisms in composite laminates

This section presents a review on the different damage mechanisms that may occur in composite laminates subjected to fatigue loads. This section distinguishes between the damage occurrence in unidirectional laminates [66, 69–71, 78, 79], plain or unnotched multi-directional laminates [55] and finally notched laminates [80,81].

1.4.1 Damage occurrence in unidirectional laminates

The different failure mechanisms that take place in unidirectional laminates strongly depend on the type of cyclic stress (tensile or compressive) and on whether or not the load is applied parallel or at some angle to the fibre direction. Less information is available regarding the fatigue behaviour under compression-compression or tension-compression loads, but this is mainly attributed to the susceptibility of composite laminates, being thin, to buckling.

The damage mechanisms that occurs under on-axis tension-tension fatigue loads are divided into three basic mechanisms. Under high cyclic strains, fibre breakage is likely to occur at the weaker fibres (see Figure 1.6a). These isolated fibre breaks may cause a shear stress concentration at the interfaces leading to cracking of the surrounding matrix, matrix plasticity, or debonding between the fibre and matrix material. Talreja [69,71,82] has also suggested that the matrix undergoes a fatigue process of crack initiation and propagation similarly to metallic materials. These cracks are oriented normal to the applied load. If the cyclic strain remains small enough, the cracks are arrested by the presence of fibres as it is shown in Figure 1.6b. However, if

the strains are larger than a threshold value, the resin cracks can turn into fibre breaks and propagate towards the next interface. When the crack reaches an interface it can also develop high shear stresses that can make the crack grow in mode II through the interface as shown in Figure 1.6c. Final failure occurs when a large enough cluster of broken fibres cause an instability, where failure of one additional fibre adjacent to the cluster leads immediately to subsequent failure of another, and so on until the laminate collapses. A experimental study on the degradation of unidirectional plies under tension-tension on-axis cyclic loads has been addressed in paper A.

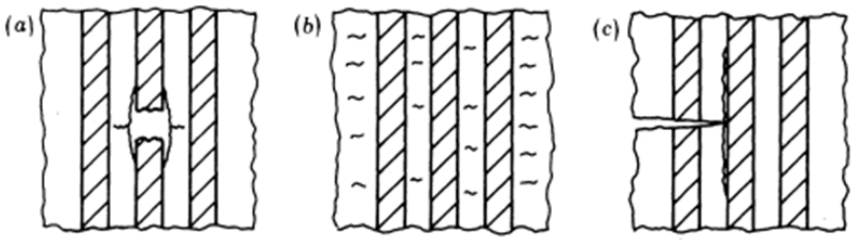

Fig. 1.6: Fatigue damage mechanisms in unidirectional laminates under loads parallel to the fibres: a. fibre fracture and fibre/matrix debonding; b. matrix cracks; c. interfacial shear failure. Figure taken from Talreja [69].

Each of these mechanisms may occur simultaneously, however Talreja has suggested that different mechanisms may dominate for different cyclic strain ranges. Under this assumption, it would be expected that the fatigue life curve would consist of different regions, each corresponding to the underlying damage mechanism. To illustrate these regions of dominance, Talreja proposed a strain-life diagram as shown in Figure 1.7. The applicability of these fatigue life diagrams has been discussed extensively in the literature and it has been concluded that they constitute a conceptual framework for interpretation of fatigue test results and damage development. According to Talreja, three main regimes can be clearly differentiated. Region I, which is the scatter-band of the composite failure strain in tension, represents the non-progressive (catastrophic) fibre breakage regime in which random fibre failure mechanism governs. Region II is the regime of progressive fibre-bridged matrix cracking in which interface debonding plays a major role. Finally, in Region III no damage initiates below this strain level, or minor micro-cracks grow but they will remain arrested by the fibres.

Gamstedt and Talreja [66] investigated the fatigue behaviour of unidirectional plies made of carbon fibre and different resin systems, one epoxy thermoset resin and one peek thermoplastic resin. They mainly concluded that the thermoset based composite has a higher fatigue resistance with few

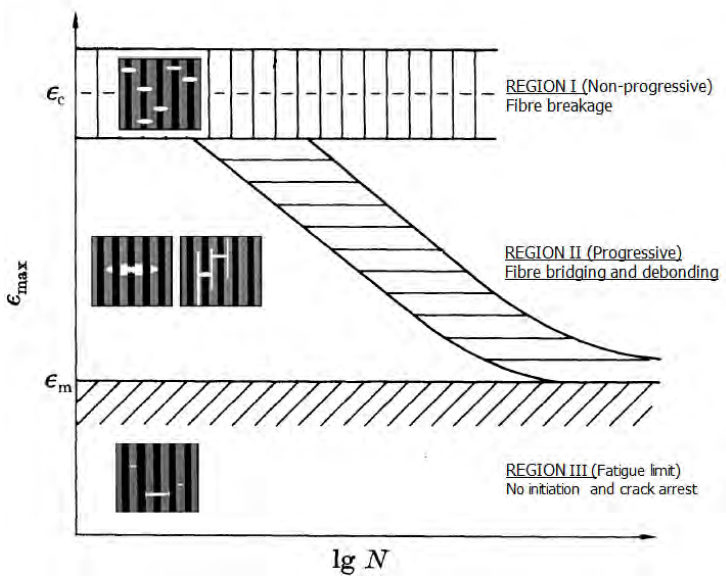

Fig. 1.7: Fatigue-life diagram for UD composites under parallel loading [71].

microcracks initiated at distributed fibre breakage growing at a decelerating rate. On the contrary, the thermoplastic composite has a more pronounced fatigue degradation with a steeper fatigue life curve (see Figure 1.8), which is caused by widespread propagating debonds and matrix cracks. The use of a tougher and more ductile matrix results in an inferior fatigue life performance, due to a more widely distributed accumulation of damage that propagates at higher rate. The carbon/epoxy shows a more brittle behaviour with small localized cracks originating from fibre breaks. These cracks propagate perpendicularly to the fibre direction, and become bridged by the adjacent fibres. Conversely, the carbon/peek has a tougher behaviour since it provides higher resistance to matrix crack growth. The damage accumulates as multiple longitudinal cracks with considerably more fibre breaks. The carbon/peek also shows a propensity to shear-induced matrix cracking or debonding in the fibre direction. This is due to a weaker interface compared to the carbon/epoxy.

The damage under off-axis loads results in a transverse crack oriented by the fibres but without breaking them. Under pure transverse stress states, the onset of these cracks usually appears at the fibre-matrix interface [67], where the hydrostatic stress in the matrix is predominant and interface debonding occurs until the complete formation of a through-the-thickness matrix crack. For off-axis loads between 0° and 90°, the tip of the crack initiated in the matrix is subjected to a mixed-mode crack growth parallel to the fibres. Un-

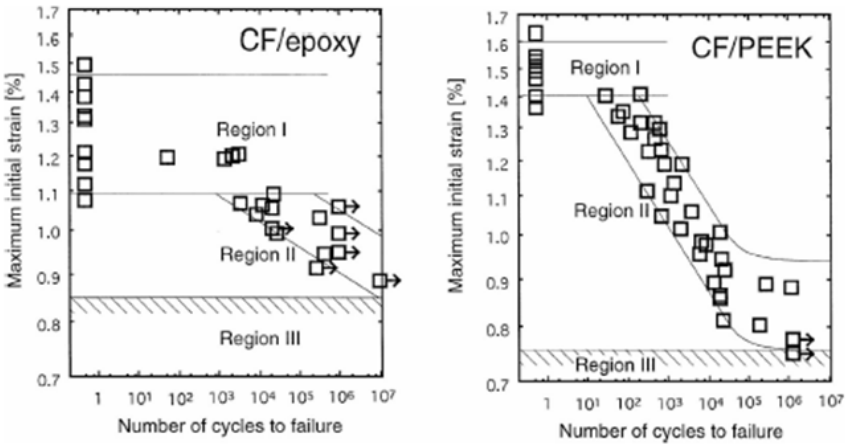

Fig. 1.8: Fatigue life diagrams of carbon/epoxy and carbon/peek (source taken from Gamstedt and Talreja [66]).

der stress states that combine transverse tension and in-plane shear, the local maximum principal stress in the matrix controls the onset and orientation of these matrix cracks. It was possible to observe in [72, 83] that the fracture surfaces are rather smooth when the shear stress component is low, whereas in the case of higher shear stress contributions the presence of shear cusps in the matrix is very significant.

Talreja's fatigue strain-life diagram for off-axis loading is shown in Figure 1.9. The fatigue life diagram for on-axis loads is also sketched with dotted lines. Note that for off-axis angles more than a few degrees, the fibre breakage scatter band is lost, as the matrix and interfacial cracking becomes the predominant damage mode. For the limiting case of $\theta = 90^\circ$, the minimum strain required for transverse fibre debonding is denoted by ε_{db}.

1.4.2 Damage occurrence in multidirectional laminates

Fatigue damage in a conventional quasi-isotropic laminate occurs as a combination of different ply failure mechanisms and delamination at the interfaces. The sequence of damage reported for unnotched specimens is usually divided in three stages of fatigue life [6, 55, 84]:

Stage I - The first mechanisms to appear is matrix cracks at the off-axis plies (first at the 90°, and later on, at the $\pm 45^\circ$). This transverse ply cracks appear spatially distributed along the specimen length, they initiate at the edges and they propagate towards the through-the-width direction. Matrix cracking induces a small reduction of the overall stiffness of CFRP laminates, and it is not considered to be a catastrophic failure mechanism as the lam-

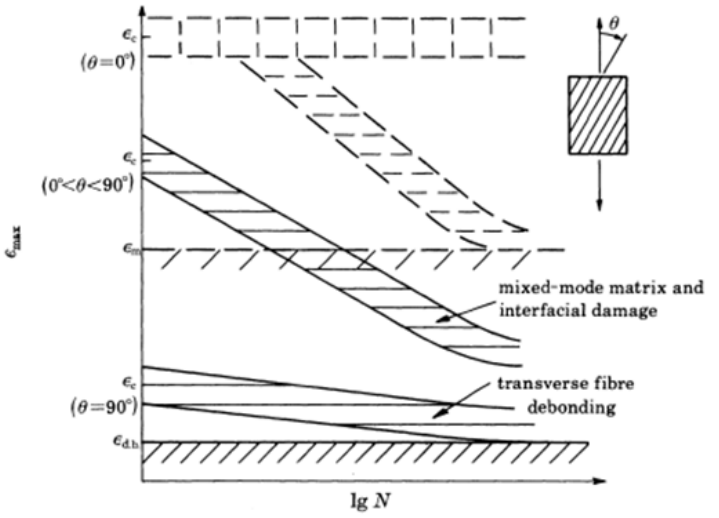

Fig. 1.9: Fatigue life diagrams for off-axis fatigue of UD composites. Dotted lines correspond to the fatigue-life for on-axis loads (source from Talreja [69]).

inate is capable of redistributing the stresses to the adjacent on-axis plies. However, it is a precursor of other sources of damage like fibre fracture and delamination. This stage of fatigue life is addressed in Paper B.

Stage II - Damage progresses with a linear decrease in stiffness with respect to the loading cycles. This is caused by the multiplication of matrix cracks at all off-axis plies along with some local delaminations that start from the free-edge or from the tip of the intralaminar cracks. Fatigue-driven delaminations have also been the subject of extensive research as delamination is one of the most dangerous and common failure modes in composite laminates subjected cyclic loads [26,77].

Stage III - The final stage corresponds to a sudden drop of stiffness triggered by an unstable delamination growth or by fibre fracture.

1.4.3 Damage occurrence in notched laminates

The study of notched specimens has received a lot of attention in open literature [80, 85–89] since it provides additional information of the fatigue behaviour of the laminate with a non-uniform stress field (i.e., stress riser). In general, notched laminates show the same mechanisms than the unnotched laminates, but it is worth noting some differences. Figure 1.10 shows the evolution of fatigue damage in a carbon/epoxy open-hole specimen under tension-tension fatigue loads. The first mechanism to appear is also trans-

verse matrix cracking at 90° plies, but now these cracks initiate at the root of the notch, and they increase in number with the increase in the number of cycles. As in the unnotched laminates, additional off-axis matrix cracks at ±45° plies grow along with matrix cracks at 0° plies, the longitudinal cracks usually referred to as splits. However, it is specially relevant in fatigue of notched laminates the initiation and propagation of the 0° splits. These longitudinal matrix cracks, that grow parallel to the fibre direction, redistribute the fibre stresses and thus reduce the stress concentration caused by the notch. In some materials, this mechanism is so effective that completely suppress fibre fracture at the 0° plies. Subsequent loading cycles induce delaminations, some of them initiate from the edge of the splits and some others from the specimen free-edge.

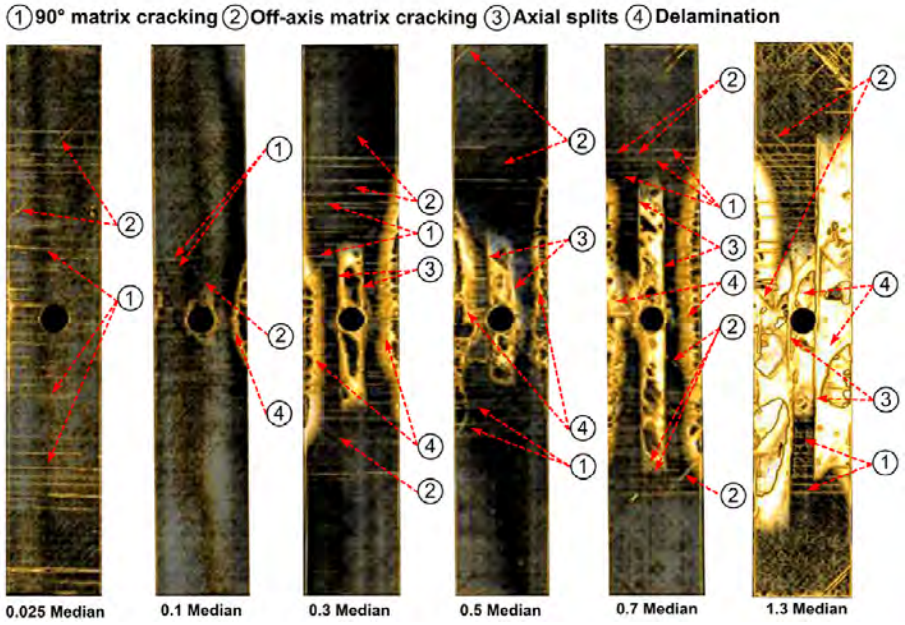

Fig. 1.10: Fatigue Damage evolution in a open-hole specimen at different fatigue life ratios. Source taken from Aidi et al. [80].

One complication is that the fatigue damage evolution in composites depends on a large number of material parameters that induces different damage mechanisms from one composite to the other. For instance, Ambu et al. [81] reported the presence of fibre fracture in a open-hole specimen at a load level of the 85% of the ultimate static, mainly due to the absence of 0° splitting in carbon/peek laminate (see Figure 1.11).

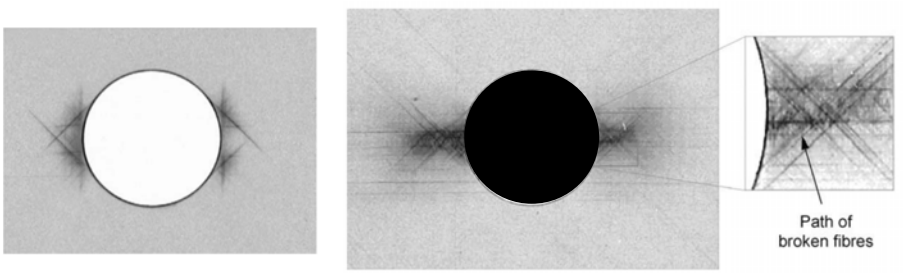

Fig. 1.11: Fatigue Damage in a $[0/\pm 45/90]_{2s}$ graphite/peek open-hole specimen at a 75% (left) and 85% (right) of the ultimate static load and 162000 cycles. Source taken from Ambu et al. [81].

1.5 Objectives

The main objective of the present thesis is to develop a computational tool capable of predicting fatigue damage and residual strength of composite structures. The point of departure is the former continuum damage mechanics (CDM) model developed during the past 10 years in AMADE research group [49,50]. Several partial objectives are identified as to pursue the main goal of this thesis:

1. To extent the framework of the CDM model presented in references [49,50] for fatigue damage and residual strength predictions.
2. To develop and implement a computational strategy into a commercial finite element code to perform fatigue simulations.
3. To investigate experimentally fatigue damage on aerospace-grade unidirectional, cross-ply and quasi-isotropic CFRP laminates under fatigue loads.
4. To validate the computational model by simulating the progressive damage and residual strength of notched laminates under fatigue loads.

The experimental works performed within this Ph.D. thesis are supported by the experimental characterization provided by Carreras in her Ph.D. thesis [26]. Carreras performed a full experimental fatigue characterization campaign on fatigue-driven delamination with the same material system.

1.6 Thesis layout

The present thesis is written as a compendium of articles, with a reproduction of the generated manuscripts that are included as appendices at the end

of the document. Although the reader is referred to the appendices, Chapter 2 provides an overview of the articles in order to expose its coherence in the context of the thesis. Each sub-objective defined above is addressed through a different paper. The first two sub-objectives are accomplished by paper C and D, where a new constitutive model for fatigue is presented and implemented into a commercial finite element code. Paper A fulfils the third sub-objective by studying the fatigue behaviour of unidirectional laminates. Analogously, Paper B addresses the third sub-objective by studying matrix cracking in cross-ply laminates under fatigue loads. The final sub-objective is fulfilled by paper D where the numerical model is validated by simulating fatigue damage and residual strength of notched laminates. The experimental works performed in this paper also cover part of the third sub-objective. Following that, in Chapters 3 and 4 a general discussion of the results and the conclusions are given as a whole.

Chapter 2

Scope of the publications

2.1 Paper A

Paper A entitled *A fatigue damage and residual strength model for unidirectional carbon/epoxy composites under on-axis tension-tension loadings* [90] investigates the reduction in the stiffness and the strength of aerospace grade unidirectional laminates subjected to tension-tension fatigue loads.

A short review of the experimental challenges found when testing high-performance unidirectional laminates under tension-tension fatigue loads is given. The review does not pretend to be exhaustive but to discuss the relevant testing parameters to ensure reasonable estimation of fatigue lives. A summary of the different fatigue tests performed is given in Table 2.1, where $\Sigma_{\max} = \frac{\sigma_{\max}}{X_T}$ is the normalized maximum cyclic stress, $R = \frac{\sigma_{\min}}{\sigma_{\min}}$ and $K = \frac{1+R}{1-R}$ are the stress ratios, $m = 1 - d$ is the complementary damage variable as defined in continuum damage mechanics, X_T and X_T^r are the static and residual strength, respectively. The tests were performed under load control and the cyclic load was defined a sinusoidal waveform of 5 Hz.

The main objective of the fatigue tests is to determine the loss of stiffness and strength with respect to the number of cycles, and to determine the cycles-to-failure for the different stress levels and stress ratios. The collected experimental data allows to determine a fatigue damage function that, in this study, depends only on the maximum cyclic stress and on the K-ratio. Only the range of tension-tension cyclic stresses is covered ($K > 1$). Since the experimental cost of residual strength testing is substantial, it is proposed to assume the common hypothesis of a constant ultimate strain for unidirectional plies. This hypothesis suggests that fatigue damage does not reduce the ultimate strain, that is, the residual stiffness and strength evolve in the same manner. Experimental evidence is provided in this respect by testing

different fatigue-damaged specimens up to final failure. Finally, a S-N curve can be derived and the life predictions are verified by comparing to the experimental fatigue life data.

$\Sigma_{max}/R(K)$	0.1 (1.22)	0.2 (1.50)	0.3 (1.86)	0.5 (3.00)
0.875	m/N_F	m/N_F	-	m/N_F
0.750	m/N_F	m/N_F	m/N_F	m/X_T^r
0.625	m/X_T^r	m/X_T^r	-	-
0.500	m/X_T^r	-	-	-

Table 2.1: Summary of fatigue tests and measurements, where m, N_F and X_T^r indicate stiffness loss, cycles-to-failure and residual strength, respectively.

2.2 Paper B

Paper B entitled *Progressive matrix cracking in carbon/epoxy cross-ply laminates under static and fatigue loading* [91] presents an experimental investigation into the growth of transverse matrix cracks in cross-ply laminates under static and fatigue loads.

Matrix cracking is usually the first mechanism to occur during the service life of multidirectional laminates. This damage mechanism is not generally considered to be as critical as delamination or fibre fracture from a structural point of view. This is mainly because matrix cracking does not cause an unacceptable loss of the laminate stiffness and strength (at least in carbon/epoxy laminates). However, this damage mechanism is considered to be the precursor of the other damage mechanisms. Matrix cracking in multi-directional laminates does not occur as a single isolated crack, rather it appears as multiple distributed cracks which in some cases can be described by one single variable, the crack density (ρ_N). The crack density is defined as the inverse distance of two consecutive cracks.

The principal objective of the experimental tests is to obtain the evolution of transverse cracks under static and fatigue loads. Two optical means are used to detect the formation of cracks, the first is a reflex camera that takes picture from the edge of the specimen, and the second is by X-ray radiography. Figure 2.1 shows the two cross-ply laminate configurations analysed in this experimental campaign. Note that four different clusters of 90° plies are considered, one outer ply with thickness t_{ply} and three embedded plies with

thickness t_{ply}, $2t_{ply}$ and $4t_{ply}$, respectively. The *in-situ* effect of thin plies is analysed.

From a fracture mechanics point of view, transverse cracks grow in mode I once the available energy release rate equals the fracture toughness of the matrix. An equation to calculate the available energy release rate for tunnelling cracks with only one material fitting parameter is proposed. This expression can be fitted experimentally thereby obtaining the crack density curves under static loading. In fatigue, two different approaches presented in literature are contemplated to describe the growth of fatigue cracks. The first is based on the concept of diffuse damage or microcracking [30], and the second is based on a modified Paris-based expression [29]. The two approaches are analysed in detail and compared with the obtained experimental data.

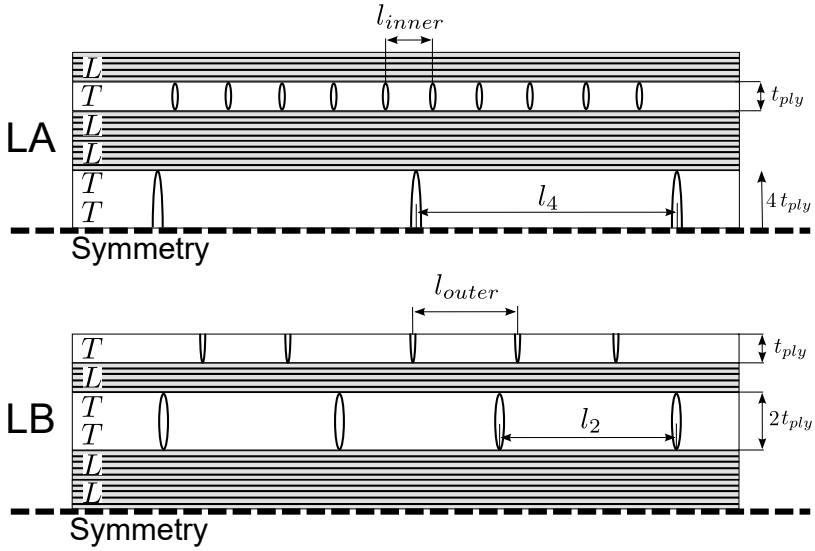

Fig. 2.1: Crack density functions for laminate A $[0/90/0_2/90_2]_S]$ termed as ρ_4 and ρ_{inner}, and for laminate B $[90/0/90_2/0_2]_S]$ termed as ρ_2 and ρ_{outer}.

2.3 Paper C

Paper C entitled *A continuum damage model for composite laminates: Part III - Fatigue* presents the extension of the previous continuum damage mechanics model published in [49, 50] for fatigue damage and residual strength predictions.

The constitutive model accounts for four intralaminar failure mechanisms that occur at ply level: fibre fracture in longitudinal tension, kink band for-

mation in longitudinal compression, and then matrix cracking under combinations of transverse tension/compression and in-plane shear loads. The LaRC loading functions [92] are used to predict the onset of damage. The softening response after damage initiation is defined according to five cohesive laws one for each loading mode. The crack-band model [63] is used to smear the cohesive law inside the continuum element. This approach ensures an objective response of the model regardless of the mesh size.

Under fatigue loads, the same damage mechanisms are considered and the same LaRC loading functions can be used to describe the onset of damage. However, fatigue damage mechanisms initiate at lower loading levels and evolve in a different manner. The original formulation is extended to account for this and all the details are explained throughout the paper. Following that, the computational strategy to implement the constitutive model in a explicit finite element code as Abaqus/Explicit [93] is given. Figure 2.2 illustrates a sequence of load steps that can be simulated within this computational framework. The numerical model allows to simulate the mechanical behaviour of composite structures subject to static, impact and fatigue loads. Note that the cycle jump approach is used in the fatigue step, and thus the fatigue simulation is performed by small cycle jumps and not cycle-by-cycle.

Two different simulation options can be set inside the cycle jump algorithm. In the first option, the maximum cyclic load is kept constant throughout the fatigue analysis and the R-ratio is thus fixed for all the integration points (i.e., usually referred to as the envelope approach). Assuming a constant R-ratio at the integration points is not necessarily true at local level and it can lead to incorrect fatigue damage predictions. The second option considers that the R-ratio at local level may change, and then, a full cycle is simulated before every cycle jump to update and evaluate the local maximum and minimum strain levels in the elements. Obviously the computational time increases significantly even though the model is able to reach more accurate predictions.

The experimental validation tests carried out and the numerical simulations to study the model performance are reported in the follow-up paper D.

2.4 Paper D

Paper D entitled *A continuum damage model for composite laminates: Part IV - Experimental and numerical tests* is the continuation of paper C, in which an experimental investigation on the damage occurrence of notched laminates in static, fatigue and residual strength tests is presented. Two notched specimens were tested, the open-hole and the double-edge notched specimens.

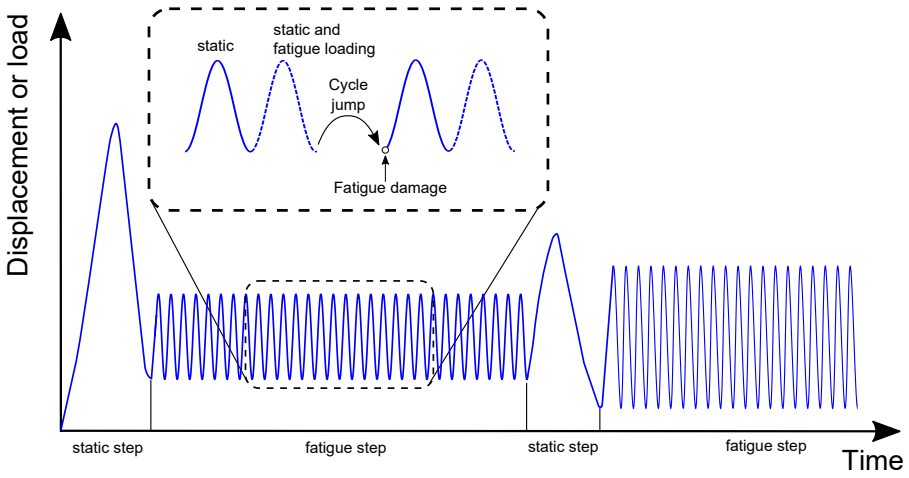

Fig. 2.2: The cycle jump approach proposed within an explicit finite element code.

The damage mechanisms are investigated by means of X-ray radiography.

The presence of extensive fatigue-driven delaminations found in the experiments forced the need to account for interlaminar fatigue damage. Thus, the fatigue cohesive zone model (CZM) developed by Turon et al. [76, 94] is implemented as a VUMAT subroutine in Abaqus/Explcit to reproduce the growth of delamination cracks under fatigue. An appropriate modelling strategy to allow the interaction between both the intra- and inter-laminar damage mechanisms is proposed, which is in line with the previous numerical studies performed at AMADE research group with impact loading cases [95–97]. Figure 2.3 exemplifies this modelling strategy.

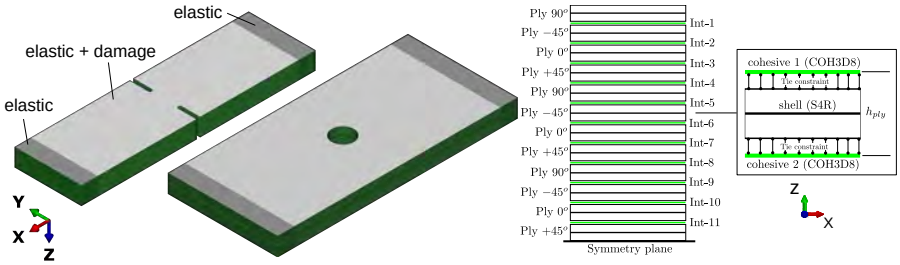

Fig. 2.3: Finite element modelling strategy and element technology.

Both intra- and inter-laminar constitutive models require extensive material characterization for static and fatigue material properties. Based on the experimental findings on notched specimens, an entire section is devoted to discuss the required material properties to feed the constitutive model. However, at this stage some of the fatigue experimental properties were not avail-

able and no experimental data could be found in open literature with the current material system. Unfortunately, the experimental campaign performed in this Ph.D thesis could not cover the characterization of all the necessary material properties. A summary of the tests and simulations performed in this paper is given in Table 2.2. The capability of the computational model to capture the main fatigue degradation mechanisms as well as the post-fatigue residual strength is examined.

	load	cycles	dent	openhole
STATIC	-	-	Exp./ FEM	Exp./ FEM
FATIGUE	$60\%\sigma_U$	$1M$	-	Exp.
	$75\%\sigma_U$	$100k$	Exp./ FEM	FEM
		$200k$	FEM	FEM
		$250k$	Exp.	-
		$300k$	FEM	FEM
		$400k$	FEM	FEM
		$500k$	FEM	FEM
		$600k$	Exp./FEM	FEM
		$700k$	FEM	FEM
		$800k$	FEM	FEM
		$900k$	FEM	FEM
		$1M$	Exp./FEM	FEM
		$2M$	-	Exp.
	$90\%\sigma_U$	$150k$	-	Exp.
		$400k$	Exp.	-

Table 2.2: Summary of experimental tests and FEM simulations performed for both geometries in static, fatigue and residual strength. The fatigue load is defined by the maximum load applied with respect to the ultimate static strength (σ_U) and the R-ratio equal to 0.1.

Chapter 3

Results and discussion

This chapter summarizes the results of the papers as a whole and discuss them in accordance with the main objectives of this thesis: fatigue damage modelling of unidirectional, cross-ply and quasi-isotropic laminates, and following that, the numerical results obtained with the novel constitutive model for fatigue implemented into a finite element code are analysed and discusses in-detail.

3.1 Fatigue damage modelling of unidirectional laminates

An extensive fatigue experimental campaign was conducted on aerospace grade unidirectional laminates under on-axis tension-tension fatigue loads parallel to the fibre direction. This type of fatigue test on high-performance unidirectional carbon/epoxy laminates made of rectangular specimens showed severe surface damage (i.e., fibre splitting), which started underneath the end tabs and extended all along the length of the specimen. This undesired mechanism is mainly caused by the shear stress concentration at the tabbed section. As a consequence, the strains at the gauge section cannot be measured accurately using the standard local sensors such as mechanical clip-on extensometers or strain gauges. The digital image correlation (DIC) technique was found to be more useful to overcome all the difficulties with the mechanical strain sensors. The DIC measurements were taken at the lateral surface of the specimens where less surface damage was observed.

The loss of stiffness was recorded at selected cycle intervals for different stress levels and K-ratios. The K-ratio is another measure to describe a cyclic load equivalent to the well-known R-ratio ($K = \frac{1+R}{1-R}$). A fatigue damage function was fitted to the experimental data with five material constants.

Figure 3.1 shows the loss of stiffness, m, with respect to the number of cycles under a constant load ratio of $R = 0.1$, but for different normalized stress levels that range from $\Sigma_{max} = 0.5$ to $\Sigma_{max} = 0.875$. m is computed as the complementary damage variable: $m = E/E_0 = 1 - d$, where E_0 and E are the pristine and fatigue-damaged Young's modulus, and d is the damage variable. Note that for stress levels below 50% of the ultimate static strength (i.e., $\Sigma_{max} = 0.5$) and R-ratio = 0.1, the measured loss of stiffness is negligible up to 2 million cycles. For stress levels higher than 75% of the ultimate strength, a large number of specimens failed at the tabbed section, which can be interpreted as an underestimation of fatigue life. The normalized stress level of $\Sigma_{max} = 0.875$ is an example of this as the fitting overestimates the fatigue life.

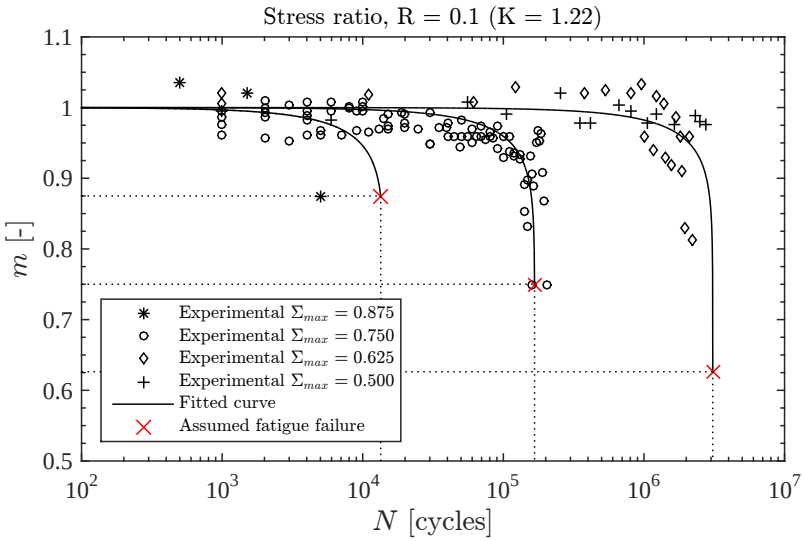

Fig. 3.1: Integrity function for different stress levels and constant R-ratio = 0.1.

In Figure 3.2, the same experimental data can be represented but keeping fixed the stress level to $\Sigma_{max} = 0.75$ and varying the R-ratio from 0.1 to 0.5 (or the K-ratio from 1.22 to 3.0). The effect of the R-ratio on the fatigue life is clearly illustrated in Figure 3.2, where the lower the R-ratio the higher the damage that takes place for a lower number of cycles. The fitting of the integrity or damage function shows reasonable correlation with the experimental data though the usual presence of scatter in fatigue data of composites.

The fatigue damage function describes the material degradation by the measured loss of stiffness but it does not provide a clear definition for failure as it does the residual strength function. A common hypothesis widely used

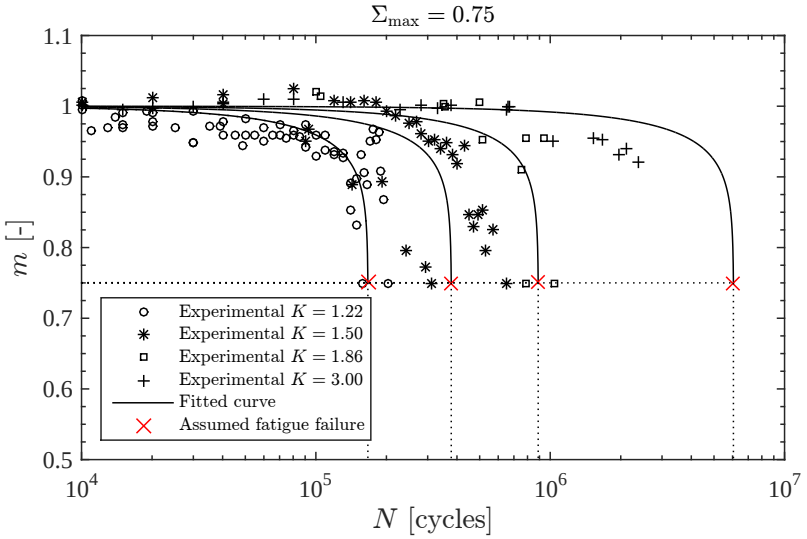

Fig. 3.2: Integrity function for different K-ratios and a constant stress level $\Sigma_{max} = 0.75$.

in open literature is to assume that the ultimate static strain remains constant after fatigue damage. This hypothesis entails many consequences, e.g., failure occurs when $\Phi_{max} = 1$ or analogously when $\Sigma_{max} = m$ which is represented by the red crosses in Figures 3.1 and 3.2, being Φ_{max} and Σ_{max} the normalized strain and stress, respectively. From a continuum damage mechanics point of view, this hypothesis suggests that a fatigue-damaged material point subjected to a mean strain and a nominal stress behaves exactly as a pristine material subjected to the same strain but under an effective stress, $\tilde{\sigma}_R$ (see Figure 3.3). This concept is well-known as the "strain equivalence principle" originally proposed by Lemaitre [98]. Fatigue-damaged specimens under different levels of damage were loaded up to final failure for residual strength measurement and plotted in Figure 3.4 for direct comparison. The obtained experimental results indicate that this hypothesis is fairly reasonable, as for increasing levels of damage, $1 - m$, the ultimate strain Φ_{max} remains within the static scatter band. Under these circumstances, it is also reasonable to assume that the residual strength evolves according to the same function as the stiffness.

Accordingly, an analytical expression for the S-N curve can be derived that allows to predict the fatigue life of unidirectional laminates subjected to tension-tension fatigue loads. The experimental fatigue lives and predictions are compared in Figure 3.5. The model predictions are consistent except for stress levels higher than 75% of the ultimate static where failure underneath the tabbed section was frequent.

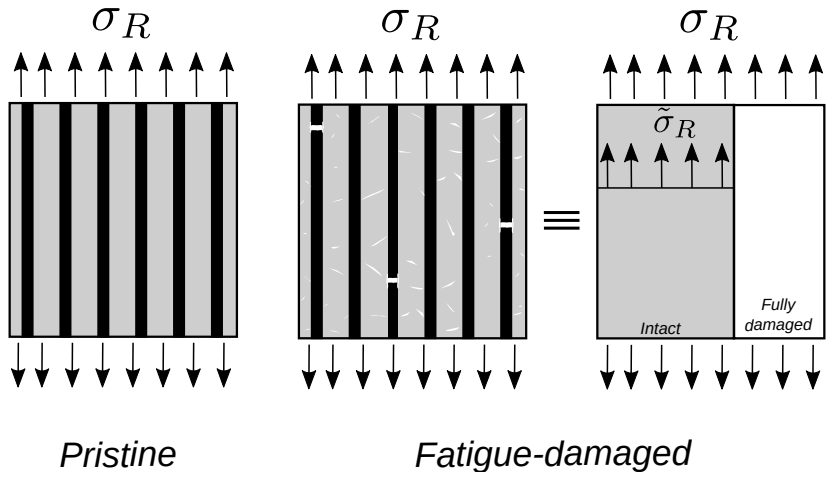

Fig. 3.3: Geometrical interpretation of the strain equivalence principle introduced by Lemaitre [98].

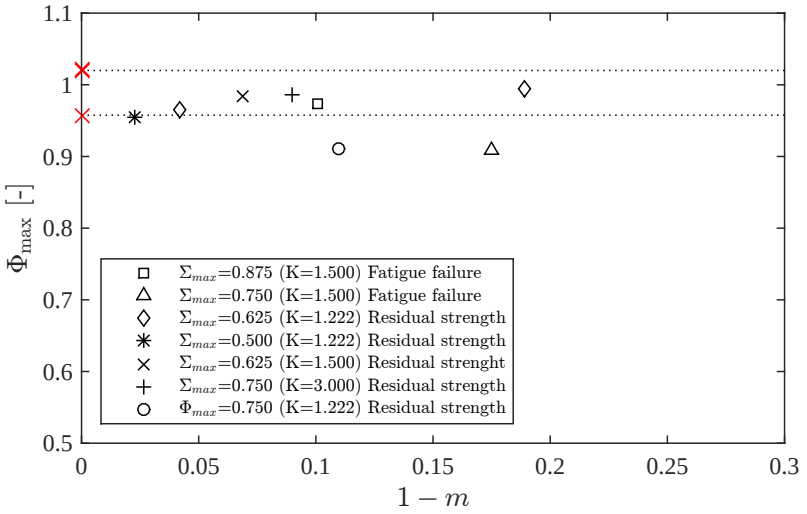

Fig. 3.4: Normalized ultimate strain, $\Phi_{\max}$, against fatigue damage, $d = 1 - m$.

It is worth mentioning that it is particularly difficult to obtain the complete path of damage states in a load-controlled fatigue test, as the stiffness drops abruptly at the very last number of cycles. Many authors claimed that controlling the strain instead of the load is by far more effective in fatigue testing of composites. Ideally, if the fatigue test is performed under strain control the laminate is not likely to fail since the lower the stiffness the lower the

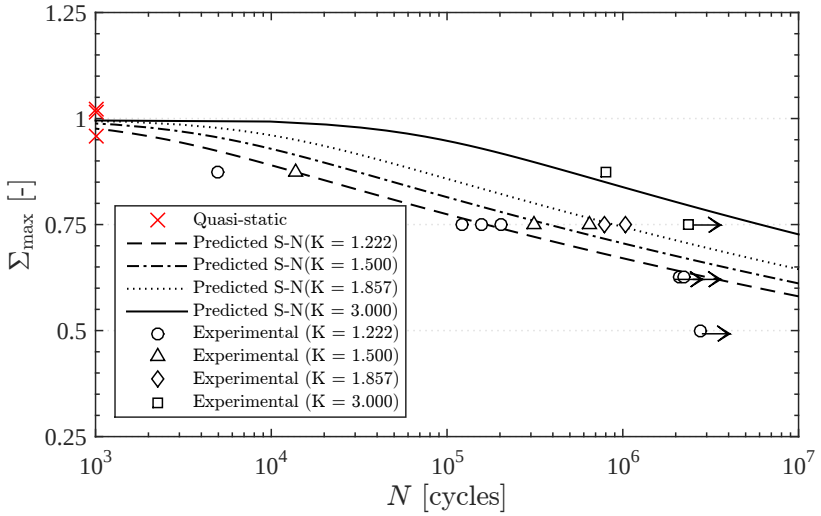

Fig. 3.5: Experimental S-N curve vs. analytical predictions

load level, and thus the path of damage states during the fatigue test can be tracked (see Figure 3.6). Nevertheless, the strain control mode in this specific fatigue test is somewhat difficult to perform. Recall that the piston displacement is not an appropriate measure due to the specimen slippage within the grips and tabs, the use of strain gauges or mechanical clip-on extensometers in the gauge is not either a good choice due to the surface damage, and the optical DIC system with a such a relatively high frequency is not so straightforward. As an alternative, a variable amplitude load-controlled fatigue test was performed as to approximate the constant strain conditions.

Figure 3.7 shows the experimental loss of stiffness and the predicted curve under a load-controlled and strain-controlled fatigue test. In the strain-controlled fatigue test, the load is reduced proportionally to the stiffness as to keep a constant cyclic strain (i.e., $\Phi = \Sigma/m = const.$), but the strains are measured quasi-statically by interrupting the fatigue test as to avoid all the above-mentioned issues when measuring the strain in real-time during fatigue testing. In any case, the strain-controlled test was stopped forcibly at 300k cycles due to the impossibility of measuring the strain even quasi-statically with such an extension of damage of specimen that occurred.

Finally, the fatigue damage function can be interpreted in the form of a master curve providing the damage growth rate per cycle in terms of the maximum cyclic strain (Φ_{max}), stress ratio (K) and current state of degradation (m), as shown in Figure 3.8. Below a certain strain threshold (assumed to be close to $\Phi_{max} = 0.5$ for this material system), the fatigue damage rate

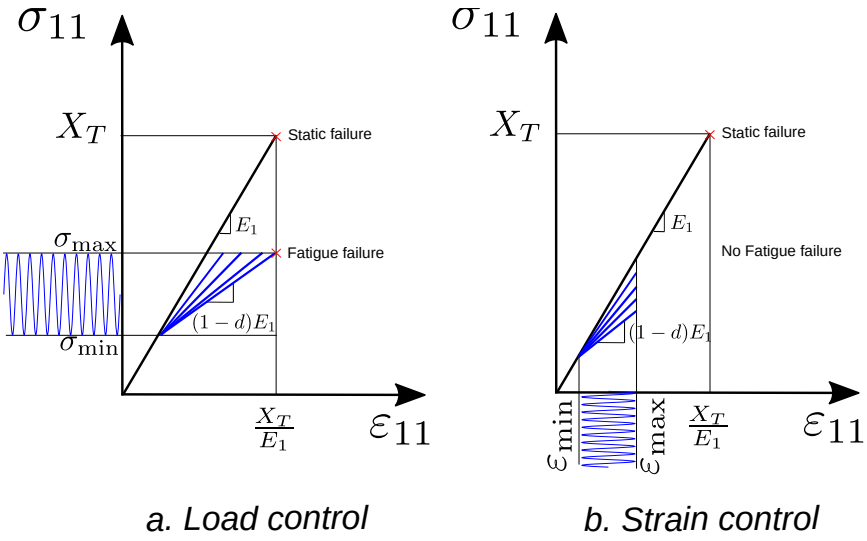

Fig. 3.6: Definition of fatigue failure by assuming a constant ultimate strain under stress and strain control.

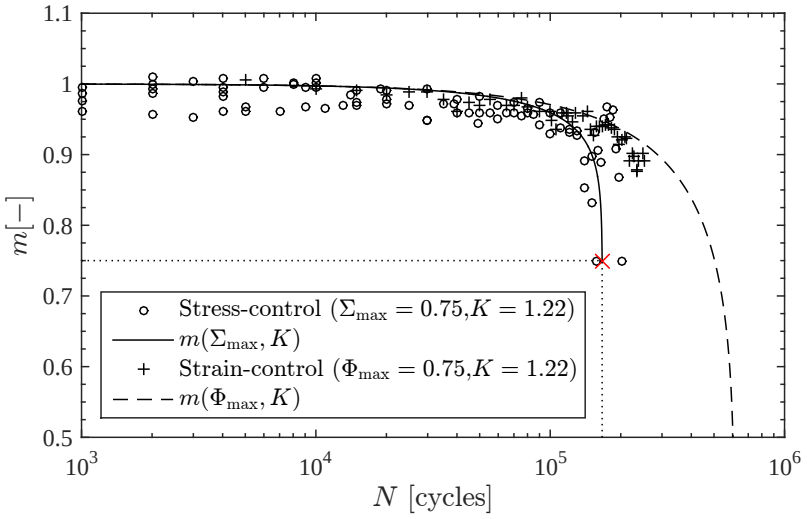

Fig. 3.7: Loss of stiffness of unidirectional laminates under constant-stress and constant-strain fatigue tests.

can be considered as negligible within a range of 2 millions cycles. This strain threshold is based on the experimental test at $\Sigma_{\max} = 0.5$ and $R = 0.1$, which it reached 2 million cycles with no apparent loss of stiffness. Above

this threshold, the rate of fatigue damage increases according to a power law function. For large enough strain levels, the material fails quasi-statically.

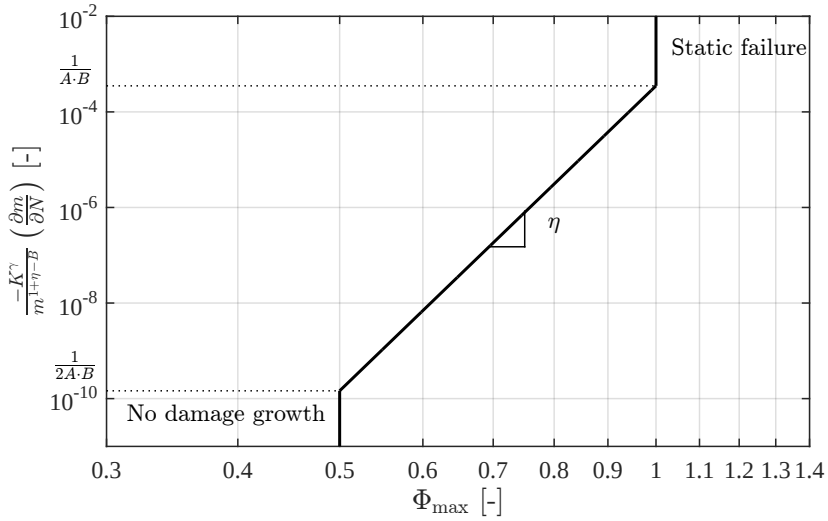

Fig. 3.8: Damage growth rate per cycle $\left(\frac{\partial m}{\partial N}\right)$ vs. normalized strain ($\Phi_{\max}$)

3.2 Fatigue damage modelling of cross-ply laminates

Matrix cracking is usually the first damage mechanisms to occur in multi-directional laminates subjected to fatigue loads. An extensive material characterization campaign was performed on two different cross-ply laminates to investigate the static and fatigue growth of transverse cracks at 90° plies. Figure 3.9 shows a camera picture with the distribution of edge cracks just an instant before static failure occurred for the two cross-ply laminate configurations investigated. The laminate configurations are identified as laminate A (LA) and laminate B (LB). Different transverse plies with different thickness and location were analysed, referred to as ρ_{inner}, ρ_{outer}, ρ_2 and ρ_4.

Linear Elastic Fracture Mechanics (LEFM) can be used to calculate the required energy release rate to propagate a mode I crack longitudinally (i.e., crack tunnelling growth). This expression is mainly valid for thin plies where cracks usually initiate at the free-edge and propagate longitudinally to the laminate centre line. However, in thick plies the crack grows first in the transverse direction and when it spans all the ply thickness, it grows in the longitudinal direction. Since the stress required for transverse crack growth is

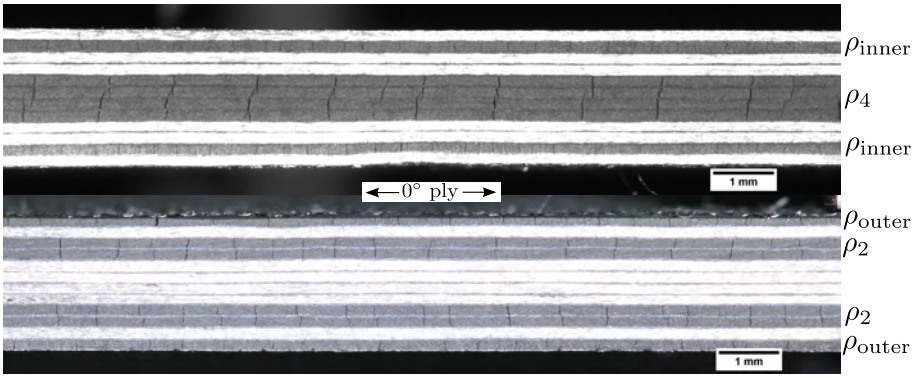

Fig. 3.9: Matrix cracks observed in laminate LA (top image) and laminate LB (bottom image) prior to static failure ($\varepsilon = 2\%$).

larger than the one for longitudinal crack growth, the propagation of transverse cracks in thick plies is considered to be unstable. It is important to note that the camera and X-ray images obtained during the static tests were enough to confirm that all transverse cracks span the entire width of the specimen and that no delamination occurs until final failure.

The expression of the energy release rate to propagate mode I transverse cracks depends on a function of the crack density $f(\bar{\rho})$, which is usually determined by solving the stress field of the laminate for different crack densities and by assuming a cracking pattern distribution. Note that, $f(\bar{\rho})$, is expressed by the normalized crack density $\bar{\rho} = t_N\rho$. In this work, $f(\bar{\rho})$ is determined by fitting the experimental data. Fortunately, experimental and numerical results found in open literature suggest that $f(\bar{\rho})$ can be assumed intrinsic and independent of the stacking sequence for most industrial laminates [31]. Hence, the experimental data can be represented as a master curve in the space $\bar{\rho}_N - \varepsilon\sqrt{t_N}$, where ε and t_N are the applied strain and the corresponding ply thickness (see Figure 3.10). The fracture mechanics based expression is plotted as a solid line. It is important to note that since $f(\bar{\rho})$ is found to be almost a constant value for low crack densities [29], the expression appears as a vertical line until a certain crack density level is reached. After this level, $f(\bar{\rho})$ decreases following an exponential function of the number of cracks leading to an excellent correlation for all the ply thicknesses. The cracking process of the thicker clusters with two and four plies, $\bar{\rho}_4$ and $\bar{\rho}_2$, is not controlled by the crack tunnelling growth assumed in the fracture mechanics based expression, instead it is controlled by the thick-ply criterion. But, once a certain crack density level is reached, the thin-ply criterion becomes higher than the thick-ply and thus the master curve follows the experimental data.

In fatigue, two different concepts to predict the growth of fatigue cracks

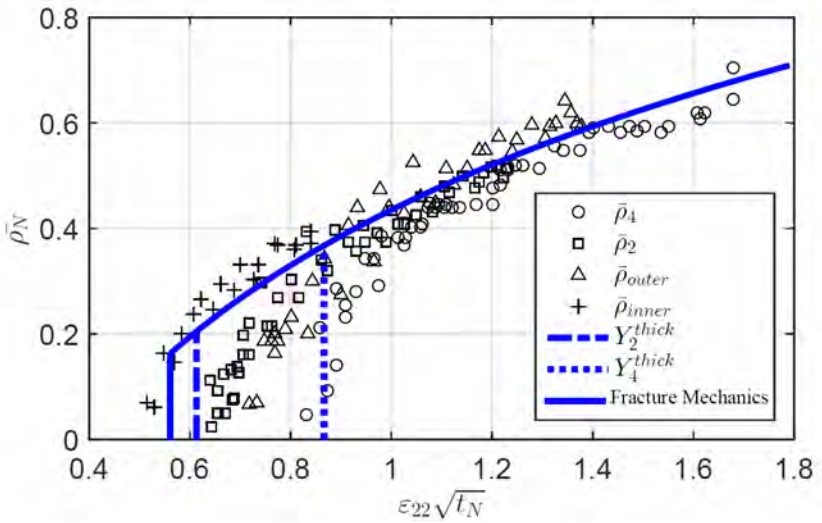

Fig. 3.10: Crack density master curve for static loads.

are analysed. The first concept, that was originally suggested by Ladèveze and co-authors [99–101], states that the growth of fatigue cracks is mainly driven by diffuse damage or micro-cracking. This mechanism is associated with fibre/matrix debonding and it occurs prior to the formation of through-the-thickness cracks. The interpretation that they take in this respect is to assume an apparent fracture toughness decrease up to the point that $\mathcal{G}_{\max}$ reaches the current fracture toughness and static propagation takes place. However, this damage form, although it exists, it appears to be very small and difficult to measure. In order to investigate the effect of diffuse damage on the growth of fatigue cracks, several specimens were first tested under fatigue and then were quasi-statically loaded up until its failure. Figure 3.11 shows the crack density levels for laminate LA and laminate LB after fatigue testing. The fatigue tests can be identified in the marker description by the maximum strain applied $\varepsilon_{\max}$ and number of cycles. The fracture mechanics criterion is plotted for direct comparison representing the static master curve for a pristine material. The markers in red represent the crack density levels immediately after the fatigue test. One would expect that the crack densities of fatigue-damaged specimens would be shifted to the left in comparison to the static master curve, meaning that diffuse damage affects the cracking process and initiates cracks earlier. For the current carbon/epoxy system, the experimental data does not support this argument as the crack density curves of the fatigue-damaged specimens tend to the master curve.

The second approach, that was introduced by Liu and Nairn [29], sug-

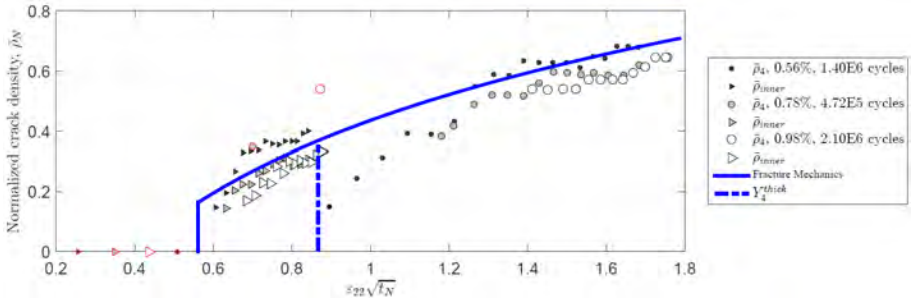

(a) Laminate LA

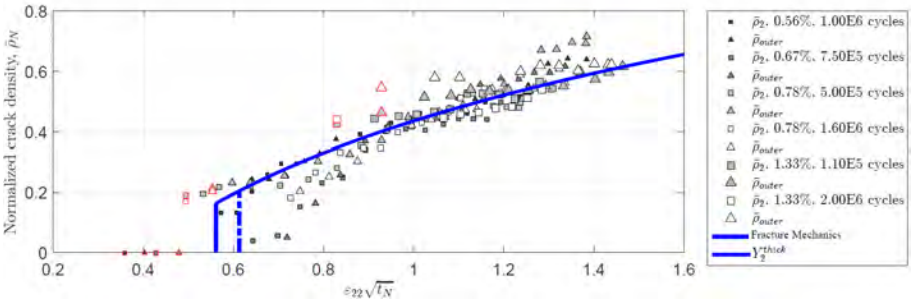

(b) Laminate LB

Fig. 3.11: Normalized crack density of a fatigued material at different strain levels and fractions of life under static loading.

gests that the crack density increases according to a modified Paris law in which the dependent variable is the crack density and the loading function is a magnitude of the energy release rate. In order to see which Paris law provides the best fitting, the experimental cracking curves are fitted by four different Paris law equations (see Figure 3.12). The top and bottom left figures correspond to the fitting with the crack density and the ones at the right with the normalized crack density as the dependent variable. At the same time, the top figures consider the loading function defined as: $g_{\Delta G} = \sqrt{\left(G_I^{\max} - G_I^{\min}\right)/G_{Ic}}$, where $G_I^{\max}$, $G_I^{\min}$, G_{Ic} are the maximum and minimum cyclic energy release rates, and mode I fracture toughness, respectively. Whereas the bottom figures consider the loading function defined as: $g_{\Delta K} = \sqrt{\left(G_I^{\max}/G_{Ic}\right)} - \sqrt{\left(G_I^{\min}/G_{Ic}\right)}$. Note that the experimental data for each ply cluster is represented by a different marker and colour (the marker colour indicates the applied maximum cyclic strain). Unfortunately, the different fittings presented in Figure 3.12 do not clarify which Paris law is more accurate.

It is worth mentioning that the crack density function ρ_{inner} was not ob-

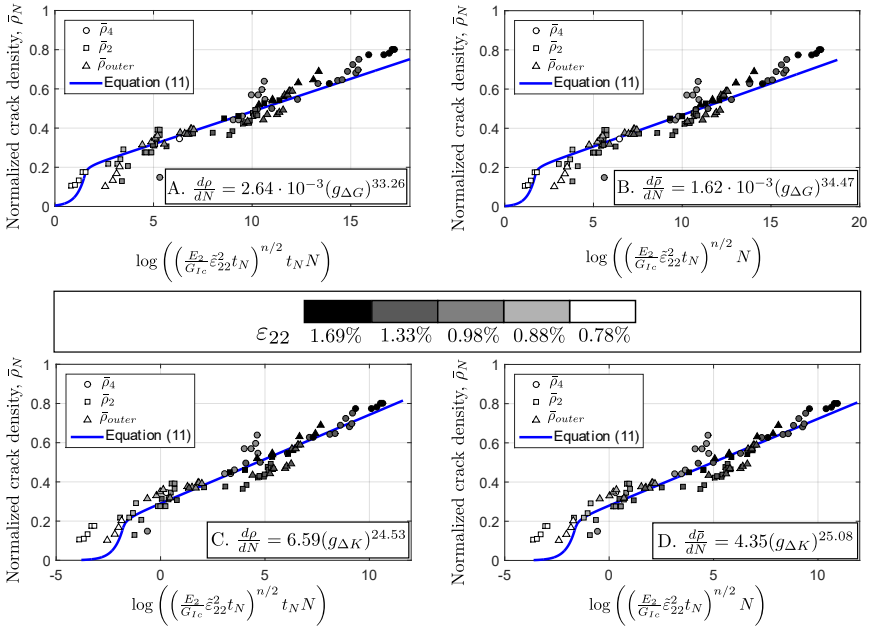

Fig. 3.12: Fitting of the Paris law function for different cases: A. Crack density and $g_{\Delta G}$, B. Normalized crack density and $g_{\Delta G}$, C. Crack density and $g_{\Delta K}$ and D. Normalized crack density and $g_{\Delta K}$.

tained in fatigue as significant fibre splitting occurred at the outermost 0° ply. The fibre splitting mechanism can change the stiffness of the outermost 0° ply and thus affecting the cracking process of the adjacent 90° ply.

3.3 Fatigue damage modelling of notched quasi-isotropic laminates

A large experimental campaign was performed on quasi-isotropic notched laminates under static, tension-tension fatigue and post-fatigue residual strength tests. Two notched geometries were used, the open-hole (OHT) and the double-edge notched (DENT) tensile specimens. Figures 3.13 and 3.14 show the X-rayed specimens after the different tests performed. In the static tests, failure of the specimens is governed by fibre fracture whereas in fatigue progressive damage grows in the form of matrix splitting cracks and delaminations. The same damage mechanisms are observed within the three stress levels tested (60 %, 75 % and 90 % of the ultimate static).

Off-axis matrix cracks start at an early stage of fatigue life in company with 0° splits that are triggered by a local peak shear stress at the notch, and

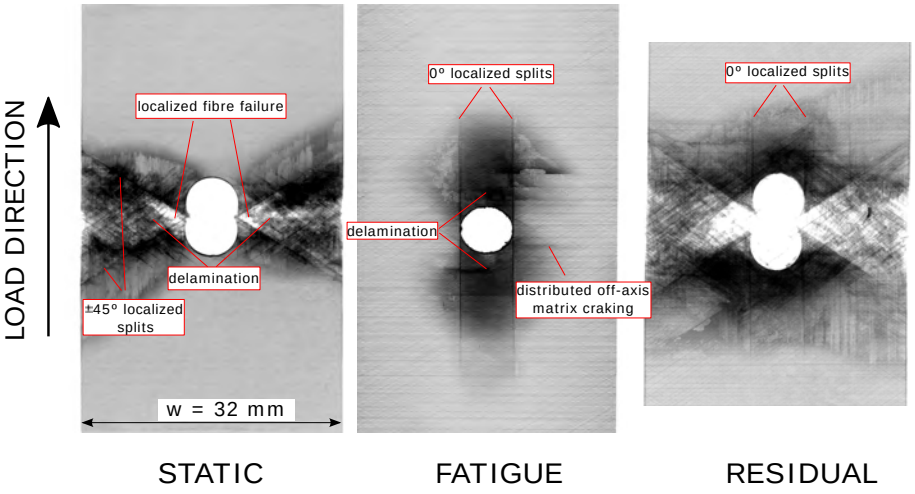

Fig. 3.13: X-ray inspections in open-hole specimens tested under static, tension-tension fatigue and residual strength.

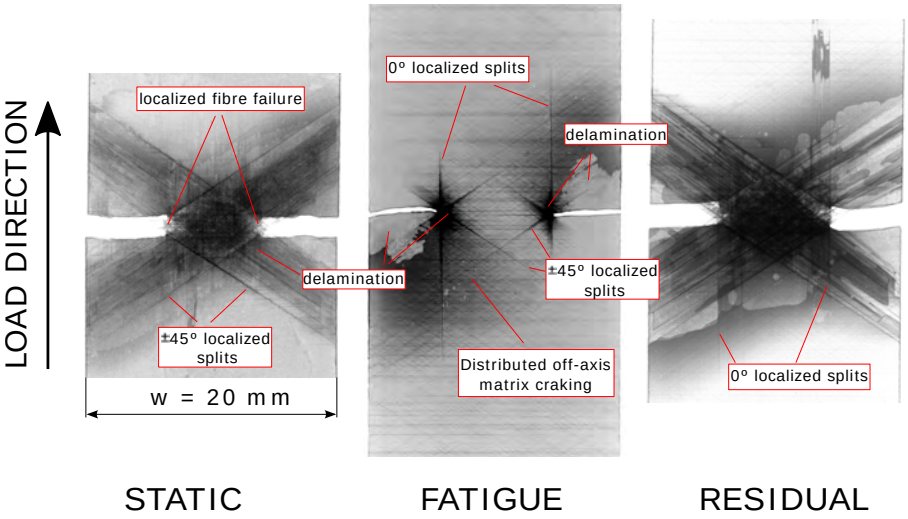

Fig. 3.14: X-ray inspections in double-edge notched specimens tested under static, tension-tension fatigue and residual strength.

then they progressively increase in length as shown in Figure 3.15. These mechanisms are accompanied by local delaminations that initiate between the splits and the edges of the hole, and then they continue to grow along with the increase in the 0° splits. In the open-hole specimen, delaminations mainly develop between the two major 0° splits at the central region of the specimen, similar to the experimental observations provided by Aidi et al.

[80] except for the free-edge delaminations. In contrast, Figure 3.16 shows a delamination front growing between the major 0° splits and the free-edge of the DENT specimen. Note that the longitudinal splits grow symmetrically in the OHT specimen (see Figure 3.15). But in the DENT specimen, they start growing symmetrically and with the increase in the number of cycles, they appear with a certain asymmetry which coincides with the formation of a large delamination front (see Figure 3.16).

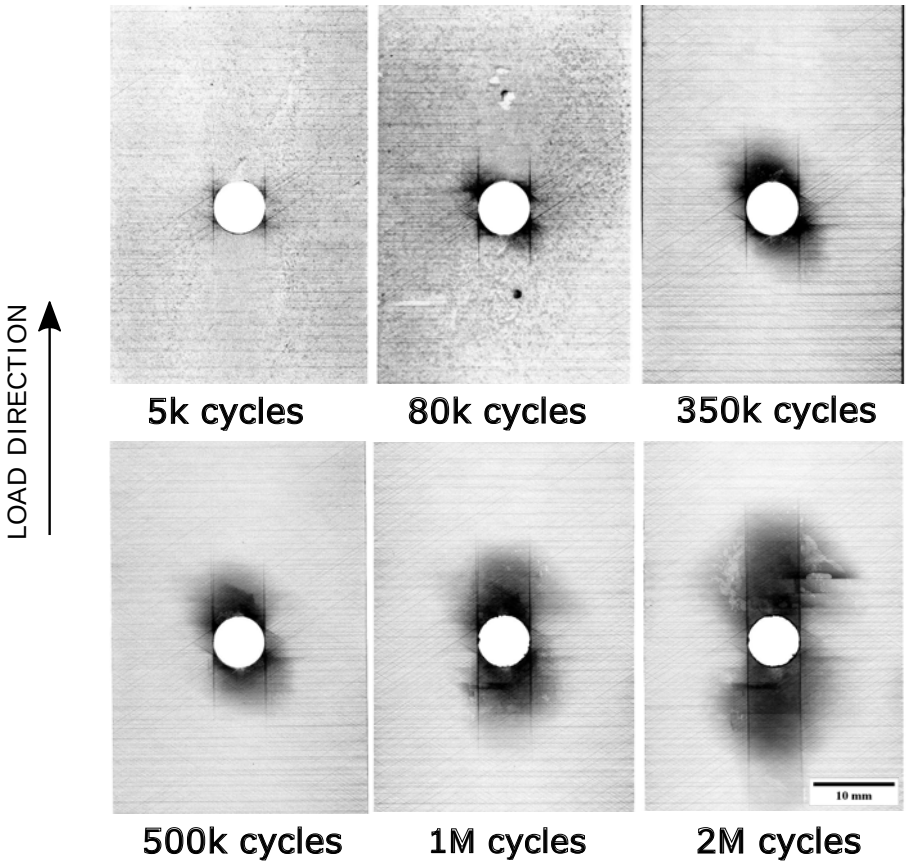

Fig. 3.15: Fatigue damage evolution in open-hole specimens subjected to the 75% of the ultimate and R-ratio=0.1.

Although the laminates suffered from fatigue damage with a relatively important loss of stiffness, the damage mechanisms that appear at the notch seems to be reducing the stress concentration as no fibre fracture was observed. The development of fatigue damage in the specimens changes completely the static scenario. Indeed, the specimens that were tested at stress levels of 75% of the ultimate static, *R*-ratio = 0.1 and 2 million cycles did not

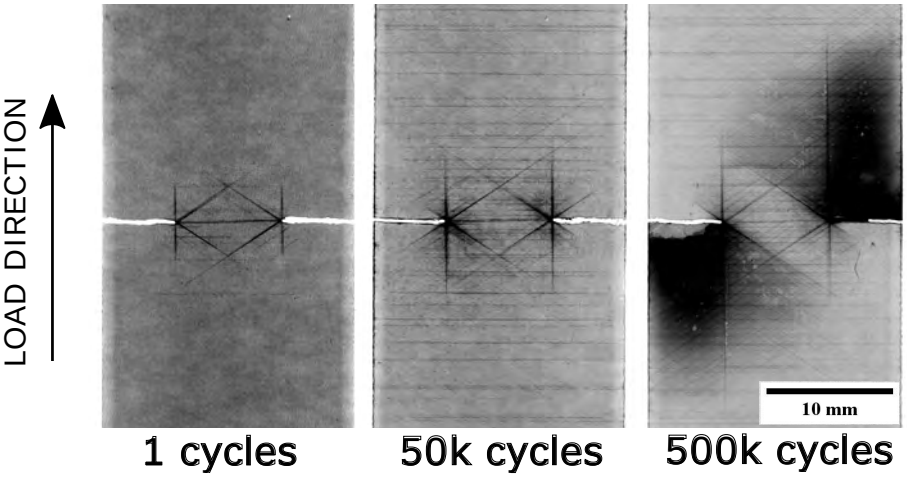

Fig. 3.16: Fatigue damage evolution in double-edge notched specimens subjected to the 90% of the ultimate and R-ratio=0.1.

reach complete failure. The post-fatigue residual strength tests confirmed that fatigue damage alleviates the stress concentration, delays localized fibre fracture and eventually results in a residual strength increase. This trend is in agreement with the experimental findings reported in literature with different carbon/epoxy notched laminates [80, 85, 86, 88]. Despite the overall damage induced by fatigue loads, it appears that the 0° splits control the increase in the tensile residual strength [89]. Figures 3.21 and 3.22 show the residual strength in the net sections with respect to the length of the 0° splits for both types of specimens.

3.4 Numerical results

This section analyses the results of the numerical simulations and discusses them by comparing the damage predictions against the experiments performed with the open-hole and double-edge notched specimens.

The X-ray inspections after the static tests showed that failure is fibre-dominated. Figures 3.17 and 3.18 show the comparison between the damage predictions and the X-ray radiographs. As shown in the left image of the figures, the numerical model predicts a localized crack at the 0° plies which promoted a load drop on the load displacement curves. It is worth mentioning that the development of 0° splits in the static simulation is very limited. The strength-to-failure at the net section of the specimens is, 647.5 MPa / 576 MPa (EXP./ FEM) for the OHT specimen, and 785 MPa / 762.5 (EXP./ FEM) for the DENT specimen.

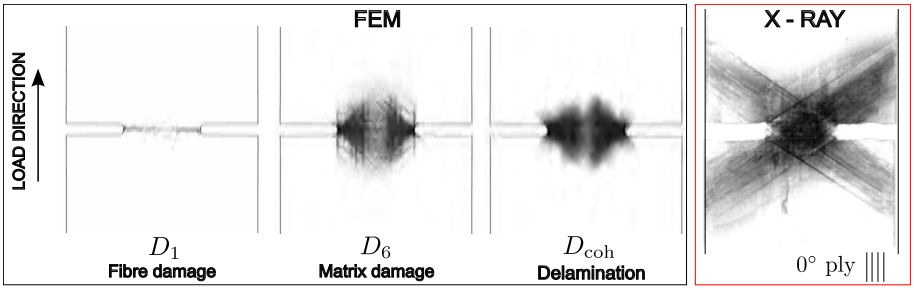

Fig. 3.17: Damage mechanisms in a quasi-isotropic carbon/epoxy double-edge notch tensile specimen under static loading (FEM vs. X-RAY).

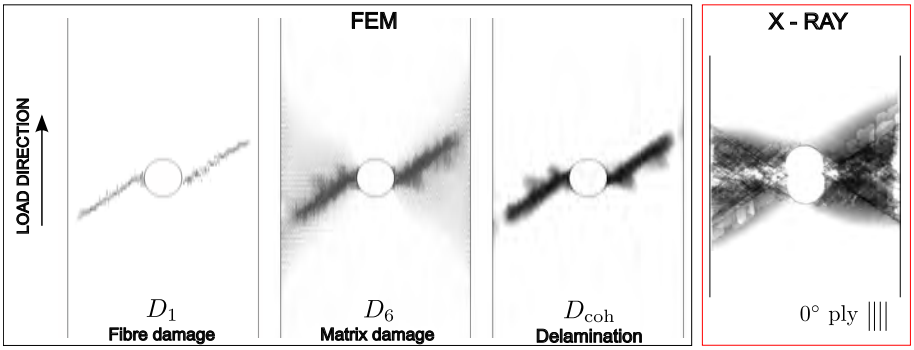

Fig. 3.18: Damage mechanisms in a quasi-isotropic carbon/epoxy open-hole specimen under static loading (FEM vs. X-RAY).

According to the experimental findings explained in section 3.3, the main fatigue damage mechanisms controlling the degradation of the laminate are the 0° splitting cracks and delaminations. Figure 3.19 shows the fatigue damage evolution predictions for the DENT specimen under a 75% of the ultimate static strength and R-ratio = 0.1. The fatigue simulation is run until 1 million cycles and then, it is restarted at cycle intervals of 100k cycles for residual strength predictions (i.e., 100k, 200k, and so on). In general, the damage predictions show good agreement with the main fatigue degradation mechanisms found in the experiments. However, it is observed that the length of the splits at the 0° plies is underestimated. The reason for this can be attributed to two different factors. The first factor is the fact that the localization band in the crack-band model takes the size of one finite element. As the element size across the crack increases, the crack effectively becomes blunter (i.e., lower stress concentration) and damage initiation is delayed. The second factor is related to the excessive distortion issues found in the numerical simulations. The adopted solution to resolve the excessive distortion errors caused by finite elements that are highly distorted due to damage is to keep

a remaining stiffness of the elements. The remaining stiffness that is kept make the elements transfer transverse and shear stresses which range from 1 to 5 MPa over the entire length of the 0° split. Eventually, this yields to a reduction of the shear stress at the crack tip which either reduces the crack growth rate or even arrests the propagation of the crack.

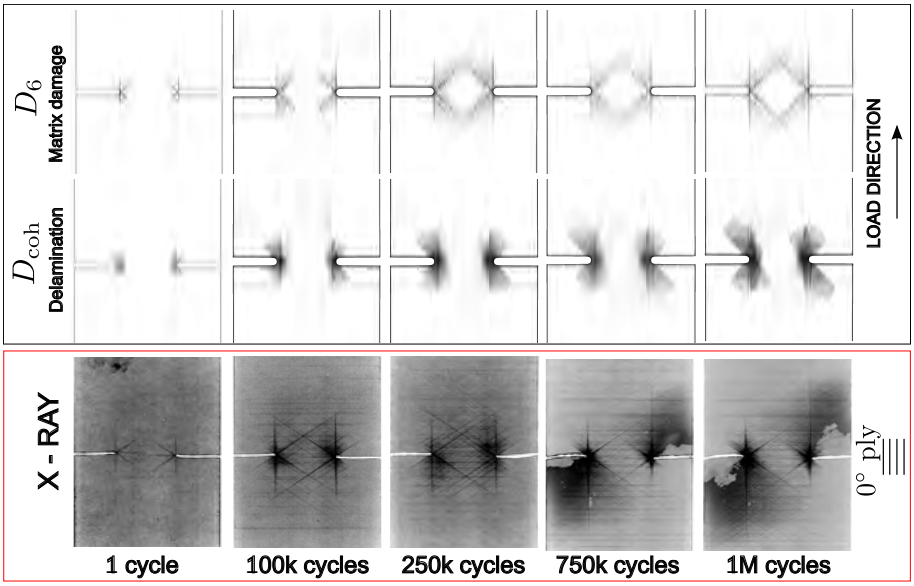

Fig. 3.19: Fatigue damage evolution in the double-edge notched specimen subjected to 75% of the ultimate static strength and R-ratio = 0.1 (FEM vs. X-RAY).

The fatigue simulation with the open-hole specimen at a fatigue load level of 75% of the ultimate static, R-ratio = 0.1 and 1 million cycles is shown in Figure 3.20. The numerical model predicts well the direction of the splitting matrix cracks and delamination locations, but again the length of the splits seems to be underestimated. As a consequence, the total delamination area is also smaller than the one observed in the radiographs.

Severe issues concerning numerical stability were found at higher fatigue loading levels (higher than 75% of the static strength), which result in most simulations unable to finish due to excessive distortion of few damaged elements undergoing large transverse and shear strains. When these elements are deleted from the mesh without fibre damage, premature failure of the specimen occurs. If they are kept active within the numerical model, then they become so distorted that may activate other more critical failure modes like fibre fracture, which eventually lead to the same excessive distortion errors. One of the reasons for this might be attributed to the concern raised by [102]. Leone suggested that the large shear deformation applied to cracked

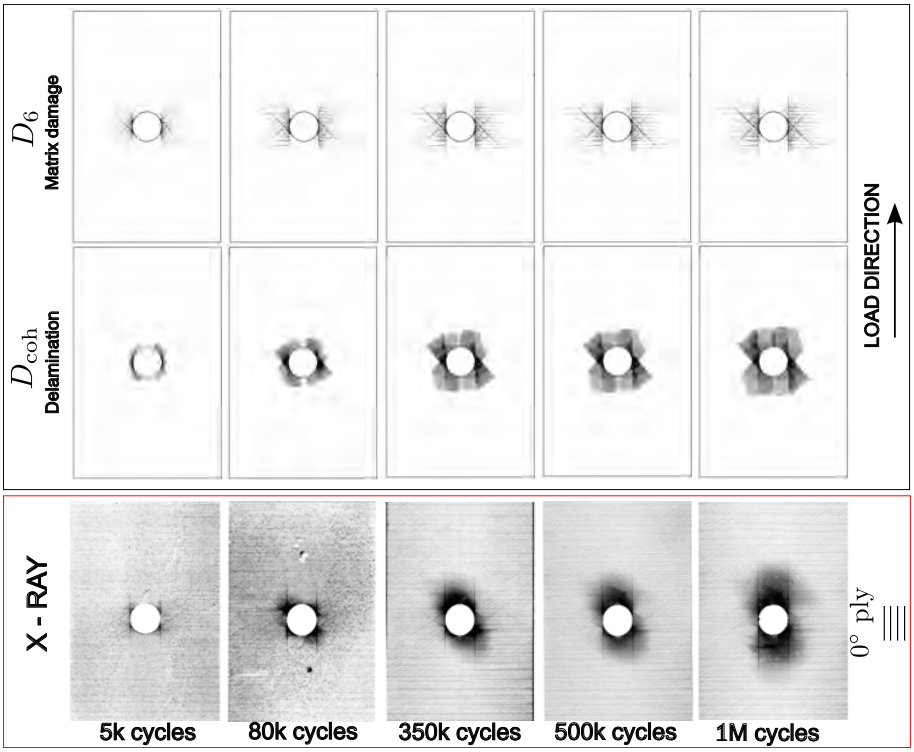

Fig. 3.20: Fatigue damage evolution in the open-hole specimen subjected to 75% of the ultimate static strength and R-ratio = 0.1.

material points results in a rotation of the local material directions. Calculating the strain in this rotated, smeared material coordinate system cause unintended load transfer across the crack faces and activate other failure modes, i.e. fibre failure. Leone figured out a method to solve this issue by decomposing the deformation gradient tensor into 'bulk' and 'cracked' material, similar to the additive strain decomposition of smeared crack models [103]. In any case, this concept has been only validated by modelling splits in unidirectional open-hole specimens and it should be benchmarked in a much more complex scenario such as the one presented in this work.

Another consideration to be made is the concern of Van deer Meer when modelling splitting cracks with meso-scale CDM models [104]. Since the homogenization of composite plies at the meso-scale level eliminates the distinction between fibres and resin, meso-scale CDM models have difficulties to predict the crack direction as they cannot distinguish between cracks that propagate along the fibre direction from those that cross fibres. Recall that the direction of the crack is driven by the local stress redistribution of dam-

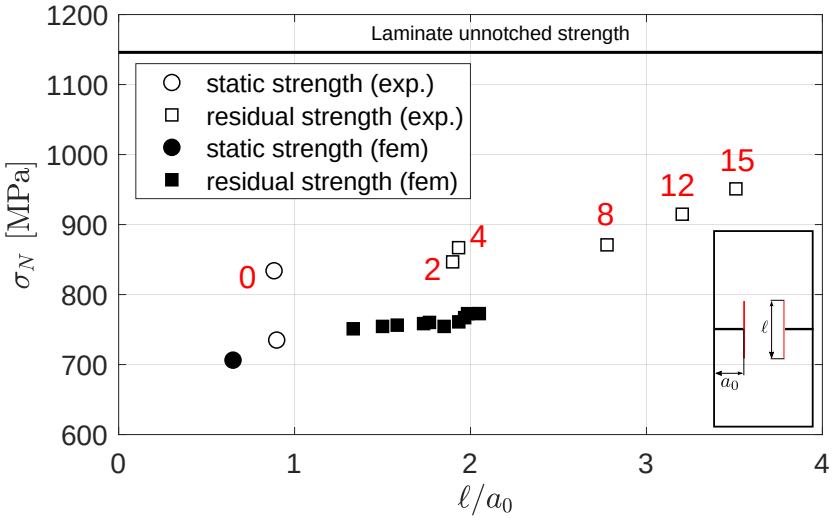

Fig. 3.21: Residual post-fatigue tensile strength in double-edge notched specimens with respect to the split length.

aged elements that are activated according to the local evaluation of a failure criteria. Although this problem seems to be alleviated by orienting the mesh with the fibre direction, it still causes some numerical difficulties in particular when a matrix crack is subjected to shear stresses [105, 106]. In the present model, the interaction between different matrix cracks at different plies results in, for instance, matrix cracks that occur at the $\pm 45^\circ$ ply are spuriously being transferred to the adjacent 90° ply.

Figures 3.21 and 3.22 show the net section strength pwith respect to the length of the 0° splits. The experimental values are plotted as white markers and the numerical predictions are plotted in black. Note that the numerical predictions of Figure 3.21 seem to follow the increase in the residual strength with the increase in the length of the splits, but the predictions are clearly shifted to the left as the length of the splits is shorter than in the experiments. In the case of the OHT specimens, the numerical model seems to be not capable of predicting the correct residual strength. Indeed, the static and post-fatigue strength predictions are relatively closer and they do not follow the experimental trend. However, it is clear by looking at Figure 3.20 that fatigue damage is significantly underestimated in the open-hole specimen, the redistribution of the stresses is not well captured and finally the numerical model underpredicts the residual strength. It is also important to note that the open-hole residual strength simulations with more than 500k cycles failed before reaching the load drop due to excessive distortion issues of few

elements next to the edge of the hole.

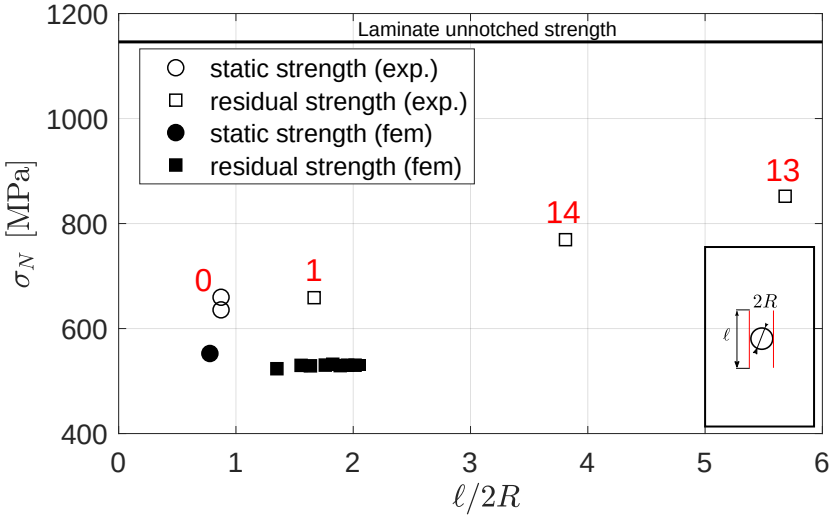

Fig. 3.22: Residual post-fatigue tensile strength in open-hole specimens with respect to the split length.

Chapter 4

Concluding remarks

4.1 Conclusions

The work developed in this Ph.D. project formulates a new constitutive model for the simulation of damage and residual strength of laminated composites under static and fatigue loads. The model has been implemented as a user material subroutine in Abaqus/Explicit and it has been validated by simulating the progressive damage and residual strength of notched quasi-isotropic laminated composites. Within the time frame of this thesis, an extensive experimental campaign has been undertaken to support the numerical works from an experimental basis.

Fatigue damage in composites has revealed as a combination of different damage mechanisms that occurs inside the plies and at the interfaces. These mechanisms may appear at different stages of fatigue life and they contribute differently to the overall laminate degradation of the stiffness and the strength. From a structural design point of view, the most dangerous damage forms in laminated composites are fibre breakage and delamination. The experimental works performed in this Ph.D thesis have focused on the fatigue damage mechanisms that occur at ply level (i.e., intra-ply mechanisms). On the other hand, an extensive experimental characterization on fatigue-driven delamination was presented in the Ph.D thesis developed by Carreras at AMADE research group [26].

The first experimental work performed in this thesis investigated the fatigue behaviour of unidirectional plies subjected cyclic loads that are parallel to the fibre direction. An experimental campaign to study the loss of stiffness and strength of unidirectional laminates under tension-tension fatigue loads was performed. A damage function to describe the loss of stiffness in the fibre direction for different stress levels and R-ratios has been determined. The assumption of a constant ultimate strain has been confirmed experimentally.

The loss of strength can be assumed to be of the same magnitude as the loss of stiffness, and hence the cost and time of the experimental campaign are significantly reduced. A S-N curve can be derived by explicit integration of the residual strength function. Finally, the life predictions correlate reasonably well with the fatigue life experimental data except for the highest stress levels where failure at the tabbed section was unavoidable.

Even though fibre failure under service fatigue loadings is unacceptable, the first damage mechanism that takes place is usually matrix cracking at off-axis plies. Matrix cracking is not considered as critical as delamination or fibre fracture, but it is usually the mechanism triggering the other two failure modes. An experimental investigation into the growth of matrix cracks in cross-ply laminates under static and fatigue loads has been done. The crack density is used as the mechanistic damage variable to describe uniquely the cracking process. The crack density is defined as the number of edge cracks divided by the observation length. The adopted definition does not account for the crack length and the model prediction do not consider the crack initiation and propagation phases separately, and thus this model is only suitable for cracks that immediately span the entire specimen width. An expression to calculate the energy release rate of mode I transverse cracks has been derived. This expression, that assumes crack tunnelling growth (i.e., thin-ply crack growth behaviour), is fitted experimentally as a master curve for all the ply thicknesses analysed. The *in-situ* strength of thin-plies can be calculated from the same expression imposing crack density equal to zero. Under fatigue loads, two different models are proposed to describe the growth of fatigue cracks. The first model attributes the growth of fatigue cracks to the presence of diffuse damage or micro-cracking (i.e, mainly fibre/matrix debonding and resin cracks). The model considers the existence of an empirical function that describes the growth of diffuse damage under fatigue by decreasing the pristine fracture toughness. In order to investigate the effect of diffuse damage on the crack density, previously fatigue-damaged specimens tested at different stress levels and number of cycles were tested again quasi-statically to determine the static crack density curves. The crack density curves of fatigue-damaged specimens tend to the master curve for pristine laminates, which indicates that diffuse damage is negligible and cannot be used to explain on its own the growth of fatigue cracks. The second model takes a completely different approach and considers a modified Paris-law based expression of the crack density. The model shows good correlation with the obtained experimental crack data.

In order to investigate a more complex damage scenario with multiple damage forms inside the plies and at the interfaces, an experimental campaign with notched quasi-isotropic laminates has been carried out. The test campaign consisted in testing two different geometries, the open-hole and the double-edge notched specimens, under static, tension-tension fatigue and

post-fatigue residual strength. The specimens were X-rayed for damage inspection at the end of each test. The fatigue experiments showed a complete different damage scenario than the static case. Whereas in static conditions failure was controlled by fibre fracture, in fatigue the main degradation mechanisms found were splitting matrix cracks and delaminations. These fatigue damage mechanisms reduce the notch stress concentration and suppress fibre fracture on the on-axis plies. It is of special importance the initiation and stable propagation of 0° splits, which redistribute the stresses and delay fibre fracture. Indeed, the residual strength experiments showed a significant increase in the tensile strength after fatigue. The splitting matrix cracks at the 0° are considered to be the main mechanism contributing to the increase in the strength. This can be clearly seen by representing the residual strength with respect to the length of the split.

With regards to the numerical aspects, the meso-scale continuum damage model developed by Maimí et al. [49,50] has been extended for fatigue damage and residual strength predictions. The new formulation and the strategy followed to implement the constitutive model into an explicit finite element framework has been presented. The model relies on a set of physically-based damage and residual strength functions that describe the degradation of the laminate under fatigue loads. The cycle jump concept is used to improve the computational performance and reduce the cost. Thus, the fatigue simulation is not performed cycle-by-cycle but with small cycle jumps that are controlled appropriately. The large extension of fatigue-driven delaminations that appeared in the experiments forced to use a cohesive zone model for the static and fatigue growth of delamination cracks. The cohesive zone model developed by Turon et al. [94,107] is used in this work. An appropriate modelling strategy based on the previous works [95,96] has been used to account for the interaction between splitting cracks and delaminations.

The numerical model has been validated by simulating the experiments performed on notched specimens. The three load cases (static, fatigue and residual strength) have been simulated, and the damage predictions have been compared with the X-ray radio-graphs. The numerical model have been shown to capture well the static failure of both the open-hole and double-edge notched specimens. Under fatigue loads, the main fatigue degradation mechanisms have been predicted well, but it is seen an underestimation of the length of the 0° splits, and as a consequence, delamination area. The overall underestimation of fatigue damage for both specimens results in an underprediction of the residual strength especially in the open-hole specimen.

Revisiting the main objective, this Ph.D thesis has contributed towards an improvement on the computational and experimental methods for fatigue of composites. However, further work is clearly needed to develop a reliable computational tool to quantitatively describe the initiation and propagation

of fatigue damage in composite structures.

4.2 Perspectives and future work

The contribution of this Ph.D. project presents a step forward for the analysis of composite structures subjected to fatigue loads. Nevertheless, several limitations have been identified from a experimental and numerical point of view, some of which are listed below as suggestions for future work.

- The uni-axial fatigue tests performed on high-performance unidirectional laminates showed some issues with the introduction of the load by shear through the tab faces. A large number of specimens failed at the tabbed section due to the stress concentration which results in an underestimation of fatigue life. The use of bending fatigue experiments with smaller forces and larger displacements is seen as a potential solution to solve the above-mentioned issues with uni-axial tests. Obviously, other complications may appear and further research is required [21].

- The vast majority of fatigue laboratory experiments are constant amplitude tests, although this type of fatigue loading is hardly present in real in-service fatigue loading conditions. However, due to the complexity and time-consuming nature of variable-amplitude experiments, their effect is often assessed by performing block loading experiments with various low–high and high–low sequences. Indeed, there is still an open discussion in open literature in which loading sequence is more detrimental for the composite [108, 109]. At the same time, it is well-known that tension-compression fatigue tests are the most severe cyclic load for composite laminates [21], especially when fatigue-driven delamination is likely to occur.

- Fatigue testing in pure shear is difficult and the candidate did not have the time to address the shear response of the laminate under fatigue loads. A tension-tension fatigue test on a $[\pm 45]_{ns}$ laminate is the most common type of test to investigate the accumulation of permanent strains during shear-dominated fatigue loading. The pioneering works by Van Paepegem et al. [110,111] would be the point of departure to address the fatigue response of a laminate under dominated shear fatigue loads.

- To develop experimental methods to characterize the fatigue cohesive law. Due to the lack of characterization methods, the CDM-based model presented here is currently based on the link between the macroscopic description of the fatigue crack growth and the local evaluation of the

damage rate within the cohesive zone. It is assumed that the quasi-static cohesive law is preserved, or when distributed damage occurs, the stiffness and the strength are reduced appropriately, but the slope of the softening branch is fixes. However, there is no experimental evidence in this regard and further experimental studies are needed.

- A complete experimental fatigue characterization of complex material systems, such as composites, appears to be unaffordable from a practical point of view due to the amount of variables involved. The determination of general material laws (as it can be the case of coupling the loss of stiffness and strength in fibre direction) is mandatory to reduce the costs associated to material characterization. In this regard, understanding the governing micromechanical mechanisms that initiate fatigue damage seems to be the path for a more general understanding of material behaviour that allows us to achieve this goal.

- Continuum damage mechanics models implemented in explicit frameworks suffer from severe numerical instabilities due to excessive distortion of damaged finite elements undergoing large strains. As of now, there is no widely accepted solution in open literature that solves this numerical issue. Further research is needed to find a remedy that can potentially improve the robustness and efficiency of these models without compromising its computational cost.

- Meso-scale continuum damage models cannot distinguish between matrix cracks that grow parallel to the fibre direction that those that grow perpendicular to it. This is mainly because of the homogenization between fibre and matrix at the meso-scale [104]. This limitation seems to be alleviated by orienting the mesh in the fibre direction, but it is considered that the constitutive model could be potentially improved by using new concepts such as the one proposed by Leone [102]. As an alternative, it is suggested to explore the capabilities of X-FEM or any of its variants [112–114], or to change the numerical approach by using cohesive elements for the discrete ply cracks [115,116].

- The cycle jump algorithm implemented in this work is simple and robust, but it reveals some limitations that penalize the computational performance. In essence, the cycle jump ensures that the damage increment per cycle is less than a predefined target limit. Obviously, this target limit must be relatively small to capture the whole process of stress redistribution. However, the cycle jump strategy is rather sensitive to the critical finite elements of the structure, which results in a consecutive large number of small cycle jumps that eventually increase the computational time. The cycle jump strategy deserves further attention since the computational model aims for modelling damage and life

of larger scale composite structures. A good point of departure could be the cycle jump approach proposed in [117].

References

[1] U. P. Breuer, *Commercial aircraft composite technology*. Springer, 2016.

[2] US Department of Defense, *Composite Materials Handbook Volume 1: Polymer Matrix Composites - Guidelines for Characterisation of Structural Materials*, vol. 1. 2002.

[3] J. Tomblin and W. Seneviratne, "Determining the fatigue life of composite aircraft structures using life and load-enhancement Factors," tech. rep., Federal Aviation Administration, 2011.

[4] G. P. Sendeckyj, "Life prediction for resin-matrix composite materials," in *Fatigue of composite materials* (K. L. Reifsnider, ed.), ch. Chapter 10, Elsevier, 1990.

[5] J. Kaminski, M.; Laurin, F.; Maire, "Fatigue Damage Modeling of Composite Structures: the ONERA viewpoint," *Aerospace lab*, no. 9, 2015.

[6] J. Degrieck and W. Van Paepegem, "Fatigue damage modelling of fibre-reinforced composite materials: Review," *Applied Mechanics Reviews*, vol. 54, no. 4, pp. 279–300, 2001.

[7] R. P. L. Nijssen, *Fatigue Life Prediction and Strength Degradation of Wind Turbine Rotor Blade Composites*. PhD thesis, Delft University of Technology, 2007.

[8] V. A. Passipoularidis and P. Brøndsted, "Fatigue Evaluation algorithms: Review," tech. rep., Risø Technical University of Denrmark, 2010.

[9] Z. Hashin and A. Rotem, "A fatigue failure criterion for fiber reinforced materials," tech. rep., 1973.

[10] Z. Hashin, "Fatigue failure criteria for unidirectional fiber composites," *Journal of Applied Mechanics, Transactions ASME*, vol. 48, no. 4, pp. 846–852, 1981.

[11] F. Ellyin and H. El-Kadi, "A Fatigue Failure Criterion for Fiber Reinforced Materials," *Composite Structures 15*, vol. 7, no. 4, pp. 61–74, 1990.

[12] Z. Fawaz and F. Ellyin, "Fatigue Failure Model for Fibre-Reinforced Materials under General Loading Conditions," *Journal of Composite Materials*, vol. 28, no. 15, pp. 1432–1451, 1994.

[13] J. Xiao and C. Bathias, "Fatigue behaviour of unnotched and notched woven glass/epoxy laminates," *Composites Science and Technology*, vol. 50, no. 2, pp. 141–148, 1994.

[14] W. Hwang and K. S. Han, "Cumulative damage models and multi-stress fatigue life prediction," *Journal of Composite Materials*, vol. 20, pp. 125–153, 1986.

[15] M. Kawai, S. Yajima, A. Hachinohe, and Y. Takano, "Off-Axis fatigue behavior of unidirectional carbon fiber-reinforced composites at room and high temperatures," *Journal of Composite Materials*, vol. 35, pp. 545–576, 2001.

[16] M. Kawai, S. Yajima, A. Hachinohe, and Y. Kawase, "High-temperature off-axis fatigue behaviour of unidirectional carbon-fiber-reinforced composites with different resin matrices," *Composites Science and Technology*, vol. 61, no. 9, pp. 1285–1302, 2001.

[17] M. Kawai, "A phenomenological model for off-axis fatigue behavior of unidirectional polymer matrix composites under different stress ratios," *Composites Part A: Applied Science and Manufacturing*, vol. 35, pp. 955–963, 2004.

[18] N. L. Post, J. J. Lesko, and S. W. Case, "Residual strength fatigue theories for composite materials," in *Fatigue Life Prediction of Composites and Composite Structures* (A. P. Vassilopoulos, ed.), ch. 3, Woodhead Publishing Limited, 2010.

[19] T. P. Philippidis and V. A. Passipoularidis, "Residual strength after fatigue in composites: Theory vs. experiment," *International Journal of Fatigue*, vol. 29, no. 12, pp. 2104–2116, 2007.

[20] V. A. Passipoularidis, *Residual strength and life prediction in composite materials after fatigue*. PhD thesis, Univeristy of Patras, 2009.

[21] W. Van Paepegem, "Fatigue damage modelling of composite materials with the phenomenological residual stiffness approach," in *Fatigue Life Prediction of Composites and Composite Structures* (A. P. Vassilopoulos, ed.), ch. 4, Woodhead Publishing Limited, 2010.

[22] W. Van Paepegem and J. Degrieck, "A new coupled approach of residual stiffness and strength for fatigue of fibre-reinforced composites," *International Journal of Fatigue*, vol. 24, no. 7, pp. 747–762, 2002.

[23] W. Van Paepegem and J. Degrieck, "Coupled residual stiffness and strength model for fatigue of fibre-reinforced composite materials," *Composites Science and Technology*, vol. 62, no. 5, pp. 687–696, 2002.

[24] ASTM D6115-97(2019), "Standard test method for mode I fatigue delamination growth onset of unidirectional fiber-reinforced polymer matrix composites," *American Society for Testing and Materials*, 2019.

[25] R. Krueger, "Development of a benchmark example for delamination fatigue growth prediction," *NASA/CR-2010-216723*, vol. 2, no. 2010, pp. 948–967, 2010.

[26] L. Carreras, *Development of efficient testing methods and cohesive zone models for analyzing fatigue-driven delamination in 3D laminated composite structures*. PhD thesis, University of Girona, 2018.

[27] J. A. Nairn, "Matrix microcracking in composites," in *Polymer Matrix Composites* (R. Talreja and J. A. E. Manson, eds.), ch. 13, pp. 403–432, Elsevier Science, 2000.

[28] J. A. Nairn, "The Strain Energy Release Rate of Composite Microcracking: A Variational Approach," *Journal of Composite Materials*, vol. 23, no. 11, pp. 1106–1129, 1989.

[29] S. Liu and J. A. Nairn, "Fracture Mechanics Analysis of Composite Microcracking: Experimental Results in Fatigue," in *Proceedings of the 5th Technical Conference on Composite Materials, American Society of Composites*, pp. 287–295, 1990.

[30] P. Ladevèze, "A computational mesodamage model for life prediction for laminates," in *Fatigue in composite materials* (B. Harris, ed.), ch. 15, Woodhead Publishing Limited, 2003.

[31] A. Thionnet and J. Renard, "Laminated composites under fatigue loading: A damage development law for transverse cracking," *Composites Science and Technology*, vol. 52, no. 2, pp. 173–181, 1994.

[32] B. Liu and L. B. Lessard, "Fatique and damage-tolerance analysis of composite laminates: Stiffness loss, damage-modelling, and life prediction," *Composites Science and Technology*, vol. 51, pp. 43–51, jan 1994.

[33] C. Li, F. Ellyin, and A. Wharmby, "A damage meso-mechanical approach to fatigue failure prediction of cross-ply laminate composites," *International Journal of Fatigue*, vol. 24, pp. 429–435, 2002.

[34] M. M. Shokrieh and L. B. Lessard, "Progressive Fatigue Damage Modeling of Composite Materials, Part I: Modeling," *Journal of Composite Materials*, vol. 34, no. 13, pp. 1056–1080, 2000.

[35] M. M. Shokrieh and L. B. Lessard, "Progressive Fatigue Damage Modeling of Composite Materials, Part II: Material Characterization and Model Verification," *Journal of Composite Materials*, vol. 34, no. 13, pp. 1081–1116, 2000.

[36] M. M. Shokrieh and F. Taheri-Behrooz, "Fatigue life prediction of composite materials based on progressive damage modelling," in *Fatigue Life Prediction of Composites and Composite Structures* (A. P. Vassilopoulos, ed.), ch. Chapter 8, Woodhead Publishing Limited, 2010.

[37] T. P. Philippidis and E. N. Eliopoulos, "A progressive damage mechanics algorithm for life prediction of composite materials under cyclic complex stress," in *Fatigue Life Prediction of Composites and Composite Structures* (A. P. Vassilopoulos, ed.), ch. Chapter 11, Woodhead Publishing Limited, 2010.

[38] E. N. Eliopoulos and T. P. Philippidis, "A progressive damage simulation algorithm for GFRP composites under cyclic loading. Part I: Material constitutive model," *Composites Science and Technology*, vol. 71, no. 5, pp. 742–749, 2011.

[39] E. N. Eliopoulos and T. P. Philippidis, "A progressive damage simulation algorithm for GFRP composites under cyclic loading. Part II: FE implementation and model validation," *Composites Science and Technology*, vol. 71, no. 5, pp. 750–757, 2011.

[40] M. Naderi and A. R. Maligno, "Fatigue life prediction of carbon/epoxy laminates by stochastic numerical simulation," *Composite Structures*, vol. 94, no. 3, pp. 1052–1059, 2012.

[41] W. Lian and W. Yao, "Fatigue life prediction of composite laminates by FEA simulation method," *International Journal of Fatigue*, vol. 32, no. 1, pp. 123–133, 2010.

[42] C. R. Kennedy, C. M. Brádaigh, and S. B. Leen, "A multiaxial fatigue damage model for fibre reinforced polymer composites," *Composite Structures*, vol. 106, pp. 201–210, 2013.

[43] B. D. Coleman and M. E. Gurtin, "Thermodynamics with internal state variables," *The Journal of Chemical Physics*, vol. 47, no. 2, pp. 597–613, 1967.

[44] R. Talreja, "Continuum Mechanics Characterization of Damage in Composite Materials.," *Proceedings of The Royal Society of London, Series A: Mathematical and Physical Sciences*, vol. 399, no. 1817, pp. 195–216, 1985.

[45] A. Matzenmiller, J. Lubliner, and R. L. Taylor, "A constitutive model for anisotropic damage in fiber-composites," *Mechanics of Materials*, vol. 20, no. 2, pp. 125–152, 1995.

[46] E. J. Barbero and L. D. Vivo, "A Constitutive Model for Elastic Damage in Fiber-Reinforced PMC Laminae," *International Journal of Damage Mechanics*, vol. 10, no. 1, pp. 73–93, 2001.

[47] P. Ladevèze, O. Allix, J. F. Deu, and D. Leveque, "A mesomodel for localisation and damage computation in laminates," *Computer Methods in Applied Mechanics and Engineering*, vol. 183, no. 1-2, pp. 105–122, 2000.

[48] P. Ladevèze and G. Lubineau, "An enhanced mesomodel for laminates based on micromechanics," *Composites Science and Technology*, vol. 62, no. 4, pp. 533–541, 2002.

[49] P. Maimí, P. P. Camanho, J. A. Mayugo, and C. G. Dávila, "A continuum damage model for composite laminates: Part I – Constitutive model," *Mechanics of Materials*, vol. 39, no. 10, pp. 897–908, 2007.

[50] P. Maimí, P. P. Camanho, J. A. Mayugo, and C. G. Dávila, "A continuum damage model for composite laminates: Part II – Computational implementation and validation," *Mechanics of Materials*, vol. 39, no. 10, pp. 909–919, 2007.

[51] J. Payan and C. Hochard, "Damage modelling of laminated carbon/epoxy composites under static and fatigue loadings," *International Journal of Fatigue*, vol. 24, pp. 299–306, apr 2002.

[52] C. Hochard, J. Payan, and C. Bordreuil, "A progressive first ply failure model for woven ply CFRP laminates under static and fatigue loads," *International Journal of Fatigue*, vol. 28, pp. 1270–1276, 2006.

[53] C. Hochard and Y. Thollon, "A generalized damage model for woven ply laminates under static and fatigue loading conditions," *International Journal of Fatigue*, vol. 32, no. 1, pp. 158–165, 2010.

[54] J. Renard and A. Thionnet, "Damage in composites: From physical mechanisms to modelling," *Composites Science and Technology*, vol. 66, pp. 642–646, may 2006.

[55] K. L. Reifsnider and R. Jamison, "Fracture of fatigue-loaded composite laminates," *International Journal of Fatigue*, vol. 4, pp. 187–197, 1982.

[56] A. Sedrakian, T. B. Zineb, and J. L. Billoet, "Contribution of industrial composite parts to fatigue behaviour simulation," *International Journal of Fatigue*, vol. 24, no. 2-4, pp. 307–318, 2002.

[57] H. Krüger and R. Rolfes, "A physically based fatigue damage model for fibre-reinforced plastics under plane loading," *International Journal of Fatigue*, vol. 70, pp. 241–251, jan 2015.

[58] B. Mohammadi, B. Fazlali, and D. Salimi-Majd, "Development of a continuum damage model for fatigue life prediction of laminated composites," *Composites Part A: Applied Science and Manufacturing*, vol. 93, pp. 163–176, 2017.

[59] P. Maimí, P. P. Camanho, J. A. Mayugo, and C. G. Dávila, "A Thermodynamically Consistent Damage Model for Advanced Composites," 2006.

[60] P. Maimí, *Modelizacion constitutiva y computacional del daño y la fractura de materiales compuestos*. PhD thesis, 2007.

[61] P. Maimi, P. P. Camanho, J. A. Mayugo, and A. Turon, "Matrix cracking and delamination in laminated composites. Part I: Ply constitutive law, first ply failure and onset of delamination," *Mechanics of Materials*, vol. 43, pp. 169–185, 2011.

[62] P. Maimi, P. P. Camanho, J. A. Mayugo, and A. Turon, "Matrix cracking and delamination in laminated composites. Part II: Evolution of crack density and delamination," *Mechanics of Materials*, vol. 43, pp. 194–211, 2011.

[63] Z. Bazant and B. Oh, "Crack band theory for fracture of concrete," *Materials and Structures*, vol. 16, p. 155, 1983.

[64] C. Hochard, S. Miot, and Y. Thollon, "Fatigue of laminated composite structures with stress concentrations," *Composites Part B: Engineering*, vol. 65, pp. 11–16, 2013.

[65] E. K. Gamstedt, L. A. Berglund, and T. Peijs, "Fatigue mechanisms in unidirectional glass-fibre-reinforced polypropylene," *Composites Science and Technology*, vol. 59, no. 5, pp. 759–768, 1999.

[66] E. K. Gamstedt and R. Talreja, "Fatigue damage mechanisms in unidirectional carbon-fibre-reinforced plastics," *Journal of Materials Science*, vol. 34, no. 11, pp. 2535–2546, 1999.

[67] E. K. Gamstedt and B. A. Sjögren, "Micromechanisms in tension-compression fatigue of composite laminates containing transverse plies," *Composites Science and Technology*, vol. 59, no. 2, pp. 167–178, 1999.

[68] E. K. Gamstedt and S. Ostlund, "Fatigue Propagation of Fibre-Bridged Cracks in Unidirectional Polymer-Matrix Composites," *Applied Composite Materials*, vol. 8, pp. 385–410, 2001.

[69] R. Talreja, "Fatigue of composite naterials: damage mechanisms and fatigue-Life diagrams," *Proceedings of the Royal Society A: Mathematical, Physical and Engineering Sciences*, vol. 378, pp. 461–475, 1981.

[70] R. Talreja, "A conceptual framework for studies of durability in composite materials," in *Fatigue of Textile Composites* (V. Carvelli and S. V. Lomov, eds.), ch. 1, Woodhead Publishing Limited, 2015.

[71] R. Talreja, "Damage and fatigue in composites – A personal account," *Composites Science and Technology*, vol. 68, no. 13, pp. 2585–2591, 2008.

[72] M. Quaresimin, P. A. Carraro, and L. Maragoni, "Early stage damage in off-axis plies under fatigue loading," *Composites Science and Technology*, vol. 128, pp. 147–154, 2016.

[73] L. Maragoni, P. Carraro, and M. Quaresimin, "Prediction of fatigue life to crack initiation in unidirectional plies containing voids," *Composites Part A: Applied Science and Manufacturing*, vol. 127, no. July, p. 105638, 2019.

[74] B. F. Sørensen and S. Goutianos, "Micromechanical model for prediction of the fatigue limit for unidirectional fibre composites," *Mechanics of Materials*, vol. 131, no. February, pp. 169–187, 2019.

[75] M. Alves and S. Pimenta, "A computationally-efficient micromechanical model for the fatigue life of unidirectional composites under tension-tension loading," *International Journal of Fatigue*, vol. 116, pp. 677–690, 2018.

[76] A. Turon, *Simulation of delamination in composites under quasi-static and fatigue loading using cohesive zone models*. PhD thesis, University of Girona, 2006.

[77] B. L. V. Bak, C. Sarrado, A. Turon, and J. Costa, "Delamination Under Fatigue Loads in Composite Laminates: A Review on the Observed Phenomenology and Computational Methods," *Applied Mechanics Reviews*, vol. 66, no. 6, 2014.

[78] R. Talreja, *Fatigue of composite materials*. PhD thesis, 1987.

[79] B. F. Sørensen, "The critical damage state controlling the tension-tension fatigue life of unidirectional fibre composites," *Composites Science and Technology*, vol. 172, no. December 2018, pp. 172–181, 2019.

[80] B. Aidi, M. K. Philen, and S. W. Case, "Progressive damage assessment of centrally notched composite specimens in fatigue," *Composites Part A: Applied Science and Manufacturing*, vol. 74, pp. 47–59, 2015.

[81] R. Ambu, F. Aymerich, and F. Bertolino, "Investigation of the effect of damage on the strength of notched composite laminates by digital image correlation," *The Journal of Strain Analysis for Engineering Design*, vol. 40, no. 5, pp. 451–461, 2005.

[82] R. Talreja, "A conceptual framework for interpretation of MMC fatigue," *Materials Science and Engineering: A*, vol. 200, no. 1-2, pp. 21–28, 1995.

[83] P. A. Carraro, L. Maragoni, and M. Quaresimin, "Prediction of the crack density evolution in multidirectional laminates under fatigue loadings," *Composites Science and Technology*, vol. 145, pp. 24–39, 2017.

[84] K. Schulte, "Stiffness reduction and development of longitudinal cracks during fatigue loading of composite laminates," in *Mechanical characterization of load bearing fibre composite laminates* (A. H. Cardon and G. Verchery, eds.), pp. 36–54, Elsevier, 1984.

[85] S. M. Spearing, P. W. R. Beaumont, and M. T. Kortschot, "The fatigue damage mechanics of notched carbon-fiber peek laminates," *Composites*, vol. 23, no. 5, pp. 305–311, 1992.

[86] S. M. Spearing and P. W. R. Beaumont, "Fatigue damage mechanics of composite materials. I: Experimental measurement of damage and post-fatigue properties," *Composites Science and Technology*, vol. 44, no. 2, pp. 159–168, 1992.

[87] S. M. Spearing, P. W. R. Beaumont, and M. F. Ashby, "Fatigue damage mechanics of composite materials. II: A damage growth model," *Composites Science and Technology*, vol. 44, pp. 169–177, jan 1992.

[88] F. Aymerich and S. Found, "Response of notched carbon/PEEK and carbon/epoxy laminates subjected to tension fatigue loading," *Fatigue & Fracture Of Engineering Materials & Structures*, pp. 675–683, 2000.

[89] O. J. Nixon-Pearson and S. R. Hallett, "An investigation into the damage development and residual strengths of open-hole specimens in fatigue," *Composites Part A*, vol. 69, pp. 266–278, 2015.

[90] J. Llobet, P. Maimí, J. A. Mayugo, Y. Essa, and F. Martin de la Escalera, "A fatigue damage and residual strength model for unidirectional carbon/epoxy composites under on-axis tension-tension loadings," *International Journal of Fatigue*, vol. 103, pp. 508–515, 2017.

[91] J. Llobet, P. Maimí, Y. Essa, and F. Martin de la Escalera, "Progressive matrix cracking in carbon/epoxy cross-ply laminates under static and fatigue loading," *International Journal of Fatigue*, vol. 119, pp. 330–337, 2018.

[92] C. G. Dávila and P. P. Camanho, "Failure Criteria for FRP Laminates in Plane Stress," tech. rep., National Aeronautics and Aerospace Administration, 2003.

[93] ABAQUS, "Abaqus 6.14 Online Documentation," 2014.

[94] A. Turon, J. Costa, P. P. Camanho, and C. G. Dávila, "Simulation of delamination in composites under high-cycle fatigue," *Composites Part A: Applied Science and Manufacturing*, vol. 38, no. 11, pp. 2270–2282, 2007.

[95] E. V. González, P. Maimí, E. Martín-Santos, A. Soto, P. Cruz, F. Martín de la Escalera, and J. R. Sainz de Aja, "Simulating drop-weight impact and compression after impact tests on composite laminates using conventional shell finite elements," *International Journal of Solids and Structures*, vol. 145, pp. 230–247, 2018.

[96] A. Soto, E. V. González, P. Maimí, F. Martín de la Escalera, J. R. Sainz de Aja, and E. Alvarez, "Low velocity impact and compression after impact simulation of thin ply laminates," *Composites Part A: Applied Science and Manufacturing*, vol. 109, no. March, pp. 413–427, 2018.

[97] A. Soto, E. V. González, P. Maimí, J. A. Mayugo, P. R. Pasquali, and P. P. Camanho, "A methodology to simulate low velocity impact and compression after impact in large composite stiffened panels," *Composite Structures*, vol. 204, no. February, pp. 223–238, 2018.

[98] J. Lemaitre, "A Course on Damage Mechanics," Springer-Verlag Berlin Heidelberg, 1992.

[99] P. Ladevèze, "A computational mesodamage model for life prediction for laminates," in *Fatigue in composite materials* (B. Harris, ed.), ch. Chapter 15, Woodhead Publishing Limited, 2003.

[100] G. Lubineau and P. Ladevèze, "Towards a micromechanics-based damage mesomodel for CFRP laminates under thermomechanical cyclic loading," *Science and Engineering of Composite Materials*, vol. 12, no. 1-2, pp. 71–82, 2005.

[101] G. Lubineau, P. Ladevèze, and D. Violeau, "Durability of CFRP laminates under thermomechanical loading: A micro - meso damage model," *Composites Science and Technology*, vol. 66, pp. 983–992, 2006.

[102] F. A. Leone, "Deformation gradient tensor decomposition for representing matrix cracks in fiber-reinforced materials," *Composites Part A: Applied Science and Manufacturing*, vol. 76, pp. 334–341, 2015.

[103] P. P. Camanho, M. A. Bessa, G. Catalanotti, M. Vogler, and R. Rolfes, "Modeling the inelastic deformation and fracture of polymer composites – Part II: Smeared crack model," *Mechanics of Materials*, vol. 59, pp. 36–49, 2013.

[104] F. P. Van Der Meer and L. J. Sluys, "Continuum Models for the Analysis of Progressive Failure in Composite Laminates," *Journal of Composite Materials*, vol. 43, no. 20, pp. 2131–2156, 2009.

[105] K. Song, Y. Li, and C. A. Rose, "Continuum Damage Mechanics Models for the Analysis of Progressive Failure in Open-Hole Tension Laminates," *American institute of Aeronautics and Astronautics*, pp. 1–18, 2011.

[106] C. A. Rose, C. G. Dávila, and F. A. Leone, "Analysis Methods for Progressive Damage of Composite Structures," *NASA Langley Research Center*, vol. NASA/TM-20, 2013.

[107] A. Turon, B. L. V. Bak, E. Lindgaard, C. Sarrado, and E. Lund, "Interface elements for fatigue-driven delaminations in advanced composite materials," in *Numerical Modelling of Failure in Advanced Composite Materials* (S. Camanho, P.P., Hallet, ed.), ch. 3, pp. 73–91, Woodhead Publishing Series in Composite Science and Engineering, 2015.

[108] E. K. Gamstedt and B. A. Sjögren, "An experimental investigation of the sequence effect in block amplitude loading of cross-ply composite laminates," *International Journal of Fatigue*, vol. 24, pp. 437–446, 2002.

[109] W. Van Paepegem and J. Degrieck, "Effects of load sequence and block loading on the fatigue response of fiber-reinforced composites," *Mechanics of Advanced Materials and Structures*, vol. 9, no. 1, pp. 19–35, 2002.

[110] W. Van Paepegem, I. De Baere, and J. Degrieck, "Modelling the nonlinear shear stress-strain response of glass fibre-reinforced composites. Part I: Experimental results," *Composites Science and Technology*, vol. 66, no. 10, pp. 1455–1464, 2006.

[111] W. Van Paepegem, I. De Baere, and J. Degrieck, "Modelling the nonlinear shear stress-strain response of glass fibre-reinforced composites. Part II: Model development and finite element simulations," *Composites Science and Technology*, vol. 66, no. 10, pp. 1465–1478, 2006.

[112] F. P. Van der Meer and L. J. Sluys, "Mesh-independent modeling of both distributed and discrete matrix cracking in interaction with delamination in composites," *Engineering Fracture Mechanics*, vol. 77, no. 4, pp. 719–735, 2010.

[113] F. P. Van der Meer, L. J. Sluys, S. R. Hallett, and M. R. Wisnom, "Computational modeling of complex failure mechanisms in laminates," *Journal of Composite Materials*, vol. 46, no. 5, pp. 603–623, 2012.

[114] E. V. Iarve, K. Hoos, M. Braginsky, E. Zhou, and D. H. Mollenhauer, "Progressive failure simulation in laminated composites under fatigue loading by using discrete damage modeling," *Journal of Composite Materials*, vol. 51, no. 15, pp. 2143–2161, 2016.

[115] V. Achard, C. Bouvet, B. Castanié, and C. Chirol, "Discrete ply modelling of open hole tensile tests," *Composite Structures*, vol. 113, no. 1, pp. 369–381, 2014.

[116] M. Q. Le, H. Bainier, D. Néron, C. Ha-Minh, and P. Ladevèze, "On matrix cracking and splits modeling in laminated composites," *Composites Part A: Applied Science and Manufacturing*, vol. 115, no. September, pp. 294–301, 2018.

[117] W. Van Paepegem, "The cycle jump concept for modelling high-cycle fatigue in composite materials," in *Fatigue of Textile Composites* (V. Carvelli and S. V. Lomov, eds.), ch. 2, Elsevier, 2015.

Appendix. Publications

Paper A

A fatigue damage and residual strength model for unidirectional carbon/epoxy composites under on-axis tension-tension loadings

J. Llobet[a], P. Maimí[a], J.A. Mayugo[a], Y.Essa[b], F. Martin de la Escalera[b]

[a] AMADE, Polytechnic School, Universitat de Girona, Girona, Spain

[b] AERNNOVA Engineering Division, Structural Integrity Department, Madrid, Spain

The paper has been published in
International Journal of Fatigue Vol. 103, pp. 508–515, 2017.

International Journal of Fatigue 103 (2017) 508–515

Contents lists available at ScienceDirect

International Journal of Fatigue

journal homepage: www.elsevier.com/locate/ijfatigue

A fatigue damage and residual strength model for unidirectional carbon/epoxy composites under on-axis tension-tension loadings

J. Llobet [a,*], P. Maimí [a], J.A. Mayugo [a], Y. Essa [b], F. Martin de la Escalera [b]

[a] AMADE, Mechanical Engineering and Industrial Construction Department, Universitat de Girona, Carrer Universitat de Girona 4, E-17003 Girona, Spain
[b] AERNNOVA Engineering Division, Structural Integrity Department, 20 Manoteras Avenue – Building B, E-28050 Madrid, Spain

ARTICLE INFO

Article history:
Received 22 March 2017
Received in revised form 16 June 2017
Accepted 18 June 2017
Available online 23 June 2017

Keywords:
Fibre reinforced material
Damage
Fatigue strength
Fatigue test methods
S-N curves

ABSTRACT

Fibre-reinforced composites experience a degradation of stiffness and strength during fatigue life. Understanding the reduction of these properties is fundamental to establish a reliable fatigue life prediction methodology. This work investigates the loss of stiffness and strength in advanced unidirectional carbon/epoxy laminates under on-axis tension-tension loads. A phenomenological stiffness-based fatigue model is formulated within the framework of continuum damage mechanics, where damage is described by the reduction of the in-plane longitudinal stiffness. The particularity of the model is to assume that the ultimate strain remains constant after fatigue damage. Thus, the residual strength model and the S-N curves are deduced from the residual stiffness model. This assumption reduces the experimental characterization of phenomenological-based approaches. The experimental challenges found in the fatigue experiments are also discussed. The accuracy of the model is verified by comparing the experimental data with the derived S-N curves.

1. Introduction

When a material is subjected to cyclic stresses, below its ultimate static strength, the response is assumed to be linear elastic. But if these cyclic stresses are repeated a sufficient number of times, the material properties degrade as microcracks nucleate and grow. This phenomenon is known as fatigue. Fatigue is widely studied in metals, mainly because fatigue loads reduce the ductility of metals resulting in a dangerous brittle failure. In metals, the main cause of fatigue degradation is the growth of a single dominant crack, which initiates from specific imperfections in the material structure and propagates perpendicularly to the loading direction. The initiation and propagation of this crack can be predicted reasonably well by the total-life and damage tolerance models, respectively [1]. In composites, fatigue damage is much more complex due to their heterogeneous and anisotropic nature, and involves the interaction of different mechanisms that are spatially distributed. This widespread damage is accompanied by stress redistribution and a large amount of dissipated energy.

In general, composite structures present an exceptional fatigue performance when compared with their metal counterparts [2–4]. In this regard, the substitution of metallic alloys by composites was a success in the aircraft industry. Currently, fatigue is not considered a key design parameter in many aerospace components [2], since composites can withstand large number of fatigue cycles, and damage does not usually increase at design strain levels (in the order of 4000 $\mu\varepsilon$ [5]). However, the lack of reliable fatigue life prediction methodologies and the need for increasing the design strain limits, entail that the no-growth design philosophy cannot be guaranteed.

According to Degrieck and Van Paepegem [6], fatigue life models (based on S-N curves), phenomenological models for residual stiffness/strength and progressive damage models (or mechanistic models) are the three fatigue modelling approaches for fibre-reinforced composite materials. Phenomenological stiffness and strength-based models are commonly used in the literature [7,8], and are selected as the framework for the current fatigue model. The stiffness is frequently used as a potential non-destructive parameter to monitor the damage progress in a structural component. Nevertheless, stiffness-based damage models present the drawback of not having a clear failure criterion unlike strength-based models. Many authors assume a failure condition which is seen as a relation between the residual stiffness and the residual strength [9–11].

For multilayered composites, usually a three-stage stiffness degradation curve is reported [12]. The first stage corresponds to transverse matrix cracks at off-axis plies. The second stage, where the stiffness loss is linear with respect to the number of cycles, marks the presence of matrix cracks at on-axis plies along with

* Corresponding author.
E-mail address: jordi.llobet@udg.edu (J. Llobet).

http://dx.doi.org/10.1016/j.ijfatigue.2017.06.026
0142-1123/

some delaminations. Finally, the last stage corresponds to fibre failure where most of the stiffness is lost. Unidirectional (UD) laminates only present two clear stages, a first linear stage corresponding to some fibre breakage and matrix cracks, and a second stage where the stiffness drops abruptly.

This work presents a phenomenological fatigue model to predict residual stiffness, residual strength and life of UD carbon/epoxy laminates under on-axis tension–tension fatigue loadings. The content of this paper is organized as follows. First, Section 2 reviews the experimental challenges found in the fatigue experiments. The key parameters that may affect the result of the test are analyzed. Section 3 introduces an appropriate test methodology to characterize the material in terms of stiffness and strength loss. Section 4 explains the fatigue modelling approach where the damage and residual strength models are formulated. The damage model describes the degradation of the stiffness due to fatigue by means of an integrity function defined in the tension-tension range of cyclic stresses. The static strength is also weakened when the material undergoes fatigue, and this weakening is described by the residual strength model. Both models are coupled by assuming a constant ultimate strain. This hypothesis reduces the experimental characterization and is appropriately validated for the material system considered in this study. The fatigue lives predicted by the model are compared to the experimental S-N data. Finally, Section 5 presents a master curve to foresee the fatigue damage evolution in terms of the applied strain.

2. Review of experimental challenges

Most articles on experimental fatigue focus on the behavior of cross-ply and quasi-isotropic laminates [13–17], either to assess the residual effective properties or to investigate the sequence and extent of damage development throughout their lifetime. Different techniques are used to characterize fatigue damage in a multidirectional laminate [18–20], mainly to analyse the presence of off-axis matrix cracks and delaminations. Nixon-Pearson et al. [18] used X-ray computed tomography with open-hole specimens, whereas Aidi et al. [19] monitored fatigue damage by combining X-ray radiography and Digital Image Correlation technique, and Montesano et al. [20] used thermography to analyse the influence of fatigue on the thermal field. However, some of these multidirectional laminates exhibit a fibre-dominated fatigue failure (or i.e., failure governed by longitudinal plies), where other damage forms such as matrix splitting, fibre/matrix debonding and fibre breaks are revealed. Several authors have centred on the fatigue behavior of UD laminates to understand this type of fibre-dominated failure mode [21–25].

Different fatigue tests are available for fibre-reinforced composites [26], but only tension-tension fatigue test with a constant-amplitude load has been standardized in both ASTM and ISO standards [27,28]. Anoshkin and Zuiko [29] presented all fatigue test methods for fibre-reinforced polymer composites from the most well-established international organizations. The lack of standard fatigue test methods gives rise to discrepancies when comparing experimental data, for instance, De Baere et al. reported different fatigue lives from rectangular-shaped and dumbbell-shaped specimens [13,14]. Other authors remarked that the loading frequency also affects the fatigue life [26,30].

2.1. Effect of gripping, specimen geometry and tabs

The main concern in all fatigue tests is to ensure a smooth introduction of the tensile load through shear forces, minimize the stress concentration in the tabbed section [31–33], but also avoid specimen slippage within the grips. This stress concentration depends on various factors, such as the geometry, the orthotropic nature of the material used (tab and specimen), gripping pressure, and adhesive. It is known that fatigue failure occurs frequently underneath the tabbed section, particularly when rectangular specimens with fibre-dominated stacking sequences are loaded at high stress levels [13,26].

In practice, shear forces are applied through friction by means of the wedge grips, which clamp the specimen surfaces at each end. The wedge grips provide a constant, hydraulically actuated preload regardless of the applied test load. This preload is adjustable to prevent specimen damage or specimen slippage during the test. Under tensile loads, the wedge principle increases the gripping force proportionally to the load applied to the specimen. However, under compressive loads the preload withstands the wedge and guarantees a minimum gripping force (Fig. 1) [34].

The gripping force applied to the specimen through the wedge grips is given by the expression [35,36]:

$$P = \frac{F}{2}\left(\frac{\cos\alpha - \mu\sin\alpha}{\sin\alpha + \mu\cos\alpha}\right) + R_A\left(\frac{\cos\alpha(1-\mu^2) - 2\mu\sin\alpha}{\sin\alpha + \mu\cos\alpha}\right) \quad (1)$$

where P is the gripping force, F is the applied load, R_A is the preload, μ is the friction coefficient and α is the angle of the wedge.

In composite materials, high clamping forces can result in excessive through-the-thickness compressive stresses, and crushing of the specimen in the gripped regions. To minimize the clamping load, grip surface roughness is increased by means of serrated grip faces which indent the surface of the tabs. In the worst-case scenario, the magnitude of the applied load can reach $F = X_T wt$, where X_T is the ultimate tensile strength, w and t are the specimen width and thickness, respectively. Then, the gripping force should satisfy the following condition:

$$P < Y_C w l_{tab} \quad (2)$$

where l_{tab} is the tab length and Y_C is the transverse compressive strength. Once the maximum gripping force is obtained, the no slip condition is ensured only if the following expression holds:

$$\mu_0 \geqslant F/2P \quad (3)$$

where μ_0 is the friction coefficient between the grip and the tab. Bailey and Lafferty [30] reported $\mu_0 \geqslant 0.43$ for metal specimens. For composites, De Baere et al. [36] and Adams [37] computed a minimum friction coefficient of $\mu_0 = 0.33$. The mean shear stress transferred through the tab can be computed as:

$$\tau = \frac{\sigma t}{2 l_{tab}} \quad (4)$$

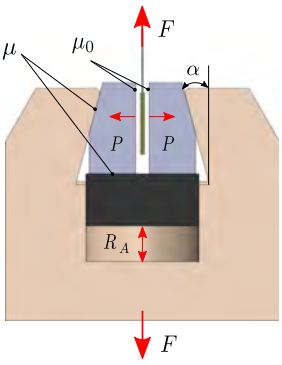

Fig. 1. MTS wedge grips mechanism.

where σ is the applied tensile stress. The use of thin specimens and long tabs is recommended to decrease the mean shear stress. But, this shear stress is not distributed uniformly throughout the tab and lengthening the tab beyond 60 mm is not effective [31,37]. Then, the tab length l_{tab} is usually derived to avoid shear failure of the adhesive at the ultimate tensile stress X_T [36].

Some authors have studied the effects of different tab geometries and materials on the stress concentration underneath the end-tab by means of finite element simulations. De Baere et al. [36] concluded that, a chamfered GFRP $[\pm 45]_{4s}$ tab gave lowest stress concentration factor, but they finally used a straight cross-ply tab of the same specimen material due to the poor bond between the GFRP tab and the carbon/PPS woven fabric specimen. Adams [37] and Kulakov et al. [31] reported slightly lower stress concentration factors for an UD carbon/epoxy and a cross-ply woven GFRP tab. The use of chamfered tabs or not gripping the whole tab length is not recommended because of the adhesive failure [13].

Note that the stress concentration can also be reduced by decreasing the specimen gauge section (typically used in fatigue of metals). Then, the mean shear stress can be rewritten as:

$$\tau = \frac{\sigma t}{2 l_{tab}} \left(\frac{w_c}{w_t} \right) \tag{5}$$

where w_c and w_t are the specimen and tab width, respectively. De Baere et al. [13,14] found that dumbbell-type specimens resulted in longer fatigue lives than rectangular specimens. They assessed the limitations of the standard rectangular geometry (ASTM D3479 [27]), and observed that most specimens failed in the tabbed section which suggests an underestimation of the fatigue life. On the contrary, other authors [37–39] suggested that rectangular specimens usually perform better in fatigue experiments, since they do not develop longitudinal splits like in dumbbell specimens [14].

2.2. Test control mode

Fatigue experiments are usually controlled by a load, displacement or strain signal. In the case of load-controlled fatigue (ASTM D3479 procedure A [27]), the grip displacement usually increases during the test as the stiffness of the specimen decreases. The specimen fails once it can no longer withstand the applied load. This control mode is the most commonly used in fatigue testing, especially to derive the standard S-N curves, to examine the load sequence effect on fatigue life and also to apply real spectrum loading patterns [40–43].

Strain-controlled fatigue is more useful to study the damage evolution process (ASTM D3479 procedure B [27]), although the specimen may not fail as decreasing the stiffness leads to decreasing the load. However, the measure of real-time strains during fatigue testing is troublesome. The applicability of different strain measurement techniques for fatigue testing is discussed in [26,44]. Any contact strain measurement technique should be restricted to an intact specimen surface. For laminates that suffer from surface damage under fatigue loading (typically observed in lay-ups with 0^0 outer plies), the best option is to interrupt the fatigue test and measure the strain quasi-statically [45,46]. However, the strain signal cannot be measured in real-time and the test cannot be performed under strain control.

Displacement-controlled fatigue through the piston displacement must also be avoided [30,44], not only because this measurement is affected by the compliance of the actuator and grip body, but also because specimen slippage within the grips can incorrectly be associated with stiffness loss. This control mode should be restricted to bending fatigue or when the specimen stiffness is relatively smaller compared to the test frame.

2.3. Cyclic load definition

Due to the complexity of applying a real in-service fatigue loading, the cyclic load used in the experiments is usually simplified by assuming a sinusoidal waveform of a particular frequency. The frequency is a limiting factor in testing of composites and can have a major impact on fatigue life. Self-heating effects, either through viscoelastic heating or energy release due to micro-fractures, result in a temperature rise in the material. Since the matrix material is usually viscoelastic, the fatigue life is considerably decreased. This is a common phenomenon observed with cross-ply and $[\pm 45]$ laminates, but is not relevant in UDs. The frequency is usually selected as a compromise between the expected heat generation and the duration of the test. A frequency range of 1–10 Hz is typically used in the literature.

A cyclic load can be defined by different stress measures: $\sigma_m, \sigma_a, \sigma_{max}, \sigma_{min}, R$ and K (refer to Table 1). Most research works make use of stress ratio R, but stress ratio K presents mathematical advantages, for instance, K does not show discontinuities with respect to the mean stress which simplifies its use in a finite element code [47]. The stress ratio indicates the nature of the cyclic stress (tension-tension, compression-compression or tension-compression loadings) and plays a major role into the fatigue behavior of composites [23,26].

3. Experimental work

3.1. Material

The material investigated in this study is a carbon/epoxy UD pre-preg (Hexcel® M21E/IMA-12K) of 0.184 mm, where the resin M21E is toughened by thermoplastic particles. The laminate consists of six UD plies that leads to a nominal thickness of 1.104 mm. The laminate was molded and cured in an autoclave under standard aeronautical conditions. The quality of the panel was verified using ultrasonic C-scan inspection. Specimens of $250 \times 15 \times 1.104$ mm were cut using a diamond coated disk. GFRP $[0/90]_{ns}$ straight tabs with dimensions 60×15 mm were bonded using Hysol 9497 epoxy adhesive. Whereas the adhesive ultimate shear strength is about 32 MPa, the mean shear stress computed from Eq. (4) at the ultimate load is about 28 MPa for this tab dimensions. The undamaged elastic and strength properties $E_1^0 = 160.8$ GPa, $\nu_{12} = 0.34$ and $X_T^0 = 3048$ MPa were obtained following the standard ASTM D3039 [48].

3.2. Test set-up

All tests were performed on a 250 kN servo-hydraulic test machine MTS 810 at room temperature. The hydraulic preload pressure was set to 7 MPa ($R_A = 35$ kN), resulting in a gripping pressure of 200 MPa at the ultimate tensile load ($P = 180$ kN from Eq. (1)). This grip pressure guarantees the inequality condition from Eq. (2), yielding a minimum friction coefficient $\mu_0 \geqslant 0.28$ from Eq. (3).

The strain was measured by two means, a contact clip-on mechanical extensometer and Digital Image Correlation (DIC)

Table 1
Cyclic stress definition.

Mean stress	$\sigma_m = \frac{\sigma_{max}+\sigma_{min}}{2}$
Amplitude stress	$\sigma_a = \frac{\sigma_{max}-\sigma_{min}}{2}$
Stress ratio R	$R = \frac{\sigma_{min}}{\sigma_{max}}$
Stress ratio K	$K = \frac{\sigma_m}{\sigma_a} = \frac{\sigma_{max}+\sigma_{min}}{\sigma_{max}-\sigma_{min}} = \frac{1+R}{1-R}$

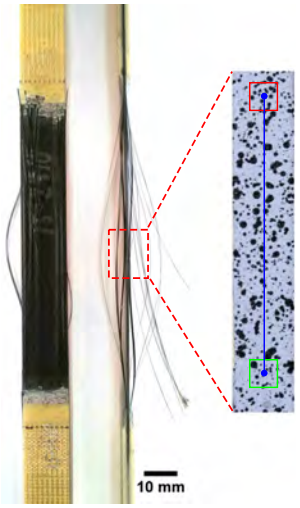

Fig. 2. Specimen top and lateral view (left), and monitored area by DIC (right) at $\Sigma_{max} = 0.75$ and $N = 50,000$ cycles.

system. A 5 MPx camera was placed approximately 150 mm from the specimen, tracking an area of 1×10 mm^2. The speckle pattern was painted on the specimen edge surface with an airbrush (see Fig. 2). As is mentioned in Section 2.2, the measure of real-time strains is not straightforward during fatigue testing. But by using DIC on the lateral surface seems to be a good solution when the specimen presents surface damage, at least under static conditions. Fortunately, this surface remained intact during almost the whole duration of the test.

3.3. Test procedure

The test follows procedure A of ASTM D3479 [27] and is in line with Brunbauer et al. [45,46] to characterize the fatigue damage in CFRP laminates through the quasi-static measure of the stiffness. The test starts with a displacement-controlled quasi-static test to measure the initial stiffness of the undamaged specimen (E_1^0). Then, a load-controlled fatigue test is performed within a selected number of cycles and the stiffness is measured again quasi-statically. The quasi-static test is run below the mean cyclic displacement in order to avoid causing additional damage. This procedure is repeated until fatigue failure occurs or the test is interrupted at 2 million cycles. After this limit, the specimen is tested up to failure to obtain the residual strength. Note that the usual range of composite fatigue data is in between 10^4 and 10^7 loading cycles [2,9,44], though some applications in the wind power industry may experience longer fatigue lives ($> 10^8$ cycles) [43].

3.4. Load cases

The load cases used to characterize the material are summarized in Table 2, where $\Sigma_{max} = \sigma_{max}/X_T^0$ is the normalized maximum stress applied to each specimen. m, N_F and X_T^r indicate the measurements performed on each specimen: stiffness loss, cycles-to-failure and residual strength, respectively.

Table 2
Summary of fatigue tests and measurements, where m, N_F and X_T^r indicate stiffness loss, number of cycles-to-failure and residual strength, respectively.

Σ_{max} \ $R\ (K)$	0.1 (1.22)	0.2 (1.50)	0.3 (1.86)	0.5 (3.00)
0.875	m/N_F	m/N_F	-	m/N_F
0.750	m/N_F	m/N_F	m/N_F	m/X_T^r
0.625	m/X_T^r	m/X_T^r	-	-
0.500	m/X_T^r	-	-	-

4. Results and modelling of fatigue damage and residual strength evolution

4.1. Fatigue damage model

The uniaxial constitutive equation for a UD laminate can be expressed as $\sigma = mE_1^0\varepsilon$, or $\Sigma = m\Phi$ in dimensionless form, where $\Sigma = \sigma/X_T^0$ is the normalized stress and $\Phi = \varepsilon E_1^0/X_T^0$ is the normalized strain. The integrity variable m defines the stiffness reduction $m = E_1/E_1^0$, and is commonly known as the complementary damage variable $m = 1 - d$ in Continuum Damage Mechanics.

On-axis quasi-static tensile loads do not degrade the material properties of UD plies prior to failure, and therefore, the ultimate strength and strain of an undamaged material are reached when $\Sigma = \Phi = 1$. Under fatigue loadings, the integrity function determines the loss of stiffness as:

$$\frac{\partial m}{\partial N} = -\frac{m^{1-B}}{AB}\tilde{\Sigma}^{\eta} \tag{6}$$

where $\tilde{\Sigma}$ is a stress measure defined in the range of stress ratios $K > 1$ as:

$$\tilde{\Sigma} = \frac{\Sigma_{max}}{K^{\tilde{\gamma}}} \tag{7}$$

with Σ_{max} being the normalized maximum stress, K the stress ratio and A, B, η and γ the four material constants. Kawai [9] proposed a similar damage evolution function, but defining $\tilde{\Sigma}$ in the range of stress ratios $|R| \geqslant 1$ and accounting for multi-axial in-plane loadings. Eq. (6) only distinguishes between the damage increase under different uni-axial stress levels and stress ratios ($K > 1$). Integrating Eq. (6) for a constant-amplitude load results in:

$$m = \left(m_0^B - \Delta N\frac{\tilde{\Sigma}^{\eta}}{A}\right)^{1/B} \tag{8}$$

where m_0 is the current value of the damage variable before applying ΔN cycles with a prescribed Σ_{max} and K.

Fig. 3 illustrates the experimental fatigue data and the corresponding fitted integrity functions for different stress levels and constant stress ratio $K = 1.22$. At stress levels $\Sigma_{max} \leq 0.5$, the measured damage is negligible up to 2 million cycles. However, fatigue damage is severe at stress levels $\Sigma_{max} \geqslant 0.75$ and many specimens failed at the tabbed section. These failure modes are considered to be an underestimation of the experimental fatigue life and they should be interpreted carefully. Fig. 4 shows how fatigue life increases with the stress ratio when maximum stress is kept con-

stant. The best fitting parameters of Eq. (8) for the conducted tests are summarized in Table 3.

4.2. Residual strength model

Residual strength models define the reduction of the static strength due to fatigue damage [7,49,50]. The residual strength X_T^r is usually characterized for a particular stress level and fraction of life, and few are the cases that investigate various stress levels throughout the entire fatigue life. The creation of such experimental data is extremely expensive and time consuming. Even an in-detail residual strength characterization at a single stress ratio requires several times the effort necessary for the determination of a single S-N curve [50].

A common hypothesis is to consider that fatigue damage does not change the ultimate static strain [10,11,51,52]. Hence, the following failure criterion can be defined:

$$\Phi \leqslant 1 \quad \text{or} \quad \Sigma \leqslant m \tag{9}$$

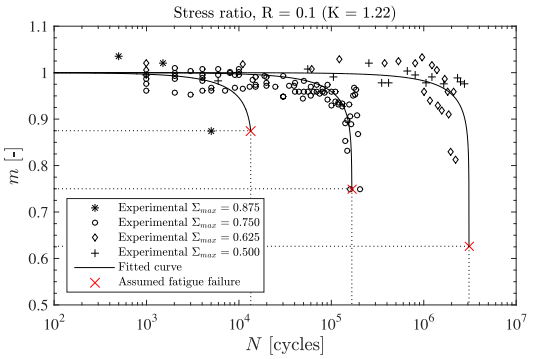

Fig. 3. Integrity functions for different stress levels and constant stress ratio $K = 1.22$.

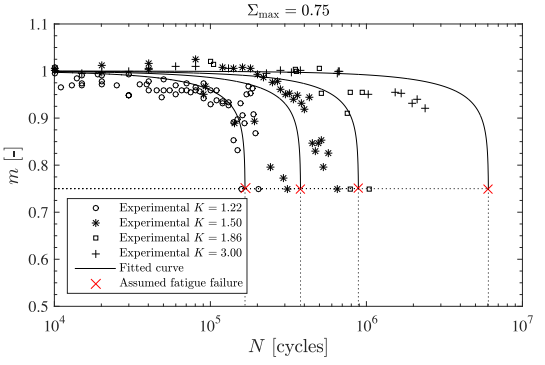

Fig. 4. Integrity functions for constant stress level $\Sigma_{max} = 0.75$ and different stress ratios.

Table 3
Fitted material constants.

$A = 750$	$B = 22$	$\eta = 16$	$\gamma = 4$

In contrast, Kawai [9] supposed fatigue failure when $m = 0$, which yields to the well-known Basquin's equation $N_F = A/\tilde{\Sigma}^\eta$ [53]. This expression appears as a straight line of slope η in a log-log plot. Interestingly, Kawai et al. [54,55] reported η between 15 and 22 depending on the material configuration and herein it is deduced $\eta = 16$. Nevertheless, the current model considers that fatigue damage occurs prior to $\Sigma_{max} = m$, when the ultimate strain is reached, and the material fractures statically. Two damage modes are clearly distinguished, distributed damage due to fatigue and localized static damage corresponding to the last loading cycles. The integrity function aims to describe the fatigue damage until $\Sigma_{max} = m$ (red[1] crosses in Figs. 3 and 4).

The assumption of a constant strain-to-failure entails that the residual strength evolves in the same manner as the residual stiffness, thus both models are coupled and described by Eq. (8). In order to validate this hypothesis, Fig. 5 illustrates the residual strain $\Phi_{max} = \Sigma_{max}/m$ obtained at different states of fatigue damage $1 - m$. When the residual strain is within the scatter of the ultimate static strain the hypothesis is acceptable. Obviously, specimens fractured under fatigue show the last measured point before failure, and therefore the residual strain is underestimated.

4.3. S-N curves

A S-N curve estimates the necessary number of cycles-to-failure under a constant-amplitude load control test. In this regard, residual strength models provide that failure occurs when the residual strength equals the maximum cyclic stress. The concept of strain equivalence assumed in this model suggests a different interpretation of failure as stated by Van Paepegem: "*Fatigue failure occurs when the effective stress $\tilde{\sigma} = \frac{\sigma}{m}$ equals the initial static strength X_T (or i.e., the static strength only decreases apparently during fatigue)*" [10]. Accordingly, the S-N curve is derived from Eq. (8) imposing $m = \Sigma_{max}$ as:

$$\Delta N_F = \frac{A}{\tilde{\Sigma}^\eta}\left(m_0^B - \Sigma_{max}^B\right) \tag{10}$$

The experimental fatigue lives and the life predictions of Eq. (10) are compared in Fig. 6.

5. Fatigue damage evolution under constant strain

The integrity function (either the residual stiffness or strength) can be rewritten in terms of strains as:

$$\frac{\partial m}{\partial N} = -\frac{m^{1+\eta-B}}{AB}\frac{\Phi_{max}^\eta}{K^\gamma} \tag{11}$$

This expression can be integrated assuming a constant-amplitude strain as:

$$m = \left(m_0^{B-\eta} - \Delta N\left(1 - \frac{\eta}{B}\right)\frac{\Phi_{max}^\eta}{AK^\gamma}\right)^{\frac{1}{B-\eta}} \tag{12}$$

A variable load-control test to keep a constant cyclic strain is used to avoid all the difficulties caused by strain-control fatigue testing. This approach allows the load to be decreased proportionally to the stiffness ($\Phi = \Sigma/m = \text{const}$), and thereby reproducing the behavior of a strain-control test. The derived integrity functions (Eqs. (8) and (12)) are compared with the experimental data of a constant-stress $\Sigma_{max} = 0.75$ and a constant-strain $\Phi_{max} = 0.75$ test, respectively. In the strain-controlled test, m was measured at intervals of $\Delta N = 5000$ cycles and the load was recalculated. After 250,000 cycles, the presence of surface damage did not allow the

[1] For interpretation of color in 'Figs. 3 and 4', the reader is referred to the web version of this article.

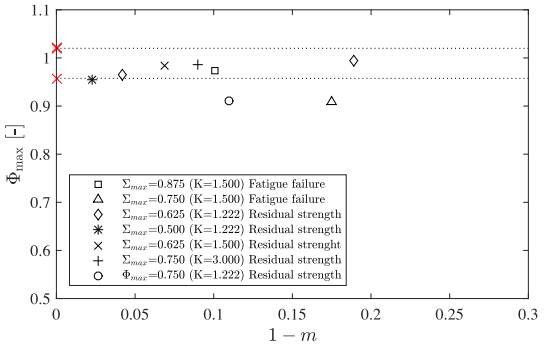

Fig. 5. Normalized ultimate strain (Φ_{max}) against damage ($d = 1 - m$).

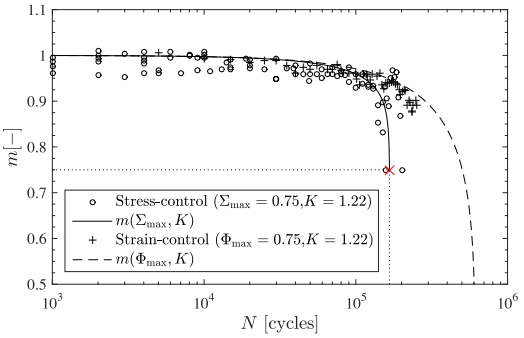

Fig. 7. Constant-stress vs. constant-strain controlled fatigue testing.

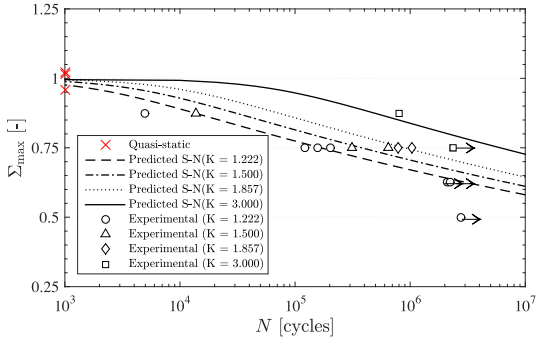

Fig. 6. Experimental vs. fitted S-N curves.

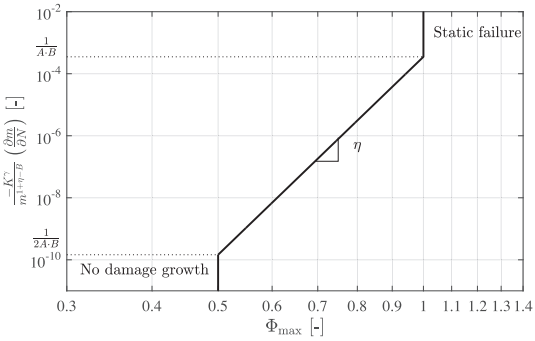

Fig. 8. Damage growth rate per cycle vs. normalized strain.

measurement of the strain. If the constant ultimate strain hypothesis is valid (refer to Fig. 5 with $\Phi_{max} = 0.75$), damage does not localize under a constant-strain cyclic load. This means that distributed damage grows but a mesocrack is never nucleated as the material never reaches the ultimate static strain.

In accordance with Talreja [21,22,56], when the maximum strain applied Φ_{max} is lower than a threshold value, the damage growth rate is zero $\frac{\partial m}{\partial N} = 0$. This corresponds to the infinite life region of Talreja's strain-life diagram [22], where no damage initiates or grows. This endurance fatigue limit, related with the fatigue properties of the matrix, is usually higher than 6000 $\mu\varepsilon$ for advanced carbon/epoxy composites [57]. For the material under study, this limit is close to 9000 $\mu\varepsilon$ ($\Phi = 0.5$). However, it is not reasonable to set this limit without performing longer fatigue tests (see Fig. 7).

Eq. (11) can be interpreted and represented as a master curve to foresee the fatigue damage evolution of UD plies in terms of the normalized strain applied (Fig. 8). Whereas below a certain strain threshold fatigue damage is null, as defined by Talreja, above this threshold the rate of fatigue damage increases according to a power law. For large enough strains the material fractures statically. Since Eq. (11) depends on the stress ratio K and the damage state m, these factors also appear in the master curve. Parameter η represents the slope of the master curve as in Basquin's equation.

6. Conclusions

An experimental investigation to characterize the residual stiffness and strength was carried out in UD carbon/epoxy laminates under on-axis tension–tension fatigue loads. A test methodology was proposed to overcome the challenges and main difficulties found during the experiments.

In order to study the damage development under cyclic loadings, strain-controlled testing is more appropriate than load-controlled testing. However, the measure of real-time strains through a local sensor is particularly difficult for laminates undergoing surface damage. The piston displacement measure is also not recommended as it is affected by the compliance of the system, the non-linearity introduced by the end-tabs and the possibility of specimen slippage inside the grips. Consequently, the fatigue tests were set to load-control. Under these circumstances, one important implication of testing advanced carbon/epoxy UD laminates is that most specimens failed underneath the end-tab, so the fatigue life obtained in the experiments should be interpreted carefully. Despite lacking a widely-accepted solution, the key parameters used to minimize premature fatigue failures were discussed.

Phenomenological stiffness/strength based models always present the drawback of large amounts of fatigue testing to characterize the material properties.An in-detail residual strength characterization at different load levels and fractions of life is extremely expensive. However, assuming a constant strain-to-failure allows the residual stiffness to be related to the residual strength, and therefore the evolution of both properties is of the same magnitude. The stiffness is considered to be a potential variable to describe the fatigue damage, it is easy to characterize in a non-destructive test and also shows less scatter than residual strength.

The residual stiffness was chosen as the framework of the fatigue model. The stiffness loss curve for a carbon/epoxy UD laminate has been obtained showing two clear stages. A first linear stage that corresponds to some fibre breakage and matrix cracks, and a second stage where stiffness drops drastically from a linkage of failed fibre regions. It is especially difficult to measure the stiffness in the last cycles because of the specimen state of damage. The fatigue damage model postulates an integrity function to define the damage growth rate per cycle for any fatigue loading defined in the tension-tension range. This function is fitted with four material constants. Forcing the failure to occur under a constant ultimate strain, the residual stiffness and strength are known at any fraction of life, and life is predicted through the derived S-N curve. The life predictions were found to be in good agreement with experimental data except for load cases with high stress levels where tab failure was unavoidable.

Acknowledgements

This work has been funded by the Spanish Government (Ministerio de Economia y Competitividad) through the project entitled ABORDA under the contract RTC-2014-1958-4, and also through the contract MAT2013-46749-R.

References

[1] Suresh S. Fatigue of materials. Cambridge University Press; 2004.
[2] Bathias C. An engineering point of view about fatigue of polymer matrix composite materials. Int J Fatigue 2006;28(10):1094–9.
[3] Kaminski M, Laurin F, Maire JF. Fatigue damage modeling of composite structures: the ONERA viewpoint. J Aerosp Lab 2015;9.
[4] Alderliesten R. Critical review on the assessment of fatigue and fracture in composite materials and structures. Eng Fail Anal 2013;35:370–9.
[5] Davies AJ, Curtis PT. Fatigue in aerospace applications. In: Harris B, editor. Fatigue in composites. Woodhead Publishing Limited; 2003 [chapter 26].
[6] Degrieck J, Van Paepegem W. Fatigue damage modelling of fibre-reinforced composite materials: review. Appl Mech Rev 2001;54(4):279–300.
[7] Post NL, Lesko JJ, Case SW. Residual strength fatigue theories for composite materials. In: Vassilopoulos AP, editor. Fatigue life prediction of composites and composite structures. Woodhead Publishing Limited; 2010 [chapter 3].
[8] Van Paepegem W. Fatigue damage modelling of composite materials with the phenomenological residual stiffness approach. In: Vassilopoulos AP, editor. Fatigue life prediction of composites and composite structures. Woodhead Publishing Limited; 2010 [chapter 4].
[9] Kawai M. A phenomenological model for off-axis fatigue behavior of unidirectional polymer matrix composites under different stress ratios. Compos Part A: Appl Sci Manuf 2004;35:955–63.
[10] Van Paepegem W, Degrieck J. A new coupled approach of residual stiffness and strength for fatigue of fibre-reinforced composites. Int J Fatigue 2002;24(7):747–62.
[11] Zhang W, Zhou Z, Zhang B, Zhao S. A phenomenological fatigue life prediction model of glass fiber reinforced polymer composites. Mater Des 2015;66:77–81.
[12] Schulte K. Stiffness reduction and development of longitudinal cracks during fatigue loading of composite laminates. In: Cardon AH, Verchery G, editors. Mechanical characterization of load bearing fibre composite laminates. Elsevier Science; 1984. p. 36–54.
[13] De Baere I, Van Paepegem W, Quaresimin M, Degrieck J. On the tension-tension fatigue behaviour of a carbon reinforced thermoplastic Part I: Limitations of the ASTM D3039/D3479 standard. Polym Test 2011;30(6):625–32.
[14] De Baere I, Van Paepegem W, Hochard C, Degrieck J. On the tension-tension fatigue behaviour of a carbon reinforced thermoplastic Part II: Evaluation of a dumbbell-shaped specimen. Polym Test 2011;30(6):663–72.
[15] Tohgo K, Nakagawa S, Kageyama K. Fatigue behaviour of CFRP cross-ply laminates under on-axis and off-axis cyclic loading. Int J Fatigue 2006;28:1254–62.
[16] Reifsnider KL, Jamison R. Fracture of fatigue-loaded composite laminates. Int J Fatigue 1982;4(4):187–97.
[17] Berthelot JM, Le Corre JF. Modelling the transverse cracking in cross-ply laminates: application to fatigue. Compos Part B: Eng 1999;30(6):569–77.
[18] Nixon-Pearson OJ, Hallett SR. An investigation into the damage development and residual strengths of open-hole specimens in fatigue. Composites: Part A 2015;69:266–78.
[19] Aidi B, Philen MK, Case SW. Progressive damage assessment of centrally notched composite specimens in fatigue. Compos Part A: Appl Sci Manuf 2015;74:47–59.
[20] Montesano J, Fawaz Z, Bougherara H. Use of infrared thermography to investigate the fatigue behavior of a carbon fiber reinforced polymer composite. Compos Struct 2013;97:76–83.
[21] Gamstedt EK, Talreja R. Fatigue damage mechanisms in unidirectional carbon-fibre-reinforced plastics. J Mater Sci 1999;34(11):2535–46.
[22] Talreja R. Fatigue of composite materials: damage mechanisms and fatigue-life diagrams. Proc Roy Soc A: Math Phys Eng Sci 1981;378:461–75.
[23] El-Kadi H, Ellyin F. Effect of stress ratio on the fatigue of unidirectional glass fibre/epoxy composite laminae. Composites 1994;25(10):917–24.
[24] Curtis PT. Tensile fatigue mechanisms in unidirectional polymer matrix composite materials. Int J Fatigue 1991;13(5):377–82.
[25] Razvan A, Reifsnider KL. Fiber fracture and strength degradation in unidirectional graphite/epoxy composite materials. Theor Appl Fract Mech 1991;16(1):81–9.
[26] Van Paepegem W. Fatigue testing methods for polymer matrix composites. In: Guedes RM, editor. Creep and fatigue in polymer matrix composites. Woodhead Publishing Limited; 2011. p. 366–405 [chapter 16].
[27] ASTM D3479/3479M-12. Standard test method for tension-tension fatigue of polymer matrix composite materials. American Society for Testing and Materials.
[28] ISO 13003:2003. Fibre-reinforced plastics – determination of fatigue properties under cyclic loading conditions. International Standard Organization.
[29] Anoshkin AN, Zuiko VY. Experimental methods and standards for fatigue of fibre-reinforced composites. In: Carvelli V, Lomov SV, editors. Fatigue of textile composites. Woodhead Publishing Limited; 2015 [chapter 3].
[30] Bailey PBS, Lafferty AD. Specimen gripping effects in composites fatigue testing – concerns from initial investigation. Express Polym Lett 2015;9(5):480–8.
[31] Kulakov VL, Tarnopol'skii YM, Arnautov AK, Rytter J. Stress-strain state in the zone of load transfer in a composite specimen under uniaxial tension. Mech Compos Mater 2004;40(2):91–100.
[32] Portnov GG, Kulakov VL, Arnautov AK. A refined stress-strain analysis in the load transfer zone of flat specimens of high-strength unidirectional composites in uniaxial tension – 1. Theoretical analysis. Mech Compos Mater 2006;42(6):787–96.
[33] Portnov GG, Kulakov VL, Arnautov AK. A refined stress-strain analysis in the load transfer zone of flat specimens of high-strength unidirectional composites in uniaxial tension – 2. Finite-Element parametric analysis. Mech Compos Mater 2007;43(1):43–58.
[34] MTS Systems Corporation. Series 647 hydraulic wedge grips reference manual. Tech rep. MTS Systems Corporations; 2013.
[35] De Baere I, Van Paepegem W, Degrieck J. Design of mechanical clamps with extra long wedge grips for static and fatigue testing of composite materials in tension and compression. Exp Tech 2008;32(3):62–9.
[36] De Baere I, Van Paepegem W, Degrieck J. On the design of end tabs for quasi-static and fatigue testing of fibre-reinforced composites. Polym Compos 2009;30(4):381–90.
[37] Adams Daniel O, Adams Donald F. Tabbing guide for composite test specimens. Tech rep. Federal Aviation Administration; 2002.
[38] Curtis PT. Durability testing of polymer composites. In: Comprehensive composite materials. Elsevier; 2000. p. 163–82.
[39] Nijssen RPL. Phenomenological fatigue analysis and life modelling. In: Vassilopoulos AP, editor. Fatigue life prediction of composites and composite structures. Woodhead Publishing Limited; 2010 [chapter 2].
[40] Van Paepegem W, Degrieck J. Effects of load sequence and block loading on the fatigue response of fiber-reinforced composites. Mech Adv Mater Struct 2002;9(1):19–35.
[41] Gamstedt EK, Sjögren BA. An experimental investigation of the sequence effect in block amplitude loading of cross-ply composite laminates. Int J Fatigue 2002;24:437–46.
[42] Harris B. Fatigue in composites. Woodhead Publishing Limited; 2003.
[43] Vassilopoulos AP. Introduction to the fatigue life prediction of composite materials and structures: past, present and future prospects. In: Vassilopoulos AP, editor. Fatigue life prediction of composites and composite structures. Woodhead Publishing Limited; 2010. p. 1–44.
[44] Brunbauer J, Pinter G. On the strain measurement and stiffness calculation of carbon fibre reinforced composites under quasi-static tensile and tension-tension fatigue loads. Polym Test 2014;40:256–64.
[45] Brunbauer J, Pinter G. Technological approach to fatigue life prediction of CFRP. In: ECCM16, Seville; 2014. p. 22–6.
[46] Brunbauer J, Arbeiter F, Stelzer S, Pinter G. Stiffness based fatigue characterisation of CFRP. Adv Mater Res 2014;891–892:166–71.
[47] Mayugo JA. Estudio constitutivo de materiales compuestos laminados sometidos a cargas cíclicas. Ph.D. thesis, Universitat Politècnica de Catalunya; 2003.
[48] ASTM D3039/D3039M-14. Standard test method for tensile properties of polymer matrix composite materials. American Society for Testing and Materials; 2014. p. 1–13.
[49] Philippidis TP, Passipoularidis VA. Residual strength after fatigue in composites: theory vs. experiment. Int J Fatigue 2007;29(12):2104–16.
[50] Passipoularidis VA. Residual strength and life prediction in composite materials after fatigue. Ph.D. thesis, Patras; 2009.
[51] Whitworth HA. A stiffness degradation model for composite laminates under fatigue loading. Compos Struct 1998;40(2):95–101.
[52] Hwang W, Han KS. Fatigue of composites–fatigue modulus concept and life prediction. J Compos Mater 1986;20:154–65.

[53] Basquin OH. The exponential law of endurance tests. In: Proc ASTM, vol. 10(2); 1910. p. 625–30.
[54] Kawai M, Yajima S, Hachinohe A, Takano Y. Off-axis fatigue behavior of unidirectional carbon fiber-reinforced composites at room and high temperatures. J Compos Mater 2001;35:545–76.
[55] Kawai M, Yajima S, Hachinohe A, Kawase Y. High-temperature off-axis fatigue behaviour of unidirectional carbon-fiber-reinforced composites with different resin matrices. Compos Sci Technol 2001;61(9):1285–302.
[56] Talreja R. Damage and fatigue in composites – a personal account. Compos Sci Technol 2008;68(13):2585–91.
[57] Talreja R. A conceptual framework for studies of durability in composite materials. In: Carvelli V, Lomov SV, editors. Fatigue of textile composites. Woodhead Publishing Limited; 2015 [chapter 1].

Paper B

Progressive matrix cracking in carbon/epoxy cross-ply laminates under static and fatigue loading

J. Llobet[a], P. Maimí[a], Y.Essa[b], F. Martin de la Escalera[b]
[a] AMADE, Polytechnic School, Universitat de Girona, Girona, Spain
[b] AERNNOVA Engineering Division, Structural Integrity Department, Madrid, Spain

The paper has been published in
International Journal of Fatigue Vol. 119, pp. 330–337, 2019.

International Journal of Fatigue 119 (2019) 330–337

Contents lists available at ScienceDirect

International Journal of Fatigue

journal homepage: www.elsevier.com/locate/ijfatigue

Progressive matrix cracking in carbon/epoxy cross-ply laminates under static and fatigue loading

J. Llobet[a,*], P. Maimí[a,*], Y. Essa[b], F. Martin de la Escalera[b]

[a] AMADE, Mechanical Engineering and Industrial Construction Department, University of Girona, Carrer Universitat de Girona 4, E-17003 Girona, Spain
[b] AERNNOVA Engineering, Structural Integrity Department, 20 Manoteras Avenue – Building B, E-28050 Madrid, Spain

ARTICLE INFO

Keywords:
Matrix cracking
Fatigue crack growth
Linear Elastic Fracture Mechanics (LEFM)
Fatigue modelling
Damage

ABSTRACT

This paper presents an experimental investigation into the growth of matrix cracks in carbon/epoxy cross-ply laminates under static and fatigue loading. Particular emphasis is placed on how to address fatigue damage. Two models are proposed to describe the evolution of fatigue cracks, where the crack density is used as the mechanistic damage variable. The first model defines the evolution of cracks according to a Paris law function. The second assumes that fatigue degradation is mainly caused by diffuse damage, resulting in an apparent decrease in the fracture energy, so that the cracking process is controlled by the static function. Both models are analysed in detail and compared against experimental data for different transverse plies and loading levels. The presence of cracks is monitored by enhanced X-ray radiography and edge camera images. Two crack density master curves are derived, one based on fracture mechanics for static and one based on a Paris law for fatigue cracking. The predictions show good correlation with the experiments.

1. Introduction

A major challenge for the aerospace industry consists of predicting the life and damage tolerance of a composite structure subjected to combined loading scenarios such as static, dynamic and fatigue. The service life and residual strength of a component can be estimated in advance by predicting the accumulation of sub-critical damage that might have grown. For a conventional composite laminate, the damage development is frequently described as a three-stage process [1]. Each stage marks the presence of a different underlying damage mechanism. The first stage corresponds to the formation of transverse matrix cracks at off-axis plies, first in the 90° and afterwards in the ± 45° plies. Within stage two, the number of matrix cracks increases along with the formation of local delaminations from the tip of these cracks. At this point, the stiffness is decreasing progressively but much more slowly. The final stage presents either a fast delamination propagation (matrix-dominated failure) or fibre fracture (fibre-dominated failure) leading both to an eventual complete loss of integrity [2].

The transverse degradation mechanisms in stage one of fatigue life have been extensively studied in cross-ply and quasi-isotropic stacking sequences [3–9]. Before the development of local delaminations, there are two main mechanisms controlling the degradation process of transverse plies, first diffuse damage as fibre/matrix debonds and micro-cracks in the resin, and subsequently the nucleation of through-the-thickness transverse cracks. In this regard, several studies pointed out that diffuse damage is the main cause of the multiplication of fatigue cracks [10–14]. Quaresimin et al. [13] proved experimentally that shear-induced diffuse damage is the first damage mechanism taking place before the nucleation of an off-axis crack in mode II shear fatigue loading. Nouri et al. [14] tested quasi-statically a cross-ply laminate under in-plane shear loading (inducing shear diffuse damage), and then monitored the static evolution of cracks in the 90° ply growing in mode I. The experimental results showed that the number of cracks increased by increasing the levels of shear-induced diffuse damage for the same strain level. This is in line with the concept introduced by Ladevèze [10], where diffuse damage induced either by static or fatigue loadings is understood as a decrease in the material fracture toughness [10,15]. As an alternative, some authors define the evolution of fatigue cracks by a modified Paris-law based function [16–20].

This paper investigates the evolution of transverse damage in 90° plies under static and fatigue loading in a carbon/epoxy cross-ply laminate. The experimental characterization consists of quasi-static testing to monitor the evolution of static cracks from a pristine material. Then, fatigue testing to monitor the evolution of fatigue cracks, and finally fatigue testing followed by static testing to monitor the evolution of static cracks after inducing different levels of diffuse damage. Fatigue tests are conducted at different stress levels with a constant R-ratio of 0.1. The number of cracks is monitored for different ply thicknesses and

* Corresponding authors.
E-mail addresses: jordi.llobet@udg.edu (J. Llobet), pere.maimi@udg.edu (P. Maimí).

https://doi.org/10.1016/j.ijfatigue.2018.10.008
Received 24 July 2018; Received in revised form 9 October 2018; Accepted 11 October 2018
Available online 17 October 2018

types (embedded and outer ply). Note that the maximum thickness of the analysed transverse plies is limited to four times the standard ply thickness as it is generally recommended for industrial applications [21]. Two models are selected to describe the process of intralaminar fatigue cracking where the crack density variable is used as the mechanistic variable. The same expression to calculate the energy release rate for mode I cracking is used in both models. The first model is based on the modified Paris law from Liu and Nairn [22] and the second model takes into account the effect of fatigue diffuse damage by decreasing the material fracture energy following the work of Ladevèze and co-authors [10–12].

The content of the paper is structured as follows. Section 2 presents a quick overview of the damage phenomenology induced in transverse plies due to the application of in-plane static or fatigue loading. The two different modelling approaches to predict the evolution of fatigue cracks are also presented in this section. Then, the experimental methodology and the different tests conducted are addressed in Section 3 followed by the summary of the experimental results in Section 4.

2. Modelling of intralaminar damage mechanisms in transverse plies

Three basic damage scenarios are introduced by Ladevèze [15,23,24] to explain the degradation process of a transverse ply. These damage forms are usually occurring sequentially under static and fatigue loading (they are all sketched in Fig. 1). The first scenario A is diffuse damage associated with the mechanism of fibre/matrix debonding. These micro-cracks in the inter-fibre region may coalesce into a through-the-thickness transverse crack leading to scenario B in Fig. 1. In some cases, matrix cracks kink into the interface as a delamination crack representing scenario C. This work focuses on scenario A and B. Scenario B is typically characterized by the crack density ρ, defined as the inverse distance l between two consecutive cracks, or it can be normalized by the ply thickness as $\bar{\rho}$:

$$\rho = \frac{1}{l} \quad \text{or} \quad \bar{\rho} = t_N \rho \tag{1}$$

where t_N is the ply thickness (for an outer ply the actual thickness t_N is multiplied by $1.12^2 \times 2$ to consider the free-edge effect of an outer cracked ply [25]).

Diffuse damage defined as a measure of the fibre/matrix debonding has already been introduced in the framework of continuum damage models for static loading cases [15,23,24]. This damage mechanism is considered to be a distributed mechanism within the ply and independent of the ply thickness [24]. Ladevèze and Lubineau [15] included this damage scenario to correctly predict the static evolution of cracks in outer transverse plies. Nouri et al. [14] also showed the effect of including shear-induced diffuse damage on mode I transverse cracking.

There is experimental evidence that transverse cracks nucleate at the free edge and propagate inwards instantaneously crossing over the entire width. So the phenomenon is typically assessed as a two-dimensional problem in the framework of Finite Fracture Mechanics [25]. However, some partial-width cracks that do not cross the entire width are observed in quasi-static loading for thin plies, and especially at low-

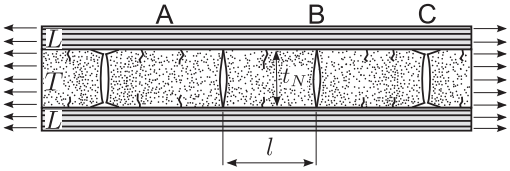

Fig. 1. Damage mechanisms at off-axis plies; (A.) diffuse damage; (B.) transverse cracking; (C.) local delamination.

stress fatigue loadings [4,26–28]. Then, the crack density is no longer constant throughout the width of the specimen. Yokozeki et al. [8,29] concluded that edge cracking and inward propagation occur usually at the same time for cross-ply laminates where cracks grow in mode I. If cracks are growing in mode II or mixed-mode conditions, as happens in ± 45° plies, edge cracking and inward propagation are not given at the same time.

2.1. In situ strength

The *in situ* strength concept reflects the apparent increase in the transverse and shear strengths when the ply is embedded in a multidirectional laminate [17,25,30–32]. This effect is commonly explained by means of Linear Elastic Fracture Mechanics (LEFM). For thin enough plies, the ply strength is defined by the mean stress at ply level required to propagate a crack in the direction of the fibres, or crack tunnelling [25]. The expression to calculate the *in situ* strength reads:

$$Y_T^{\text{Thin}} = \sqrt{\frac{4\overline{E}_2 G_{Ic}}{t_N \kappa_2}} \tag{2}$$

where G_{Ic} is the mode I fracture toughness, $\overline{E}_2$ is the plain strain transverse Young modulus, t_N is the ply thickness, and κ_2 is a parameter that depends on the elastic properties of the adjacent plies, the relative thickness of each ply, the laminate stacking sequence, and the position of the considered ply within the laminate.

The *in situ* strength decreases with the increase in the ply thickness until the thick-ply strength is reached. For thick plies, the cracking process is governed by an unstable transverse crack growth and not by crack tunnelling. Thick plies show a constant *in situ* strength with respect to the ply thickness but larger than UD ply strength, which is usually explained by the constraining (or free-edge) effect of adjacent plies. Note that an unidirectional laminate can be considered a special case of a thick laminate in which the outer surfaces are unconstrained so that surface cracks can develop. This observation allows the prediction of the *in situ* strength of thick plies using experimental data from unidirectional laminates. Thus, the thick ply *in situ* strength can be estimated as [25,30–32]:

$$Y_T^{\text{Thick}} = \kappa_T Y_T^{\text{UD}} \tag{3}$$

where κ_T is taken as $1.12\sqrt{2}$ [25,32]. The use of thick-ply laminates for structural purposes is not recommended since they are less resistant to matrix cracking and also to delamination [21].When the analysed ply is external (not constrained by longitudinal plies), there in no such *in situ* effect so that parameter $\kappa_T = 1$.

Matrix cracking also occur when the ply is loaded under in-plane shear stresses with mode II crack growth. Moreover, the ply shows a non-linearity with some diffuse damage and plastic deformation which must be taken into account for an accurate crack evolution prediction [30–32]. It is also usual that plies withstand combined normal and shear so that cracks grow under mixed-mode conditions. Mode II and mixed-mode cracking are not analysed in this study.

2.2. Residual thermal-induced stresses

When the laminate is cooled down from the curing temperature (or the stress-free temperature) to room temperature some residual stresses are induced into the laminate plies due to the mismatch between the longitudinal and transverse thermal expansion coefficients (CTEs). The equivalent laminate CTE can be obtained by enforcing force equilibrium into the laminate [33]. The difference between the total laminate contraction and the transverse ply contraction determines the induced strains that cause thermal stresses. The average thermal-induced strain in the transverse ply is calculated as:

$$\varepsilon_{22}^{\text{t}} = (\alpha_{xx} - \alpha_{22}^{T})\Delta T \tag{4}$$

Table 1
M21E/IMA carbon/epoxy unidirectional properties.

Elastic properties			
E_1 [GPa]	E_2 [GPa]	G_{12} [GPa]	ν_{12}
160.8	9.3	–	0.34
Strength properties			
X_T/X_c [MPa]	Y_T/Y_c [MPa]	S_L [MPa]	
3048 / 1196	47 / 230	96	
Fracture properties			
G_{Ic} [N/mm]	G_{IIc} [N/mm]	t_{ply} [mm]	
0.309	2.780	0.184	
Thermal properties			
α_{11} [$\mu\epsilon/°C$]	α_{22} [$\mu\epsilon/°C$]	ΔT [$°C$]	
2.1	24	−160	

where $\alpha_{xx} = 3.6\ \mu\epsilon/°C$ is the laminate CTE in the global longitudinal direction, α_{22}^T is the transverse ply CTE and ΔT is the thermal jump. Hereafter, ε_{22} refers to the total strain applied (mechanical and thermal) as:

$$\varepsilon_{22} = \varepsilon_{22}^{m} + \varepsilon_{22}^{t} \tag{5}$$

where the average thermal-induced strain for the material under study is approximated to $\varepsilon_{22}^{t} = 0.33\%$ (see thermal properties in Table 1).

2.3. Matrix cracking under static loading

From a fracture mechanics point of view, the expression to calculate the available energy release rate for crack tunneling under a mode I loading case reads [10,15]:

$$G_I = \frac{\overline{E}_2}{2}\varepsilon_{22}^2 t_N f(\bar{\rho}) \leqslant G_{IC} \tag{6}$$

where function $f(\bar{\rho})$ is determined by solving the stress field of the laminate with different crack densities. Indeed, $f(\bar{\rho})$ depends on the solution of the elasticity problem and also on the assumed crack pattern distribution [31,34,35]. In this work, it is assumed that the cracks are uniformly distributed (i.e periodic spaced cracking) so that the cracking process can be described objectively by the mechanistic variable $\bar{\rho}$. It is also considered that the evolution of transverse cracks in one ply does not affect the cracking process in other plies, since the stiffness provided by the longitudinal plies is high enough. Then, the use of a staggered sequence of cracking reported for some cross-ply laminates with outer ply cracks is no longer a good option [36,37].

There are several methods available to solve the stress field and the corresponding energy release rate in cracked laminates [38,39], some of them are based on the shear-lag model [40–45], variational methods [17,37,46,47], finite element methods [15,48–50] or by analytical models [51–53]. Fortunately, experimental and numerical results suggest that $f(\bar{\rho})$ can be assumed intrinsic and independent of the laminate stacking sequence for most industrial laminates [15,31,54,55]. Note that $f(\bar{\rho})$ is constant for low crack densities. However, above a certain crack density level (i.e., when the cracks are sufficiently close so that their stress field interacts), $f(\bar{\rho})$ decreases with the increase in the number of cracks. Note that the *in situ* strength (or strain) of thin plies defined by Eq. (2) can also be computed with $f(\bar{\rho} = 0)$ in Eq. (6). Within this study, function $f(\bar{\rho})$ is experimentally fitted by the static cracking curves.

2.4. Matrix cracking under fatigue loading

Paris-law based functions have been extensively used to describe the crack growth rate under fatigue loading, especially for delamination cracks in laminated composites [56,57]. The conventional Paris law relates the crack growth rate to a power law of the stress intensity factor (ΔK) range during one cycle. Note that for certain materials, the increase in the crack density can be assumed to be proportional to the increase in the crack extension, thus the use of a Paris-law based function with the crack density is justified [16–18,58]:

$$\frac{d\rho}{dN} = \alpha[g(\Delta K,\ \Delta G,\ G_{\max},\ ...)]^n \tag{7}$$

Note that g is a loading function that depends on numerous factors other than ΔK mainly used in metal fatigue [59]. Also, the calculation of K is not straightforward for matrix cracking and in general for composites since it can lead to complex solutions [56]. This is usually solved by taking G instead. The basic relation between them is written as $G = K^2/E$, but E being a measure of the stiffness may also result in a complex form for most of the cases with composites. Taking these considerations, Eq. (7) can be expressed by different loading functions, such as $g_{\Delta K} = (\sqrt{G_I^{\max}} - \sqrt{G_I^{\min}})/\sqrt{G_{Ic}}$, or in some cases and materials directly with $g_{G_{\max}} = \sqrt{G_I^{\max}}$ [56,57], or even with $g_{\Delta G} = \sqrt{(G_I^{\max} - G_I^{\min})/G_{Ic}}$ [16,17,19,20]. It is worth noting that Liu an Nairn [17] figured out a Paris-law master curve for Eq. (7) for different materials and ply thicknesses by considering $g_{\Delta G}$. This will be further investigated with the current material system and ply thicknesses.

A completely different physical explanation of the growth of fatigue cracks is introduced by Ladevèze and co-workers [10–12]. They suggested that diffuse damage (micro-cracking in the resin and in the interfibre region) is the main damage mechanism degrading the transverse and shear-stiffness of the ply. Quaresimin et al. [13] experimentally proved that suggestion by testing $[45/-45/0]_s$ glass/epoxy specimens in fatigue loading, where they observed an early stage of shear-induced diffuse damage consisting of micro-cracks before the nucleation of full thickness transverse cracks. However, this damage, although it exists, appears to be small. Therefore, the definition of diffuse damage through the loss of stiffness is not appropriate for quantifying the cyclic weakening of the material. So they defined a new concept of reducing the fracture energy under fatigue loading. Here this idea is taken to explain the growth of mode I fatigue cracks. In this regard, Eq. (6) is modified by adding a function termed β_N as follows:

$$G_I \leqslant \beta_N(\varepsilon_{22}^{\max}, \varepsilon_{22}^{\min}, \bar{\rho})G_{Ic} \tag{8}$$

β_N is defined as a decreasing function that quantifies the reduction in the mode I fracture toughness G_{Ic} due to the progressive growth of diffuse damage under fatigue loading. β_N depends on the maximum and minimum stress (or strain), and for large crack densities also on $\bar{\rho}$, but not on the ply thickness. In the experimental tests, it is investigated some evolution function like $d\beta_N/dN$. Note that, it is assumed that the increase in diffuse damage under static loading is negligible.

Some authors take the Paris-law based approach by using Eq. (7) [16–20] and neglecting the effect of diffuse damage, while others explain the evolution of fatigue cracks with β_N by means of Eq. (8) [10–12].

3. Experimental method

3.1. Material

The material system used in this study is a carbon/epoxy pre-preg (Hexcel® M21E/IMA-12K) of 0.184 mm nominal ply thickness. The laminate was moulded and cured in an autoclave under standard aeronautical conditions. The quality of the panel was verified using ultrasonic C-scan inspection. The specimens were cut by water abrasive jet with dimensions 200 × 20 × 2.2 mm. Cross-ply GFRP tabs of 50 mm length were used to avoid gripping problems. After being cut and measured, the specimens edges were polished. The polishing process was performed under wet conditions with a medium grit (472 mesh) and followed by fine grit (1200 mesh).

The in-plane elastic, strength and fracture properties were obtained according to the corresponding ASTM standards at AMADE research lab

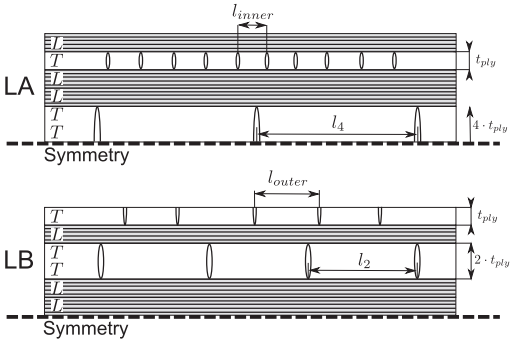

Fig. 2. Crack density functions for LA $[0/90/0_2/90_2]_s$ termed as ρ_4 and ρ_{inner}, and for LB $[90/0/90_2/0_2]_s$ as ρ_2, and ρ_{outer}.

(see Table 1). The interlaminar fracture properties were obtained from Carreras [60,61] and the thermal coefficients were taken from Sebaey et al. [62].

Two different stacking sequences are considered for this study, laminate A (LA) $[0/90/0_2/90_2]_s$ and laminate B (LB) $[90/0/90_2/0_2]_s$. Both are obtained from the same panel but LB is rotated 90 degrees (no differences associated with the manufacturing process). Fig. 2 depicts the two lay-up configurations and the four crack density functions analysed. These density functions correspond to the four types of transverse plies identified as ρ_4, ρ_2, ρ_{inner} and ρ_{outer}, a cluster of four and two plies, inner embedded and outer individual plies, respectively.

3.2. Equipment

All tests were performed using a universal servo-hydraulic test machine 810 MTS. The force was measured by a load cell of 250 kN. The strain was measured by a clip-on extensometer with a 25 mm gauge length.

Matrix cracks were monitored by two optical means, by a digital reflex camera CANON EOS550D with a 100 mm macro lens and by X-ray radiography. The camera was used to detect transverse cracks at the specimen edge and the X-ray images captured through-the-width transverse cracks. The most important camera settings are: raw format, ISO 100, shutter speed of 1/200 and aperture size of f/7.1. This configuration is only achieved by providing intense led light into the specimen and by using a dark background. X-ray radiographs were made using a Hamamatsu unit at AMADE Research lab. The following settings were used: 35 kV, 120 μA, analogue integration of 5 images within a exposure time of 3000 ms. To enhance X-ray contrast, a solution comprised of 520 g of zinc iodide, 86.5 ml distilled water, 86.5 ml alcohol and 26 ml Kodak Photo-Flo 200 was used. The specimens were immersed into this solution and were placed inside a vacuum chamber for some minutes.

3.3. Test procedure

The static tests were conducted under displacement control with a displacement rate of 1 mm/min until eventual failure. The methodology used to count the number of cracks under static conditions is described by Sebaey et al. [62] and Zubillaga et al. [63]. This methodology consists in real-time monitoring of edge matrix cracks in which images are taken every 5s while load is being increased.Three specimens for each stacking sequence were tested, although one of the specimens was interrupted at an intermediate strain level of 1.46% and x-rayed.

Tension-tension load-controlled fatigue tests were run at different stress levels of constant amplitude (stress ratio $R = 0.1$), and a frequency $f = 5$ Hz. Two different groups of fatigue tests were conducted. In the first group, the evolution of fatigue cracks in a pristine specimen was investigated for different stress levels reaching strains of 0.56%, 0.78%, 0.88%, 0.98%, 1.33% and 1.69%. The crack density functions were monitored until $2{\cdot}10^6$ cycles unless complete failure occurred. The tests were periodically interrupted to count the number of cracks through the edge camera pictures and sometimes by the X-ray images. During the image capture, a small displacement was applied to the specimens in order to open the already formed cracks. The second group of tests was used to investigate the effect of diffuse damage. This was accomplished by testing specimens under fatigue loading and afterwards monitoring the evolution of transverse cracks in a quasi-static test. This type of test has been performed for different stress levels and fractions of life but with special emphasis on the early stages of fatigue life. For laminate LA, three specimens tested at 0.56% and $1.4{\cdot}10^6$ cycles, 0.78% and 472000 cycles and 0.98% and $2.1{\cdot}10^6$ cycles were considered. For laminate LB, six specimens tested at 0.56% and $1.0{\cdot}10^6$ cycles, 0.67% and 750000 cycles, 0.78% and 500000 cycles, 0.78% and $1.6{\cdot}10^6$ cycles, 1.33% and 110000 cycles, 1.33% and $2.0{\cdot}10^6$ cycles were considered.

4. Results and discussion

4.1. Crack density under static loading for a pristine material

Both LA and LB laminates behave linearly elastic prior reaching the ultimate fibre strain and fracture. The presence of transverse cracking does not change the global laminate stiffness which is typically the case for laminates with stiff carbon layers and relatively thin plies [25,62]. Fig. 3 illustrates the crack density curves ρ_N vs. the total transverse strain applied ε_{22} computed by Eq. (5) in the quasi-static tests. The intersection of these curves when the crack density becomes zero corresponds to the *in situ* strain. Figs. 4 and 5 show X-ray and camera images obtained for LA and LB at a intermediate strain level of $\varepsilon_{22} = 1.46\%$ before failure. The radiographs confirm that all cracks span the entire width and no delamination occurs. It should be mentioned that Fig. 4 does not show the correct crack density in the embedded individual ply for this strain level. The detection of transverse cracks within this ply thickness and constraint under small displacements is rather complicated. The edge polishing and the camera settings are found to be crucial to detect them. Finally, Fig. 6 illustrates the crack density stage prior to the final collapse of the laminate.

So by taking into account Eq. (6), the experimental data of Fig. 3 can be plotted in the space $\bar{\rho} - \varepsilon_{22}\sqrt{l_N}$ defining a master curve as shown in Fig. 7. Because its simplicity and good correlation with the experimental results, it is suggested $f(\bar{\rho})$ as:

$$f(\bar{\rho}) = \min\left\{\frac{\kappa_2}{2}, \kappa_2 \exp(-\kappa_2 \bar{\rho})\right\} \tag{9}$$

where κ_2 is a material fitting parameter. The minimum condition of Eq. (9) determines the intersection point from low to high crack densities

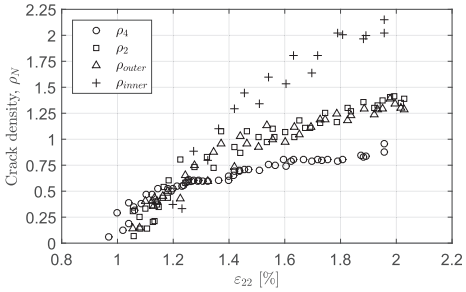

Fig. 3. Crack density ρ_N as a function of the total transverse strain ε_{22}.

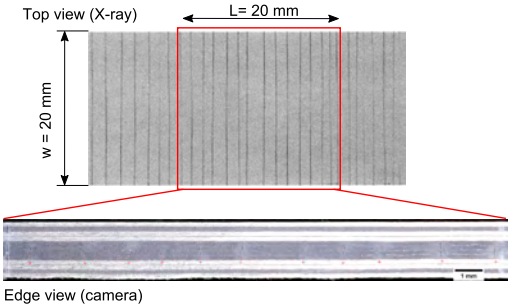

Fig. 4. Matrix cracks observed in LA under static loading (ε_{22} = 1.46%).

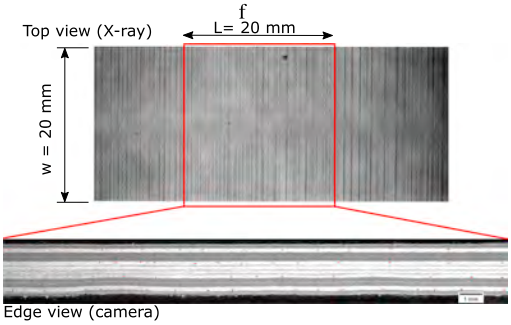

Fig. 5. Matrix cracks observed in LB under static loading (ε_{22} = 1.46%).

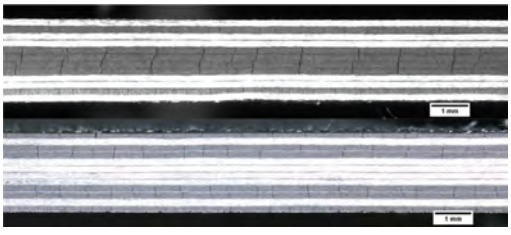

Fig. 6. Matrix cracks observed in LA and LB prior to failure (ε_{22} = 1.96%).

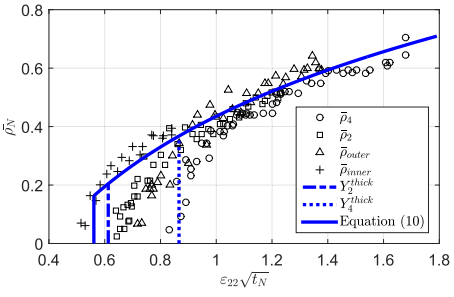

Fig. 7. Static crack density master curve.

[25]. For $\rho_N = 0$ the *in situ* strain of Eq. (2) is recovered. Rearranging terms in Eqs. (6) and (9), the static evolution of cracks is defined as:

$$\bar{\rho} = -\frac{1}{\kappa_2}\ln\left(\frac{2G_{Ic}}{\kappa_2 \overline{E}_2 \varepsilon_{22}^2 t_N}\right) \quad \text{for} \quad \varepsilon_{22} \geqslant \frac{Y_T^{IS}}{\overline{E}_2} \tag{10}$$

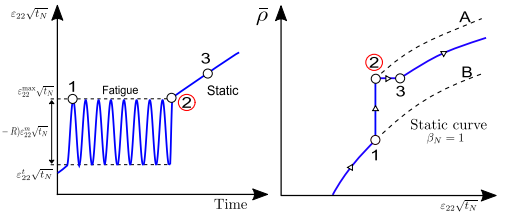

Fig. 8. Crack density evolution under fatigue loading followed by static loading.

where Y_T^{IS} is the *in situ* strength determined by the maximum of Eqs. (2) and (3): $Y_T^{IS} = \max\{Y_T^{Thin}, Y_T^{Thick}\}$. The best-fit of Eq. (10) is obtained with $\kappa_2 = 4.15$. Note that the *in situ* strength $Y_T^{Thin} < Y_T^{Thick}$ in $\bar{\rho}_2$ and $\bar{\rho}_4$.

The cracking process of the thicker clusters $\bar{\rho}_4$ and $\bar{\rho}_2$ is not governed by crack tunneling assumed in Eq. (10), instead it is driven by *in situ* effect of thick plies. But, above a certain crack density level the crack tunneling criterion is higher than the thick ply criterion, thus the response tends to the master curve.

4.2. Crack density under static loading for a fatigue-damaged material

The growth of fatigue diffuse damage $d\beta_N/dN$, where β_N represents the reduction in the neat material fracture energy G_{Ic} with respect to the loading cycles [10–12], is further investigated by first testing specimens under tension-tension fatigue loading, and then by loading them quasi-statically until failure. Fig. 8 exemplifies this concept. During the first fatigue cycle, the crack density might be increased statically depending on the maximum stress level applied (see point 1 in Fig. 8). Subsequent fatigue cycles increase the density until point 2. After this state, a static test is performed. The static loading starts to increase and the crack density is kept constant until reaching point 3, and further to this point, the crack density follows the solid line in between curve A and B. If point 3 merges with point 2 and the cracks evolve following the dashed line of curve A, this would indicate that the evolution of fatigue cracks is explained uniquely by Eq. (8). On the contrary, if point 3 reaches curve B thereby suggesting that the fatigue evolution is well explained by the Paris law of Eq. (7). Note that if point 3 lies in between curve A and B, as it is illustrated in Fig. 8, both mechanisms are influencing the crack density growth.

Fig. 9 shows the static evolution of the normalized crack density after different levels of fatigue diffuse damage (specimens were fatigue-damaged at different strain levels ε_{22}^{max} and number of cycles). The static master curve from Eq. (10) is plotted as a reference curve for the evolution of static cracking in a pristine material. The red markers represent the crack density after the fatigue test (point 2 in Fig. 8). If fatigue cracks are governed by the effect of diffuse damage, one would expect a shift to the left on the experimental crack density data, which is not the case for the tests conducted. For the current carbon/epoxy material under study, the experimental data indicates that transverse-induced fatigue diffuse damage appears to be small so that $\beta_N = 1$.

4.3. Crack densities under fatigue loading

If the Paris law based approach is taken, Eq. (7) combined with Eqs. (6) and (9) can be integrated as follows:

$$\begin{aligned} \bar{\rho} &= \bar{\rho}_0 + \alpha\left(\frac{\kappa_2 \overline{E}_2}{4G_{Ic}}\tilde{\varepsilon}^2 t_N\right)^{\frac{n}{2}}\widetilde{\Delta N} && \text{if} \quad \bar{\rho} \leqslant \frac{-1}{\kappa_2}\ln\left(\frac{1}{2}\right) \\ \bar{\rho} &= \frac{2}{n\kappa_2}\ln\left[\frac{\alpha\kappa_2 n}{2}\left(\frac{\kappa_2 \overline{E}_2}{2G_{Ic}}\tilde{\varepsilon}^2 t_N\right)^{\frac{n}{2}}\widetilde{\Delta N} + \exp\left(\frac{\kappa_2 n}{2}\bar{\rho}_0\right)\right] && \text{if} \quad \bar{\rho} \geqslant \frac{-1}{\kappa_2}\ln\left(\frac{1}{2}\right) \end{aligned} \tag{11}$$

where $\tilde{\varepsilon}$ is the equivalent strain that depends on the loading function g considered in the Paris law of Eq. (7). For example, if

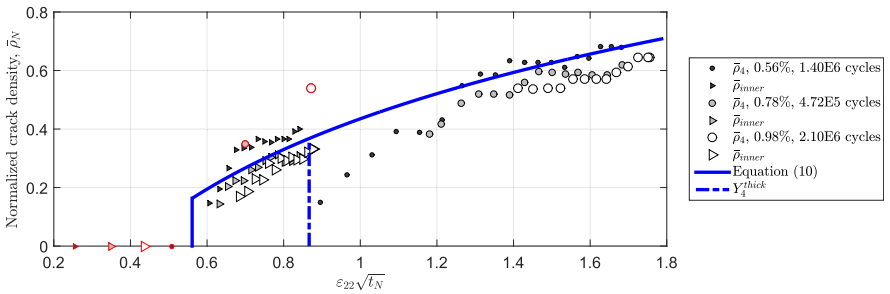

(a) laminate LA

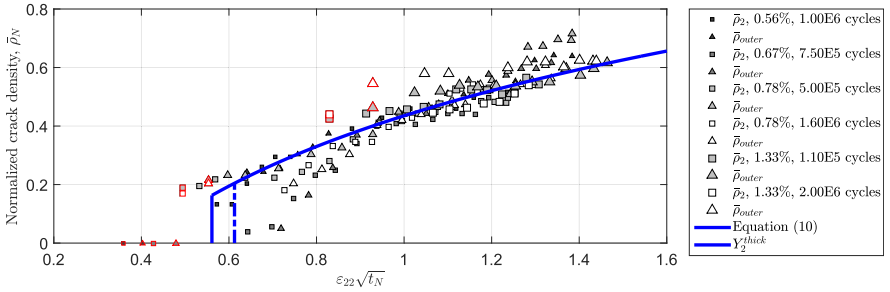

(b) laminate LB

Fig. 9. Normalized crack density of a fatigued material at different strain levels and fractions of life under static loading.

$g_{\Delta K} = \sqrt{G_I^{\max}/G_{Ic}} - \sqrt{G_I^{\min}/G_{Ic}}$ is considered as in the original Paris law, then the equivalent strain becomes $\widetilde{\varepsilon} = \varepsilon_{22}^{\max} - \varepsilon_{22}^{\min}$. If $g_{\Delta G} = \sqrt{(G_I^{\max} - G_I^{\min})/G_{Ic}}$ is taken as proposed by Liu and Nairn [22], then the equivalent strain turns out to be: $\widetilde{\varepsilon} = \sqrt{(\varepsilon_{22}^{\max})^2 - (\varepsilon_{22}^{\min})^2}$.

As it has been mentioned in Section 2.4, the crack density ρ is the dependent variable in the Paris law function. However, the normalized crack density $\bar{\rho}$ is found to be more appropriate, since the distance in between two cracks is not measured in millimetre but in units of crack size [28]. Consequently, the $\widetilde{\Delta N}$ defines the number of cycles if the Paris law is expressed by the normalized crack density: $d\bar{\rho}/dN$, or $\widetilde{\Delta N} = t_N \Delta N$ if it is expressed by the crack density: $d\rho/dN$. The Paris law defined by $d\rho/dN$ results in a master curve of the form: ρ - $(\widetilde{\varepsilon}^2 t_N)^{n/2} t_N \Delta N$. In contrast, if it is expressed by $d\bar{\rho}/dN$, the master curve is of the form: $\bar{\rho}$ - $(\widetilde{\varepsilon}^2 t_N)^{n/2} \Delta N$. Fig. 10 shows the best-fit of Eq. (11) for different loading functions g and for the two different dependent variables analysed (ρ and $\bar{\rho}$). The results presented do not clarify which fitting is better.

Note that the crack density function ρ_{inner} is not shown under fatigue since significant fibre splitting has been found at the outermost ply. It is experimentally observed that this mechanism is affecting the cracking process so that this crack density curve has not been considered. The presence of any other damage form, such as fibre splitting or delamination, may result in an inaccurate prediction of the crack density curves. This undesirable effect has already been reported by Togho [5] and also by the authors [2] when testing unidirectional laminates.

5. Conclusions

The process of matrix cracking has been analysed for two different carbon/epoxy cross-ply laminates under static and fatigue loading. The study of these two laminates allows to compare the evolution of transverse cracks in mode I for different ply thicknesses and types (embedded and outer plies) in both loading scenarios. Damage detection has been accomplished by edge camera images and X-ray radiography.

A simple expression to calculate the energy release rate for mode I cracking has been derived based on the assumption of crack tunnelling growth. The best-fit of this function with only one fitting parameter results in a master curve for all transverse plies. The good correlation found with the experimental data confirms that this expression can be assumed intrinsic and independent of the stacking sequence for the studied laminates. However, the crack densities in the cluster of four and two plies do not match the master curve at low densities, because they are controlled by the *in situ* effect of thick plies. Above a certain crack density, their response tends to the master curve where crack tunnelling growth is dominant. It should be highlighted that the thermal-induced stresses after the curing process play a major role so they must be considered throughout the analysis.

Two different fatigue models available in open literature have been evaluated in order to describe the development of fatigue cracks. The first model describes the crack density increase by a modified Paris law. The definition of the Paris law is assessed by introducing two loading functions and also two dependent variables (the crack density and the normalized crack density). The derived curves can be plotted as master curve with good correlation with the fatigue experimental data (crack density vs. cycles). However, the best-fit for the proposed Paris laws does not show relevant differences. The second model considers that the multiplication of fatigue cracks can be attributed to the growth of diffuse damage (micro-cracks in the inter/fibre region). Therefore, it is suggested to investigate the evolution of static cracks in fatigue-damaged specimens. One would expect to advance the process of cracking (shift to the left in the crack density curves) compared to the pristine material (without fatigue damage). The experimental results indicate that this is not the case for this material system where the crack density curves tend to the pristine static ones. Consequently, it is concluded that fatigue cracking cannot be explained by only considering diffuse damage.

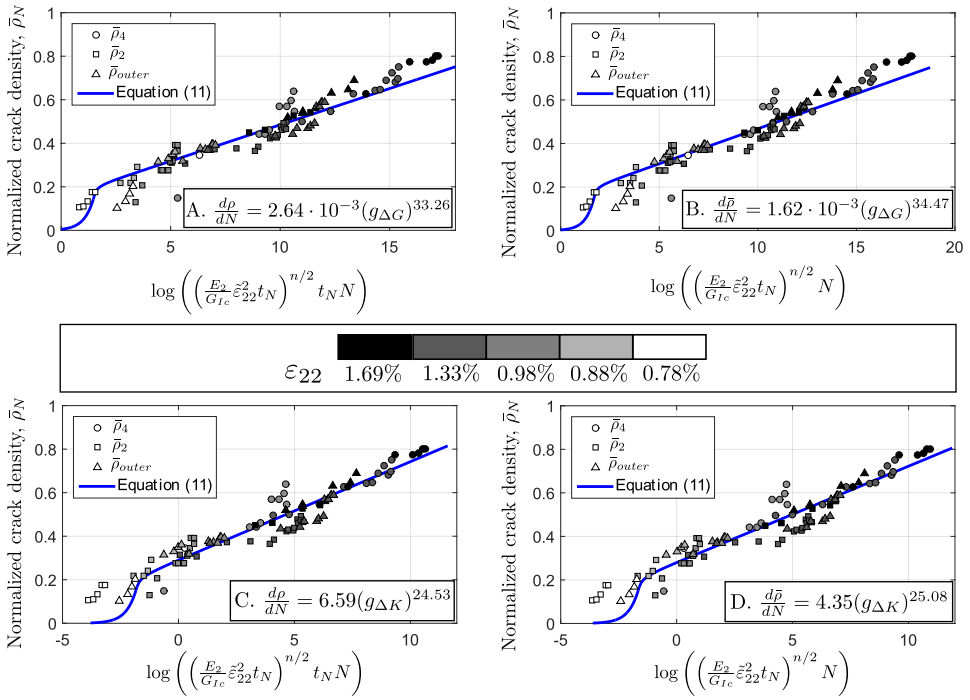

Fig. 10. Fitting of the Paris law function for different cases: (A.) Crack density and $g_{\Delta G}$, (B.) Normalized crack density and $g_{\Delta G}$, (C.) Crack density and $g_{\Delta K}$ and (D.) Normalized crack density and $g_{\Delta K}$.

Acknowledgements

This work has been funded by the Spanish Government (Ministerio de Economia y Competitividad) through the project entitled ABORDA under the contract RTC-2014-1958-4.

References

[1] Schulte K. Stiffness reduction and development of longitudinal cracks during fatigue loading of composite laminates. In: Cardon AH, Verchery G, editors. Mechanical characterization of load bearing fibre composite laminates. Elsevier; 1984. p. 36–54.

[2] Llobet J, Maimi P, Mayugo JA, Essa Y, de la Escalera F Martin. A fatigue damage and residual strength model for unidirectional carbon/epoxy composites under on-axis tension-tension loadings. Int J Fatigue 2017;103:508–15. https://doi.org/10.1016/j.ijfatigue.2017.06.026.

[3] Berthelot JM. Transverse cracking and delamination in cross-ply glass-fiber and carbon-fiber reinforced plastic laminates: static and fatigue loading. Appl Mech Rev 2003;56(1):111–47. https://doi.org/10.1115/1.1519557.

[4] Berthelot JM, Le Corre JF. Modelling the transverse cracking in cross-ply laminates: application to fatigue. Compos Part B: Eng 1999;30:569–77. https://doi.org/10.1016/S1359-8368(99)00023-2.

[5] Tohgo K, Nakagawa S, Kageyama K. Fatigue behaviour of CFRP cross-ply laminates under on-axis and off-axis cyclic loading. Int J Fatigue 2006;28:1254–62. https://doi.org/10.1016/j.ijfatigue.2006.02.011.

[6] Henaff-Gardin C, Lafarie-Frenot MC. The use of a characteristic damage variable in the study of transverse cracking development under fatigue loading in cross-ply laminates. Int J Fatigue 2002;24:389–95. https://doi.org/10.1016/S0142-1123(01)00094-9.

[7] Taheri-Behrooz F, Shokrieh MM, Lessard LB. Residual stiffness in cross-ply laminates subjected to cyclic loading. Compos Struct 2008;85:205–12.

[8] Yokozeki T, Aoki T, Ishikawa T. Fatigue growth of matrix cracks in the transverse direction of CFRP laminates. Compos Sci Technol 2002;62:1223–9. https://doi.org/10.1016/S0266-3538(02)00068-4.

[9] Shen H, Yao W, Qi W, Zong J. Experimental investigation on damage evolution in cross-ply laminates subjected to quasi-static and fatigue loading. Compos Part B: Eng 2017;120:10–26. https://doi.org/10.1016/j.compositesb.2017.02.033.

[10] Ladevèze P. A computational mesodamage model for life prediction for laminates. In: Harris B, editor. Fatigue in composite materials. Woodhead Publishing Limited; 2003. ch 15.

[11] Lubineau G, Ladevèze P. Towards a micromechanics-based damage mesomodel for CFRP laminates under thermomechanical cyclic loading. Sci Eng Compos Mater 2005;12(1–2):71–82. https://doi.org/10.1515/SECM.2005.12.1-2.71.

[12] Lubineau G, Ladevèze P, Violeau D. Durability of CFRP laminates under thermo-mechanical loading: a micro – meso damage model. Compos Sci Technol 2006;66:983–92. https://doi.org/10.1016/j.compscitech.2005.07.031.

[13] Quaresimin M, Carraro PA, Maragoni L. Early stage damage in off-axis plies under fatigue loading. Compos Sci Technol 2016;128:147–54. https://doi.org/10.1016/j.compscitech.2016.03.015.

[14] Nouri H, Lubineau G, Traudes D. An experimental investigation of the effect of shear-induced diffuse damage on transverse cracking in carbon-fiber reinforced laminates. Compos Struct 2013;106:529–36. https://doi.org/10.1016/j.compstruct.2013.06.026.

[15] Ladevèze P, Lubineau G. On a damage mesomodel for laminates: micromechanics basis and improvement. Mech Mater 2003;35:763–75. https://doi.org/10.1016/S0167-6636(02)00204-1.

[16] Takeda N, Ogihara S, Kobayashi A. Microscopic fatigue damage progress in CFRP cross-ply laminates. Composites 1995;26(12):859–67. https://doi.org/10.1016/0010-4361(95)90879-5.

[17] Nairn JA. Matrix microcracking in composites. In: Talreja R, Manson JAE, editors. Polymer matrix composites. Elsevier Science; 2000. p. 403–32. ch. 13.

[18] Hosoi A, Arao Y, Kawada H. Transverse crack growth behavior considering free-edge effect in quasi-isotropic CFRP laminates under high-cycle fatigue loading. Compos Sci Technol 2009;69:1388–93. https://doi.org/10.1016/j.compscitech.2008.09.003.

[19] Kobayashi S, Terada K, Ogihara S, Takeda N. Damage-mechanics analysis of matrix cracking in cross-ply CFRP laminates under thermal fatigue. Compos Sci Technol 2001;61:1735–42. https://doi.org/10.1016/S0266-3538(01)00077-X.

[20] Kobayashi S, Takeda N. Experimental and analytical characterization of transverse cracking behavior in carbon/bismaleimide cross-ply laminates under mechanical fatigue loading. Compos Part B: Eng 2002;33(6):471–8.

[21] US Department of Defense. Handbook of polymer matrix composites, vol.3, materials usage, design and analysis; 2002. https://doi.org/10.1016/0378-3804(85)90127-5.

[22] Liu S, Nairn JA. Fracture mechanics analysis of composite microcracking: experimental results in fatigue. Proceedings of the 5th technical conference on composite materials. American Society of Composites; 1990. p. 287–95.

[23] Ladevèze P, Lubineau G. On a damage mesomodel for laminates: micro-meso relationships, possibilities and limits. Compos Sci Technol 2001;61(15):2149–58.

https://doi.org/10.1016/S0266-3538(01)00109-9.
[24] Ladevèze P, Lubineau G. An enhanced mesomodel for laminates based on micromechanics. Compos Sci Technol 2002;62:533–41. https://doi.org/10.1016/S0266-3538(01)00145-2.
[25] Maimí P, Rodríguez H, Blanco N, Mayugo JA. Numerical modelling of matrix cracking and intralaminar failure in advanced composite materials. In: Camanho PP, Hallett SR, editors. Numerical modelling of failure in advanced composite materials. Elsevier; 2015. p. 196–214. ch 7.
[26] Lafarie-Frenot MC, Henaff-Gardin C. Formation and growth of 90 ply fatigue cracks in carbon/epoxy laminates. Compos Sci Technol 1991;40:307–24. https://doi.org/10.1016/0266-3538(91)90087-6.
[27] Lafarie-Frenot MC, Henaff-Gardin C, Gamby D. Matrix cracking induced by cyclic ply stresses in composite laminates. Compos Sci Technol 2001;61:2327–36. https://doi.org/10.1016/S0266-3538(01)00125-7.
[28] Varna J, Loukil MS. Effective transverse modulus of a damaged layer: potential for predicting symmetric laminate stiffness degradation. J Compos Mater 2016;51(14):1945–59. https://doi.org/10.1177/0021998316658965.
[29] Yokozeki T, Aoki T, Ishikawa T. Transverse crack propagation in the specimen width direction of CFRP laminates under static tensile loadings. J Compos Mater 2002;36(17):2085–99. https://doi.org/10.1106/002199802026978.
[30] Maimí P, Camanho PP, Mayugo JA, Turon A. Matrix cracking and delamination in laminated composites. Part I: ply constitutive law, first ply failure and onset of delamination. Mech Mater 2011;43:169–85. https://doi.org/10.1016/j.mechmat.2010.12.003.
[31] Maimí P, Camanho PP, Mayugo JA, Turon A. Matrix cracking and delamination in laminated composites. Part II: evolution of crack density and delamination. Mech Mater 2011;43:194–211. https://doi.org/10.1016/j.mechmat.2011.01.002.
[32] Camanho PP, Dávila CG, Pinho ST, Iannucci L, Robinson P. Prediction of in situ strengths and matrix cracking in composites under transverse tension and in-plane shear. Compos Part A: Appl Sci Manuf 2006;37(2):165–76. https://doi.org/10.1016/j.compositesa.2005.04.023.
[33] Herakovich CT. Mechanics of fibrous composites; 1998. https://doi.org/10.1007/s13398-014-0173-7.2.
[34] Lim SH, Li S. Energy release rates for transverse cracking and delaminations induced by transverse cracks in laminated composites. Compos Part A: Appl Sci Manuf 2005;36(11):1467–76. https://doi.org/10.1016/j.compositesa.2005.03.015.
[35] Kashtalyan M, García IG, Mantič V. Coupled stress and energy criterion for multiple matrix cracking in cross-ply composite laminates. Int J Solids Struct 2018;139–140:189–99. https://doi.org/10.1016/j.ijsolstr.2018.01.033.
[36] Maimí P, Mayugo JA, Camanho PP. A three-dimensional damage model for transversely isotropic composite laminates. J Compos Mater 2008;42(25):2717–45. https://doi.org/10.1177/0021998308094965.
[37] Nairn JA, Hu S. The formation and effects of outer-ply microcracks in cross-ply laminates: a variational approach. Eng Fract Mech 1992;41(2):203–21. https://doi.org/10.1016/0013-7944(92)90181-D.
[38] McCartney LN, Schoeppner GA, Becker W. Comparison of models for transverse ply cracks in composite laminates. Compos Sci Technol 2000;60(12–13):2347–59. https://doi.org/10.1016/S0266-3538(00)00030-0.
[39] Farrokhabadi A, Mohammadi B, Hosseini-Toudeshky H. A generalized plane-strain crack density-based model for evaluating the finite fracture toughness of composite laminates. Mech Adv Mater Struct 2017;24(2):131–41. https://doi.org/10.1080/15376494.2015.1120906.
[40] Parvizi A, Bailey JE. On multiple transverse cracking in glass fibre epoxy cross-ply laminates. J Mater Sci 1978;13(10):2131–6. https://doi.org/10.1007/BF00541666.
[41] Krasnikovs A, Varna J. Transverse cracks in cross-ply laminates. 1. Stress analysis. Mech Compos Mater 1997;33(6):565–82. https://doi.org/10.1007/BF02269616.
[42] Varna J, Krasnikovs A. Transverse cracks in cross-ply laminates 2. Stiffness degradation. Mech Compos Mater 1998;34(2):153–70. https://doi.org/10.1007/BF02256035.
[43] Berthelot JM, El Mahi A, Leblond P. Transverse cracking of cross-ply laminates: Part 2. Progressive widthwise cracking. Compos Part A: Appl Sci Manuf 1996;27(10):1003–10. https://doi.org/10.1016/1359-835X(96)00064-4.
[44] Nairn JA, Mendels DA. On the use of planar shear-lag methods for stress-transfer analysis of multilayered composites. Mech Mater 2001;33(6):335–62. https://doi.org/10.1016/S0167-6636(01)00056-4.
[45] Mayugo JA, Camanho PP, Maimí P, Dávila CG. Analytical modelling of transverse matrix cracking of {θ/90 n } s composite laminates under multiaxial loading. Mech Adv Mater Struct 2010;17(4):237–45. https://doi.org/10.1080/15376490903056577.
[46] Hashin Z. Analysis of cracked laminates: a variational approach. Mech Mater 1985;4(2):121–36. https://doi.org/10.1016/0167-6636(85)90011-0.
[47] Vinogradov V, Hashin Z. Variational analysis of cracked angle-ply laminates. Compos Sci Technol 2010;70(4):638–46. https://doi.org/10.1016/j.compscitech.2009.12.018.
[48] Xia ZC, Carr RR, Hutchinson JW. Transverse cracking in fiber-reinforced brittle matrix, cross-ply laminates. Acta Metall Mater 1993;41(8):2365–76. https://doi.org/10.1016/0956-7151(93)90316-K.
[49] Leblond P, El Mahi A, Berthelot JM. 2D and 3D numerical models of transverse cracking in cross-ply laminates. Compos Sci Technol 1996;56(7):793–6. https://doi.org/10.1016/0266-3538(96)00022-X.
[50] Berthelot JM, El Mahi A, Le Corre JF. Development of transverse cracking in cross-ply laminates during fatigue tests. Compos Sci Technol 2001;61(12):1711–21. https://doi.org/10.1016/S0266-3538(01)00068-9.
[51] McCartney LN. Theory of stress transfer in a 0-90-0 cross-ply laminate containing a parallel array of transverse cracks. J Mech Phys Solids 1992;40(1):27–68. https://doi.org/10.1016/0022-5096(92)90226-R.
[52] McCartney L. Model to predict effects of triaxial loading on ply cracking in general symmetric laminates. Compos Sci Technol 2000;60(12-13):2255–79. https://doi.org/10.1016/S0266-3538(00)00086-5.
[53] McCartney LN. Predicting transverse crack formation in cross-ply laminates. Compos Sci Technol 1998;58(7):1069–81. https://doi.org/10.1016/S0266-3538(96)00142-X.
[54] Thionnet A, Renard J. Laminated composites under fatigue loading: a damage development law for transverse cracking. Compos Sci Technol 1994;52:173–81. https://doi.org/10.1016/0266-3538(94)90203-8.
[55] Renard J, Thionnet A. Damage in composites: from physical mechanisms to modelling. Compos Sci Technol 2006;66(5):642–6.
[56] Bak BLV, Sarrado C, Turon A, Costa J. Delamination under fatigue loads in composite laminates: a review on the observed phenomenology and computational methods. Appl Mech Rev 2014;66(November). https://doi.org/10.1115/1.4027647.
[57] Turon A, Bak BLV, Lindgaard E, Sarrado C, Lund E. Interface elements for fatigue-driven delaminations in advanced composite materials. In: Camanho S, Hallet PP, editors. Numerical modelling of failure in advanced composite materials Woodhead Publishing Series in Composite Science and Engineering; 2015. p. 73–91. https://doi.org/10.1016/B978-0-08-100332-9.00003-7. ch 3.
[58] Ogin SL, Smith PA, Beaumont PWR. Matrix cracking and stiffness reduction during the fatigue of a (0/90)s GFRP laminate. Compos Sci Technol 1985;22:23–31. https://doi.org/10.1016/0266-3538(85)90088-0.
[59] Ritchie RO. Mechanisms of fatigue-crack propagation in ductile and brittle solids. Int J Fract 1999;100:55–83. https://doi.org/10.1023/A:1018655917051.
[60] Carreras L, Renart J, Turon A, Costa J, Essa Y, de la Escalera F Martin. An efficient methodology for the experimental characterization of mode II delamination growth under fatigue loading. Int J Fatigue 2017;95:185–93. https://doi.org/10.1016/j.ijfatigue.2016.10.017.
[61] Carreras L. Development of efficient testing methods and cohesive zone models for analyzing fatigue-driven delamination in 3D laminated composite structures. PhD thesis, University of Girona; 2018.
[62] Sebaey TA, Costa J, Maimí P, Batista Y, Blanco N, Mayugo JA. Measurement of the in situ transverse tensile strength of composite plies by means of the real time monitoring of microcracking. Compos Part B: Eng 2014;65:40–6. https://doi.org/10.1016/j.compositesb.2014.02.001.
[63] Zubillaga L, Turon A, Renart J, Costa J, Linde P. An experimental study on matrix crack induced delamination in composite laminates. Compos Struct 2015;127:10–7. https://doi.org/10.1016/j.compstruct.2015.02.077.

Paper C

A continuum damage model for composite laminates: Part III - Fatigue

J. Llobet[a], P. Maimí[a], Y. Essa[b], F. Martin de la Escalera[b]
[a] AMADE, Polytechnic School, Universitat de Girona, Girona, Spain
[b] AERNNOVA Engineering Division, Structural Integrity Department, Madrid, Spain

The paper has been submitted to
Mechanics of Materials.

A continuum damage model for composite laminates: Part III - Fatigue

J. Llobet[a,*], P. Maimí[a,*], Y. Essa[b], F. Martin de la Escalera[b]

[a]AMADE, Mechanical Engineering and Industrial Construction Department, University of Girona, Carrer Universitat de Girona 4, E-17003 Girona, Spain
[b]AERNNOVA Engineering Division SA, Llano Castellano Avenue 13, E-28034 Madrid, Spain

Abstract

The meso-scale continuum damage model for laminated composites that has been developed for the past 10 years at AMADE research group is extended for fatigue life and residual strength predictions. The same intralaminar damage mechanisms are considered by using the LaRC loading functions, but a new set of physically-based functions are introduced to contemplate fatigue damage initiation and evolution. The cycle jump approach is adopted within the finite element code to reduce the computational cost. The model is validated by simulating the progressive failure mechanisms of open-hole and double-edge notched specimens under static, tension-tension fatigue and residual strength load cases. The experimental tests and simulations to validate the computational model are reported in the follow-up paper.

Keywords: Fatigue, Composite laminates, Continuum Damage Mechanics, Residual strength, Finite Element Modelling

1. Introduction

This paper follows on from the previous work developed by (Maimí et al., 2007a,b), in which a meso-scale continuum damage mechanics (CDM) model was framed to predict the accumulation of intra-laminar damage and final failure of composite laminates under static loads. The CDM model has been proved to be a reliable predictive computational tool whose capabilities have been tested extensively under static and dynamic loading scenarios (Camanho et al., 2007; González et al., 2018; Maimí et al., 2006; Soto et al., 2018).

Fatigue in composites is fundamentally different than in metals (Alderliesten, 2013; Bathias, 2006). While fatigue damage in metals often reveals in a localized manner (unique crack leading to failure), fatigue damage in composites occurs in multiple forms that can be described at the meso-scale as distributed or localized damage. The fatigue design philosophies used for metals, from safe-life design principles, via fail-safe concepts and towards damage tolerance designs have been improved over the years by increasing the understanding of metal fatigue. In composites, the maximum strains are limited to proven values that will not cause fatigue issues and the no-growth concept (or safe-life) is commonly adopted. Despite the continuous improvement to have reliable life prediction methodologies, the aerospace sector is seeking for more advanced computational tools to allow damage-tolerance designs with composites and thus reduce the necessary number of tests for certification.

Several authors have shown that the observed damage mechanisms are identical for laminates under static and fatigue loads (Kaminski et al., 2015). However, the threshold of damage initiation in fatigue is lower than the threshold in static, and the damage evolution laws differ. The fact that no new damage mechanisms occur under fatigue loads implies that CDM can be the appropriate framework to reproduce the physics of fatigue degradation in composites. Different CDM-based models exist in open literature that allow to describe fatigue damage and life of composites under certain conditions (Hochard and Thollon, 2010; Ladevèze, 2003; Mohammadi et al., 2017; Payan and Hochard, 2002; Sedrakian et al., 2002; Zhang et al., 2016, 2014). The vast majority of these models share the common limitations of "classical" strain-softening constitutive models, that is, mesh-dependency when damage localizes and damage evolution depending on thermodynamic restrictions rather than physically-based material properties. The model presented in Maimí et al. (2007a,b), besides satisfying the thermodynamic restrictions, is based on the actual failure mechanisms, i.e., the damage activation functions are related to the physics of the different ply failure mechanisms and the damage variables evolve according to the cohesive laws of the governing mechanism. The model ensures an objective response regardless of the mesh refinement by means of the crack band model (Bazant and Oh, 1983), provided that a structured mesh of the ply oriented in the fibre direction is used (Camanho et al., 2007). It is worth pointing out relevant aspects of some fatigue damage models such as Van Paepegem et al. (2006a,b) that include the accumulation of cyclic permanent strains, Hochard et al. (2013) that introduce a non-local approach to predict the fatigue failure of composite structures with stress concentrations, Krüger and Rolfes (2015) that account for the length of the finite element in the constitutive law (i.e., crack band model) and introduce an energy-based approach to relate the damage states under static and fatigue loads, Naderi and Maligno (2012) and Lian and Yao (2010) that include the effect of a random distribution of the material properties to predict the scatter of fatigue data, among so many others (Eliopoulos and Philippidis, 2011a,b; Kordkheili et al.,

*Corresponding author.
Email addresses: jordi.llobet@udg.edu (J. Llobet), pere.maimi@udg.edu (P. Maimí)

2017; Shokrieh and Lessard, 2000a,b). Most of these damage models cannot be strictly classified as CDM-based models as such, however they are considered as remarkable fatigue models in the literature. Note that none of these models account for fatigue-driven delamination, except for Naderi and Maligno (2012) that define a stress-based delamination onset criterion, and then apply the ply-discount method to degrade the ply properties. Several of these fatigue models make use of the simplified ply discount method once the failure criterion is met. The ply discount method is not sufficient to predict the progressive failure of composite structures which can accumulate damage before structural collapse. Finally, fatigue models based on discrete damage modelling such as Nixon-Pearson et al. (2013) that represent the growth of intra- and inter-laminar fatigue cracks by means of cohesive interface elements, and Iarve et al. (2016) that account for intra-laminar matrix cracks by regularized X-FEM and delamination using cohesive interface elements. Iarve et al. (2016) highlighted the importance of modelling fatigue damage initiation of matrix cracks which was done by defining a S-N curve and a linear damage accumulation rule (i.e., Miner), and then crack propagation with a Paris-based function that allowed to simulate the progressive damage of open-hole specimens.

Based on the previous considerations, the main objective of this work is to present an extended version of the previous CDM model (Maimí et al., 2006, 2007a,b) for fatigue life and residual strength predictions. The constitutive model assumes a change in the constitutive response when fatigue damage takes place. This change is directly related to the form of fatigue damage mechanism that occurs and the way that can be described at the meso-scale, i.e., distributed or localized intra-ply damage. Different empirical functions are contemplated to define the constitutive response of a fatigue-damaged material point. First, the early initiation of fatigue distributed damage is considered by modifying the elastic response prior to the localization of a macro crack. Once a localized crack is formed, the subsequent growth can be defined by means of the crack growth rate data. The methodology to characterize some of these functions is presented in the previous experimental works performed by the authors (Llobet et al., 2018, 2017). Delamination is also an important mechanism during the fatigue degradation process of a carbon/epoxy material, and thus it is necessary to include its effect on the numerical model. The follow-up paper presents a modelling strategy that couples the intra-laminar fatigue model presented here and the fatigue cohesive zone model developed in (Turon, 2006; Turon et al., 2015, 2007).

The content of this paper is organized as follows. First, section 2 introduces the fatigue damage mechanisms that occur in a laminated composite and emphasizes the differences between static and fatigue. Section 3 provides a short summary of the key features of the published CDM model but also stands out the updates and changes made to the original formulation. The new concepts that are introduced to include fatigue damage are also described in this section. Hereafter, the reader is referred to (Maimí et al., 2006, 2007a,b) for further details of the model formulation. Section 4 shows how to implement a fatigue analysis inside a finite element code using a cycle jump strategy. Finally, Section 5 exposes the conclusions of the present work.

2. Mechanisms of damage and fracture in laminated composites: static vs. fatigue

The model describes any complex state of degradation in a laminated composite by four intralaminar damage modes that occur at ply level. The interlaminar damage (or delamination) at the interfaces is not considered here, but the reader is referred to the follow-up paper where an interlaminar damage model is presented.

Under a longitudinal tension static load, failure occurs in a fracture plane normal to the fibre direction where both constituents break. Under a longitudinal compression load, fibre breaks as a result of shear kinking and damage in the supporting matrix, which leads to the nucleation of a kink-band. However, failure in the transverse direction leads to a matrix crack. This matrix crack appears in the fibre/matrix interface and in the resin. In tension, it is formed parallel to the fibre direction, but for higher levels of transverse compression the angle of the fracture plane changes (Maimí et al., 2006, 2007a). In general, all the ply damage mechanisms produce a brittle failure in unidirectional laminates. Nevertheless, a relevant non-linear region with hardening occurs before cracking if the ply is loaded under in-plane shear. When the unidirectional ply is embedded into a multidirectional laminate, two considerations need to be made. First, transverse matrix cracking occurs (multiple cracks rather than one isolated crack), and this mechanism can be considered as non-localized by using the crack density variable. Second, the increase in the transverse and shear ply strengths by reducing its thickness (known as the *in-situ* effect).

Under fatigue loads, the same damage mechanisms are identified but they initiate at lower loading levels and evolve in a different manner. The sequence of fatigue damage in conventional quasi-isotropic unnothed laminates is usually divided in three stages (Reifsnider and Jamison, 1982; Schulte, 1984; Van Paepegem and Degrieck, 2002a):

Stage I - The first damage mechanism that appears is matrix cracking at off-axis plies. This transverse ply cracks appear spatially distributed along its specimen length and they propagate into the through-the-width direction. This damage mechanism causes a small reduction in the overall stiffness of carbon/epoxy laminates, but these cracks redistribute stresses to adjacent plies causing fibre fractures and delamination. This stage of fatigue life has been analysed extensively in Berthelot and Le Corre (1999); Hosoi et al. (2015); Liu and Nairn (1990); Llobet et al. (2018); Nairn (2000); Yokozeki et al. (2002).

Stage II - Damage progresses with a linear decrease in stiffness with respect to the number of cycles (Brøndsted et al., 1996). This is caused by the multiplication of matrix cracks accompanied by local delaminations. Fatigue growth of delamination cracks has also been the subject of many investigations (Bak et al., 2014).

Stage III -The final stage III corresponds to a sudden drop of stiffness triggered by an unstable delamination growth

(delamination-dominated failure) or by a fibre fracture (fibre-dominated failure).

Extensive fatigue experimental campaigns are available in open-literature that provide decreasing functions of the number of cycles for the loss of stiffness and strength at a given load magnitude. These functions distinguish between fibre and matrix degradation, and also the types of stress (normal, transverse, in-plane and out-of-plane shear) (Eliopoulos and Philippidis, 2011a,b; Passipoularidis, 2009; Philippidis and Passipoularidis, 2007; Shokrieh and Lessard, 2000a,b; Shokrieh and Taheri-Behrooz, 2010).

In notched specimens, transverse cracks at the 90° plies initiate at the root of the notch, while additional matrix cracks occur in the 0° and ±45° plies, referred to as splitting. Figure 1 shows an example of this with an X-ray image taken from a carbon/epoxy open-hole specimen. In the static case (left), the strength is governed by the translaminar cohesive law with fibre fracture (Ortega, 2017; Ortega et al., 2016), whereas in fatigue it is controlled by the progressive growth of splitting and by delamination (Aidi et al., 2015; Ambu et al., 2005; Aymerich and Found, 2000; Nixon-Pearson and Hallett, 2015). The development of splitting cracks parallel to the 0-degree fibres is of prime importance as it alleviates the stress concentration factor and suppresses the fibre fracture. Indeed, these splitting cracks and delaminations play a beneficial role since they increase the open-hole tensile residual strength (Aymerich and Found, 2000; Spearing and Beaumont, 1992; Spearing et al., 1992a,b).

3. Constitutive damage model

The constitutive damage model is summarized in this section and the changes made to the original formulation are highlighted, but the reader is referred to (Maimí et al., 2007a,b, 2008) for further details on the derivation of the model. It should be noted that the notation used in this work follows the former publications except for a minor change in the subscripts of the variables. The notation, terms and coefficients used here are progressively introduced throughout the paper, but the reader is referred to Table 1 for clarification.

	$\sigma_{11} > 0$	$\sigma_{11} < 0$	$\sigma_{22} > 0$	$\sigma_{22} < 0$	σ_{12}
n:	1+	1−	2+	2−	6
k:	$L+$	$L-$	$T+$	$T-$	$T+$
E_n:	E_1	E_1	E_2	E_2	G_{12}
X_n:	X_T	X_C	Y_T	Y_C	S_L
$\mathcal{G}_n$:	$\mathcal{G}_{1+}$	$\mathcal{G}_{1-}$	$\mathcal{G}_{2+}$	$\mathcal{G}_{2-}$	$\mathcal{G}_6$
ϑ_n:	0	$\frac{\nu_{12}\nu_{21}-\nu_{21}(1-\eta_L X_C/S_L)}{1-\nu_{12}\nu_{21}}$	$\frac{\nu_{12}\nu_{21}}{1-\nu_{12}\nu_{21}}$	$\frac{\nu_{12}\nu_{21}}{1-\nu_{12}\nu_{21}}$	0

Table 1: Notation, coefficients and terms used throughout the paper for each uni-axial stress type, where σ_{11}, σ_{22} and σ_{12} are the normal, transverse and in-plane shear stresses. The subscript 1 indicates the longitudinal direction (fibre) and the subscript 2 the transverse in-plane direction (matrix). Subscripts L and T define the four damage mechanisms considered. L stands for fibre failure and T for matrix failure, in both tension (+) and compression (−) cases.

3.1. Potential energy function, constitutive law and energy dissipation

The constitutive law of a composite material can be established based on the framework of thermodynamics and the use of a scalar potential function (Houlsby and Puzrin, 2000). Assuming that the constitutive model is defined at the meso-scale (i.e., the composite lamina is homogeneous and transversally isotropic), small strains and a state of plane-stress, the scalar complementary Gibbs free energy (G) can be used to describe the stored elastic energy:

$$G = \frac{\sigma_{11}^2}{2(1-D_1)E_1} + \frac{\sigma_{22}^2}{2(1-D_2)E_2} - \frac{\nu_{12}}{E_1}\sigma_{11}\sigma_{22} + \frac{\sigma_{12}^2}{2(1-D_6)G_{12}} + \sigma_{12}\varepsilon_{12}^p + (\alpha_{11}\sigma_{11} + \alpha_{22}\sigma_{22})\Delta T + (\beta_{11}\sigma_{11} + \beta_{22}\sigma_{22})\Delta M \tag{1}$$

where σ_{11}, σ_{22} and σ_{12} are the normal, transverse and in-plane shear stresses. E_1, E_2, ν_{12} and G_{12} are the in-plane elastic properties. α_{11}, α_{22}, β_{11} and β_{22} are the thermal and hygroscopic expansion coefficients. ΔT and ΔM are the change in temperature and moisture content. Note that a new term ε_{12}^p is added into the expression to consider shear permanent strains. The damage state is described by a set of scalar damage variables D_1, D_2 and D_6 whose values range from 0, for a pristine material, to 1 for a fully damaged material. The damage variable D_1 is associated with longitudinal (fibre) failure, D_2 is the damage variable associated with transverse (matrix) failure and D_6 is a damage variable influenced by longitudinal and transverse cracks. In order to account for crack closure effects, the model tracks the damage caused by tensile (D_{n+}) or by compressive loads (D_{n-}). Depending on the sign of the stress, the longitudinal and transverse damage variables are computed as follows:

$$\begin{aligned} D_1 &= D_{1+}\frac{\langle\sigma_{11}\rangle}{|\sigma_{11}|} + D_{1-}\frac{\langle-\sigma_{11}\rangle}{|\sigma_{11}|} \\ D_2 &= D_{2+}\frac{\langle\sigma_{22}\rangle}{|\sigma_{22}|} + D_{2-}\frac{\langle-\sigma_{22}\rangle}{|\sigma_{22}|} \end{aligned} \tag{2}$$

where $2\langle x\rangle = x + |x|$ is the Macaulay operator. The model assumes that the shear damage variable, D_6, is not affected by the closure effect (Maimí et al., 2007a).

The constitutive model must ensure the irreversibility of the damage process by imposing the rate of energy dissipated, Ξ, to be positive. The evolution of damage without energy dissipation is physically not admissible in constitutive modelling. Assuming an isothermal process, the Clausius-Duhem inequality can be postulated such that the externally supplied mechanical power, $\sigma : \dot{\varepsilon}$, minus the rate of change of the Helmholtz free energy, $\dot{\Psi}$, must be positive:

$$\Xi = \boldsymbol{\sigma} : \dot{\boldsymbol{\varepsilon}} - \dot{\Psi} \geq 0 \tag{3}$$

Alternatively, one can express the rate of dissipated energy, Ξ, with respect to the rate of change of the complementary Gibbs free energy, $\dot{G}$, minus the externally supplied work, $\dot{\sigma} : \varepsilon$

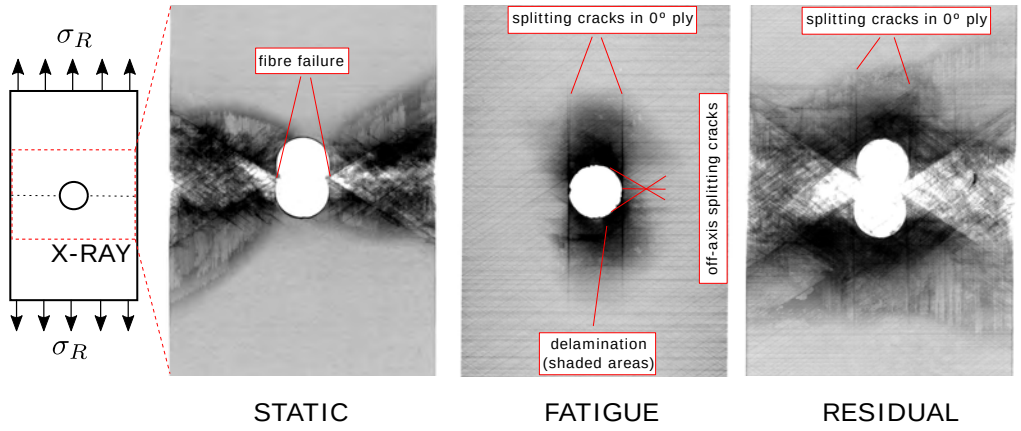

Figure 1: Damage mechanisms found in a quasi-isotropic carbon/epoxy open-hole specimen subjected to static, tension-tension fatigue and post-fatigue residual strength tests (original tests and X-ray images performed by the authors). Refer to the follow-up paper for further details.

using the Legendre transformation (Houlsby and Puzrin, 2000; Quintanas-Corominas et al., 2018). It follows that:

$$\Xi = \dot{G} - \dot{\boldsymbol{\sigma}} : \boldsymbol{\varepsilon} = \left(\frac{\partial G}{\partial \boldsymbol{\sigma}} - \boldsymbol{\varepsilon}\right) : \dot{\boldsymbol{\sigma}} + \frac{\partial G}{\partial D_n} : \dot{D}_n + \frac{\partial G}{\partial \varepsilon_{12}^p} : \dot{\varepsilon}_{12}^p \geq 0 \quad (4)$$

Since the stress variables can change without restrictions, the positive rate of Ξ is guaranteed only if the term inside the brackets in Eq. (4) equals zero, provided that the damage variables increase monotonically ($\dot{D}_n \geq 0$) and $\dot{\varepsilon}_{12}^p$ has the same sign as σ_{12}. Thus, the strain tensor is obtained by taking the derivative of the complementary free energy with respect to the stress tensor:

$$\boldsymbol{\varepsilon} = \frac{\partial G}{\partial \boldsymbol{\sigma}} = \mathbf{H} : \boldsymbol{\sigma} + \boldsymbol{\varepsilon}^{\boldsymbol{p}} + \boldsymbol{\alpha}\Delta T + \boldsymbol{\beta}\Delta M \quad (5)$$

where $\mathbf{H}$ is the compliance tensor, $\boldsymbol{\sigma}$ is the stress tensor, $\boldsymbol{\varepsilon}^{\boldsymbol{p}}$ is the plastic strain tensor, $\boldsymbol{\alpha}$ and $\boldsymbol{\beta}$ are the thermal and moisture dilatation tensors. Due to the symmetry of the stress and strain tensors, the tensors of Eq. (5) can be written using Voigt notation as:

$$\mathbf{H} = \frac{\partial^2 G}{\partial \sigma^2} = \begin{bmatrix} \frac{1}{(1-D_1)E_1} & -\frac{\nu_{21}}{E_2} & 0 \\ -\frac{\nu_{12}}{E_1} & \frac{1}{(1-D_2)E_2} & 0 \\ 0 & 0 & \frac{1}{(1-D_6)G_{12}} \end{bmatrix} \quad (6)$$

$$\begin{aligned} [\boldsymbol{\sigma}]^{\mathrm{T}} &= [\sigma_{11}, \sigma_{22}, \sigma_{12}] \\ [\boldsymbol{\varepsilon}]^{\mathrm{T}} &= [\varepsilon_{11}, \varepsilon_{11}, \varepsilon_{12}] \\ [\boldsymbol{\varepsilon}^{\boldsymbol{p}}]^{\mathrm{T}} &= [0, 0, \varepsilon_{12}^p] \\ [\boldsymbol{\alpha}]^{\mathrm{T}} &= [\alpha_{11}, \alpha_{22}, 0] \\ [\boldsymbol{\beta}]^{\mathrm{T}} &= [\beta_{11}, \beta_{22}, 0] \end{aligned} \quad (7)$$

3.2. Damage onset functions

The elastic domain is enclosed by four damage onset functions F_k, associated with the longitudinal and transverse failure modes in tension and compression ($k = L+, L-, T+, T-$):

$$\begin{aligned} F_{L+} &= \phi_{L+} - r_{L+}\beta_{L+} \leq 0 \quad , \quad F_{L-} = \phi_{L-} - r_{L-}\beta_{L-} \leq 0 \\ F_{T+} &= \phi_{T+} - r_{T+}\beta_{T+} \leq 0 \quad , \quad F_{T-} = \phi_{T-} - r_{T-}\beta_{T-} \leq 0 \end{aligned} \quad (8)$$

where ϕ_k are the loading functions which define a norm of the strain (and the shape of the failure surface) and $r_k(D_n)$ are the internal variables that track the state of damage in a material point. When the material is undamaged, the internal variables r_k take a value of 1, and $D_n = 0$. But once the material is completely damaged, the strain is localized in a fracture plane with $D_n(r_k \to \infty) = 1$. β_k is defined as a new variable that measures the reduction of the ultimate strain due to fatigue damage. β_k and r_k are internal variables of the model describing the static and fatigue response of the material, respectively. Under shear loads, the material undergoes plastic deformation once reaches the yield stress prior to the localization of a matrix crack with softening. If one considers the idealized case of linear hardening, the yield condition can be written as:

$$F_P = |\tilde{\sigma}_{12}| - \left(\beta_{T+} S_{LP} + \varsigma_L \varepsilon_{12}^I\right) \leq 0 \quad (9)$$

where $\tilde{\sigma}_{12}$ is the effective shear stress component (see Section 3.3), ε_{12}^I is the isotropic hardening variable, S_{LP} and ς_L are material parameters that can be obtained from the in-plane shear test with a $[\pm 45^\circ]$ laminate (see ASTM D3518-13). Eq. (9) defines linear hardening as soon as the yield stress S_{LP} is reached with a plastic modulus of $\varsigma_L G_{12} / (G_{12} + \varsigma_L)$ as shown in Figure 2.

3.3. Damage modes and loading functions

The four intralaminar damage modes that are considered at ply level (see Figure 2), longitudinal tensile and compressive

failure, transverse tensile and compressive failure, are activated depending on the magnitude of the strain or the effective stress (stress acting on the intact material). The effective stress is computed as $\tilde{\boldsymbol{\sigma}} = \mathbf{H}_0^{-1} : (\boldsymbol{\varepsilon} - \boldsymbol{\varepsilon}^{\boldsymbol{p}})$, where $\mathbf{H}_0$ is the undamaged compliance tensor. The loading functions ϕ_k are defined by the LaRC03-04 failure criterion (Dávila and Camanho, 2003; Maimí et al., 2006; Pinho et al., 2005):

$$\phi_{L+} = \frac{\langle \tilde{\sigma}_{11} - \nu_{12}\tilde{\sigma}_{22} \rangle}{X_T} \qquad \text{if} \quad \tilde{\sigma}_{11} \geq 0 \tag{10a}$$

$$\phi_{L-} = \frac{\left\langle \left|\tilde{\sigma}^m_{12}\right| + \eta^L \tilde{\sigma}^m_{22} \right\rangle}{S_L} \qquad \text{if} \quad \tilde{\sigma}_{11} < 0 \tag{10b}$$

$$\phi_{T+} = (1-g)\frac{\tilde{\sigma}_{22}}{Y_T} + \sqrt{g^2\left(\frac{\tilde{\sigma}_{22}}{Y_T}\right)^2 + \left(\frac{\tilde{\sigma}_{12}}{S_L}\right)^2} \qquad \text{if} \quad \tilde{\sigma}_{22} \geq 0 \tag{10c}$$

$$\phi_{T+} = \frac{1}{S_L}\left\langle |\tilde{\sigma}_{12}| + \eta^L \tilde{\sigma}_{22} \right\rangle \qquad \text{if} \quad \tilde{\sigma}_{22} < 0 \tag{10d}$$

$$\phi_{T-} = \sqrt{\left(\frac{\tilde{\tau}^T_{eff}}{S_T}\right)^2 + \left(\frac{\tilde{\tau}^L_{eff}}{S_L}\right)^2} \qquad \text{if} \quad \tilde{\sigma}_{22} < 0 \tag{10e}$$

where the stress tensor $\tilde{\boldsymbol{\sigma}}^{\boldsymbol{m}}$ in Eq. (10b) refers to the stress components in a coordinate system (m) representing the fibre misalignment, and η^L is the longitudinal friction coefficient (Dávila and Camanho, 2003; Maimí et al., 2007a). Note that Eq. (10c) is modified with respect the original expression (Maimí et al., 2007a) as to make the expression linear-wise with respect to the effective stress.

3.4. Internal variables evolution

The damage activation functions can be explicitly integrated by considering the consistency condition, $\dot{F}_k = 0$, which yields to the following equations:

$$\begin{aligned} r_{L+} &= \max_{s=0,t}\left\{1, \left(\phi_{L+}\beta_{L+}^{-1}\right)^s, \left(\phi_{L-}\beta_{L-}^{-1}\right)^s\right\}, \quad r_{L-} = \max_{s=0,t}\left\{1, \left(\phi_{L-}\beta_{L-}^{-1}\right)^s\right\} \\ r_{T+} &= \max_{s=0,t}\left\{1, \left(\phi_{T+}\beta_{T+}^{-1}\right)^s, \left(\phi_{T-}\beta_{T-}^{-1}\right)^s\right\}, \quad r_{T-} = \max_{s=0,t}\left\{1, \left(\phi_{T-}\beta_{T-}^{-1}\right)^s\right\} \end{aligned} \tag{11}$$

Analogously, the rate of plastic deformation can be determined by the consistency condition, $\dot{F}_P = 0$, and also by considering that $\dot{\varepsilon}^I_{12} = \left|\dot{\varepsilon}^p_{12}\right|$:

$$\dot{\varepsilon}^p_{12} = \frac{G_{12}}{G_{12} + \varsigma_L}\dot{\varepsilon}_{12} \tag{12}$$

3.5. Damage: static and fatigue

Damage is distinguished between two different regions: distributed damage and localized damage once a crack is formed. This damage can grow either in static or fatigue loads. Each damage function can be expressed by different terms:

$$D_n = 1 - m_n^{Df} m_n^{Ds} m_n^{Lf} m_n^{Ls} \tag{13}$$

where $m_n = 1 - D_n$ is the complementary damage variable, superscript D refers to distributed damage due to the intrinsic dissipation mechanisms in the bulk material and L refers to localized damage due to the extrinsic dissipation mechanisms in the cohesive zone (Ritchie, 1999). f stands for fatigue damage and s for static damage. Figure 3 exemplifies the two different forms of damage in a composite ply.

3.6. Static damage functions

The static response of a unidirectional composite ply is assumed to be linear elastic prior to failure so that the static distributed damage can be neglected for almost all the static cases. An exception to this occurs when a ply is loaded under a longitudinal compression or under in-plane shear, the former case resulting in a small region of hardening during the nucleation of a kink-band, and the latter resulting in a large non-linear zone with permanent strains. Another case of non-localized material degradation is transverse matrix cracking, which occurs when a ply is embedded in a multi-directional laminate. The crack density is used as the mechanistic variable rather than the first ply failure of one individual isolated matrix crack (Berthelot and Le Corre, 1999; Hosoi et al., 2015; Llobet et al., 2018). But with the appropriate kinematic description, these transverse cracks can also be modelled as localized damage (Maimí et al., 2008; Quintanas-Corominas et al., 2018).

When localization takes place, the strains are no longer defined in the continuum and the material constitutive law must be expressed by the cohesive law. The crack-band model (Bazant and Oh, 1983) is used to guarantee an objective response regardless of the mesh size. Thus, the fracture energy dissipated by the different damage modes (g_n) is adjusted for each finite element accounting its size:

$$g_n = \int_1^\infty Y_n \frac{\partial D_n}{\partial r_k} dr_k = \frac{\mathcal{G}_n}{l^*} \tag{14}$$

where l^* is the characteristic length of the finite element and $Y_n = \partial G / \partial D_n$ are the so-called thermodynamic forces conjugated to the damage variables (Maimí et al., 2007a). Figure 4 illustrates the transformation from a traction-displacement cohesive law to a stress-strain cohesive law by the crack-band approach. The element is split into two parts, and the mean strain in a material point is computed by using the additive decomposition of the strain tensor: $\boldsymbol{\varepsilon} = \boldsymbol{\varepsilon}^{\boldsymbol{D}} + \boldsymbol{\varepsilon}^{\boldsymbol{L}} + \boldsymbol{\varepsilon}^{\boldsymbol{p}}$. The strain components are determined by considering the same stress in

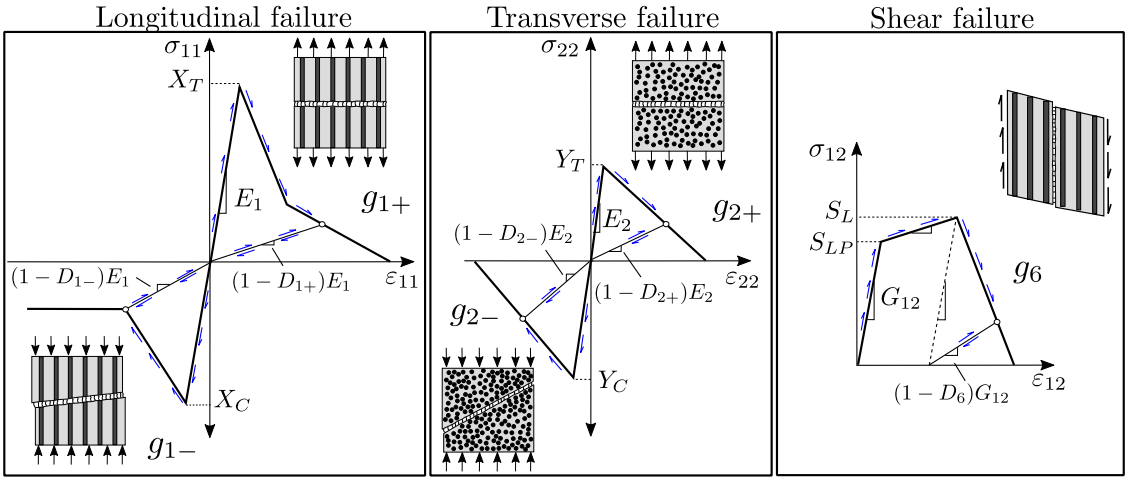

Figure 2: Ply-based failure modes (longitudinal, transverse and in-plane shear cracks) and corresponding constitutive laws.

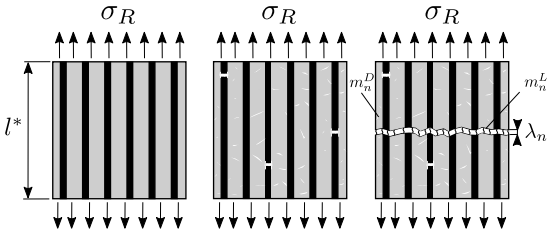

Figure 3: Pristine material (left), distributed damage (centre) and combination of distributed and localized damage (right).

the distributed and localized parts as: $\boldsymbol{\sigma} = \boldsymbol{\sigma^D} = \boldsymbol{\sigma^L}$. The localized strain tensor $\boldsymbol{\varepsilon^L}$ reads:

$$\boldsymbol{\varepsilon^L} = \mathbf{M}^L(\boldsymbol{\varepsilon} - \boldsymbol{\varepsilon}^p); \quad \mathbf{M}^L = \begin{bmatrix} \frac{D_1^L}{1-m_1m_2\nu_{12}\nu_{21}} & \frac{m_2\nu_{21}D_1^L}{1-m_1m_2\nu_{12}\nu_{21}} & 0 \\ \frac{m_1\nu_{12}D_2^L}{1-m_1m_2\nu_{12}\nu_{21}} & \frac{D_2^L}{1-m_1m_2\nu_{12}\nu_{21}} & 0 \\ 0 & 0 & D_6^L \end{bmatrix} \tag{15}$$

Recall that the localized strain is defined as the crack opening with respect to the length of the element: $\varepsilon_n^L = \lambda_n / l^*$.

In the former formulation, exponential cohesive laws were used for all the fracture modes. In the current version, linear and bilinear laws are chosen for the ease of integration. In longitudinal tension response, it is found that a significant load drop at a relatively small crack opening precedes a large tail with small stresses. This response can be described by a bilinear cohesive law such as the one shown in Figure 4. In longitudinal compression, it is also observed a similar load drop prior to a zone with a constant residual stress that is related to the kink-band broadening. The failure modes related to the matrix can be simply reproduced by a linear (or exponential) cohesive law, where the only fitting parameter is the fracture toughness $\mathcal{G}_n$.

Under an uniaxial stress state, the interval variables r_k can be related to the damage variable D_n through the use of the loading functions ϕ_k:

$$r_k = \phi_k = (1 + D_n^{Ls}\vartheta_n)\frac{E_n}{X_n}\varepsilon_n \tag{16}$$

where the term ϑ_n is defined in Table 1 for each uniaxial case, D_n^{Ls} is the static localized damage and the rest are material parameters. By using Eq. (16), the static damage can be calculated as follows:

$$D_n^{Ls} = \frac{r_k X_n - s_{n_i}}{r_k X_n \left(\frac{E_n}{E_n - l^* H_{n_i}}\right) + S_{n_i}\vartheta_n} \quad \begin{cases} i = 1 & \text{for} \quad r_k \le r_k^F \\ i = 2 & \text{for} \quad r_k > r_k^F \end{cases} \tag{17}$$

where the parameters defining the shape of the cohesive law H_{n_i} and s_{n_i} are expressed by the material properties:

$$\begin{aligned} H_{n_1} &= \frac{X_n^2(1-f_{X_n})}{2f_{\mathcal{G}_n}\mathcal{G}_n}, & s_{n_1} &= X_n \\ H_{n_2} &= \frac{s_{n_2}X_n f_{X_n}}{2(1-f_{\mathcal{G}_n})\mathcal{G}_n}, & s_{n_2} &= \frac{f_{X_n}X_n(1-f_{\mathcal{G}_n})}{1-f_{\mathcal{G}_n}(1-f_{X_n})} \end{aligned} \tag{18}$$

r_k^F is the threshold value of the internal variables at which the second stage of the cohesive law is activated:

$$r_k^F = \frac{f_{X_n}}{(1-D_n^F)} \quad \text{and} \quad D_n^F = \frac{2E_n f_{\mathcal{G}_n}\mathcal{G}_n}{f_{X_n}X_n^2 l^* + 2E_n f_{\mathcal{G}_n}\mathcal{G}_n} \tag{19}$$

Note that for a longitudinal compression load (see Figure 2), the second branch of the cohesive law keeps a constant residual

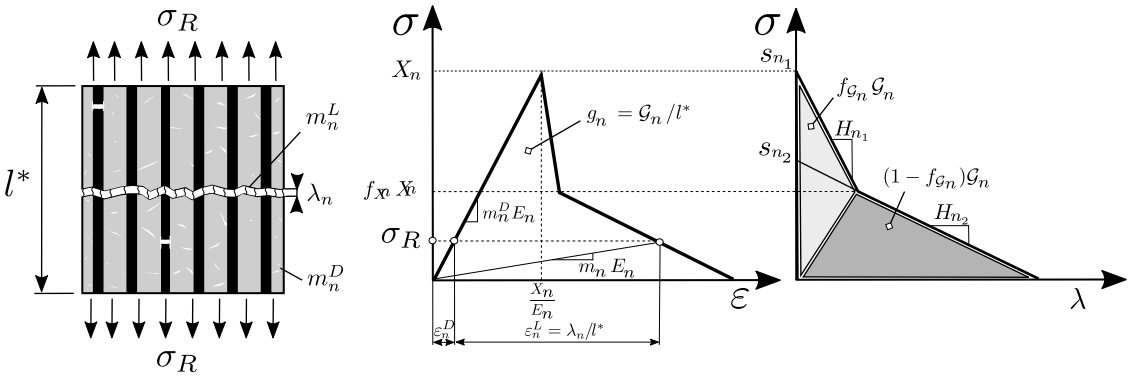

Figure 4: (a) Stress-strain $\sigma(\varepsilon)$ response by introducing the crack-band model. (b) Traction-displacement $\sigma(\lambda)$ bilinear cohesive law.

stress with $H_{n_2} = 0$. The transverse modes with a linear cohesive law are simply defined with H_{n_1}. Under pure shear with linear hardening, the shear damage reduces to:

$$D_{6*}^{Ls} = \frac{G_{12}}{G_{12} - l^* H_n} \left(1 - \frac{S_L \varsigma_L}{r_{T+} S_L (G_{12} + \varsigma_L) - S_{LP} G_{12}}\right) \quad (20)$$

Note that the model computes the total shear damage as: $D_6^{Ls} = 1 - \left(1 - D_{6*}^{Ls}\right)\left(1 - D_{1+}^{Ls}\right)$. The size of the finite elements must be less than a critical value to avoid a local snap-back in the stress-strain response, but it is generally recommended to define elements several times smaller (Leone et al., 2017):

$$l^* \leq \min\left(\frac{E_n}{H_n}\right) \quad (21)$$

3.7. Fatigue damage functions

Fatigue loads induce different damage mechanisms into the laminate plies and these mechanisms can be represented as distributed or localized damage. A set of empirical functions is postulated based on empirical knowledge accounted in the bibliography and on the experimental fatigue tests performed by the authors (Llobet et al., 2018, 2017). The phenomenological functions, that describe the physics of fatigue degradation and its evolution at the mesoscale, are defined as follows:

$$\frac{dD_n^{Df}}{d\mathrm{N}}, \quad \frac{dD_n^{Lf}}{d\mathrm{N}}, \quad \frac{d\beta_k}{d\mathrm{N}} \quad (22)$$

where $dD_n^{Df}/d\mathrm{N}$ and $dD_n^{Lf}/d\mathrm{N}$ are the rates of distributed and localized damage, $d\beta_n/d\mathrm{N}$ is the rate of reduction of the ultimate strain and N is the number of cycles. Figure 5 shows the change of the constitutive response after distributed or localized fatigue damage.

3.7.1. Distributed fatigue damage

The distributed damage functions, D_n^{Df}, are directly related to the decrease in the longitudinal, transverse and shear elastic modulus before localization takes place (refer to Figure 5a). The evolution of the different stages of fatigue damage (in accordance with section 2) is obtained as a combination of different mechanisms at different plies. The distributed damage function at ply level can be generally written as:

$$\frac{dD_n^{Df}}{d\mathrm{N}}\left(D_n^{Df}, \phi_k^{\max}, \phi_k^{\min}, ...\right) \quad (23)$$

where $\phi_k^{\max}$ and $\phi_k^{\min}$ are the maximum and minimum value of the loading functions reached during one fatigue cycle. The loading functions are computed with respect to the distributed strains. Different strategies are adopted to define these functions based on the available data from the experimental characterization tests, some authors expressed them by a magnitude of the strain ϕ_k or the stress $m_n^{Df}\phi_k$ (Degrieck and Van Paepegem, 2001; Llobet et al., 2017; Peerlings, 1999; Van Paepegem and Degrieck, 2002a; Zhang et al., 2014), although other authors make use of the strain energy density $m_n^{Df}(\phi_k)^2$ (Movaghghar and Lvov, 2011, 2012a,b), or the thermodynamic force conjugated to the damage variables $(m_n^{Df}\phi_k)^2$ (Hochard et al., 2006; Mohammadi et al., 2017; Payan and Hochard, 2002; Vasiukov et al., 2015). The definition of Eq. (23) is general enough to cover all possibilities.

3.7.2. Residual strain

Residual strain or strength functions define the reduction of the ultimate strain (or strength) due to the growth of fatigue damage. The residual strength is usually defined as a decreasing function of the number of cycles for a given fatigue load. Similarly, β_k is defined as:

$$\frac{d\beta_k}{d\mathrm{N}}\left(\beta_k, \phi_k^{\max}, \phi_k^{\min}, ...\right) \quad (24)$$

where $\phi_k^{\max}$ and $\phi_k^{\min}$ are also computed with respect to the distributed strains. Contrarily to the distributed damage functions,

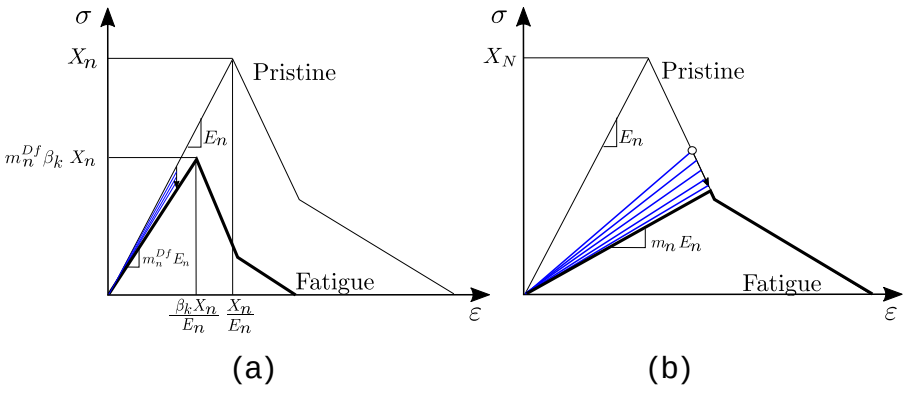

Figure 5: (a) Fatigue response under distributed damage. (b) Fatigue response under localized damage.

the β_k functions are obtained by destructive tests which make them experimentally expensive. In this regard, a common hypothesis is to consider that fatigue damage does not change the ultimate longitudinal strain (Hwang and Han, 1986; Llobet et al., 2017; Van Paepegem and Degrieck, 2002a,b; Whitworth, 1998; Zhang et al., 2015), i.e., $\beta_{L+} = \beta_{L-} = 1$. This assumption, that is deduced from the strain equivalence principle introduced by (Lemaitre, 1992), was validated experimentally by the authors (Llobet et al., 2017). Note that if $\beta_{L+} = \beta_{L-} = 1$, the loss of strength in the fibre direction is of the same magnitude as the loss of stiffness.

3.7.3. *Localized fatigue damage*

The localized damage functions, D_n^{Lf}, describe the growth of a crack after the onset of localization through the cohesive law. Turon et al. (Turon, 2006; Turon et al., 2015, 2007) combined damage mechanics and fracture mechanics concepts to figure out a consistent way to relate the damage rate, $dD_n^{Lf}/d\mathrm{N}$, and the crack growth rate, $da/d\mathrm{N}$. This approach was successfully used to simulate the fatigue growth of delamination cracks. The localized damage rate, $dD_n^{Lf}/d\mathrm{N}$, reduces to the expression postulated by Turon et al. (Turon et al., 2007), namely:

$$\frac{dD_n^{Lf}}{d\mathrm{N}} = -\frac{l^*}{l_{cz}} \frac{\left[D_n X_n^2 + 2m_n E_n \mathcal{G}_n / l^*\right]^2}{2X_n^2 E_n \mathcal{G}_n} \frac{da}{d\mathrm{N}} \tag{25}$$

where l_{cz} is the length of the cohesive zone that has to be estimated analytically, $da/d\mathrm{N}$ is the crack growth rate and the rest of terms are known material properties. The crack growth rate $da/d\mathrm{N}$ is evaluated point-wise according to a Paris law:

$$\frac{da}{d\mathrm{N}} = \begin{cases} A(\omega_{\mathrm{tot}})^p & \text{for} \quad \mathcal{G}_{th}(\Phi) < \omega_{\mathrm{tot}} < \mathcal{G}_c(\Phi) \\ 0 & \text{otherwise} \end{cases} \tag{26}$$

where the exponent $p(\Phi)$ and coefficient $A(\Phi)$ are mode-dependent parameters that can be computed following the work developed by Blanco et al. (2004). $\mathcal{G}_{th}$ is the energy release rate threshold below which no propagation occurs (Turon et al., 2007). ω_{tot} is the specific work that is calculated as the area bounded by the cohesive law and the maximum crack opening displacement for each material point. The calculation of the total specific work depends on the selected shape of the cohesive law, thus for a linear softening the expression reads:

$$\omega_n^{\max} = \frac{l^* E_n \left(\varepsilon_n^{L\max}\right)^2}{\phi_k^{\max}} \left(1 - \frac{l^* X_n \varepsilon_n^{L\max}}{4\mathcal{G}_n}\right) \quad \text{for} \quad \varepsilon_n^{L\max} < \frac{2\mathcal{G}_n}{l^* X_n} \tag{27}$$

where $\phi_k^{\max}$ is computed with the localized strain $\varepsilon_n^{L\max}$ of Eq. (15). Note that the term $\varepsilon_n^{L\max}$ becomes $\left\langle \varepsilon_{22}^{L\max} \right\rangle$ for the transverse strain ($n = 2+, 2-$) and $|\varepsilon_{12}^{L\max}|$ for the in-plane shear strain ($n = 6$). Under mixed-mode conditions, the total specific work is equal to the sum of the mode I and mode II specific works: $\omega_{\mathrm{tot}} = \omega_{2+}^{\max} + \omega_6^{\max}$. The local mode mixity evaluated point-wise is computed as follows: $\Phi = \omega_6^{\max}/\omega_{\mathrm{tot}}$.

4. Computational strategy

The constitutive model is implemented as a fortran-written user material subroutine (VUMAT) in Abaqus/Explicit (ABAQUS, 2014). Figure 6 shows a sequence of loading cases that can be simulated such as static, impact and fatigue load steps. The fatigue step requires two stress levels and the number of cycles in which these two stress levels will be repeated. The fatigue step is performed by means of cycle jumps, since performing cycle-by-cycle simulations result in prohibitive computational times. This approach has been widely used to simulate large-scale components under high-cycle fatigue simulations (Kaminski et al., 2015; Turon et al., 2007; Van Paepegem, 2015).

The fatigue step consists of a first full cycle where the static internal variables can still increase. A second full cycle is simulated to compute and store the maximum and minimum local stresses at each material point. Once these stresses are known,

a local cycle jump is computed. The local cycle jump is determined as to guarantee that the damage increment in the elements is less than a predefined limit. This limit must be relatively small if one aims to represent the correct stress redistribution process, but obviously the lower this limit the larger the computation time. After that, the minimum value of all the cycle jump variables is computed and stored as the global cycle jump (this value corresponds to the critical element). Finally, the fatigue damage variables are increased according to the global cycle jump and the sequence is repeated until the predefined number of cycles is attained or when complete loss of integrity takes place.

Within this computational strategy, the fatigue model can take into account the effect of the R-ratio at each material point. An alternative to reduce the computational time is to consider the envelope approach (Bak et al., 2014; Turon et al., 2007). This method keeps the maximum stress constant during the fatigue step, and assumes a constant R-ratio for all the material points (calculated from the remote load).

4.1. Main modules

Figure 7 shows the four main modules (static, fatigue, cycle jump and fatigue damage) that are executed every time increment. The inputs and outputs of these modules are summarized below.

The static module reads the deformation gradient tensor (F), the static and fatigue internal variables. It returns the stress tensor and updates static internal variables. The fatigue module takes the strain tensor and the static damage variables, calculates the distributed and localized strains, and determines the maximum and minimum strain reached within the cycle. Then, the local cycle jump can be computed, $\Delta N_t^{\text{local}}$, as to guarantee that the damage increment is less than a predefined target limit (e.g., $\Delta D^f = 0.1$). Once the second condition is flagged as true, the cycle jump module simply reads the local cycle jump at all the material points and returns the global minimum of the entire model. This value is stored in a global variable, called global cycle jump: $\Delta N_t^{\text{global}} = \min(\Delta N_t^{\text{local}})$. Finally, the fatigue damage module takes the global cycle jump, the fatigue loading functions and the fatigue internal variables, and it returns the updated fatigue damage variables.

These modules are activated by solving the conditionals and by the definition of time flags. These flags are controlled by the VEXTERNALDB subroutine (ABAQUS, 2014). This subroutine gives control to the user at key moments of the analysis (e.g. at the end of the time increment) so that data can be exchanged among Abaqus user subroutines and in between different Abaqus processes via MPI-based communication. Note that the implementation of a cycle jump approach within a finite element code requires information of all the gauss points of the model, but this information is not available inside the VUMAT subroutine especially in cases where Abaqus/Explicit is executed in parallel in a computer cluster. By default, Abaqus/Explicit utilizes a domain-level parallelization and a MPI-based implementation. This means that the entire model is decomposed into separate topological domains (partitions) that are assigned to a separate MPI process, and memory is not shared between them. Abaqus provides well-defined synchronization points in which it is possible to exchange information across all MPI processes by using MPI communications facilities. Then, the only thing missing is the definition of a global variable across all MPI processes as a common block in fortran. The use of common block variables in fortran code should be taken carefully, since a common block is only global in a single MPI process. However, the calculation of the global cycle jump for the entire model should be computed by using a MPI library at a certain synchronization point. A thread-based parallelization method (shared-memory) is available in Abaqus/Explicit, where the common block variables are true global variables. In this case, there exists the possibility to write in the global variables from different processes at the same time. Abaqus/Explicit provides the mutexes function to protect them from being updated simultaneously from different processes.

4.2. Algorithm

The main actions executed in each module for every stable time increment are numbered below:

Static module:

1.	Read static and fatigue material data:	X_n, E_n, $\mathcal{G}_n$
2.	Read the previous threshold values:	r_k^{t-1},$\left(\varepsilon_{12}^p\right)^{t-1}$,$\left(\varepsilon_{12}^I\right)^{t-1}$
3.	Read the deformation gradient tensor:	$\boldsymbol{F}^t$
4.	Compute the strain tensor and shear plastic strain:	$\boldsymbol{\varepsilon}^t$, $\left(\varepsilon_{12}^p\right)^t$
5.	Compute the effective stress tensor:	$\tilde{\boldsymbol{\sigma}}^t = \mathbf{H}_0^{-1} : \left(\boldsymbol{\varepsilon}^t - (\boldsymbol{\varepsilon}^p)^t\right)$
6.	Compute the loading functions:	$\phi_k^t(\tilde{\boldsymbol{\sigma}}^t)$
7.	Compute the damage thresholds:	$r_k^t(r_k^{t-1}, \phi_k^t)$
8.	Compute the damage variables:	$D_n^t(r_k^t)$
9.	Compute the Cauchy stress tensor:	$\boldsymbol{\sigma}^t = (\mathbf{H}^t)^{-1} : \left(\boldsymbol{\varepsilon}^t - (\boldsymbol{\varepsilon}^p)^t\right)$

Fatigue module:

1.	Read the input data:	$\boldsymbol{\varepsilon}^t$, $\left(\varepsilon_{12}^p\right)^t$, $\left(\phi_k^{t-1}\right)$, $(D_n^s)^t$
2.	Compute the distributed and localized strains:	$\left(\boldsymbol{\varepsilon}^D\right)^t$, $\left(\boldsymbol{\varepsilon}^L\right)^t$
3.	Compute the fatigue loading functions:	$\left(\phi_k^D\right)^t$, $\left(\phi_k^L\right)^t$
4.	Determine max/min of the loading functions:	$\left(\phi_k^{\max}\right)^t$, $\left(\phi_k^{\min}\right)^t$
5.	Compute the local cycle jump:	$\Delta N_{\text{local}}^t$

Cycle jump:

1.	Compute the global cycle jump:	$\Delta N_{\text{global}}^t = \min\left(\Delta N_{\text{local}}^t\right)$
2.	Compute the number of cycles:	$N^t = N^{t-1} + \Delta N_{\text{global}}^t$

Fatigue damage:

1.	Compute the fatigue damage variables:	$\left(D_n^f\right)^t = \left(D_n^f\right)^{t-1} + \int_{N^{t-1}}^{N^t} \frac{dD_n^f}{dN} dN$

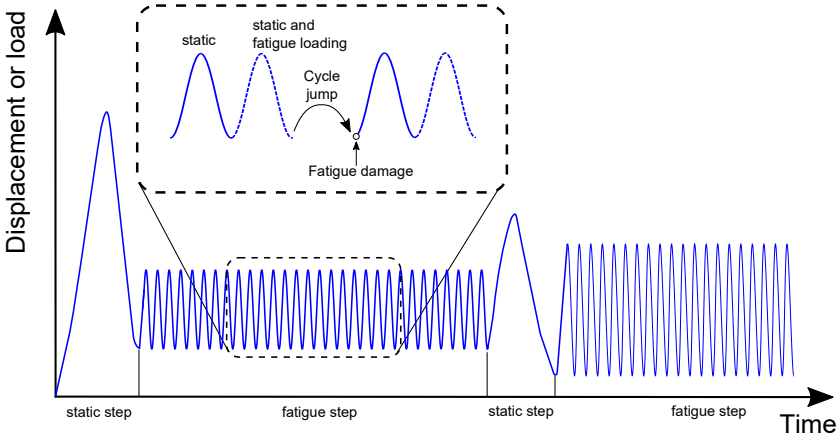

Figure 6: Cycle jump approach within an explicit finite element code.

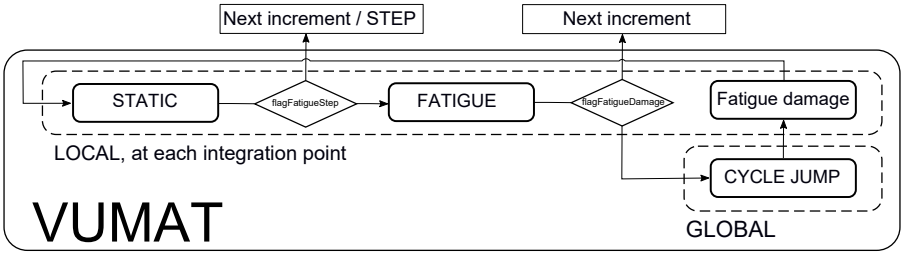

Figure 7: Flow chart of the constitutive model for static and fatigue loading.

5. Conclusions

The meso-scale continuum damage model from the previous papers (Maimí et al., 2006, 2007a,b) has been extended for fatigue life and residual strength predictions. First, two key features were updated that concerns the static part:

- An isotropic hardening model for plasticity has been added into the constitutive response under in-plane shear.
- The exponential softening laws have been changed to linear or bilinear functions for greater simplicity.

Under fatigue loads, the same ply damage mechanisms are considered but they initiate at lower loading levels and evolve in a different manner. Fatigue damage is introduced using different empirical functions that modify the elastic and softening response of a pristine material point. A cycle jump algorithm is implemented inside the finite element code. The constitutive model is validated in the following part by simulating the progressive failure mechanisms of open-hole and double-edge notched specimens under static, tension-tension fatigue and residual strength tests. The experimental tests performed by the authors are also reported in the following part.

Acknowledgements

The authors would like to acknowledge the financial support of the Spanish Government through the Spanish Ministerio de Ciencia, Innovación y Universidades under the contracts RTC-2014-1958-4 and RTI2018-097880-B-I00.

References

ABAQUS, 2014. Abaqus 6.14 documentation.

Aidi, B., Phillen, M. K., Case, S. W., 2015. Progressive damage assessment of centrally notched composite specimens in fatigue. Composites Part A: Applied Science and Manufacturing 74, 47–59.

Alderliesten, R., 2013. Critical review on the assessment of fatigue and fracture in composite materials and structures. Engineering Failure Analysis 35, 370–379.

Ambu, R., Aymerich, F., Bertolino, F., 2005. Investigation of the effect of damage on the strength of notched composite laminates by digital image correlation. The Journal of Strain Analysis for Engineering Design 40 (5), 451–461.

Aymerich, F., Found, S., 2000. Response of notched carbon/PEEK and carbon/epoxy laminates subjected to tension fatigue loading. Fatigue & Fracture Of Engineering Materials & Structures, 675–683.

Bak, B. L. V., Sarrado, C., Turon, A., Costa, J., jun 2014. Delamination Under Fatigue Loads in Composite Laminates: A Review on the Observed Phenomenology and Computational Methods. Applied Mechanics Reviews 66 (6), 060803.

Bathias, C., oct 2006. An engineering point of view about fatigue of polymer matrix composite materials. International Journal of Fatigue 28 (10), 1094–1099.

Bazant, Z. P., Oh, B. H., 1983. Crack band theory for fracture of concrete. Materials and Structures 16, 155–177.

Berthelot, J. M., Le Corre, J. F., 1999. Modelling the transverse cracking in cross-ply laminates: application to fatigue. Composites Part B: Engineering 30, 569–577.

Blanco, N., Gamstedt, E. K., Asp, L. E., Costa, J., 2004. Mixed-mode delamination growth in carbon-fibre composite laminates under cyclic loading. International Journal of Solids and Structures 41 (15), 4219–4235.

Brøndsted, P., Andersen, S. I., Lilholt, H., 1996. Fatigue performance of glass/polyester laminates and the monitoring of material degradation. Mechanics of Composite Materials 32 (1), 21–29.

Camanho, P. P., Maimí, P., Dávila, C. G., 2007. Prediction of size effects in notched laminates using continuum damage mechanics. Composites Science and Technology 67 (13), 2715–2727.

Dávila, C. G., Camanho, P. P., 2003. Failure Criteria for FRP Laminates in Plane Stress. Tech. rep., National Aeronautics and Aerospace Administration.

Degrieck, J., Van Paepegem, W., 2001. Fatigue damage modelling of fibre-reinforced composite materials: Review. Applied Mechanics Reviews 54 (4), 279–300.

Eliopoulos, E. N., Philippidis, T. P., 2011a. A progressive damage simulation algorithm for GFRP composites under cyclic loading. Part I: Material constitutive model. Composites Science and Technology 71 (5), 742–749.

Eliopoulos, E. N., Philippidis, T. P., 2011b. A progressive damage simulation algorithm for GFRP composites under cyclic loading. Part II: FE implementation and model validation. Composites Science and Technology 71 (5), 750–757.

González, E. V., Maimí, P., Martín-Santos, E., Soto, A., Cruz, P., Martín de la Escalera, F., Sainz de Aja, J. R., 2018. Simulating drop-weight impact and compression after impact tests on composite laminates using conventional shell finite elements. International Journal of Solids and Structures 145, 230–247.

Hochard, C., Miot, S., Thollon, Y., 2013. Fatigue of laminated composite structures with stress concentrations. Composites Part B: Engineering 65, 11–16.

Hochard, C., Payan, J., Bordreuil, C., 2006. A progressive first ply failure model for woven ply CFRP laminates under static and fatigue loads. International Journal of Fatigue 28, 1270–1276.

Hochard, C., Thollon, Y., 2010. A generalized damage model for woven ply laminates under static and fatigue loading conditions. International Journal of Fatigue 32 (1), 158–165.

Hosoi, A., Sakuma, S., Fujita, Y., Kawada, H., jan 2015. Prediction of initiation of transverse cracks in cross-ply CFRP laminates under fatigue loading by fatigue properties of unidirectional CFRP in 90 direction. Composites Part A: Applied Science and Manufacturing 68, 398–405.

Houlsby, G. T., Puzrin, A. M., 2000. Thermomechanical framework for constitutive models for rate-independent dissipative materials. International journal of plasticity 16 (9), 1017–1047.

Hwang, W., Han, K. S., 1986. Fatigue of Composites–Fatigue Modulus Concept and Life Prediction. Journal of Composite Materials 20, 154–165.

Iarve, E. V., Hoos, K., Braginsky, M., Zhou, E., Mollenhauer, D. H., 2016. Progressive failure simulation in laminated composites under fatigue loading by using discrete damage modeling. Journal of Composite Materials 51 (15), 2143–2161.

Kaminski, M., Laurin, F., Maire, J. F., 2015. Fatigue damage modeling of composite structures: the ONERA viewpoint. Journal Aerospace Lab (9).

Kordkheili, S. A. H., Toozandehjani, H., Soltani, Z., 2017. A progressive multiscale fatigue model for life prediction of laminated composites. Journal of Composite Materials 51 (20), 2949–2960.

Krüger, H., Rolfes, R., jan 2015. A physically based fatigue damage model for fibre-reinforced plastics under plane loading. International Journal of Fatigue 70, 241–251.

Ladevèze, P., 2003. A computational mesodamage model for life prediction for laminates. In: Harris, B. (Ed.), Fatigue in composite materials. Woodhead Publishing Limited, Ch. 15.

Lemaitre, J., 1992. A Course on Damage Mechanics. Springer-Verlag Berlin Heidelberg.

Leone, F. A., Dávila, C. G., E., M. G., Madhavadas, R., Hyder, I., 2017. Fracture-Based Mesh Size Requirements for Matrix Cracks in Continuum Damage Mechanics Models. In: 58th AIAA/ASCE/AHS/ASC Structures, Structural Dynamics, and Materials. No. January. pp. 1–14.

Lian, W., Yao, W., 2010. Fatigue life prediction of composite laminates by FEA simulation method. International Journal of Fatigue 32 (1), 123–133.

Liu, S., Nairn, J. A., 1990. Fracture Mechanics Analysis of Composite Microcracking: Experimental Results in Fatigue. In: Proceedings of the 5th Technical Conference on Composite Materials, American Society of Composites. pp. 287–295.

Llobet, J., Maimí, P., Essa, Y., Martin de la Escalera, F., 2018. Progressive matrix cracking in carbon/epoxy cross-ply laminates under static and fatigue loading. International Journal of Fatigue 119, 330–337.

Llobet, J., Maimí, P., Mayugo, J. A., Essa, Y., Martin de la Escalera, F., 2017. A fatigue damage and residual strength model for unidirectional carbon/epoxy composites under on-axis tension-tension loadings. International Journal of Fatigue 103, 508–515.

Maimí, P., Camanho, P. P., Mayugo, J. A., Dávila, C. G., 2006. A Thermodynamically Consistent Damage Model for Advanced Composites. Tech. Rep. March.

Maimí, P., Camanho, P. P., Mayugo, J. A., Dávila, C. G., 2007a. A continuum damage model for composite laminates: Part I Constitutive model. Mechanics of Materials 39 (10), 897–908.

Maimí, P., Camanho, P. P., Mayugo, J. A., Dávila, C. G., 2007b. A continuum damage model for composite laminates: Part II Computational implementation and validation. Mechanics of Materials 39 (10), 909–919.

Maimí, P., Mayugo, J. A., Camanho, P. P., 2008. A three-dimensional damage model for transversely isotropic composite laminates. Journal of Composite Materials 42 (25), 2717–2745.

Mohammadi, B., Fazlali, B., Salimi-Majd, D., 2017. Development of a continuum damage model for fatigue life prediction of laminated composites. Composites Part A: Applied Science and Manufacturing 93, 163–176.

Movaghghar, A., Lvov, G. I., 2011. An Energy Model for Fatigue Life Prediction of Composite Materials Using Continuum Damage Mechanics. Applied Mechanics and Materials 110-116 (Icmae), 1353–1360.

Movaghghar, A., Lvov, G. I., 2012a. A Method of Estimating Wind Turbine Blade Fatigue Life and Damage using Continuum Damage Mechanics. International Journal of Damage Mechanics 21 (6), 810–821.

Movaghghar, A., Lvov, G. I., 2012b. Theoretical and experimental study of fatigue strength of plain woven glass/epoxy composite. Journal of Mechanical Engineering 58 (3), 175–182.

Naderi, M., Maligno, A. R., 2012. Fatigue life prediction of carbon/epoxy laminates by stochastic numerical simulation. Composite Structures 94 (3), 1052–1059.

Nairn, J. A., 2000. Matrix microcracking in composites. In: Talreja, R., Manson, J. A. E. (Eds.), Polymer Matrix Composites. Elsevier Science, Ch. 13, pp. 403–432.

Nixon-Pearson, O. J., Hallett, S. R., 2015. An investigation into the damage development and residual strengths of open-hole specimens in fatigue. Composites Part A 69, 266–278.

Nixon-Pearson, O. J., Hallett, S. R., Harper, P. W., Kawashita, L. F., 2013. Damage development in open-hole composite specimens in fatigue. Part 2: Numerical modelling. Composite Structures 106, 890–898.

Ortega, A., 2017. Characterization of the translaminar cohesive law. Ph.D. thesis, University of Girona.

Ortega, A., Maimi, P., Gonzalez, E. V., Trias, D., 2016. Characterization of the translaminar fracture Cohesive Law. Composites Part A: Applied Science and Manufacturing 91, 501–509.

Passipoularidis, V. A., 2009. Residual strength and life prediction in composite materials after fatigue. Ph.D. thesis, Patras.

Payan, J., Hochard, C., apr 2002. Damage modelling of laminated carbon/epoxy composites under static and fatigue loadings. International Journal of Fatigue 24 (2-4), 299–306.

Peerlings, R. H. J., 1999. Enhanced damage modelling for fracture and fatigue. Ph.D. thesis, Technische Universiteit Eindhoven.

Philippidis, T. P., Passipoularidis, V. A., 2007. Residual strength after fatigue in composites: Theory vs. experiment. International Journal of Fatigue 29 (12), 2104–2116.

Pinho, S. T., Davila, C. G., Camanho, P. P., Iannucci, L., Robinson, P., 2005. Failure Models and Criteria for FRP Under In-Plane or Three-Dimensional Stress States Including Shear Non-Linearity. Tech. rep., Nattional Aeronautics and Space Administration.

Quintanas-Corominas, A., Maimí, P., Casoni, E., Turon, A., Mayugo, J. A., Guillamet, G., Vázquez, M., 2018. A 3D transversally isotropic constitutive model for advanced composites implemented in a high performance computing code. European Journal of Mechanics - A/Solids 71 (May 2017),

278–291.
Reifsnider, K. L., Jamison, R., 1982. Fracture of fatigue-loaded composite laminates. International Journal of Fatigue 4, 187–197.
Ritchie, R. O., 1999. Mechanisms of fatigue-crack propagation in ductile and brittle solids. International Journal of Fracture 100, 55–83.
Schulte, K., 1984. Stiffness reduction and development of longitudinal cracks during fatigue loading of composite laminates. In: Cardon, A. H., Verchery, G. (Eds.), Mechanical characterization of load bearing fibre composite laminates. Elsevier, pp. 36–54.
Sedrakian, A., Zineb, T. B., Billoet, J. L., 2002. Contribution of industrial composite parts to fatigue behaviour simulation. International Journal of Fatigue 24 (2-4), 307–318.
Shokrieh, M. M., Lessard, L. B., 2000a. Progressive Fatigue Damage Modeling of Composite Materials, Part I: Modeling. Journal of Composite Materials 34 (13), 1056–1080.
Shokrieh, M. M., Lessard, L. B., 2000b. Progressive Fatigue Damage Modeling of Composite Materials, Part II: Material Characterization and Model Verification. Journal of Composite Materials 34 (13), 1081–1116.
Shokrieh, M. M., Taheri-Behrooz, F., 2010. Fatigue life prediction of composite materials based on progressive damage modelling. In: Vassilopoulos, A. P. (Ed.), Fatigue Life Prediction of Composites and Composite Structures. Woodhead Publishing Limited, Ch. Chapter 8.
Soto, A., González, E. V., Maimí, P., Mayugo, J. A., Pasquali, P. R., Camanho, P. P., 2018. A methodology to simulate low velocity impact and compression after impact in large composite stiffened panels. Composite Structures 204 (February), 223–238.
Spearing, S. M., Beaumont, P. W. R., 1992. Fatigue damage mechanics of composite materials. I: Experimental measurement of damage and post-fatigue properties. Composites Science and Technology 44 (2), 159–168.
Spearing, S. M., Beaumont, P. W. R., Ashby, M. F., jan 1992a. Fatigue damage mechanics of composite materials. II: A damage growth model. Composites Science and Technology 44 (2), 169–177.
Spearing, S. M., Beaumont, P. W. R., Kortschot, M. T., 1992b. The fatigue damage mechanics of notched carbon-fiber peek laminates. Composites 23 (5), 305–311.
Turon, A., 2006. Simulation of delamination in composites under quasi-static and fatigue loading using cohesive zone models. Ph.D. thesis, University of Girona.
Turon, A., Bak, B. L. V., Lindgaard, E., Sarrado, C., Lund, E., 2015. Interface elements for fatigue-driven delaminations in advanced composite materials. In: Camanho, P.P., Hallet, S. (Ed.), Numerical Modelling of Failure in Advanced Composite Materials. Woodhead Publishing Series in Composite Science and Engineering, Ch. 3, pp. 73–91.
Turon, A., Costa, J., Camanho, P. P., Dávila, C. G., 2007. Simulation of delamination in composites under high-cycle fatigue. Composites Part A: Applied Science and Manufacturing 38 (11), 2270–2282.
Van Paepegem, W., 2015. The cycle jump concept for modelling high-cycle fatigue in composite materials. In: Carvelli, V., Lomov, S. V. (Eds.), Fatigue of Textile Composites. Elsevier, Ch. 2.
Van Paepegem, W., De Baere, I., Degrieck, J., 2006a. Modelling the nonlinear shear stress-strain response of glass fibre-reinforced composites. Part I: Experimental results. Composites Science and Technology 66 (10), 1455–1464.
Van Paepegem, W., De Baere, I., Degrieck, J., 2006b. Modelling the nonlinear shear stress-strain response of glass fibre-reinforced composites. Part II: Model development and finite element simulations. Composites Science and Technology 66 (10), 1465–1478.
Van Paepegem, W., Degrieck, J., 2002a. A new coupled approach of residual stiffness and strength for fatigue of fibre-reinforced composites. International Journal of Fatigue 24 (7), 747–762.
Van Paepegem, W., Degrieck, J., apr 2002b. Coupled residual stiffness and strength model for fatigue of fibre-reinforced composite materials. Composites Science and Technology 62 (5), 687–696.
Vasiukov, D., Panier, S., Hachemi, A., 2015. Direct method for life prediction of fibre reinforced polymer composites based on kinematic of damage potential. International Journal of Fatigue 70, 289–296.
Whitworth, H. A., 1998. A stiffness degradation model for composite laminates under fatigue loading. Composite Structures 40 (2), 95–101.
Yokozeki, T., Aoki, T., Ishikawa, T., 2002. Fatigue growth of matrix cracks in the transverse direction of CFRP laminates. Composites Science and Technology 62, 1223–1229.
Zhang, W., Zhou, Z., Scarpa, F., Zhao, S., 2016. A fatigue damage meso-model for fiber-reinforced composites with stress ratio effect. Materials & Design 107, 212–220.
Zhang, W., Zhou, Z., Zhang, B., Zhao, S., 2015. A phenomenological fatigue life prediction model of glass fiber reinforced polymer composites. Materials and Design 66, 77–81.
Zhang, W., Zhou, Z., Zheng, P., Zhao, S., 2014. The fatigue damage mesomodel for fibre-reinforced polymer composite lamina. Journal of Reinforced Plastics and Composites.

Paper D

A continuum damage model for composite laminates: Part IV - Experimental and numerical tests

J. Llobet[a], P. Maimí[a], A. Turon[a], B.L.V. Bak[b], E. Lindgaard[b], L. Carreras[b] Y. Essa[c], F. Martin de la Escalera[c]

[a] AMADE, Polytechnic School, Universitat de Girona, Girona, Spain

[b] Department of Materials and Production, Aalborg University, Aalborg, Denmark

[c] AERNNOVA Engineering Division, Structural Integrity Department, Madrid, Spain

The paper has been submitted to
Mechanics of Materials.

A continuum damage model for composite laminates: Part IV- Experimental and numerical tests

J. Llobet[a,*], P. Maimí[a,*], A. Turon[a], B.L.V. Bak[b], E. Lindgaard[b], L. Carreras[b], Y. Essa[c], F. Martin de la Escalera[c]

[a]*AMADE, Mechanical Engineering and Industrial Construction Department, University of Girona, Carrer Universitat de Girona 4, E-17003 Girona, Spain*
[b]*Department of Materials and Production, Aalborg University, Fibigerstraede 16, 9220 Aalborg East, Denmark*
[c]*AERNNOVA Engineering Division SA, Llano Castellano Avenue 13, E-28034 Madrid, Spain*

Abstract

This paper follows on from part III where a meso-scale continuum damage mechanics (CDM) model for static and fatigue loads has been presented. An experimental investigation on the damage occurrence and the strength of carbon/epoxy notched laminates that are tested in static, tension-tension fatigue and post-fatigue is provided. The large extension of fatigue-driven delaminations in the experiments forced the need to account for the growth of delamination cracks under fatigue. A cohesive zone (CZ) model is suggested to achieve this purpose. An appropriate modelling strategy is used to allow the interaction between both damage models, and thus to simulate the initiation and propagation of intra- and inter-laminar fatigue damage. The capability of the computational model to capture the main fatigue degradation mechanisms as well as the post-fatigue tensile residual strength is examined. The numerical predictions captured most experimental trends and showed good agreement with the X-ray inspections. However, further experimental and modelling work are required to develop a reliable computational tool for quantitative evaluation of fatigue and damage tolerance of composite structures.

Keywords: Residual strength, Fatigue, Continuum damage mechanics, Cohesive zone models

1. Introduction

This paper is the follow-up of part III (Llobet et al., 2020) in which the meso-scale continuum damage mechanics (CDM) model presented in references (Maimí et al., 2006, 2007a,b) is extended for fatigue and residual strength predictions. Part III focused on describing the constitutive model and the computational framework to implement a fatigue analysis inside an explicit finite element code, while the computational model is numerically tested and validated in the present work. The extensive presence of fatigue-driven delamination that showed up in the experiments made the authors consider the growth of interlaminar damage under fatigue. Thus, the CDM model for intralaminar damage is coupled with the fatigue cohesive zone (CZ) model developed by Turon et al. (Turon, 2006; Turon et al., 2015, 2010, 2007) to account for interlaminar damage. The experimental tests consist of a set of static, tension-tension fatigue and post-fatigue residual strength tests of a quasi-isotropic carbon/epoxy notched laminate. Two specimen geometries, the open-hole (OHT) and the double-edge notched (DENT) tensile specimens, are analysed.

It is a common aerospace practice to develop notched design allowables to account for various stress concentrations since they provide a damage-tolerant point of view in the certification process of composite airframes. The study of this type of notched specimens under fatigue loads has also become the subject of extensive experimental and numerical investigations. For example, the slot-shaped specimen representing severe damage inflicted by a service accident (Spearing and Beaumont, 1992; Spearing et al., 1992a,b), the DENT specimen (Hallett and Wisnom, 2005a,b), or the OHT specimen to study the circular hole that is commonly cut into the laminate for fasteners, or to allow the pass of electrical and hydraulic lines (Aidi et al., 2015; Ambu et al., 2005; Aymerich and Found, 2000; Daken and Mar, 1985; Hochard et al., 2013; Nixon-Pearson and Hallett, 2015; Nixon-Pearson et al., 2013b).

This paper is organized as follows. First, section 2 reports the experimental test campaign carried out with the OHT and DENT specimens. Next, section 3 introduces the key features of the computational model. Following that, section 4 describes the material card that is needed to feed the constitutive model. Special emphasis is placed on the fatigue properties and on the assumptions made due to the lack of some experimental data at this stage. Section 5 discusses the comparison between the damage mechanisms predicted by the simulations and the experimental observations from X-ray inspections. Finally, section 6 presents some concluding remarks that can be drawn from the numerical analysis as well as some suggestions for future work.

2. Experimental test campaign

This section reports all the tests that have been done to investigate the damage mechanisms under static, fatigue and

*Corresponding author.
Email addresses: jordi.llobet@udg.edu (J. Llobet), pere.maimi@udg.edu (P. Maimí)

post-fatigue tests. All the validation tests were conducted at AMADE Research lab, the composite testing laboratory of the University of Girona, which is NADCAP (AC7122/1 RevB, 2017) and ISO 17025 (ISO/IEC 17025:2017, 2017) accredited.

2.1. Material

The material system used in this study is a carbon/epoxy prepreg of 0.184 mm nominal ply thickness. The laminate was moulded and cured in an autoclave under standard aeronautical conditions. The quality of the panel was verified using ultrasonic C-scan inspection. The laminate lay-up consists of 24 plies $[90\ {-45}\ 0\ {+45}]_{3s}$ with a nominal laminate thickness of 4.4 mm. Two geometries were cut by water abrasive jet with the following dimensions: 280x32 mm (length and width) and diameter $2R = 6.35$ mm for the OHT specimen, 250x20 mm (length and width) and notch size $a_0 = 6$ mm for the DENT specimen. GFRP tabs of 60 mm length were used in both specimens to avoid compressive damage in the gripping area.

2.2. Equipment

All tests were performed at room temperature using a universal servo-hydraulic test machine 810 MTS with a load cell of 250 kN. The tests were interrupted periodically for non-destructive inspection of damage progression through X-ray radiography. All radiographs were conducted at AMADE Research facility. The following settings were used: 35 kV, 120 μA, analogue integration of 5 images within a exposure time of 3000 ms. To enhance X-ray contrast, a solution comprised of 520 g of zinc iodide, 86.5 ml distilled water, 86.5 ml alcohol and 26 ml Kodak Photo-Flo 200 was used. The specimens were immersed into this solution for some minutes inside a vacuum chamber.

2.3. Test procedure

Quasi-static tests for the pristine laminates and residual strength for the damaged ones were conducted at a displacement rate of 2 mm/min. Tension-tension load-controlled fatigue tests were run at 90%, 75% and 60% of the ultimate static load, with a constant amplitude (stress ratio $R = 0.1$), a sinusoidal waveform and a frequency of 5 Hz. All fatigue tests were interrupted at selected cycle intervals and the specimens were removed from the testing machine for X-ray inspection, and eventually loaded up until failure for tensile residual strength measurement.

2.4. Experimental results

Figures 1 and 2 show the X-rayed specimens after static, fatigue and residual strength tests. While static failure is governed by fibre tensile fracture, in fatigue progressive damage grows in the form of matrix splitting cracks and delaminations. The same fatigue damage patterns are observed in the three stress levels tested (60%, 75% and 90% of the ultimate static). The splits start at an early stage triggered by a local peak shear stress at the notch (Daken and Mar, 1985; Wisnom and Chang, 2000), and then progressively increase in length as shown in the OHT specimen of Figure 3. This is accompanied by local delaminations that initiate between the splits and the notch edges, and continue to grow along with the increase in the splits. In the open-hole specimen, delaminations mainly develop between the two major 0° splits at the central part of the specimen, similar to the experimental findings by (Aidi et al., 2015), but no free-edge delamination is observed here. Note also the presence of transverse matrix cracking from an early stage of fatigue life. In contrast, the DENT specimen shows a delamination front growing between the principal 0° splits and the free-edge. Both geometries develop delaminations that grow from the notch towards the specimen tabs in both directions.

The evolution of fatigue damage for a stress level of 75% of the ultimate static load is illustrated in Figure 3 for the OHT and for a 90% of the ultimate static load in Figure 4 for the DENT. The 0° splits grew symmetrically in the OHT specimen. However, in the DENT specimen, they start to grow symmetric and with the increase in the loading cycles they progress asymmetrically once an extensive delamination front appears between the free-edge and the split. The fatigue damage patterns are in agreement with the findings reported by other authors (Aymerich and Found, 2000; Nixon-Pearson and Hallett, 2015; Nixon-Pearson et al., 2013a; Spearing and Beaumont, 1992). Although the laminates suffered from fatigue damage with a significant loss of stiffness, the damage mechanisms that appear at the notch reduce the stress concentration and suppress fibre fracture. Once fatigue damage takes place, the strength is no longer controlled by fibre failure. Indeed, the redistribution of stresses caused by fatigue damage results in specimens tested at stress levels of 75% of the ultimate static and 2 million cycles without specimen complete failure.

3. Numerical model

3.1. Coupled intra- and inter-laminar damage model

Fatigue degradation in carbon/epoxy laminates occurs as a combination of intra- and inter-laminar damage mechanisms that grow and interact during fatigue loadings. It is thus essential to include both forms of damage in order to describe adequately the physics of fatigue degradation and the process of stress redistribution that takes place in composite laminates. The most common idealization for representing damage of composites at structural level is at the meso-scale (Rose et al., 2013), where the individual plies are represented as homogeneous and orthotropic materials and the interfaces are represented by cohesive elements or by cohesive surfaces. At this scale, the intra-laminar or intra-ply damage is defined by CDM models while the inter-laminar or inter-ply damage is described by CZ models. Numerous examples exist of coupled damage models that have been successfully used to simulate complex failure events under static and impact loading cases (Achard et al., 2014; Cox and Yang, 2006; Falcó et al., 2018; González et al., 2018; Rose et al., 2013; Soto et al., 2018a,b).

Several fatigue CZ models are available in open literature (Bak et al., 2014, 2017; Carreras et al., 2019c; Harper and Hallett, 2010; Turon et al., 2015). Turon's model is used herein (Turon, 2006; Turon et al., 2007). This model

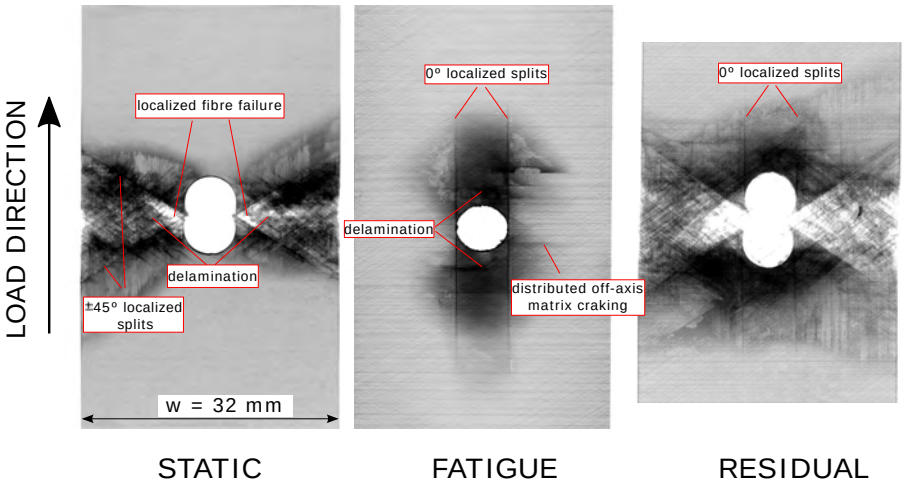

Figure 1: X-ray inspections in open-hole specimens tested under static, tension-tension fatigue and residual strength.

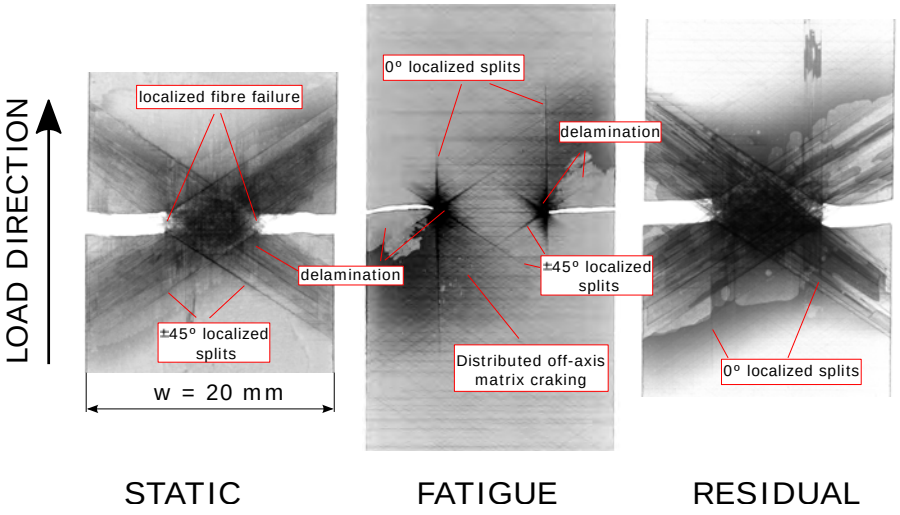

Figure 2: X-ray inspections in double-edge notched specimens tested under static, tension-tension fatigue and residual strength.

that was originally implemented as a user element subroutine (UEL) for Abaqus/Standard is coded into a VUMAT subroutine for Abaqus/Explicit taking the previous static CZ model by González et al. (González et al., 2009) as point of departure. Turon's model offers the advantage of being point-wise evaluable so that its implementation as a constitutive model is somewhat straightforward. In contrast, the computation of the energy release rate, the mode mixity and the crack growth rate are evaluated locally (likewise the CDM model), which it is known to be less accurate than computing the contour J-integral (see Bak et al., 2016, 2017; Carreras et al., 2019c). Thus, the implementation of non-local models in finite element codes to compute the J-integral is by far much more complex (Carreras et al., 2019a,c). Turon et al. (Turon et al., 2015, 2007) expressed the stiffness-based interlaminar damage rate variable, D^f_{coh}, as a function of the crack growth rate:

$$\frac{dD^f_{\text{coh}}}{d\text{N}} = \frac{1}{l_{cz}} \frac{(\lambda_c(1-D_{\text{coh}}) + D_{\text{coh}}\lambda_o)^2}{\lambda_c\lambda_o} \frac{da}{d\text{N}} \tag{1}$$

where l_{cz} is the length of the fracture process zone, λ_o and λ_c are the onset and critical displacement jumps, respectively. The

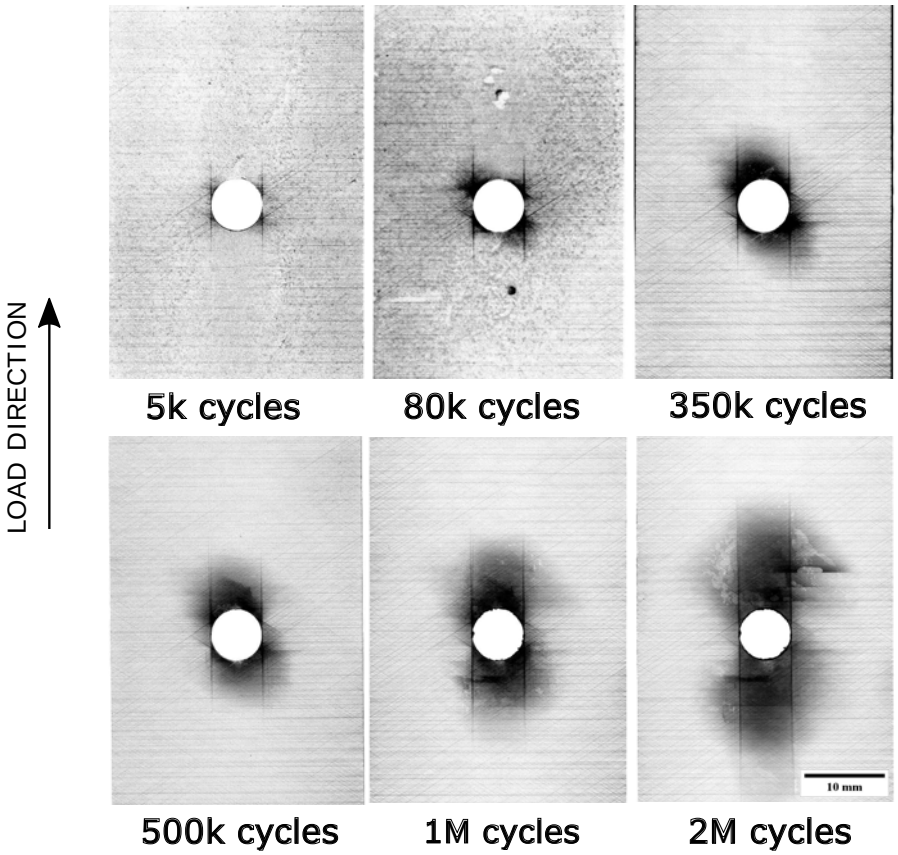

Figure 3: X-ray radiographs showing the evolution of fatigue damage in open-hole specimens subjected to the 75% of the ultimate and R-ratio = 0.1.

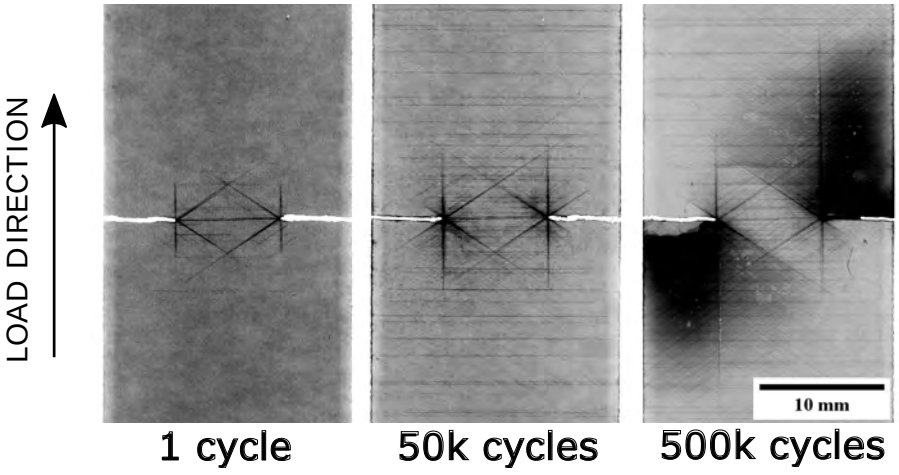

Figure 4: X-ray radiographs showing the evolution of fatigue damage in double-edge notched specimens subjected to the 90% of the ultimate and R-ratio = 0.1.

following expression for the crack growth rate, $da/d\mathrm{N}$, is used:

$$\frac{da}{d\mathrm{N}} = \begin{cases} A(\omega_{tot})^p & \text{for} \quad \mathcal{G}_{th}(\Phi) < \omega_{tot} < \mathcal{G}_c(\Phi) \\ 0 & \text{otherwise} \end{cases} \tag{2}$$

where $A(\Phi)$ and $p(\Phi)$ are mode-dependent material constants, ω_{tot} is the specific work computed as the area under the quasi-static cohesive law using local information for each integration point and Φ is the local mode mixity. The mode-dependent fitting parameters of the Paris law, $p(\Phi)$ and $A(\Phi)$, are calculated by the expressions derived by Blanco et al. (2004):

$$\begin{aligned} p &= \Phi^2 \left(p_{II} - p_I - p_m\right) + \Phi p_m + p_I \\ \log(A) &= \Phi^2 \left(\frac{A_{II}}{A_m A_I}\right) + \Phi \log(A_m) + \log(A_I) \end{aligned} \tag{3}$$

where p_I and A_I are the Paris law material fitting parameters for pure mode I, p_{II} and A_{II} are the Paris law material fitting parameters for pure mode II, p_m and A_m are mode interpolation parameters. $\mathcal{G}_c$ is the fracture toughness and $\mathcal{G}_{th}$ is the fatigue threshold (energy release rate below which the crack does not grow). Its dependence with the mode mixity is assumed to follow a Benzeggagh and Kenane based expression (Benzeggagh and Kenane, 1996), as stated in Turon et al. (2007):

$$\begin{aligned} \mathcal{G}_c &= \mathcal{G}_{Ic} + (\mathcal{G}_{IIc} - \mathcal{G}_{Ic})\Phi^{\eta} \\ \mathcal{G}_{th} &= \mathcal{G}_{Ith} - (\mathcal{G}_{IIth} - \mathcal{G}_{Ith})\Phi^{\eta_2} \end{aligned} \tag{4}$$

where η and η_2 are material interpolation parameters.

3.2. Cycle jump computation

The cycle jump concept is used when the fatigue simulation deals with a large number of cycles (i.e., high-cycle fatigue). Thus, the simulation is not conducted cycle-by-cycle (as it may take prohibitive computational times) but with small cycle jumps. It is worth mentioning that the cycle jump concept was first developed for metallic materials by (Lesne and Savalle, 1984) in the late 80's, and shortly after was proposed by (Lemaitre and Doghri, 1994). Van Paepegem was the first to apply the cycle jump concept to composite structure simulations (Van Paepegem, 2002, 2015).

The cycle jump is determined as to guarantee that the damage increment in the finite elements is less than a predefined target damage increment. This target must be relatively small since the exact damage increment per cycle, $dD_n^f/d\mathrm{N}$, is unknown for $\mathrm{N} \in [\mathrm{N}^t, \mathrm{N}^t + \Delta\mathrm{N}^t]$. The local cycle jump at time t for each integration point, $\Delta\mathrm{N}^t_{\text{local}}$, is computed as:

$$\Delta\mathrm{N}^t_{\text{local}} = \min\left\{\frac{\Delta D_n^f}{\max\left\{\frac{dD_n^f}{d\mathrm{N}}\right\}}\right\} \quad \text{for} \quad n = 1+, 2+, 6, \text{coh} \tag{5}$$

where ΔD_n^f is the target damage increment for each damage mode. The current active damage growth rates, $dD_n^f/d\mathrm{N}$, correspond to the stiffness-based longitudinal tension $n = 1+$, transverse tension $n = 2+$, in-plane shear $n = 6$ and interface $n = \text{coh}$ damage variables, respectively. It can happen that the target damage increment is higher than the critical damage increment (increment in damage to dissipate all the remaining fracture energy). Then, the target damage increment is reduced to the critical. In order to prevent penalizing the computational time, the local cycle jump is forced to be at least larger than a minimum threshold:

$$\Delta\mathrm{N}^t_{\text{local}} = \max\left\{\Delta\mathrm{N}^t_{\text{local}}, \Delta\mathrm{N}_{\min}\right\} \tag{6}$$

Once the minimum local cycle jump is known, the model determines the global minimum for all the integration points as: $\Delta\mathrm{N}^t_{\text{global}} = \min\left\{\Delta\mathrm{N}^t_{\text{local}}\right\}$. The damage at a given number of cycles is determined by the integration of the damage rates, $dD_n^f/d\mathrm{N}$:

$$D_n^f(\mathrm{N}^t + \Delta\mathrm{N}^t_{\text{global}}) = D_n^f(\mathrm{N}^t) + \int_{\mathrm{N}^t}^{\mathrm{N}^t+\Delta\mathrm{N}^t_{\text{global}}} \frac{dD_n^f}{d\mathrm{N}} d\mathrm{N} \quad \text{for} \quad n = 1+, 2+, 6, \text{coh} \tag{7}$$

where N^t is the current number of cycles and $\Delta\mathrm{N}^t_{\text{global}}$ is the global cycle jump at time t. Refer to part III to see further details on the implemented computational methodology to perform a cycle jump based fatigue simulation (Llobet et al., 2020).

3.3. Modelling strategy

The FE model consists of plane-stress reduced-integration shell elements (S4R) for the plies (one shell element in the thickness direction per ply), and zero-thickness cohesive elements (COH3D8) for the interfaces. The elements are connected via tie constraints according to Figure 5. The adopted modelling strategy is the result of an extensive numerical investigation performed at AMADE research group (González et al., 2018; Soto et al., 2018a), mainly with the intention of simulating complex failure events in large-scale structures but in reasonable calculation times. The main advantage of this modelling strategy is the elimination of the detrimental effect of the ply thickness on the computational time since shell elements are used. Recall that the explicit integration algorithm computes the minimum stable time increment as $\Delta t \approx l_{\min}/c_d$, where $l_{\min}$ is the smallest element dimension, c_d is the dilatational wave speed (ABAQUS, 2014). The small ply thickness given in laminated composites results in a very small Δt when using solid or continuumm shell elements. A transition region with elastic behaviour is defined at the boundaries to ensure a smooth introduction of the load.

3.4. Mesh generation

The sensitivity of CDM models to the orientation of the mesh is well-known to cause difficulties in predicting the correct crack path. Although the independence of the solution with

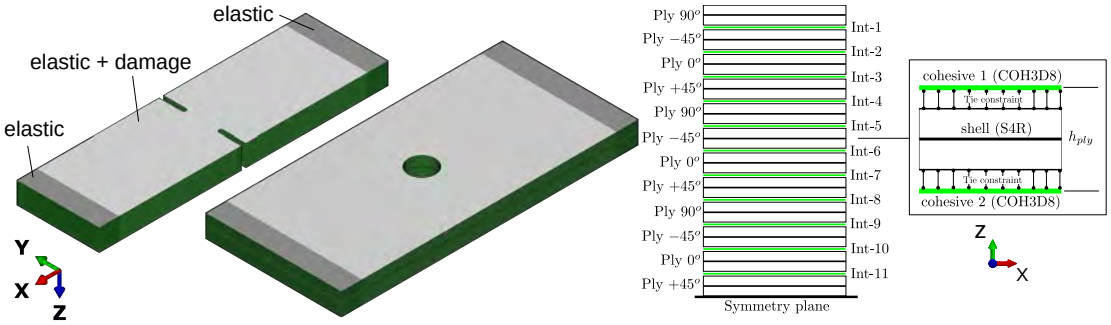

Figure 5: FE modelling strategy and element technology.

respect to the element size is guaranteed by the crack-band approach, damage tends to propagate along the mesh lines. The common solution adopted is to mesh with elements aligned with the fibre direction so that the mesh-dependency is alleviated (Falcó et al., 2018; Iarve, 2003; Iarve et al., 2005; Jirásek, 2001; Jirásek and Zimmermann, 1998; Song et al., 2011). The adopted modelling strategy with tie constraints allows to use different meshes for the different ply orientations. The medial axis algorithm is used for the structured mesh along with a process of partitioning and seeding, which leads to the mesh shown in Figures 6 and 7.

The crack-band approach requires a minimum element size to ensure that when damage initiates the elastic strain energy does not exceed the fracture energy. The maximum element size can be calculated for a linear softening law as:

$$l^*_{\max} = \frac{2E_n\mathcal{G}_n}{X_n^2} \quad \text{for} \quad n = 1\pm, 2\pm, 6 \tag{8}$$

where E_n, X_n and $\mathcal{G}_n$ are elastic, strength and fracture ply material properties for each damage mode n, respectively. With element sizes larger than $l^*_{\max}$, a local snap-back in the stress-strain relation is expected to occur which cannot be solved by common implicit Newton-Raphson solvers. In dynamic explicit integration procedures such as the one used in this work, the model would most likely over-predict the energy dissipation by damping the nodal velocities (Falcó et al., 2018). In any case, it is usually recommended to use elements several times smaller than $l^*_{\max}$ as to represent appropriately the stress field along the length of the damage process zone and thus avoiding to have mesh-dependent failures (Leone et al., 2017). The selected element size is 0.25 mm. Analogously, the size of the cohesive elements is chosen as to be the same size as the continuum elements which follow the guidelines provided by Turon et al. (Turon et al., 2015) of having at least three elements within the length of the damage process zone.

3.5. Load steps and boundary conditions

Three different load steps are defined in Figure 8. The first step corresponds to a static step up to the maximum cyclic displacement. Following that, the fatigue step starts. The fatigue

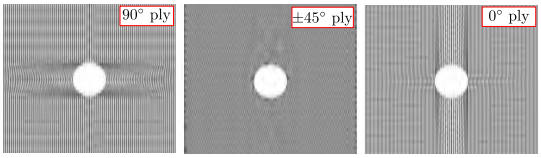

Figure 6: Open-hole (OHT) specimen with fibre-oriented mesh

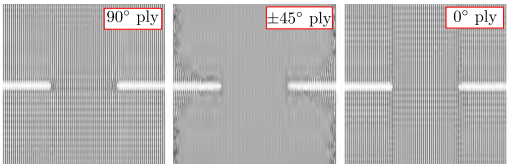

Figure 7: Double-edge notched (DENT) specimen with fibre-oriented mesh

load step can be run in two different manners (see part III for further details (Llobet et al., 2020)). The first simulates one full cycle before every cycle jump in order to calculate the local maximum and minimum displacements, and thus to evaluate the local R-ratio. The second takes the envelope approach, which it is computationally less expensive than the former, but it assumes that the R-ratio is constant for all the finite elements and it is fixed by the remote loading applied. However, this is not necessarily true at local level as the local R-ratio may change when damage takes place. The latter method to control fatigue degradation, i.e. the envelope approach, is used in this work. The last step in Figure 8 corresponds to the residual strength step where the displacement is increased smoothly until the load drops.

The load is introduced by a prescribed displacement at one of the edges while the other edge is constrained. In order to avoid dynamic oscillations, the displacement is introduced by smooth amplitude curves. The transitions between steps are controlled via the VEXTERNALDB subroutine (ABAQUS, 2014), in which it is possible to conclude the step execution and advance to the next step (for example by the given number of cycles). Note that only half of the laminate is represented with through-the-thickness symmetry boundary conditions as shown

in Figure 5.

3.6. Element deletion criterion

One of the major shortcomings of modelling damage in continuum theories with the crack band model is the excessive distortion of elements undergoing large strains. This is a frequent problem when modelling structures with severe damage which can eventually crash the explicit simulations. Different measures have been adopted in the literature (Falcó et al., 2018; Soto et al., 2018a,b); from deleting the continuum elements when a certain value of the fibre damage is reached, to limit the damage variables to a certain value without element deletion. Recall that limiting the damage variables without element deletion entails that the energy dissipated could be far from the actual material fracture toughness (see comparisons provided by Soto et al., 2018a). Moreover, the elements with remaining stiffness can still transfer stresses and store an important amount of elastic energy.

In the present model, the continuum elements are deleted only if $D_1 \geq 0.999$. However, the low transverse and shear strengths of the matrix give rise to excessive distortion of elements undergoing higher levels of matrix damage that are not being deleted from the mesh. Thus, the matrix damage variables D_2 and D_6 must be limited to some extent. In part III (Llobet et al., 2020), it was shown that the in-plane effective stresses are used to evaluate the failure criteria that determines the initiation of damage. The effective stress vector $\tilde{\boldsymbol{\sigma}} = [\tilde{\sigma}_{11}, \tilde{\sigma}_{22}, \tilde{\sigma}_{12}]^{\mathrm{T}}$ is computed as: $\tilde{\boldsymbol{\sigma}} = \mathbf{H}_0^{-1} : (\boldsymbol{\varepsilon} - \boldsymbol{\varepsilon}^p)$, where $\mathbf{H_0^{-1}}$ is the undamaged stiffness tensor defined as follows:

$$\mathbf{H}_0^{-1} = \begin{bmatrix} \frac{E_1}{1-\nu_{12}\nu_{21}} & \frac{\nu_{12}E_2}{1-\nu_{12}\nu_{21}} & 0 \\ \frac{\nu_{12}E_2}{1-\nu_{12}\nu_{21}} & \frac{E_2}{1-\nu_{12}\nu_{21}} & 0 \\ 0 & 0 & G_{12} \end{bmatrix} \tag{9}$$

Note that if $D_2 = 1$ and the strain ε_{22} becomes relatively large, the coupling with the Poisson coefficients can produce high $\tilde{\sigma}_{11}$ stresses, which in some cases can activate spurious damage in the fibre and crashing of the simulations due to excessive distortion. There is one alternative (see Matzenmiller et al., 1995) that solves this issue by slightly modifying the stiffness tensor with a term that cancels out the effect of Poisson under large damage states. Then, the stiffness tensor reduces to:

$$\mathbf{H}_0^{-1} = \begin{bmatrix} \frac{E_1}{\Delta} & \frac{(1-D_1)(1-D_2)\nu_{12}E_2}{\Delta} & 0 \\ \frac{(1-D_1)(1-D_2)\nu_{12}E_2}{\Delta} & \frac{E_2}{\Delta} & 0 \\ 0 & 0 & G_{12} \end{bmatrix} \tag{10}$$

where $\Delta = 1 - (1 - D_1)^2(1 - D_2)^2\nu_{12}\nu_{21}$. Note that when the damage is small the stiffness tensor takes the original form of Eq. (9), while under large damage states the Poisson effect is reduced according to Eq. (10). In case of undesired additional distortion issues, the transverse and shear damage variables are limited to $D_2 = D_6 \leq 0.999$. The interface damage variable D_{coh} is not limited and the cohesive elements are not deleted from the mesh as they keep the penalty stiffness under compression to resist interpenetration between plies.

3.7. Numerical parameters

In order to conduct efficient quasi-static simulations in Abaqus/Explicit, the mass of the model can be artificially increased for those elements whose stable time increment are less than a user-supplied time increment. This is defined by the variable mass scaling. A stable time increment of $5\text{x}10^{-6}$ s is set for all the simulations, and Abaqus/Explicit determines the necessary mass scaling factors. The quasi-static nature of the simulations is guaranteed by keeping the kinetic energy two orders of magnitude lower than the internal energy.

The interface penalty stiffness for the zero-thickness cohesive elements is set to $K = 10^5$ N/mm^3. Ideally, the penalty stiffness should be as large as possible to avoid adding compliance to the specimen. However, the larger the penalty stiffness the lower the stable time increment computed in the cohesives. A high value of K can also introduce spurious oscillations in explicit codes (Soto et al., 2018a). Other numerical parameters that need to be defined for the fatigue simulation are shown in Table 1. The target fatigue damage increments, ΔD_n^f, for the fibre, matrix and interface are defined as a compromise between the computational time and the accuracy to describe the process of stress redistribution due to fatigue damage.

Parameter	Description	Value
ΔD_{1+}^f	fibre damage increment	0.01
ΔD_{2+}^f, Δd_6^f	matrix damage increment	0.1
$\Delta D_{\mathrm{coh}}^f$	interface damage increment	0.1
$\Delta \mathrm{N}_{\mathrm{min}}$	minimum allowed cycle jump	25 cycles
$\mathrm{N}_{\mathrm{cycles}}$	number of cycles	10^6 cycles

Table 1: Fatigue analysis parameters

4. Material card

The computational model requires the characterization of several static and fatigue properties that are presented in this section.

4.1. Static properties

The static material properties are summarized in Table 2 and Table 3 for the intra- and inter-laminar model, respectively. The standard test procedures followed are also included in these tables along with the source from which the property is taken or measured.

The longitudinal (or fibre) fracture is described by a bilinear cohesive law. The data reduction method developed by Ortega et al. (2016) is used to deduce the longitudinal cohesive

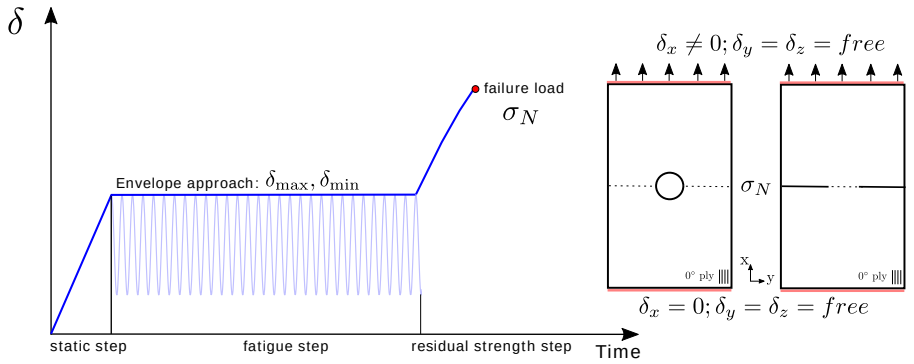

Figure 8: Load steps and boundary conditions.

laws in tension and in compression. This method is based on an inverse analytical approach that best fits the experimental load displacement curves obtained in the compact tension (CT) and compact compression (CC) experiments. Figure 9 shows the cohesive laws obtained by this method. It has to be noted that the CT test resulted in an invalid failure mode with back-end compressive failure. When this happens the measure of the fracture toughness that is taken from the last point available in the load-displacement curve is strongly underestimated. Therefore, this material property is adjusted in the static numerical simulations.

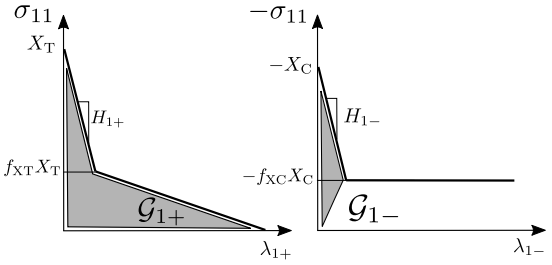

Figure 9: Fibre bilinear cohesive laws in tension (f_{XT} = 0.15 and H_{1+} = 62755 N/mm^3) and compression (f_{XC} = 0.2 and H_{1-} = 11520 N/mm^3).

The transverse and shear (or matrix) fracture are described by linear cohesive laws so that only the ply strengths and the fracture energies are required. Note that the intralaminar fracture energies for matrix cracking in tension and shear are usually assumed to be the same as the interlaminar fracture energies. However, this carbon/epoxy material has a much tougher interface than other traditional carbon/epoxy systems. The greater toughness is the result of a prepreg manufacturing technique that concentrates the toughening agents between plies, rather than uniformly distributing them throughout the ply. This yields to higher interlaminar fracture energies compared to the intralaminar ones. Thus, assuming the same fracture energy for intralaminar and interlaminar cracking is no longer valid.

The interface static fracture properties (see Table 3) are directly taken from the works done by Carreras et al. (Carreras et al., 2019b, 2017), Renart et al. (Renart et al., 2018) and Jaeck et al. (Jaeck et al., 2018). These experimental works reported mode I, mode II and B-K interpolation parameter to describe interlaminar fracture under mixed-mode conditions.

4.2. Fatigue properties

The fatigue experiments with notched quasi-isotropic carbon/epoxy laminates did not show significant fibre damage as it occurred when testing plain laminates (Llobet et al., 2017). The authors confirmed experimentally the loss of stiffness and strength in unnotched unidirectional laminates under tension-tension longitudinal loads. A fatigue damage function to describe the fibre loss of stiffness and strength under tension-tension longitudinal loads can be introduced (Llobet et al., 2017):

$$\frac{dD_{1+}^{Df}}{dN} = \frac{\phi_{L+}^{16}}{16500\left(1 - D_{1+}^{Df}\right)^5}\left(\frac{1-R}{1+R}\right)^4 \tag{11}$$

where D_{1+}^{Df} is the fibre distributed damage, ϕ_{L+} is the longitudinal loading function in tension and R is the stress ratio. Note that it was also confirmed in (Llobet et al., 2017) that the ultimate strain-to-failure in the fibre direction remains constant after fatigue damage, meaning that the function β_{L+} can be assumed to be equal to one. These two fatigue material properties are illustrated in Figure 10a. The reader is referred to the former part III (Llobet et al., 2020) for further details on the intralaminar fatigue damage model.

For the matrix-dominated fatigue damage, there is experimental evidence that diffuse fatigue damage or microcracking occurs prior to a through-the-thickness matrix crack especially under shear stresses (May and Hallett, 2010; Quaresimin et al., 2016). This mechanism is considered to be essential to simulate fatigue crack initiation in crack-free specimens. Indeed, the works from Nojavan et al. (2016) and Iarve et al. (2016) remarked that fatigue damage should be included as a strength reduction mechanism. The strength to initiate a matrix crack

Property				Standard test	Source
Elastic	E_1	[GPa]	160	ASTM D3039	AMADE lab
	E_2	[GPa]	9.3	ASTM D3039	AMADE lab
	$G12$	[GPa]	5.2		Estimated (Sebaey et al., 2014)
	ν_{12}		0.34	ASTM D3039	AMADE lab
Strength	X_T	[MPa]	3050	ASTM D3039	AMADE lab
	X_C	[MPa]	1200	ASTM D6641	AMADE lab
	Y_T	[MPa]	47	ASTM D3039	AMADE lab
	Y_C	[MPa]	230	ASTM D6641	AMADE lab
	S_L	[MPa]	96	ASTM D2344	AMADE lab
Fracture toughness	$\mathcal{G}_{1+}$	[N/mm]	315	Compact Tension	AMADE lab
	$\mathcal{G}_{1-}$	[N/mm]	250	Compact Compression	AMADE lab
	$\mathcal{G}_{2+}$	[N/mm]	0.3		AMADE lab (Llobet et al., 2018)
	$\mathcal{G}_{2-}$	[N/mm]	1.5		Estimated ($\mathcal{G}_6/\cos 53°$)
	$\mathcal{G}_6$	[N/mm]	0.9		Estimated (Sebaey et al., 2014))

Table 2: Ply-based unidirectional material properties

Property				Standard test	Source
Interface strength	τ_{Io}	[MPa]	32	–	$\tau_{IIo}\sqrt{\frac{\mathcal{G}_{Ic}}{\mathcal{G}_{IIc}}}$ (Turon et al., 2010)
	τ_{IIo}	[MPa]	96	ASTM D2344	
Fracture toughness	$\mathcal{G}_{Ic}$	[N/mm]	0.305	ASTM D5528	AMADE lab (Carreras et al., 2019b)
	$\mathcal{G}_{IIc}$	[N/mm]	2.766	ASTM D7905	AMADE lab (Carreras et al., 2019b)
B-K interpolation parameter	η		2.051	ASTM D6671	AMADE lab (Carreras et al., 2019b,c)
Paris law mode I	p_I, A_I		8.399, 564.4		AMADE lab (Carreras et al., 2019c; Renart et al., 2018)
Paris law mode II	p_{II}, A_{II}		3.620, 0.0121		AMADE lab (Carreras et al., 2019c)
Mixed mode interpolation parameter	p_m, A_m		-4.991, $1.197{\cdot}10^{-6}$		AMADE lab (Carreras et al., 2019c; Jaeck et al., 2018)
Mode I and II thresholds	$\mathcal{G}_{Ith}$, $\mathcal{G}_{IIth}$	[N/mm]	0.085, 0.083		AMADE lab (Carreras et al., 2019b)

Table 3: Interface material static and fatigue properties

is reduced to the stress given by the S-N curve. The constitutive model presented in part III (Llobet et al., 2020) distinguishes the initiation and propagation phases of a matrix crack. The initiation can be defined by a function called β_{T+} that reduces both the transverse and shear static strengths Y_T and S_L, but it keeps the elastic modulus constant until localized damage initiates as is exemplified in Figure 10b and c. There is no experimental data available that can be easily taken to account for the matrix damage initiation mechanism. The authors investigated the β_{T+} function for mode I transverse cracks in cross-ply laminates Llobet et al. (2018). The experimental results did not show any strength reduction mechanisms at least for mode I transverse cracks. However, the authors propose to define β_{T+} function for the initiation of shear cracks similarly to the function used for the loss of strength in the fibre (Llobet et al., 2017), but with different fitting material constants that are adjusted in the numerical simulations. It should be mentioned that no shear plasticity is taken into account at this stage since the fatigue model is unclear in this respect. The propagation of matrix cracks is done by embedding a Paris law based function inside the continuum elements. The crack growth rates given by the Paris law are linked to the corresponding matrix damage variables as in Turon's model (Turon et al., 2007). See part III for further details on the derivation of the damage rates (Llobet et al., 2020). The same crack growth rates are used for the intra- and inter-laminar matrix cracks.

The fatigue interlaminar properties are taken from the works (Carreras et al., 2019b, 2017, 2019c; Jaeck et al., 2018; Renart et al., 2018). The reader is referred to these references for further details on the experimental and data reduction methods used to obtain crack growth rate curves (or Paris law curves). The parameters of the Paris law-based expression are obtained from interlaminar fatigue crack propagation tests at different mode mixities: p_I, A_I (mode I), p_{II}, A_{II} (mode II), p_m, A_m (mixed-mode interpolation parameters). The mode I and II energy release thresholds $\mathcal{G}_{Ith}$, $\mathcal{G}_{IIth}$ are obtained from onset curves (defined by a 5% increase in the specimen compliance), and considering run-out specimen at 2 millions cycles.

5. Results and discussion

This section shows the numerical predictions and discusses the results with respect to the experimental findings for each loading case: static, tension-tension fatigue and residual

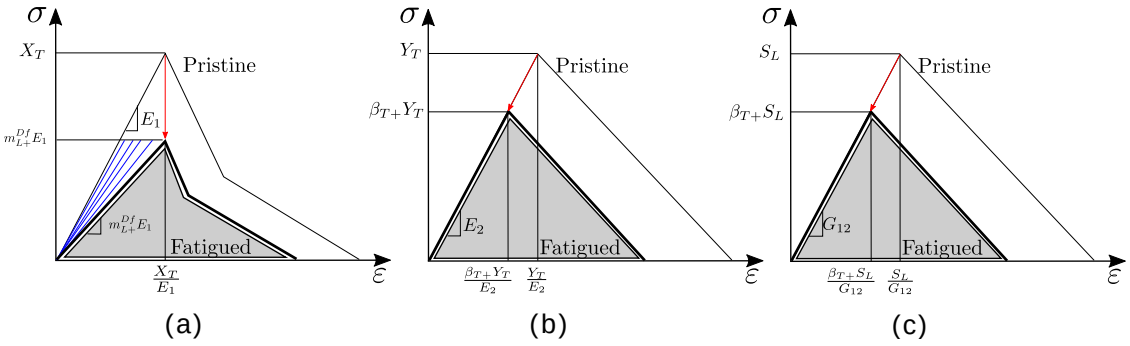

Figure 10: Fatigue intralaminar cohesive laws for the longitudinal (a) fibre response, transverse (b) and shear (c) matrix response, respectively.

strength. Table 4 summarizes all the simulated and tested load cases which are identified by the Id. number.

	load	cycles	dent	openhole	Id. number
STATIC	-	-	Exp./ FEM	Exp./ FEM	[**0**]
FATIGUE	60%σ_U	1M	-	Exp.	[**1**]
	75%σ_U	100k	Exp./ FEM	FEM	[**2**]
		200k	FEM	FEM	[**3**]
		250k	Exp.	-	[**4**]
		300k	FEM	FEM	[**5**]
		400k	FEM	FEM	[**6**]
		500k	FEM	FEM	[**7**]
		600k	Exp./FEM	FEM	[**8**]
		700k	FEM	FEM	[**9**]
		800k	FEM	FEM	[**10**]
		900k	FEM	FEM	[**11**]
		1M	Exp./FEM	FEM	[**12**]
		2M	-	Exp.	[**13**]
	90%σ_U	150k	-	Exp.	[**14**]
		400k	Exp.	-	[**15**]

Table 4: Summary of experimental tests and FEM simulations performed for both geometries in static, fatigue and residual strength. σ_U refers to the ultimate static load and the R-ratio is equal to 0.1 for all the load cases.

5.1. Static simulation

Figures 11 and 12 show the comparison between the damage predicted by the numerical model and the damage patterns observed in the X-rayed specimens after static failure. The load drop in the static simulations occurs when a fibre crack localizes at the 0° plies, which means that static failure is fibre-dominated. The initiation and propagation of a fibre crack is controlled by the longitudinal strength X_T and by the first slope H_{1+} of the cohesive law (see Figure 9 and Maimí et al., 2012). As it was mentioned in section 4, the slope H_{1+} is adjusted numerically since invalid failure occurred in the compact tension tests. It is worth mentioning that the experiments and numerical predictions do not show significant 0° splits in static conditions (the split length is less than the notch length in the DENT and less than the diameter size in the OHT). The strength-to-failure at the net section for the OHT specimen is 647.5 MPa (experiment) and 575.9 MPa (numerical prediction). The strength-to-failure at the net section for the DENT specimen results in 784.6 MPa (experiment) and 706.5 MPa (numerical prediction).

5.2. Fatigue simulation

Figure 13 shows the fatigue damage evolution of the DENT specimen under a 75% of the ultimate static strength and R-ratio equal to 0.1. The X-ray images at this stress level reveals that damage grows progressively without specimen complete failure even up to 1 million loading cycles. No fibre fracture is observed due to the redistribution of stresses that the splitting crack produces at the 0° plies.

The fatigue simulations were run until 1M cycles and then, the simulations were restarted at intervals of 100k cycles for residual strength measurement (i.e., 100k, 200k and so on). In general, the damage predictions show good agreement with the main fatigue degradation mechanisms found in the experiments. However, it is observed that the length of the splits at the 0° plies is underestimated. The reason for this can be attributed to two different factors. The first is the fact that the localization band with the crack-band approach takes the size of one finite element. As the element size across the crack increases, the crack effectively becomes blunter (having a lower stress concentration associated with it) and damage initiation is delayed (Leone et al., 2017). The second is given by the limitation of the magnitude of the transverse and shear damage variables to reduce the excessive distortion problems. The remaining stiffness of these elements makes them transfer transverse and shear stresses ranging from 1 to 5 MPa over the entire length of the 0° split. Eventually, this yields to a reduction of the shear stress at the crack tip which either reduces the crack growth rate or even arrests the propagation of the crack.

To deal with such limitations many authors concluded the absolute need to use discrete models to simulate splitting cracks (Achard et al., 2014; Le et al., 2018; Nixon-Pearson et al., 2013a,b). In those models they insert cohesive elements at the potential crack locations if the crack paths are known beforehand.

A fatigue simulation with the open-hole specimen at a fatigue load of 75% of the static strength, R-ratio = 0.1 and 1 million cycles is shown in Figure 14. The numerical model

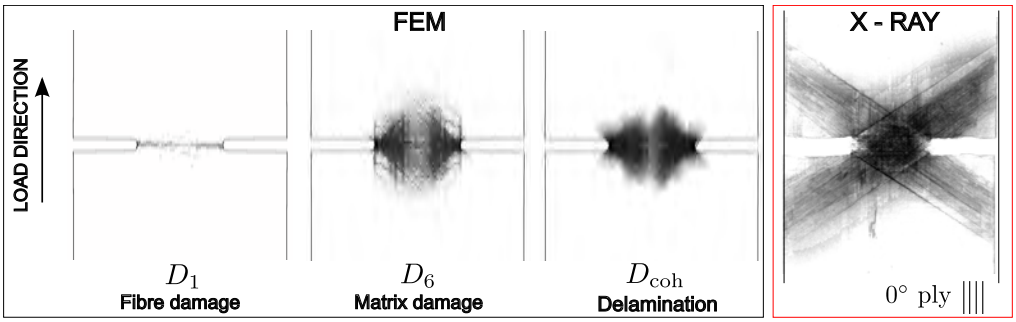

Figure 11: Damage mechanisms in a quasi-isotropic carbon/epoxy double-edge notch tensile specimen under static loading (FEM vs. X-RAY).

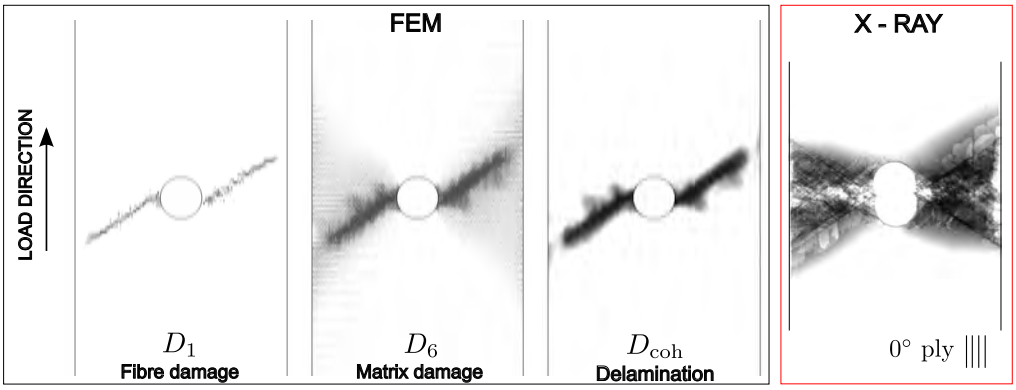

Figure 12: Damage mechanisms in a quasi-isotropic carbon/epoxy open-hole specimen under static loading (FEM vs. X-RAY).

predicts well the direction of the splitting cracks and delamination locations, but again the length of the intra-laminar cracks is underestimated as in the DENT specimens. Thus, the extension of delamination is also smaller than the one observed in the radiographs.

It is worth mentioning that severe issues concerning numerical stability were found at higher fatigue loading levels (higher than 75% of the static strength), resulting in most simulations unable to complete due to excessive distortion issues of few elements undergoing large transverse and shear strains. If these elements are deleted from the mesh without fibre damage, premature failure of the specimen occurs. If they are kept active within the model, then they become so distorted that may activate other more critical failure modes like fibre fracture, which eventually lead to the same excessive distortion errors. One of the reasons for this is attributed to the concern raised by Leone (2015). Leone suggested that the large shear deformation applied to cracked material points results in a rotation of the local material directions. Calculating the strain in this rotated, smeared material coordinate system cause unintended load transfer across the crack faces and activate other failure modes, i.e. fibre failure. Leone figured out a method to solve this issue by decomposing the deformation gradient tensor into 'bulk' and 'cracked' material, similar to the additive strain decomposition of smeared crack models (Camanho et al., 2013). In any case, this concept has been only validated by modelling splits in unidirectional open-hole specimens and it should be benchmarked in a much more complex scenario such as the one presented in this work.

Another consideration to be made is the concern of Van deer Meer when modelling splitting cracks with meso-scale CDM models (Van Der Meer and Sluys, 2009). Since the homogenization of composite plies at the meso-scale level eliminates the distinction between fibres and resin, meso-scale CDM models have difficulties to predict the crack direction as they cannot distinguish between cracks that propagate along the fibre direction from those that cross fibres. Recall that the direction of the crack is driven by the local stress redistribution of damaged elements that are activated according to the local evaluation of a failure criteria. Although this problem seems to be solved by orienting the mesh with the fibre direction, it still causes some numerical difficulties in particular when a matrix crack is subjected to shear stresses (Rose et al., 2013; Song et al., 2011). In the present model, the interaction between different matrix cracks at different plies results in, for instance, matrix cracks that occur at the ±45° ply are spuriously being transferred to

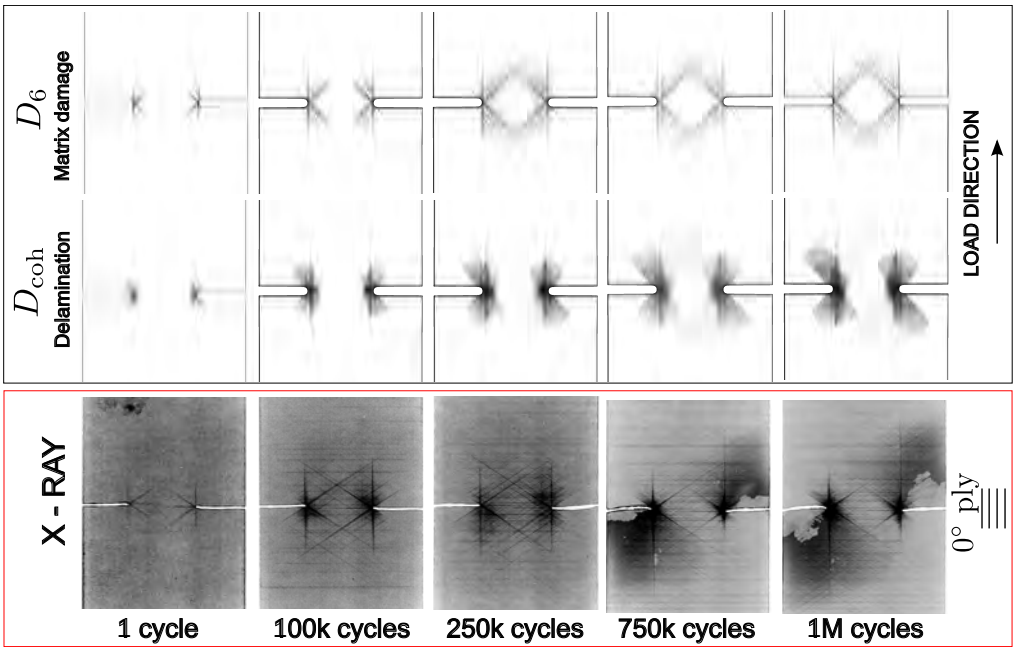

Figure 13: Fatigue damage evolution in the double-edge notched specimen subjected to 75% of the ultimate static strength and R-ratio = 0.1 (FEM vs. X-RAY).

the adjacent 90° ply.

5.3. Residual strength simulation

The post-fatigue residual strength experiments revealed that fatigue damage alleviates the stress concentration and delays localized fibre fracture. This trend is in agreement with the findings in open literature with different carbon/epoxy notched laminates (Aidi et al., 2015; Aymerich and Found, 2000; Spearing and Beaumont, 1992; Spearing et al., 1992b). Despite the overall damage induced by fatigue loads, it appears that the 0° ply splits control the increase in the tensile residual strength (Nixon-Pearson and Hallett, 2015). Figure 15 and 16 show the net section strength predictions and the experimental values with respect to the length of the 0° splits. Note that the predicted DENT strengths of Figure 15 seem to capture well the increase in the strength, but they clearly show that the length of the splits is shorter than in the experiments, and thus the predictions are shifted to the left. The experimental fatigue load cases can be identified through the Id. number given in table 4.

In the case of the OHT specimen, the model seems to be not capable of predicting the correct residual strengths. Indeed, the static and residual strengths are relatively closer and they do show the strength increase observed in the experiments. It is clear shown in Figure 14 that fatigue damage is underestimated and thus the increase in the strength is not well captured. It is also important to note that the residual strength simulations after more than 500k cycles failed before reaching the load drop due to excessive distortion errors.

6. Conclusions

A new computational model for composite laminates has been presented to simulate fatigue damage and post-fatigue residual strengths. The model is based on an extension of the meso-scale continuum damage model developed by Maimí et al. (2007a,b) and the fatigue cohesive zone model developed by Turon et al. (2007). Both models are controlled by a cycle jump strategy that is implemented inside an explicit finite element code. The computational model has been numerically tested by simulating notched carbon/epoxy quasi-isotropic laminates. Two different geometries such as the open-hole and the double-edge notched specimens have been tested.

The experimental results have shown that the presence of fatigue damage affects the overall stiffness and the ultimate strength of notched laminates. While the static strength is controlled by fibre fracture, the fatigue strength is driven by the progressive failure of the matrix and by delamination. These forms of damage reduce the notch sensitivity and delay fibre fracture. The direct consequence of this is that the post-fatigue residual strength in tension is higher than the pristine static strength. This experimental results are in line with the previous observations in open literature.

The numerical predictions have captured the most relevant fatigue damage mechanisms and showed qualitatively good correlation with the X-rayed specimens. The numerical model has been able to capture the strength increase in the double-edge notched specimen but not in open-hole specimen. This problem has been attributed to the underestimation of the length of

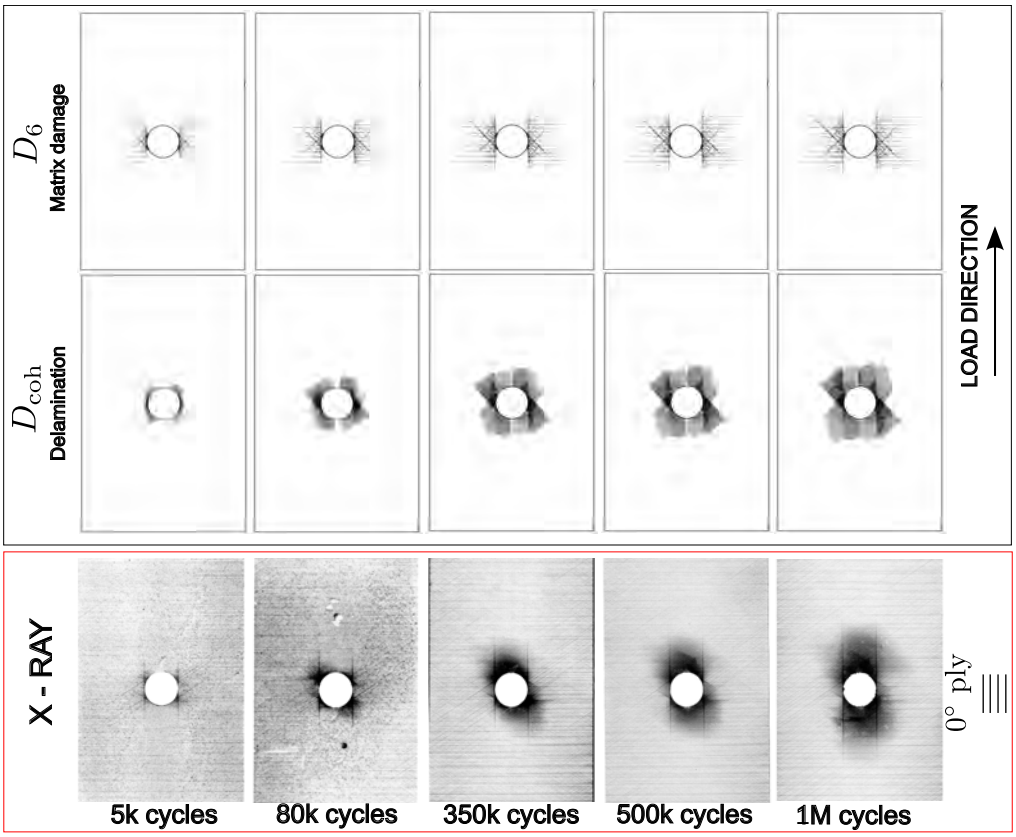

Figure 14: Fatigue damage evolution in the open-hole specimen subjected to 75% of the ultimate static strength and R-ratio = 0.1.

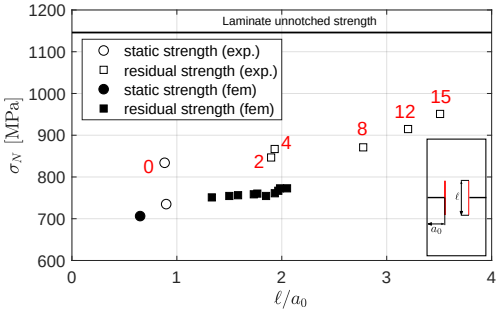

Figure 15: Residual post-fatigue tensile strength in double-edge notched specimens with respect to the length of the 0° splits normalized by the notch length (a_0).

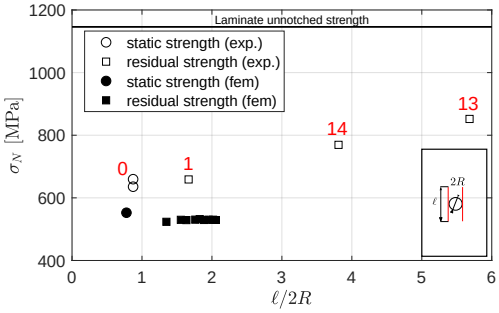

Figure 16: Residual post-fatigue tensile strength in open-hole specimens with respect to the length of the 0° splits normalized by the hole diameter ($2R$).

0° splits after fatigue. Several difficulties were identified and further work is needed to develop a robust and reliable computational tool for quantitative evaluation of fatigue damage. The following numerical issues have been identified that deserves further attention:

- Continuum elements undergoing large transverse and shear strains (due to matrix damage) lead to a large num-

ber of uncompleted simulations with excessive distortion errors. If these elements are deleted from the mesh without fibre damage, premature failure of the specimen occurs. If they are kept active within the model, then they become so distorted that may activate other more critical failure modes like fibre fracture, which eventually led to the same excessive distortion errors. The concept proposed by Leone (Leone, 2015) is seen as a potential improvement to solve this issue, but it needs to be further investigated under more complex laminate configurations.

- The continuum damage model has proved its capability of predicting the correct direction of isolated splitting matrix cracks by aligning the mesh of each ply with the fibre direction. However, the homogenization between fibre and matrix at the meso-scale level can give rise to some limitations when modelling isolated matrix cracks. The problem stems from the fact that the direction of the propagation crack is controlled by the local evaluation of the failure criteria and not by the fibre direction. In other words, the model cannot distinguish between matrix cracks that grow perpendicular to the fibres or matrix cracks that grow parallel to the fibre direction, where in reality the inhomogeneity of the composite material causes the crack to grow differently (see Van Der Meer and Sluys, 2009). It is considered that this problem deserves further investigation and it should be analysed in more detail. As an alternative, it is suggested to explore the capabilities of X-FEM or any of its variants in order to describe the propagation of splitting matrix cracks (Iarve et al., 2016; Van der Meer and Sluys, 2010; Van der Meer et al., 2012).

- The cycle jump algorithm adopted in the explicit finite element code was found to be rather sensitive to the critical finite elements (i.e., resulting in a consecutive set of small cycle jumps), and thus leading to simulations that currently can take a considerable computational time, even though the methodology can be executed in parallel in multiple cpus. In order to address problems of industrial interest, it is considered that the cycle jump strategy must be improved to some extent especially when dealing with larger scale composite structures.

Acknowledgements

The authors would like to acknowledge the financial support of the Spanish Government through the Spanish Ministerio de Ciencia, Innovación y Universidades under the contracts RTC-2014-1958-4 and RTI2018-097880-B-I00.

References

ABAQUS, 2014. Abaqus 6.14 documentation.

AC7122/1 RevB, 2017. Nadcap Audit Criteria for Non-Metallic Materials Testing - Mechanical Testing. Tech. rep.

Achard, V., Bouvet, C., Castanié, B., Chirol, C., 2014. Discrete ply modelling of open hole tensile tests. Composite Structures 113 (1), 369–381.

Aidi, B., Philen, M. K., Case, S. W., 2015. Progressive damage assessment of centrally notched composite specimens in fatigue. Composites Part A: Applied Science and Manufacturing 74, 47–59.

Ambu, R., Aymerich, F., Bertolino, F., 2005. Investigation of the effect of damage on the strength of notched composite laminates by digital image correlation. The Journal of Strain Analysis for Engineering Design 40 (5), 451–461.

Aymerich, F., Found, S., 2000. Response of notched carbon/PEEK and carbon/epoxy laminates subjected to tension fatigue loading. Fatigue & Fracture Of Engineering Materials & Structures, 675–683.

Bak, B. L. V., Sarrado, C., Turon, A., Costa, J., jun 2014. Delamination Under Fatigue Loads in Composite Laminates: A Review on the Observed Phenomenology and Computational Methods. Applied Mechanics Reviews 66 (6), 060803.

Bak, B. L. V., Turon, A., Lindgaard, E., Lund, E., 2016. A simulation method for high-cycle fatigue-driven delamination using a cohesive zone model. International Journal for Numerical Methods in Engineering.

Bak, B. L. V., Turon, A., Lindgaard, E., Lund, E., 2017. A benchmark study of simulation methods for high-cycle fatigue-driven delamination based on cohesive zone models. Composite Structures 164, 198–206.

Benzeggagh, M. L., Kenane, M., 1996. Measurement of mixed-mode delamination fracture toughness of unidirectional glas/epoxy composites with mixed-mode bending apparatus. Composite Science and Technology 56 (4), 439–449.

Blanco, N., Gamstedt, E. K., Asp, L. E., Costa, J., 2004. Mixed-mode delamination growth in carbon-fibre composite laminates under cyclic loading. International Journal of Solids and Structures 41 (15), 4219–4235.

Camanho, P. P., Bessa, M. A., Catalanotti, G., Vogler, M., Rolfes, R., 2013. Modeling the inelastic deformation and fracture of polymer composites Part II: Smeared crack model. Mechanics of Materials 59, 36–49.

Carreras, L., Lindgaard, E., Renart, J., Bak, B. L. V., Turon, A., 2019a. An evaluation of mode-decomposed energy release rates for arbitrarily shaped delamination fronts using cohesive elements. Computer Methods in Applied Mechanics and Engineering 347, 218–237.

Carreras, L., Renart, J., Turon, A., Costa, J., Bak, B. L. V., Lindgaard, E., Martin de la Escalera, F., Essa, Y., 2019b. A benchmark test for validating 3D simulation methods for delamination growth under quasi-static and fatigue loading. Composite Structures 210 (December 2018), 932–941.

Carreras, L., Renart, J., Turon, A., Costa, J., Essa, Y., Martin de la Escalera, F., 2017. An efficient methodology for the experimental characterization of mode II delamination growth under fatigue loading. International Journal of Fatigue 95, 185–193.

Carreras, L., Turon, A., Bak, B. L. V., Lindgaard, E., Renart, J., Martin de la Escalera, F., Essa, Y., 2019c. A simulation method for fatigue-driven delamination in layered structures involving non-negligible fracture process zones and arbitrarily shaped crack fronts. Composites Part A 122 (April), 107–119.

Cox, B., Yang, Q. D., 2006. In quest of virtual tests for structural composites. Science 314 (5802), 1102–1107.

Daken, H. H., Mar, J. W., 1985. Splitting initiation and propagation in notched unidirectional graphite/epoxy composites under tension-tension cyclic loading. Composite Structures 4 (2), 111–133.

Falcó, O., Ávila, R., Tijs, B., Lopes, C., 2018. Modelling and simulation methodology for unidirectional composite laminates in a Virtual Test Lab framework. Composite Structures 190 (September 2017), 137–159.

González, E. V., Maimí, P., Martín-Santos, E., Soto, A., Cruz, P., Martín de la Escalera, F., Sainz de Aja, J. R., 2018. Simulating drop-weight impact and compression after impact tests on composite laminates using conventional shell finite elements. International Journal of Solids and Structures 145, 230–247.

González, E. V., Maimí, P., Turon, A., Camanho, P. P., Renart, J., 2009. Simulation of delamination by means of cohesive elements using an explicit finite element code. CMC-Computers Materials & Continua 9 (1), 51–92.

Hallett, S. R., Wisnom, M. R., 2005a. Experimental investigation of progressive damage and the effect of layup in notched tensile tests. Journal of Composite Materials 40 (2).

Hallett, S. R., Wisnom, M. R., 2005b. Numerical investigation of progressive damage and the effect of layup in notched tensile tests. Journal of Composite Materials 40 (14).

Harper, P. W., Hallett, S. R., 2010. A fatigue degradation law for cohesive interface elements - Development and application to composite materials. International Journal of Fatigue 32 (11), 1774–1787.

Hochard, C., Miot, S., Thollon, Y., 2013. Fatigue of laminated composite struc-

tures with stress concentrations. Composites Part B: Engineering 65, 11–16.
Iarve, E. V., 2003. Mesh independent modelling of cracks by using higher order shape functions. International Journal for Numerical Methods in Engineering 56 (6), 869–882.
Iarve, E. V., Hoos, K., Braginsky, M., Zhou, E., Mollenhauer, D. H., 2016. Progressive failure simulation in laminated composites under fatigue loading by using discrete damage modeling. Journal of Composite Materials 51 (15), 2143–2161.
Iarve, E. V., Mollenhauer, D., Kim, R., 2005. Theoretical and experimental investigation of stress redistribution in open hole composite laminates due to damage accumulation. Composites Part A: Applied Science and Manufacturing 36 (2 SPEC. ISS.), 163–171.
ISO/IEC 17025:2017, 2017. General requirements for the competence of testing and calibration laboratories.
Jaeck, I., Carreras, L., Renart, J., Turon, A., Martin de la Escalera, F., Essa, Y., 2018. Experimental methodology for obtaining fatigue crack growth rate curves in mixed-mode I-II by means of variable cyclic displacement tests. International Journal of Fatigue 110 (November 2017), 63–70.
Jirásek, M., 2001. Modeling of localized damage and fracture in quasibrittle materials. In: Vermeer P.A., H.J., H., S., L., W., E., S., D., E., R. (Eds.), Continuous and Discontinuous Modelling of Cohesive-Frictional Materials. Springer, pp. 17–18.
Jirásek, M., Zimmermann, T., 1998. Analysis of a rotating crack. Journal of Engineering Mechanics, 842–851.
Le, M. Q., Bainier, H., Néron, D., Ha-Minh, C., Ladevèze, P., 2018. On matrix cracking and splits modeling in laminated composites. Composites Part A: Applied Science and Manufacturing 115 (September), 294–301.
Lemaitre, J., Doghri, I., 1994. Damage 90: a post processor for crack initiation. Computer Methods in Applied Mechanics and Engineering 115 (3-4), 197–232.
Leone, F. A., 2015. Deformation gradient tensor decomposition for representing matrix cracks in fiber-reinforced materials. Composites Part A: Applied Science and Manufacturing 76, 334–341.
Leone, F. A., Dávila, C. G., E., M. G., Madhavadas, R., Hyder, I., 2017. Fracture-Based Mesh Size Requirements for Matrix Cracks in Continuum Damage Mechanics Models. In: 58th AIAA/ASCE/AHS/ASC Structures, Structural Dynamics, and Materials. No. January. pp. 1–14.
Lesne, P. M., Savalle, S., 1984. An efficient cyle jump technique for viscoplastic structure calculations involving large number of cycles. In: 2nd International Conference on Computational Plasticity. Models, Software and Applications. Barcelona.
Llobet, J., Maimí, P., Essa, Y., Martin de la Escalera, F., 2018. Progressive matrix cracking in carbon/epoxy cross-ply laminates under static and fatigue loading. International Journal of Fatigue 119, 330–337.
Llobet, J., Maimí, P., Essa, Y., Martin de la Escalera, F., 2020. A continuum damage model for composite laminates: Part III - Fatigue. Submitted for publication in Mechanics of Materials.
Llobet, J., Maimí, P., Mayugo, J. A., Essa, Y., Martin de la Escalera, F., 2017. A fatigue damage and residual strength model for unidirectional carbon/epoxy composites under on-axis tension-tension loadings. International Journal of Fatigue 103, 508–515.
Maimí, P., Camanho, P. P., Mayugo, J. A., Dávila, C. G., 2006. A Thermodynamically Consistent Damage Model for Advanced Composites. Tech. Rep. March.
Maimí, P., Camanho, P. P., Mayugo, J. A., Dávila, C. G., 2007a. A continuum damage model for composite laminates: Part I Constitutive model. Mechanics of Materials 39 (10), 897–908.
Maimí, P., Camanho, P. P., Mayugo, J. A., Dávila, C. G., 2007b. A continuum damage model for composite laminates: Part II Computational implementation and validation. Mechanics of Materials 39 (10), 909–919.
Maimí, P., Trias, D., González, E. V., Renart, J., 2012. Nominal strength of quasi-brittle open hole specimens. Composites Science and Technology 72 (10), 1203–1208.
Matzenmiller, A., Lubliner, J., Taylor, R. L., 1995. A constitutive model for anisotropic damage in fiber-composites. Mechanics of Materials 20 (2), 125–152.
May, M., Hallett, S. R., 2010. An assessment of through-thickness shear tests for initiation of fatigue failure. Composites Part A: Applied Science and Manufacturing 41 (11), 1570–1578.
Nixon-Pearson, O. J., Hallett, S. R., 2015. An investigation into the damage development and residual strengths of open-hole specimens in fatigue. Composites Part A 69, 266–278.
Nixon-Pearson, O. J., Hallett, S. R., Harper, P. W., Kawashita, L. F., dec 2013a. Damage development in open-hole composite specimens in fatigue. Part 1: Experimental investigation. Composite Structures 106, 890–898.
Nixon-Pearson, O. J., Hallett, S. R., Harper, P. W., Kawashita, L. F., 2013b. Damage development in open-hole composite specimens in fatigue. Part 2: Numerical modelling. Composite Structures 106, 890–898.
Nojavan, S., Schesser, D., Yang, Q. D., 2016. An in situ fatigue-CZM for unified crack initiation and propagation in composites under cyclic loading. Composite Structures 146, 34–49.
Ortega, A., Maimí, P., Gonzalez, E. V., Trias, D., 2016. Characterization of the translaminar fracture Cohesive Law. Composites Part A: Applied Science and Manufacturing 91, 501–509.
Quaresimin, M., Carraro, P. A., Maragoni, L., 2016. Early stage damage in off-axis plies under fatigue loading. Composites Science and Technology 128, 147–154.
Renart, J., Budhe, S., Carreras, L., Mayugo, J. A., Costa, J., 2018. A new testing device to simultaneously measure the mode I fatigue delamination behavior of a batch of specimens. International Journal of Fatigue 116 (February), 275–283.
Rose, C. A., Dávila, C. G., Leone, F. A., 2013. Analysis Methods for Progressive Damage of Composite Structures. NASA Langley Research Center NASA/TM-20.
Sebaey, T. A., Costa, J., Maimí, P., Batista, Y., Blanco, N., Mayugo, J. A., 2014. Measurement of the in situ transverse tensile strength of composite plies by means of the real time monitoring of microcracking. Composites Part B: Engineering 65, 40–46.
Song, K., Li, Y., Rose, C. A., 2011. Continuum Damage Mechanics Models for the Analysis of Progressive Failure in Open-Hole Tension Laminates. American institute of Aeronautics and Astronautics, 1–18.
Soto, A., González, E. V., Maimí, P., Martín de la Escalera, F., Sainz de Aja, J. R., Alvarez, E., 2018a. Low velocity impact and compression after impact simulation of thin ply laminates. Composites Part A: Applied Science and Manufacturing 109 (March), 413–427.
Soto, A., González, E. V., Maimí, P., Mayugo, J. A., Pasquali, P. R., Camanho, P. P., 2018b. A methodology to simulate low velocity impact and compression after impact in large composite stiffened panels. Composite Structures 204 (February), 223–238.
Spearing, S. M., Beaumont, P. W. R., 1992. Fatigue damage mechanics of composite materials. I: Experimental measurement of damage and post-fatigue properties. Composites Science and Technology 44 (2), 159–168.
Spearing, S. M., Beaumont, P. W. R., Ashby, M. F., jan 1992a. Fatigue damage mechanics of composite materials. II: A damage growth model. Composites Science and Technology 44 (2), 169–177.
Spearing, S. M., Beaumont, P. W. R., Kortschot, M. T., 1992b. The fatigue damage mechanics of notched carbon-fiber peek laminates. Composites 23 (5), 305–311.
Turon, A., 2006. Simulation of delamination in composites under quasi-static and fatigue loading using cohesive zone models. Ph.D. thesis, University of Girona.
Turon, A., Bak, B. L. V., Lindgaard, E., Sarrado, C., Lund, E., 2015. Interface elements for fatigue-driven delaminations in advanced composite materials. In: Camanho, P.P., Hallet, S. (Ed.), Numerical Modelling of Failure in Advanced Composite Materials. Woodhead Publishing Series in Composite Science and Engineering, Ch. 3, pp. 73–91.
Turon, A., Camanho, P. P., Costa, J., Renart, J., 2010. Accurate simulation of delamination growth under mixed-mode loading using cohesive elements: Definition of interlaminar strengths and elastic stiffness. Composite Structures 92 (8), 1857–1864.
Turon, A., Costa, J., Camanho, P. P., Dávila, C. G., 2007. Simulation of delamination in composites under high-cycle fatigue. Composites Part A: Applied Science and Manufacturing 38 (11), 2270–2282.
Van Der Meer, F. P., Sluys, L. J., 2009. Continuum Models for the Analysis of Progressive Failure in Composite Laminates. Journal of Composite Materials 43 (20), 2131–2156.
Van der Meer, F. P., Sluys, L. J., 2010. Mesh-independent modeling of both distributed and discrete matrix cracking in interaction with delamination in composites. Engineering Fracture Mechanics 77 (4), 719–735.
Van der Meer, F. P., Sluys, L. J., Hallett, S. R., Wisnom, M. R., 2012. Computational modeling of complex failure mechanisms in laminates. Journal of Composite Materials 46 (5), 603–623.

Van Paepegem, W., 2002. Development and finite element implementation of a damage model for fatigue of fibre-reinforced polymers. Ph.D. thesis, Ghent University.
URL http://hdl.handle.net/1854/LU-153455

Van Paepegem, W., 2015. The cycle jump concept for modelling high-cycle fatigue in composite materials. In: Carvelli, V., Lomov, S. V. (Eds.), Fatigue of Textile Composites. Elsevier, Ch. 2.

Wisnom, M. R., Chang, F. K., 2000. Modelling of splitting and delamination in notched cross-ply laminates. Composites Science and Technology 60 (15), 2849–2856.